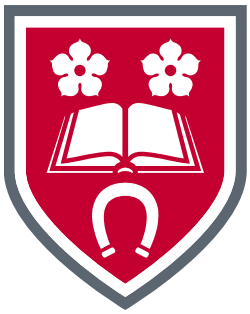

UNIVERSITY OF LEICESTER

REGULATION OF MONOCYTE ANTI-THROMBOTIC GENE AND PROTEIN EXPRESSION THROUGH PLATELET-DERIVED MATERIAL

Thesis submitted for the degree of Doctor of Philosophy at the University of Leicester

by

Robert Edward Turnbull BSc

Department of Cardiovascular Sciences

University of Leicester

2016

Abstract

Activated platelets can recruit monocytes into thrombi through the P-selectin•PSGL-1 interaction. Cross-talk between the cells may regulate monocyte gene and protein expression. A previous genome-wide transcriptomic study identified >3000 genes upregulated in monocytes in response to activated platelets, including a number of antithrombotic genes; in particular *tfpi* and *procr*. This thesis aimed to establish the mechanisms by which platelets regulate these genes, and if this was through the nuclear receptor PPARγ.

Using the same experimental model as in previous studies, in which platelets were activated in whole blood with the platelet-specific GPVI agonist CRP-XL, monocyte *tfpi* and *procr* expression was confirmed, shown to be affected by inhibitors of COX-1 (aspirin) and 12-LOX (esculetin and baicalein), and regulated through soluble factors released from platelets, which were shown to be oxylipins for *tfpi* and proteins ~10kDa for *procr*. Expression of *pparγ* was also increased and largely regulated through direct platelet-monocyte contact, although oxylipins potentiated expression. An associated increase in protein expression was partially confirmed for all three genes. Mass spectrometry (MS) of platelet-derived releasate measured 386 proteins and identified platelet factor 4 (PF4) and RANTES (CCL5) as likely candidates for *procr* regulation. Expression was attenuated with releasate incubated with heparin agarose (HA) but this was not rescued with exogenous PF4. LC-MS/MS measured no change in PF4 levels in the releasate incubated with HA but complete removal of RANTES. MS identified 10 oxylipins released from platelets (AA, 8-, 9-, 11-, 12-, 15-HETE, 9-, 13-HODE, PGD/E2 and TxA2) of which four (11-, 15-HETE, 9-, 13-HODE) were significantly, and TxA2 and PGD/E2 completely reduced by aspirin, and all but AA and 9-HETE reduced with 12-LOX inhibitors. These oxylipins included known PPARγ agonists. Incubation with 15d-PGJ2 and rosiglitazone confirmed potentiation of *tfpi* expression in monocytes. Using a transactivation assay 12- and 15-HETE were shown to activate PPARγ expression *in vitro*, while X-ray crystallography indicated, for the first time, interaction of both with PPARγ.

These results are the first to show regulation of antithrombotic genes in monocytes by factors released from platelets. It is the first to profile oxylipins released from GPVI-activated platelets and identify PPARγ as a regulator of *tfpi,* and RANTES as a potential regulator of *procr* expression in monocytes. The observation that aspirin attenuates expression of both these genes raises issues with its use in the treatment of cardiovascular disease, for which it is relied on heavily.

Acknowledgements

Firstly, I would like to express huge thanks to my primary supervisor, Professor Alison Goodall, who has provided unwavering support throughout the entire project and given me the freedom to plan and conduct interesting experiments. She also provided many opportunities to attend and present at national and international conferences, helping me develop as a researcher. I must also thank my second supervisor, Professor John Schwabe, who offered valuable support and space even though he often had no idea when I was returning. There are a number of other people who have provided valuable support during the project and without whom, this project would not have been possible. In general, I would like to thank everyone in Alison's group who shared many enjoyable, as well as frustrating moments,the many, many colleagues who regularly donated blood for my experiments (even though they had no idea what it was being used for!) and the phlebotomists for being the take the blood for me. Specifically, I would like to thank Katrin Sander and Professor David Barrett for running the oxylipin LC-MS/MS; Jatinderpal Sandhu, Pauline Quinn, Amirmansoor Hakimi and Don Jones for running the protein LC-MS/MS and helping with the analysis; Peter Watson, Greg Hudson and Chris Millard for their support and advice when I was at Biochemistry; Toshimasa Itoh for kindly gifting the 15-HETE he synthesised; and Louise Fairell for her help in collecting and analysing crystallography data sets.

Outside of the University, I would like to thank my parents for getting me to where I am today, constantly believing in me and providing numerous short term 'loans'. I must also thank my wife, Charlotte, who has not only accepted that we will never be millionaires but also for listening to me go on about my research and pretending to believe me when I insist an international conference classifies as a 'hard weeks work'.

Table of contents

Table of tables

Table of figures

Publications arising from this thesis

Presentations

Robert E Turnbull, Jatinderpal K Sandhu, Amirmansoor Hakimi, Leong L Ng, Donald J L Jones, Alison H Goodall. Identification of low molecular weight factors released from platelets that induce *procr* in monocytes. Presented at the UK Platelet meeting, Leicester, UK; September 2015

Robert E Turnbull, Julian van Capelleveen, Unni Krishnan, Joy R Wright, Nilesh J Samani, Meike Trip, Suthesh Sivapalaratnam, Alison H Goodall. Aspirin inhibits the platelet-mediated expression of antithrombotic genes in monocytes. BSHT Abstr. O21, 2012. *(Oral)*

Sameer A Kurmani, Daniel Chan, **Robert E Turnbull**, Chris Jones, Joy R Wright, Alison H Goodall. Regulation of PAI-1 expression within an arterial thrombus. Atherosclerosis; 2012 Dec; 225 (2): E1-E1.

Manuscripts in preparation

R.E. Turnbull, K.N. Sander, D.A. Barrett, A.H. Goodall. *Oxylipins derived from GPVI-activated platelets and the effects of inhibiting arachidonic acid metabolism.*

R.E. Turnbull, P.J. Watson, J.W. Schwabe, A.H. Goodall. *Mechanism of regulation of platelet-induced monocyte tfpi expression.*

R.E. Turnbull, J. Sandhu, A. Hakimi, L.L. Ng, D.J.L. Jones, A.H. Goodall. *Mechanism of regulation of platelet-induced monocyte procr expression.*

R.E Turnbull, P.J Watson, L. Fairrell, J.W. Schwabe, A.H. Goodall. *Structural characteristics of PPARγ with bound 12- and 15-HETE.*

Abbreviations

7-AAD	7-aminoactinomycin D
12-LOX	12-lipoxygenase
15d-PGJ2	15-deoxy-$\Delta^{12,14}$-prostaglandinJ2
AA	Arachidonic acid
AAA	Abdominal aortic aneurysm
ACD	Acid citrate dextrose
ADAM	A disintegrin and metalloproteinase
ADH	Alcohol dehydrogenase
ADP	Adenosine di-phosphate
AMV-RT	Avian myeloblastoma virus reverse transcriptase
ANO6/TMEM16f	Anoctamin 6
ANRIL	Antisense non-coding RNA in the INK4 locus
APC	Activated protein C
APS	Ammonium persulphate
ASA	Aspirin / acetyl salicylic acid
AT	Anti-thrombin
ATCC	American tissue culture collection
ATP	Adenosine tri-phosphate
ATTC	Antithrombotic Trialists' Collaboration
AUC	Area under the curve
B-Gal	β-galactosidase
B2M	β2-microglobulin
BCA	Bicinchoninic acid
BHT	Butylated hydroxytoluene
BSA	Bovine serum albumin
C/EBPβ	CCAAT/enhancer binding protein β
CAD	Coronary artery disease
CalDAP-GEFI	Calcium and diacylglycerol-regulated guanidine nucleotide exchange factor
CCD	Charge-couple device
CCL(♯)	C-C (chemokine motif) ligand (number)
CCP4	Collaborative Computational Project number 4

CD	Cluster of differentiation
CoAPB	Acyl CoA binding protein
COX	Cyclooxygenase
CRP-XL	Cross-linked collagen related peptide
C_T	Cycle threshold
CVD	Cardiovascular disease
CXCL	C-X-C motif ligand
Cys (C)	Cysteine
DAG	Diacyl glycerol
DBD	DNA-binding domain
DHET	Dihydroxyeicosatrienoic acid
DMEM	Dulbecco's modified eagles media
DMSO	Dimethyl sulphoxide
DNA	Deoxyribose nucleic acid
dNTP	Deoxynucleotide triphosphate
DPBS	Dulbecco's phosphate buffered saline
DR	Direct repeat
DTS	Dense tubular system
DTT	Dithiothreitol
DU	Densitometry units
DVT	Deep vein thrombosis
E	Glutamic acid
EC's	Endothelial cells
EDTA	Ethylenediaminetetraacetic acid
EET	Epoxyeicosaenoic acid
ELISA	Enzyme-linked immunosorbent assay
EPCR/*procr*	Endothelial protein C receptor (protein / *gene*)
ER	Endoplasmic reticulum
ESI	Electrospray ionisation
F(x)	Factor (coagulation)
FAc	Formic acid
FA	Final aggregation
FCS	Foetal calf serum
FDA	Food and drug administration

FDR	False discovery rate
FITC	Fluorescein isothiocyanate
FLAP	5-lipoxygenase activating protein
FRET	Fluorescence resonance energy transfer
FSc	Forward scatter
FS	Formyl saline
FT-ICR	Fourier transform-ion cyclotron resistance
GAGs	Glycosaminoglycans
GLA	Gamma carboxyglutamic acid
GO	Gene ontology
GP(x)	Glycoprotein
GPCR	G-protein coupled receptor
GPI	Glycosylphosphatidylinositol
GPO	Glycine – Proline – Hydroxyproline
GWE	Genome wide expression
H-bond	Hydrogen bond
HA	Heparin agarose
HAT	Histone acetyl transferase
HBS	HEPES-buffered saline
HBSS	Hanks balanced salt solution
HDAC	Histone deacetylase
HDHA	Hydroxydocosahexaenoic acid
HDL	High-density lipoproteins
HEPE	Hydroxyeicosapentaenoic acid
HESI II	High-energy electrospray ionisation source
HETE	Hydroxyeicosatetraenoic acid
HF	Heart failure
HHT	Hydroxyheptadecatrienoic acid
His (H)	Histadine
HODE	Hydroxyoctadecadienoic acid
HPLC	High performance liquid chromatography
HRP	Horseradish peroxidase
Hx	Helix
IAA	Iodoacetic acid

IFNγ	Interferon γ
Ig	Immunoglobulin
IL	Interleukin
IP3	Inositol triphosphate
IPI	International protein identifier
IPTG	Isopropyl β-D -1-thiogalactopyranoside
IR	Isomorphous replacement
IT	Ion trap
ITAM	Immune tyrosine activation motif
JAM-C	Junctional adhesion molecule C
K	Lysine
KO	Knockout
KPI	Kunitz-like protease inhibitor domain
L	Leucine
LA	Linoleic acid
LAT	Linker for activation of T-cells
LBD	Ligand-binding domain
LC-MS/MS	Liquid chromatography tandem mass spectrometry
LDL	Low-density lipoprotein
LPS	Lipopolysaccharide
M-CSF	Macrophage-colony stimulating factor
MHC-1	Major histocompatibility complex 1
M-SFM	Macrophage-serum free media
MAC-1	Macrophage-1 antigen
MAD	Multiwavelength anomalous dispersion
MALDI	Matrix assisted laser desorption ionisation
MCP-1	Monocyte chemotractant protein 1
Md X	Median fluorescence
MI	Myocardial infarction
miRNA	MicroRNA
MMP	Matrix metalloproteinase
MPA	Monocyte platelet aggregate
MPC	Magnetic particle concentrator
MPs	Microparticles

MR	Molecular replacement
mRNA	MessengerRNA
MS	Mass spectrometry
Munc18	Mammalian uncoordinated 18
MVs	Microvesicles
MW	Molecular weight
MWCO	Molecular weight cut off
NADPH	Nicotinamide adenine dinucleotide phosphate
N-CoR1	Nuclear co-repressor receptor 1
NF-κB	Nuclear factor kappa B
NMR	Nuclear magnetic resonance
NR	Nuclear receptor
NRF2	Nuclear factor like-2
NR-LBD	Nuclear receptor ligand-binding domain
NS	Not significant
NSAIDs	Non-steroidal anti-inflammatory drugs
OD	Optical density
ONPG	Ortho-Nitrophenyl-b-galactoside
oxLDL	Oxidised low density lipoprotein
oxoDHA	Oxodocosahexaenoic acid
oxoETE	Oxidised eicosatetraenoic acid
oxoOTE	Oxooctadecatrienoic acid
PAD	Peripheral artery disease
PAGE	Polyacrylamide gel electrophoresis
PAI-1	Plasminogen activator inhibitor 1
PAR	Protease activated receptor
PBMCs	Peripheral blood mononuclear cells
PBP	Platelet basic protein
PBS	Phosphate buffered saline
PC	Protein C
PCR	Polymerase chain reaction
PDI	Protein disulphide isomerase
PDB	Protein data bank
PE	Phycoerythrin

PEI	Polyethenimin
Pen/Strep	Penicillin / streptomycin
PF4	Platelet factor 4
PF4v	Platelet factor 4 varient
PG(x)	Prostaglandin
PGC1α	PPARγ Co-activator 1α
PI	Phosphatidylinositol
PI3K	Phosphoinositol-3 kinase
PKC	Protein kinase C
PLCγ2	Phospholipase C γ2
PLA2α	Phospholipase A 2α
PI-PLC	Phosphatidylinositol-phospholipase C
PMA	Phorbol-myristate-acetate
PMT	Photomultiplier tube
PPARγ	Peroxisome proliferator-activating receptor gamma
PPI	Peptidyl prolyl isomerase
PPM	Parts per million
PPP	Platelet poor plasma
PPRE	Peroxisome proliferator response element
PRP	Platelet rich plasma
PrS	Protein S
PS	Phosphatidylserine
PSGL-1	P-selectin glycoprotein ligand 1
PTFE	Polytetrafluoroethylene
PVC	Polyvinylchloride
PVDF	Polyvinylidene fluoride
Q	Glutamine
QC	Quality control
R	Arganine
RANTES (CCL5)	Regulated on activation, normal T-cell expressed and secreted
RER	Rough endoplasmic reticulum
rhTFPI	recombinant human tissue factor pathway inhibitor
RISC	RNA-induced silencing complex
RT	Reverse transcription

RT-qPCR	Real time polymerase chain reaction
RXR	Retinoid X receptor
SDS	Sodium dodecylsulphate
SDS-PAGE	SDS-polyacrylamide gel elctrophoresis
SEM	Standard error of the mean
sEPCR	Soluble endothelial protein C receptor
Ser (S)	Serine
SH2	Src homology 2
SLS	Swiss lightsource
SMC	Smooth muscle cell
SMRT	Silencing mediator for retinoid and thyroid hormone receptor
SNAP-23	Synaptosomal-activated protein 23
SNP	Single nucleotide polymorphism
SOCE	Store operated calcium entry
SRC-1	Steroid receptor co-activator 1
SREBP	Sterol regulatory element binding protein
SS	Side scatter
STEMI	ST-elevated myocardial infarction
STIM1	Stromal interaction molecule 1
Syk	Spleen tyrosine kinase
T007	T0070907
TAE	Tris–acetate–EDTA
TBP	TATA-binding protein
TBS	Tris-buffered saline
TBS/T	Tris-buffered saline with Tween
TCEP	Tris(2-carboxyethyl)phosphine
TEMED	Tetramethylethylenediamine
TEV	Nuclear Inclusion A protein (TEV protease) encoded by the tobacco etch virus
TF	Tissue factor
TFPI/*tfpi*	Tissue factor pathway inhibitor (protein/*gene*)
TGF-β	Transforming growth factor β
TGS	Tris–Glycine–SDS
TK-Luc	TK-luciferase plasmid

TNFα	Tumour necrosis factor alpha
ToF	Time of flight
TREM-1	Triggering receptor expressed on myeloid cells 1
TxA2	Thromboxane A2
TxB2	Thromboxane B2
Tyr (Y)	Tyrosine
V	Valine
VCAM-1	Vascular cell adhesion molecule 1
vWf	von Willebrand factor
WR	Working reagent

Chapter 1: Introduction

1.1 Cardiovascular disease (CVD)

Cardiovascular disease (CVD) is a term used to cover a number of pathological processes involving the cardiac muscle and blood vessels. It is currently the leading cause of death in the developed world and the prevalence is only set to increase with the growing incidence of diabetes and obesity. CVD is more commonly associated with pathologies affecting the heart such as angina, myocardial infarction (MI), coronary artery disease (CAD) and heart failure (HF), but stroke, peripheral artery disease (PAD), deep vein thrombosis (DVT) and abdominal aortic aneurysm (AAA) are also included. The majority of diseases encompassed by CVD result as a consequence of atherosclerosis and can be considered as a manifestation of this. Diseases not associated with atherosclerosis are often congenital and cover structural modifications of the heart such as bicuspid aortic valve disease. Whilst all of these are important areas, this project will mainly focus on CAD.

1.2 Risk factors for CAD

CAD is a disease of the arteries supplying oxygen to the heart. The primary cause of CAD is atherosclerosis, which can narrow the lumen of the artery and cause angina. Atherosclerosis is the build up of fatty deposits and necrotic cells in the tunica intima that forms a characteristic atherosclerotic plaque. The ultimate consequence of atherosclerosis is plaque rupture that leads to formation of a thrombus. This can completely occlude an artery, leading to ischemia, MI and, in the worst case, death (Hansson, 2005).

Although atherosclerosis is a major contributor to CAD, it can be considered a consequence of aging rather than a disease, as the process is thought to begin at adolescence (Strong et al., 1999). The rate of progression, however, can be largely influenced through genetics and environment / lifestyle.

Risk of CAD is increased if there is a family history and if previous generations have had an MI below the age of 50. Whilst this is probably multifactorial, a number of inherited diseases can contribute to atherosclerosis. An example of this is familial hypercholesterolemia, an inherited disease resulting in higher levels of cholesterol, specifically low-density lipoprotein (LDL), in the circulation resulting from mutations in the LDL receptor (Goldstein and Brown, 1985; Goldstein et al., 1983). Cholesterol and LDL are known to be important in the progression of atherosclerosis. There are also

a number of single nucleotide polymorphisms (SNPs) associated with CAD, the most prominent being the chromosome 9p21 locus, which encodes, among genes, the antisense non-coding RNA in the INK4 locus (*ANRIL*) (McPherson et al., 2007; Pasmant et al., 2007; Samani et al., 2007).

Environment and lifestyle represent a category of modifiable factors that increase the risk of CAD. These include smoking (Howard et al., 1998), diet, inactivity (Kadoglou et al., 2008) and excessive alcohol consumption (Kiechl et al., 1998) that manifest as high blood cholesterol, high blood pressure, obesity and diabetes. All of these can speed up the development of atherosclerosis or increase plaque instability, rupture and thrombus formation.

Taken together, there are a number of factors that increase a person's risk of CAD that may include a combination of non-modifiable and modifiable risk factors.

1.3 Atherosclerosis

Atherosclerosis is found mainly at arterial branch points and areas of disturbed laminar flow (GLAGOV et al., 1988; Zand et al., 1999) and results from the build up of necrotic cells and fatty deposits in the tunica intima.

The process begins with an influx of LDL through leaky endothelial cells (EC's) and its oxidation (oxLDL) by molecules released from EC's and smooth muscle cells (SMC's) (Moore and Tabas, 2011). oxLDL upregulates adhesion molecules such as vascular cell adhesion molecule-1 (VCAM-1) and P-selectin on EC's, as well as the release of monocyte chemotractants (GEBUHRER et al., 1995; Moore and Tabas, 2011; ROSS, 1993). P-selectin on EC's binds to P-selectin glycoprotein ligand 1 (PSGL-1) on monocytes; promoting rolling across the endothelium and monocyte arrest (Huo and Ley, 2001; Weyrich et al., 1995). Chemokines and cytokines released from endothelial cells also promote the activation of surface integrins such as α4β1. The importance of α4β1 is demonstrated by a significant reduction in monocyte attachment after neutralisation (Ramos et al., 1999). Chemokines are also important for firm adhesion, as shown in monocyte chemotactic protein-1 (MCP-1) deficient mice that have reduced monocyte content in lesions (Braunersreuther et al., 2008; 2007; Combadiere et al., 2008).

Monocytes extravate into the tunica intima and differentiate into macrophages. The phenotype of a differentiated macrophage is dependent on factors present in the local environment; in atherosclerotic regions the main phenotypes are M1 and M2 although

others have been described. M1 macrophages are predominantly phagocytes and, in atherosclerosis, engulf oxLDL, eventually forming foam cells. This process was thought to be mediated by the scavenger receptors SRA and cluster of differentiation (CD) 36 (Kunjathoor et al., 2002) but more recent studies using a double knockout (KO) mouse strain showed no decrease in foam cell formation (Manning-Tobin et al., 2009). Ingested oxLDL undergoes hydrolysis of cholesterol esters to cholesterol, which is either trafficked to the cell membrane and removed or re-esterified to cholesterol fatty acid esters (Brown et al., 1980). These new cholesterol esters form the characteristic lipid droplets in macrophages that eventually give rise to foam cells (BERLINER et al., 1995; Brown et al., 1980; Maxfield and Tabas, 2005). Cholesterol laden macrophages undergo apoptosis initiated through stress responses, reactive oxygen species and nutrient deprivation. Apoptotic macrophages are cleared in a process known as efferocytosis, however, inefficient clearance leads to necrosis. The build up of necrotic cells leads to formation of a necrotic core, characteristic of an advanced atherosclerotic lesion (Tabas, 2010a; 2010b) (figure 1.1).

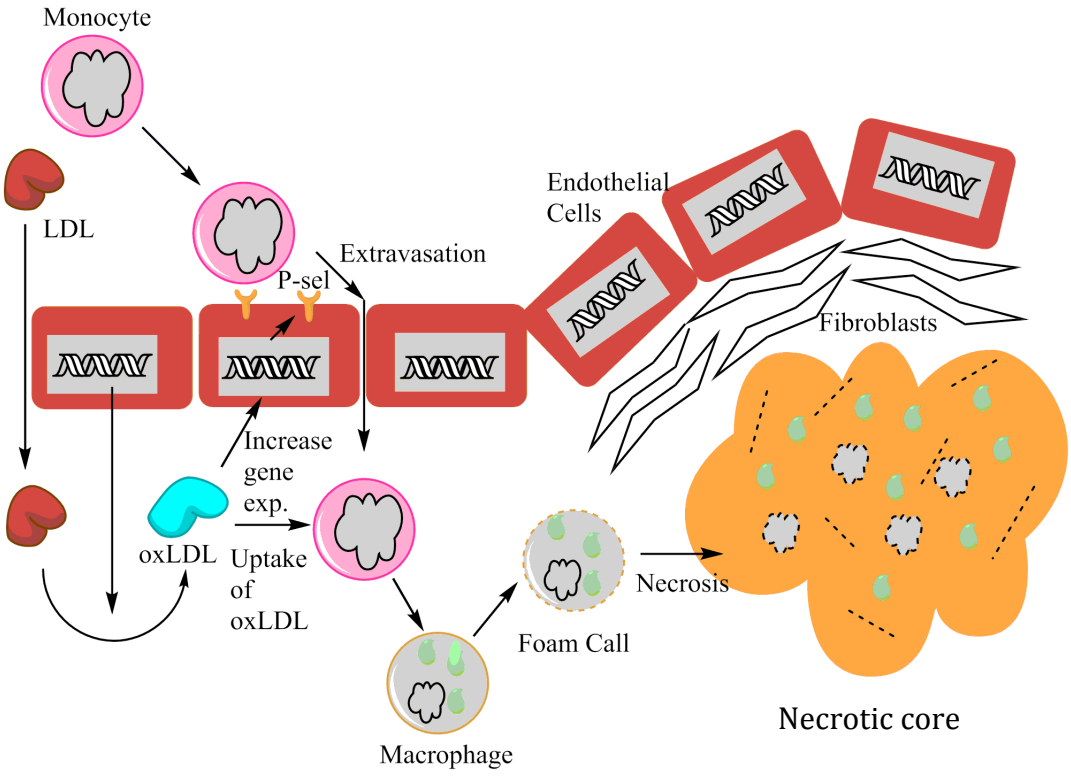

Figure 1.1: Model of atherosclerosis

Diagram depicting the mechanism of atherosclerosis, beginning with the upregulation of adhesion molecules by oxLDL, extravasation of monocytes into the intima and differentiation into foam cells. The latter stages show foam cell necrosis leading to the development of a necrotic core, commonly referred to as an atheroma.

Progression of stable plaques to unstable plaques occurs when the fibrous cap collagen, formed from fibroblast-like SMC's, starts to thin. This can result from increased SMC death induced by macrophage-derived pro-apoptotic molecules activating the Fas pathway (Boyle et al., 2003) or through direct degradation by matrix metalloproteinases (MMPs), specifically MMP-2 and MMP-9 (GALIS et al., 1994; Gough et al., 2006).

Continual growth of the necrotic core, death of SMC's and degradation of the fibrous cap all contribute to the instability of the atherosclerotic plaque, which may eventually rupture and lead to thrombosis. Thrombosis is the pathological term given to the process of haemostasis and can result in vessel occlusion, ischemia and tissue death.

1.4 Haemostasis and thrombosis

Haemostasis and thrombosis are used interchangeably to describe the process of clot formation at sites of vascular damage; haemostasis is used to describe the normal response to vascular injury whereas thrombosis usually refers to clot formation in response to abnormal pathologies such as atherosclerotic plaque rupture creating a hypercoagulatory environment. In simple terms, clots form at sites where blood can exit the vasculature into tissues and organs. It is a process that results in the transformation of fluid blood into a gel-like substance that seals the damaged area. The factors that contribute to haemostasis and thrombosis have historically been divided into the broad categories of stasis (of blood), endothelial injury and hypercoagulability, referred to as Virchow's triad.

Normal haemostasis occurs in response to endothelial damage, where molecules such as von Willebrand factor (vWf) and collagen become exposed, recruiting and activating platelets to form a platelet plug. In addition, exposed tissue factor (TF) interacts with coagulation factors present as zymogens in the blood, resulting in their activation and a downstream cascade leading to the cleavage of pro-thrombin to thrombin and fibrinogen to fibrin (section 1.11). Fibrin polymerises and forms a large protein meshwork holding the thrombus together. Activated platelets also recruit leukocytes into the thrombus through specific interactions with surface receptors. Cross-talk between cells enables regulation of thrombus growth and stability. Rupture of an atheroma results in thrombosis and is dependent on a number of factors including plaque stability, foam cell and SMC content (Davies, 1996). When thrombosis occurs as a result of atherosclerotic plaque rupture, growth is more likely to become dis-regulated and arterial occlusion may result, leading to MI or stroke.

Treatment of this disease through drugs has been most beneficial in the secondary prevention of MI, with the use of the cyclooxygenase (COX) inhibitor aspirin (acetylsalicylic acid; ASA) (Hennekens et al., 1989), the most commonly used antiplatelet agent, adenosine diphosphate (ADP) receptor antagonists such as clopidogrel and prasugrel (Jakubowski et al., 2012; Tran et al., 2006) and cholesterol lowering drugs such as pravastatin (Tonin et al., 1998). However, treatment for primary MI's has not had the same success. This is mainly due to the difficulty in predicting a person's predisposition to a primary event (Antithrombotic Trialists' (ATT) Collaboration et al., 2009; "Collaborative overview of randomised trials of antiplatelet therapy Prevention of death, myocardial infarction, and stroke by prolonged antiplatelet therapy in various categories of patients," 1994).

1.5 Role of platelets in haemostasis and thrombosis

Platelets are essential to thrombus formation as well as a number of other processes including immune function and cancer metastasis. They are anucleate cells produced by megakaryocytes in the bone marrow and released into the circulation at a rate of ~10^{11}/day (Harker, 1977). Platelets circulate for around 10 days before they are cleared by spleen macrophages or the liver (Italiano et al., 1999; Trowbridge et al., 1984). Although anucleate, platelets do contain messengerRNA (mRNA) and the machinery needed for translation (Denis et al., 2005) along with microRNA (miRNA) (Landry et al., 2009) and proteins. In addition to mitochondria and endoplasmic reticulum (ER), platelets also contain specialised granules; ~80 α-granules (Blair and Flaumenhaft, 2009), 5 dense granules (McNicol and Israels, 1999) and lysosomes (Bentfeld-Barker and BAINTON, 1982) that release their contents upon activation. The role of platelets in haemostasis and thrombosis can be loosely divided into 3 phases: initiation (adhesion), activation and aggregation.

1.5.1 Adhesion

If vascular damage has occurred, platelets bind to the vessel wall through a number of interactions dependent on the shear conditions. The shear stress of a vessel is dependent on the diameter, with arterioles and microvasculature having high shear stress, arteries having lower shear stress and veins the least. Vascular damage results in the removal of anti-thrombotic endothelial cells and the exposure of molecules able to bind to platelets. It is recognised that the two major molecules in platelet adhesion are collagen and vWf (Cosemans et al., 2013).

vWf is found in plasma, endothelial weibal palade bodies and platelets in the form of high molecular weight multimers (Clemetson, 2012). In the plasma, these multimers are unable to bind platelets, however at sites of vascular damage, vWf, either already bound to collagen or from the circulation, is stretched as a result of the high shear stress. Stretching makes the A1 domain accessible (Schneider et al., 2007) to the platelet receptor complex glycoprotein (GP) Ib-V-IX (Savage et al., 1996) (figure 1.2).

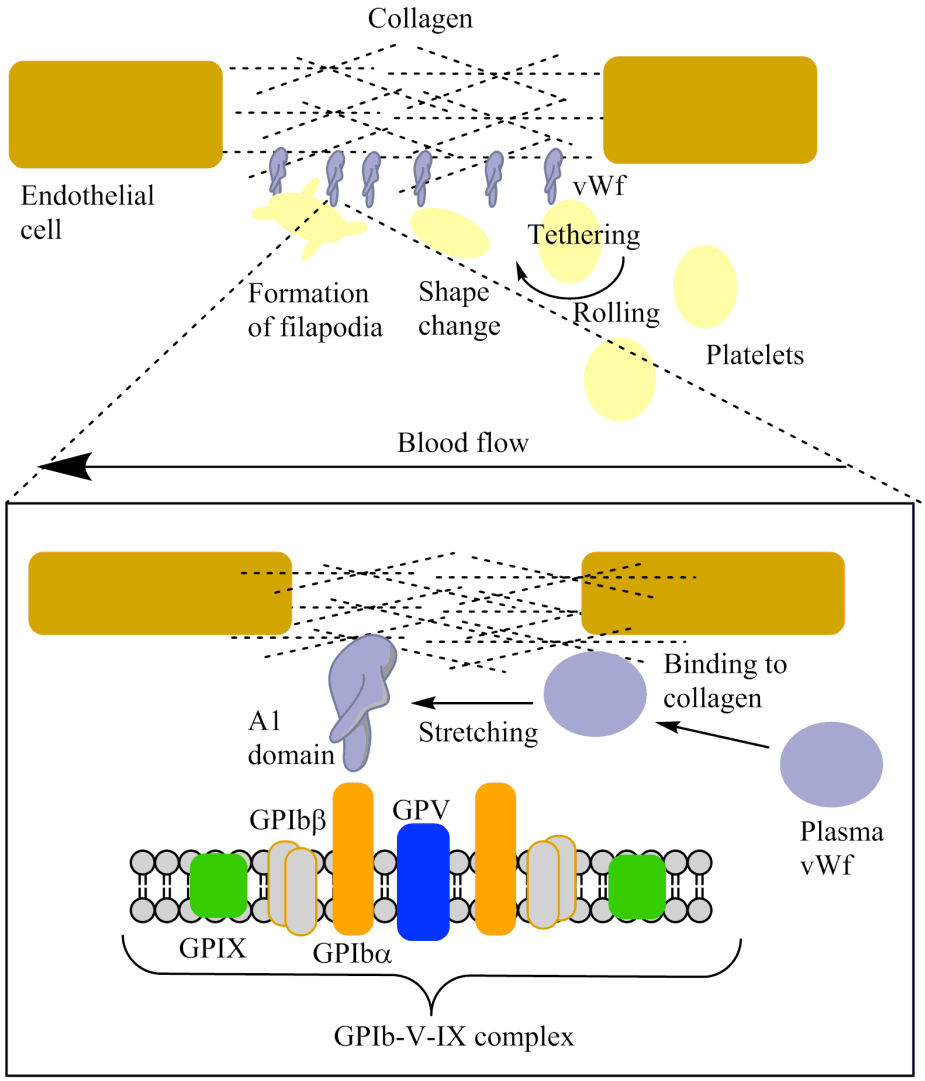

Figure 1.2: Platelet adhesion to vWf and the GPIb-V-IX complex

Diagram showing the adhesion of platelets to vWf bound to exposed collagen. Binding of vWf to platelets is transient and promotes platelet rolling, shape change and eventually filapodia formation. Binding of vWf to platelets is mediated through the GPIb-V-IX complex and specifically the A1 domain of vWf and the GPIbα protein.

The GPIb complex is made up of GPIbα and GPIbβ that are covalently linked, and GPV and GPIX that are associated non-covalently with the stoichiometry 2:4:1:2 respectively (S.-Z. Luo et al., 2007). vWf causes the clustering of GPIb complexes and, along with

the tethering of GPIb to filamin, results in the formation of an elongated tether (Dopheide et al., 2002; Kasirer-Friede et al., 2002; Williamson et al., 2002). This tether is usually transient due to the high on / off rate of the vWf•GPIb complex but is sufficient to slow the rolling platelets and allow for more stable attachment (Cosemans et al., 2013).

The higher order of vWf multimer the more haemostatically efficient for tethering, either because the multimer is larger when stretched at equivalent shear stress or increased binding sites for the GPIb complexes (Clemetson, 2012). Whilst the vWf•GPIb interaction is important for attachment of platelets, outside-in signalling through this complex is minimal, although reports have suggested some Ca^{2+} signalling, ADP release and integrin activation can occur, which may account for the absence of bleeding phenotype in patients that lack other receptors (Yap et al., 2000). This could be explained by the ability of the GPIb complex to interact with other signalling proteins such as GPVI in lipid rafts (López et al., 2005). Mice lacking the GPIb complex fail to form arterial thrombi (Bergmeier et al., 2006) and the human bleeding disorder Bernard Soulier syndrome is associated with lack of functional GPIb-V-IX (López et al., 1998).

The second major interaction mediating platelet attachment is collagen, which is recognised by two platelet receptors; the GPVI signalling receptor and the integrin α2β1. GPVI recognises the sequence glycine-proline-hydroxyproline (GPO) present in collagens with triple helical structure (Knight et al., 1999). GPVI is co-expressed, and forms a complex with, the FCR-γ chain. This interaction is important as signalling occurs through the immunoreceptor tyrosine-based activation motif (ITAM) present within FCR-γ. Signalling through GPVI results in platelet activation. Further stable adhesion is mediated through integrins such as α2β1, α5β1, α6β1, αIIbβ3 and αVβ3 that, once activated, bind, respectively, primarily to collagen, fibronectin, laminin, fibrinogen and vitronectin to mediate stable adhesion.

1.5.2 Activation

Platelet activation is mediated through overlapping intracellular pathways that ultimately result in the activation of integrins through inside-out signalling, and to granule secretion. The major activation pathway of platelets *in vivo* is through GPVI and the signalosome. Upon binding of collagen, GPVI is cross-linked and the constitutively associated Src kinases phosphorylate tyrosine residues within the ITAM (Ezumi et al., 1998; Gibbins et al., 1997). This leads to the formation of the

signalosome consisting of Src homology 2 (SH2) domain containing proteins such as spleen tyrosine kinase (Syk) (Gibbins et al., 1996). Syk phosphorylates linker for activation of T-cells (LAT), which activates phosphoinositol-3 kinase (PI3K) and phospholipase Cγ2 (PLCγ2) (Pasquet et al., 1999). PI3K phosphorylates phosphatidylinositol (PI) 4,5-bisphosphate to PI 3,4,5-trisphosphate (PIP3), which recuits PLCγ2 to the membrane. PLCγ2 cleaves PIP2 to diacyl glycerol (DAG) and inositol trisphosphate (IP3) (S. P. Watson et al., 2005) (figure 1.3).

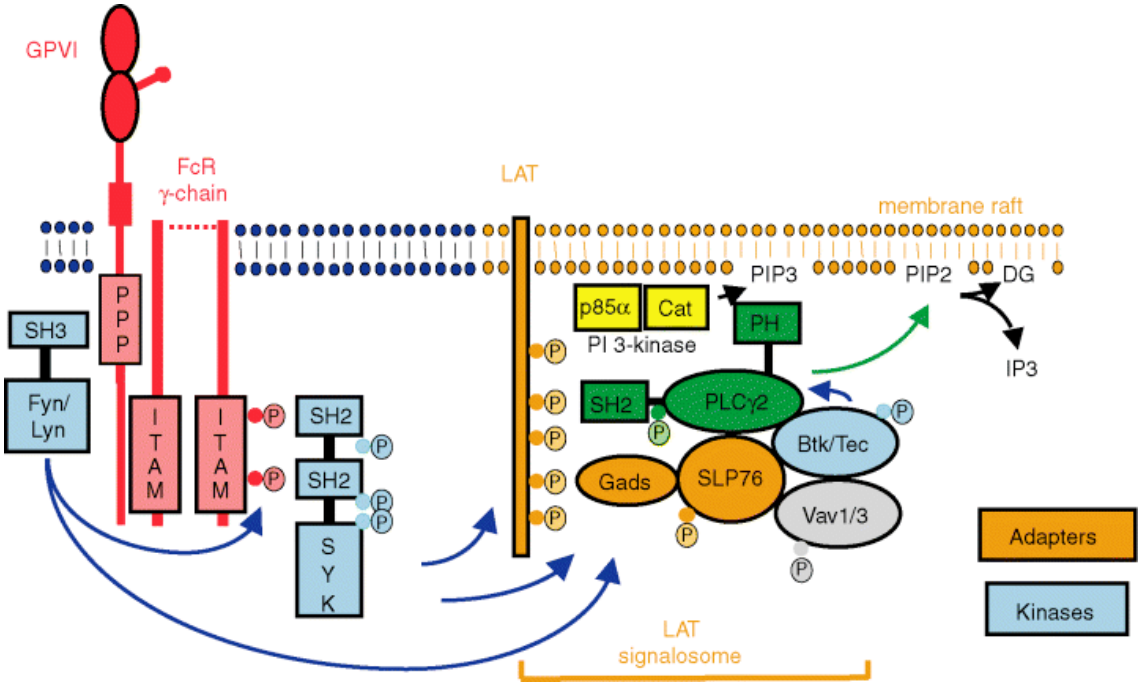

Figure 1.3: Signalling through GPVI

Activation of GPVI by collagen results in phosphorylation of the associated ITAM by Srk tyrosine kinases leading to the recruitment of Syk through its SH2 domains. Syk is activated and phosphorylates LAT leading the formation of the signalosome and eventually the cleavage of PIP3 to DAG and IP3. Figure from S. P. Watson et al., 2005.

IP3 binds to calcium channels in the dense tubular system (DTS) and promotes a rise in intracellular calcium levels (Berridge et al., 2003) whilst DAG is an activator of protein kinase C (PKC) (Harper and Poole, 2010). The depletion of calcium from internal stores is sensed by stromal interaction molecule 1 (STIM1) (Roos et al., 2005) that opens the calcium channel ORAI1 (Feske et al., 2006) at the plasma membrane resulting in store-operated calcium entry (SOCE) (Gilio et al., 2010; Soboloff et al., 2006). SOCE has been shown to be important in the procoagulant but not proadhesive actions of platelets (Ahmad et al., 2011).

Integrin activation is mediated by both the increase in intracellular calcium and PKC activation. Calcium transiently activates integrins through activation of Ca^{2+} and DAG-regulated guanidine nucleotide exchange factor (CalDAP-GEFI), which activates Rap1b. Rap1b is able to regulate integrin activation through cytosolic rearrangements. Sustained Rap1b activation is dependent on the PKC mediated ADP release (Stegner and Nieswandt, 2011). The activation of integrins is through conformational changes; from a low affinity to high affinity ligand binding state (B.-H. Luo et al., 2007; Takagi et al., 2002). Through binding of ligands, integrins mediate outside-in signalling leading to further reorganisation of the cytoskeleton, resulting in cell spreading and clot retraction (Stegner and Nieswandt, 2011).

Platelet activation also results in degranulation; a process requiring PKC-dependent phosphorylation of a number of proteins involved in vesicle fusion such as synaptosomal-activated protein 23 (SNAP23) (Polgar et al., 2003), mammalian uncoordinated-18 (Munc18) (Barclay et al., 2003) and syntaxins (Chung et al., 2000). Granule secretion itself plays a role in platelet activation and thrombus progression. The small molecule ADP, released from dense granules, binds to the G-protein coupled receptors (GPCRs) P2Y1 and P2Y12 (Offermans, n.d.) and has a role in maintaining activation induced by primary agonists, integrin activation and in microparticle (MP) release (Cifuni et al., 2008).

The resultant rise in intracellular Ca^{2+} from GPVI signalling further promotes the formation and/or release of additional platelet responses. For example, calcium binds to and activates the membrane scramblase, anoctamin 6 (ANO6/TMEM16F), that translocates negatively charged phospholipids to the outer membrane providing a procoagulant surface for thrombin production, a potent platelet agonist (Lhermusier et al., 2011; Yang et al., 2012). Calcium also activates phospholipase A2α (PLA2α) that cleaves arachidonic acid (AA) from the membrane and results in thromboxane A2 (TxA2) production, a short-lived platelet agonist described as an amplifying signal for other agonists (FitzGerald, 1991) (figure 1.4).

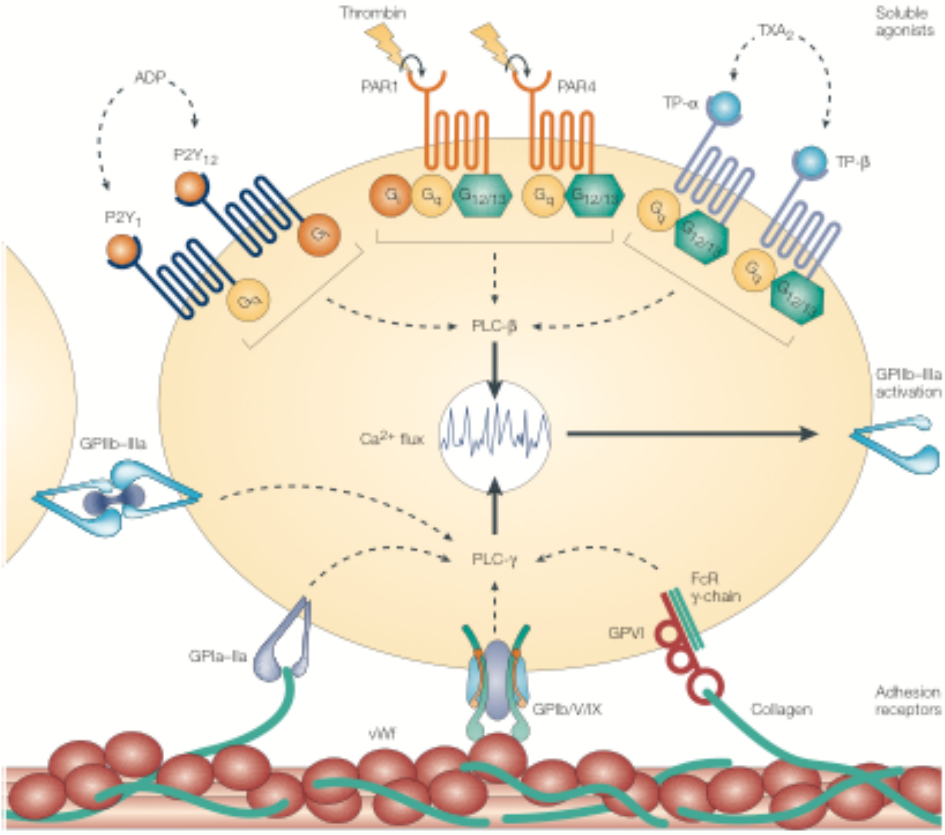

Figure 1.4: Major agonists and interactions leading to platelet activation

Major pathways of platelet activation through GPCRs, integrins and ITAMs. Figure from S. P. Jackson and Schoenwaelder, 2003.

1.5.3 Aggregation

After a platelet monolayer has formed at the site of injury, additional platelets are recruited to form the platelet aggregate. This process is, in the majority, mediated by integrin αIIbβ3. Inside-out signalling activates this integrin and when in its high affinity state is able to bind fibrinogen either present in the plasma or released from platelets. Fibrinogen is a bivalent ligand and can bind two αIIbβ3 molecules on different platelets. The large number of integrin molecules on each platelet (50000-80000) means one platelet can form bridges with many other platelets leading to the formation of large aggregates (Lefkovits et al., 1995). The aggregate is then stabilised further through multiple receptor ligand complexes between the platelets such as ephrins and eph kinases; semaphorin 4D to CD72/Plexin B; and Gas6 with Axl/Tyro3/Mer tyrosine kinase receptors which all act to increase the stability of the platelet aggregate (Ruggeri, 2002).

1.6 The platelet 'secretome'

Upon activation platelets release a number of molecules into the extracellular medium. These can be derived from granules (α, dense and lysosomes), shed from the membrane or derived from AA metabolism. Platelets are also able to release microvesicles (MVs) of different sizes termed exosomes and microparticles (MPs) (figure 1.5).

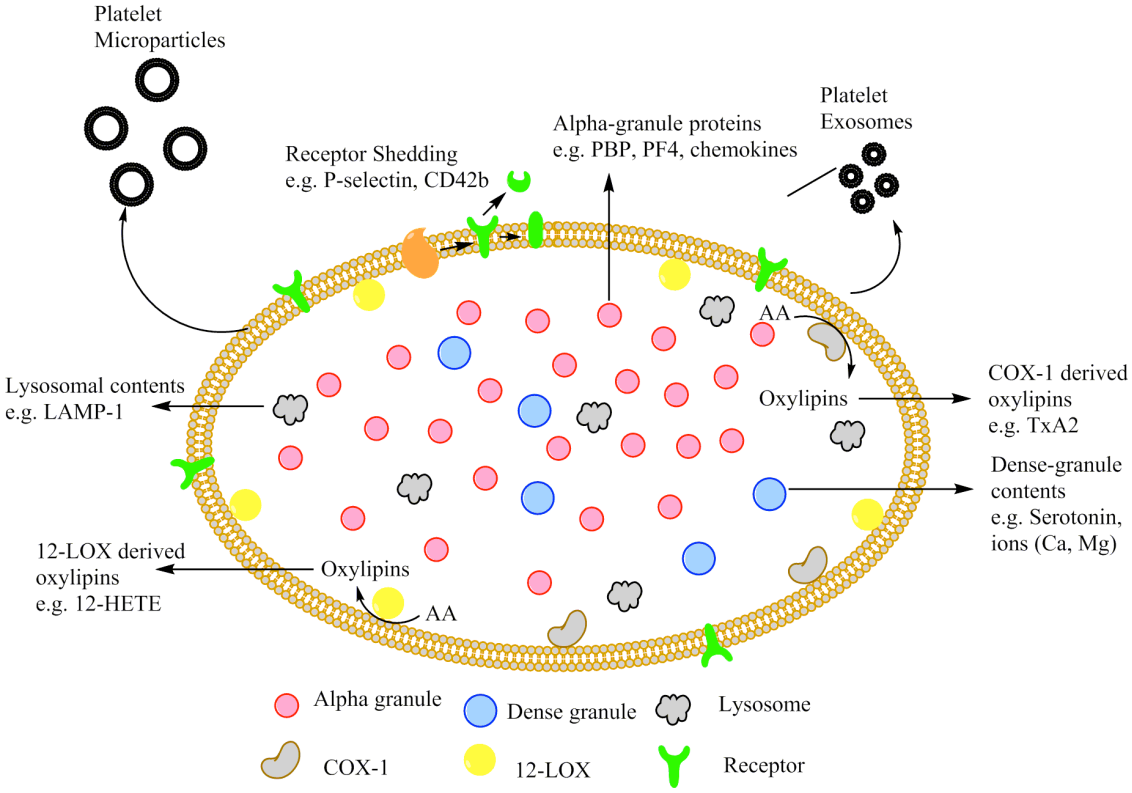

Figure 1.5: Sources of molecules comprising the platelet secretome

Activation of platelets leads to the release of a number of molecules such as proteins and oxylipins as well as MVs. The sources of some of these are shown above.

Proteins released from platelets by different agonists have largely been identified by mass spectrometry (MS) (Coppinger et al., 2004; Corte et al., 2008; Piersma et al., 2009) and some studies show the profile is dependent on the type of agonist used (Coppinger et al., 2007; Jonnalagadda et al., 2012). Currently, it is estimated that activated platelets release more than 1000 proteins including 69 potential shed proteins (sometimes referred to as the 'sheddome'). Protein shedding is thought to occur by disintegrin and metalloproteinase (ADAM) proteins and includes release of fragments of sema7a, GPIbα, GPVI and P-selectin (Fong et al., 2011). Proteins derived from α-granules include a number of cytokines and chemokines, e.g. C-X-C motif ligand (CXCL) 4, C-C motif ligand (CCL) 5, which are involved in chemotactic responses, as

well as proteins involved in thrombus formation, e.g. fibrinogen and vWf, and immune modulation, e.g. major histocompatibility complex 1 (MHC1) (Zufferey et al., 2014). There has been some evidence that α-granules are heterogeneous with regards to content that has led some researchers to stipulate that different populations may be released in response to different environmental signals (Italiano et al., 2008; Sehgal and Storrie, 2007). Lysosomes release hydrolases, e.g. cathepsin, that may play a role in platelet activation within a clot (Si-Tahar et al., 1996). Dense granules release small molecules into the extracellular medium. These include the nucleotides ADP and adenosine tri-phosphate (ATP), divalent cations Ca^{2+} and Mg^{2+} and serotonin and histamine (Rendu and Brohard-Bohn, 2001).

MVs released from platelets are a heterogeneous population that can be divided into exosomes, which are less than 200nm and MPs, which are between 200-1000nm. Exosomes mainly contain miRNA with some mRNA and proteins, specifically tetraspanins. MPs contain little miRNA, many proteins derived from the platelet cytoplasm and membrane (Yáñez-Mó et al., 2015a). Exosomes are thought to be derived from exocytosis of multi-vesicular bodies whereas microparticles are released from the plasma membrane (Heijnen et al., 1999). Once released, MVs can fuse with other cells to deliver their contents and regulate cell processes. The MV proteome consists of >550 proteins (Benjamin A Garcia et al., 2005) and includes integrins, chemokines and receptors. For example, peroxisome proliferator-activating receptor gamma (PPARγ) has been shown to be present in microparticles and could be transferred to other cell types to regulate gene transcription (Lannan et al., 2015; Ray et al., 2008).

AA and linoleic acid (LA)-derived oxylipins released from activated platelets have largely been identified by enzyme-linked immunosorbant assay (ELISA) and chromatography but recent advances in MS have allowed a more complete profile to be formed (Jarrar et al., 2013) (and our own data). TxA2 is well characterised and plays an important role in platelet activation (FitzGerald, 1991). Another well-measured oxylipin is 12-hydroxyeicosatetraenoic acid (12-HETE) whose roles include promoting cancer metastasis (Honn et al., 1994). Other identified oxylipins include 11- and 15-HETE (HENDERSON et al., 1992) and 12(S)-hydroxy-5-cis-8,10-trans-heptadecatrienoic acid (12-HHT) as well as some epoxyeicosatetraenoic acids (EETS) (Jarrar et al., 2013).

1.7 Arachidonic acid (AA) metabolism

AA is an important oxylipin released from the platelet plasma membrane after activation. The majority is metabolised by two enzymes, COX-1 and 12-lipoxygenase (12-LOX) that produce TxA2 and 12-HETE respectively as well as other minor metabolites. Whilst the role of TxA2 in platelet function is well known, the role of 12-HETE is controversial with reports suggesting both anti- and pro-thrombotic functions (Porro et al., 2014). As described in the previous section, AA release is mediated by the calcium-dependent activation of PLA2α (figure 1.6).

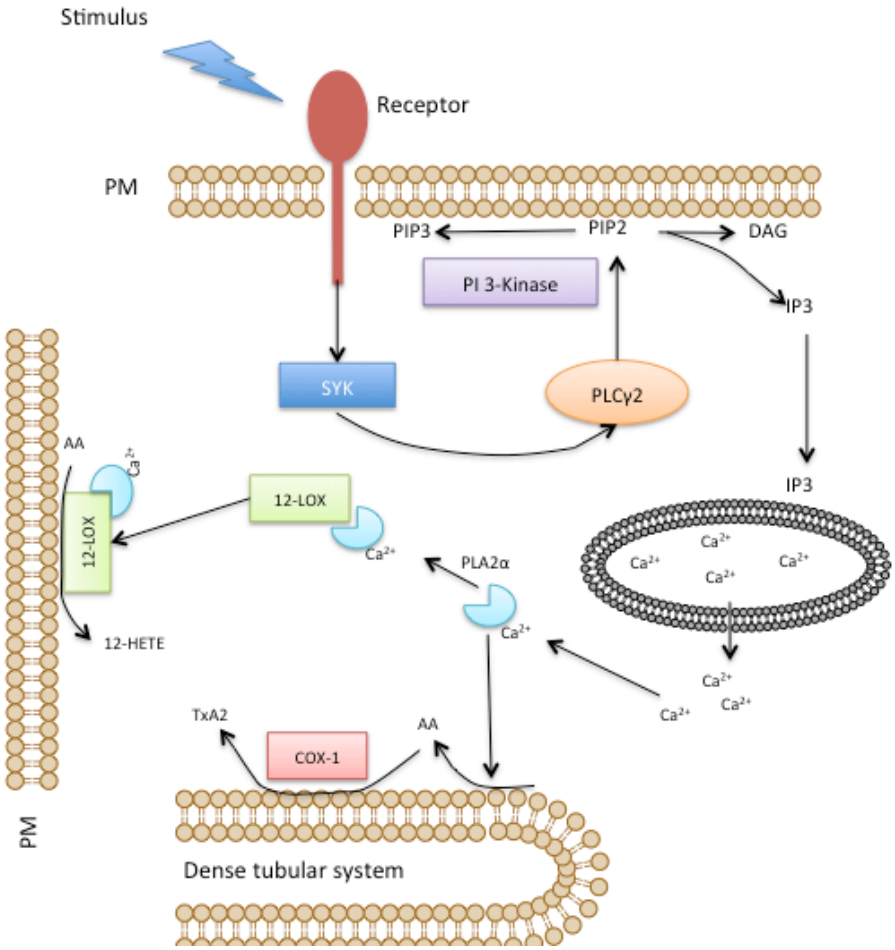

Figure 1.6: Mechanism of AA release from the platelet membrane

Representation of steps required for release of AA from the plasma membrane of platelets and its metabolism to 12-HETE and TxA2 by 12-LOX and COX-1 respectively.

Interestingly, inhibition of PI3K, which converts PIP2 to PIP3 for full activation of PKCγ2, abolishes oxylipin production from COX-1 but not from 12-LOX raising the hypothesis that 12-LOX may utilise an alternative pool of AA. This is supported by evidence showing that 12-HETE formation by 12-LOX continues after TxA2 formation

has peaked (Holinstat et al., 2011). The activity of both however, remains dependent on PLA2α, as null mutations prevent the activity of both COX-1 and 12-LOX (Adler et al., 2008).

12-LOX is a non-heme iron containing protein produced from the *alox12* gene on chromosome 17 (Kühn et al., 2014). It has 662 residues, ~75kDa, and forms an N-terminal β-barrel domain and large C-terminal catalytic domain where the non-heme iron is coordinated by conserved histidine (His) residues (Aleem et al., 2008). In resting platelets 12-LOX is found in the cytosol and translocates to the plasma membrane on activation; a process dependent on intracellular as well as extracellular Ca^{2+} (Baba et al., 1989; Coffey et al., 2004a). In the cytosol as well as at the membrane, 12-LOX is found associated with both cytosolic and secretory PLA2α isoforms (Coffey et al., 2004a). In their activated conformation, at the membrane, other LOX enzymes bind membrane-activating proteins (for example 5-LOX and 5-LOX activating protein (FLAP) (Dixon et al., 1990)) and whilst the same is thought to be true for 12-LOX, platelets do not contain FLAP and identification of a similar protein has remained elusive. Acquisition of the substrate at the membrane is currently unknown but theories include transfer of AA from an associated membrane protein (as in 5-LOX and FLAP (MANCINI et al., 1993)) or membrane insertion of the N-terminal β-barrel domain as is the case with lipases, whose β-barrel domain is homologous to lipoxygenase's (Gillmor et al., 1997). Once AA is acquired, the iron cofactor needs to be in its oxidised active form (Fe^{3+}), which enables reduction (Fe^{2+}) of AA and incorporation of oxygen. The free radical produced then oxidises Fe (Fe^{3+}) and the product is released (Andreou and Feussner, 2009; Ivanov et al., 2010).

Activity of 12-LOX in platelets can be inhibited with molecules such as esculetin and baicalein (Keizo and Hiromichi, 1982; Keizo et al., 1982). These have some off target effects (Y. Huang et al., 2005) and more specific inhibitors such as NCTT-956 have been developed recently (Kenyon et al., 2011; Luci et al., 2010). Blocking 12-LOX results in a number of anti-platelet effects such as inhibition of platelet aggregation, integrin activation, dense granule release and intracellular calcium mobilisation (Yeung et al., 2013; 2014). Whilst the role of 12-HETE in platelets is still hotly debated it is clear from these results that 12-LOX activity is fundamental for platelet activation. This discrepancy could be explained if 12-LOX has a product independent function in platelets. This could be possible, as roles of the other LOX enzymes have been

described, including membrane lipid peroxidation (Schewe et al., 1975), organelle degradation (van Leyen et al., 1998) and membrane pore formation.

COX-1, unlike 12-LOX, is a heme iron containing protein formed from the *pghs1* gene on chromosome 9 (FUNK et al., 1991). It has 576 residues, ~70kDa, that is divided into 3 domains, an N-terminal EGF domain, a membrane binding domain and a large C-terminal catalytic domain. COX-1 is continuously associated with the membrane through four amphipathic α-helices (Picot et al., 1994) and in platelets is associated with the DTS (Gerrard et al., 1976). The catalytic domain, in addition to the heme iron, also contains two spatially separated catalytic sites, cyclooxygenase and peroxidase (Garavito et al., 2002). COX-1 activity is dependent on the activation of PI3K and PLA2α activation for the liberation of AA from the membrane (Holinstat et al., 2011).

The COX-1 enzyme is first activated by a 2-electron reduction from a peroxide substrate, oxidising ferric heme to an oxo-ferryl porphyrin radical cation able to abstract an electron from tyrosine (Tyr) 385. In turn the Tyr385 radical abstracts hydrogen from carbon 13 of AA, initiating cyclooxygenase activity to form prostaglandin (PG) G2 and regenerate the Tyr385 radical. The unstable PGG2 is converted to PGH2 by the peroxidase activity (Smith and Song, 2002). It is this PGH2 that is metabolised by PG and thromboxane synthase enzymes to the corresponding PGs and TxA2.

The activity of COX-1 can be inhibited with non-steroidal anti-inflammatory drugs (NSAIDs) and aspirin by non-covalent and covalent mechanisms respectively. Aspirin is most commonly used to inhibit COX-1 in platelets in patients that have suffered an MI. The mechanism of action of aspirin was first documented in 1975 by Gerald Roth, who reported the transfer of an acetyl group to the active site (Roth and Majerus, 1975). Further evidence for irreversible inhibition came from studies correlating the 10% recovery of COX-1 activity with platelet turnover (Catella-Lawson et al., 2001). Inhibition of COX-1 by aspirin is through the acetylation of serine (Ser) 530 in the hydrophobic pocket. This modification blocks the entry and metabolism of AA (DeWitt et al., 1990; Roth and Majerus, 1975). NSAIDS, although non-covalent, work in a similar way to aspirin, blocking entry of AA through non-covalent contacts with residues (Díaz-González and Sánchez-Madrid, 2015; Vane and Botting, 1998).

1.8 Platelet-mediated recruitment of monocytes

Whilst platelets are the main constituent of thrombi other cells are also present. Some, such as erythrocytes, are non-specifically trapped in the fibrin network whilst others,

such as leukocytes can be recruited specifically through receptors. One of the key leukocytes recruited from the circulation are monocytes. These bind to platelets through an interaction between platelet P-selectin, which is translocated to the plasma membrane from α-granules upon activation (Stenberg et al., 1985), and monocyte PSGL-1. The interaction of P-selectin and PSGL-1 is paramount to supporting monocyte platelet aggregate formation (van Gils et al., 2009a), although other interactions also occur to stabilise this interaction (figure 1.7).

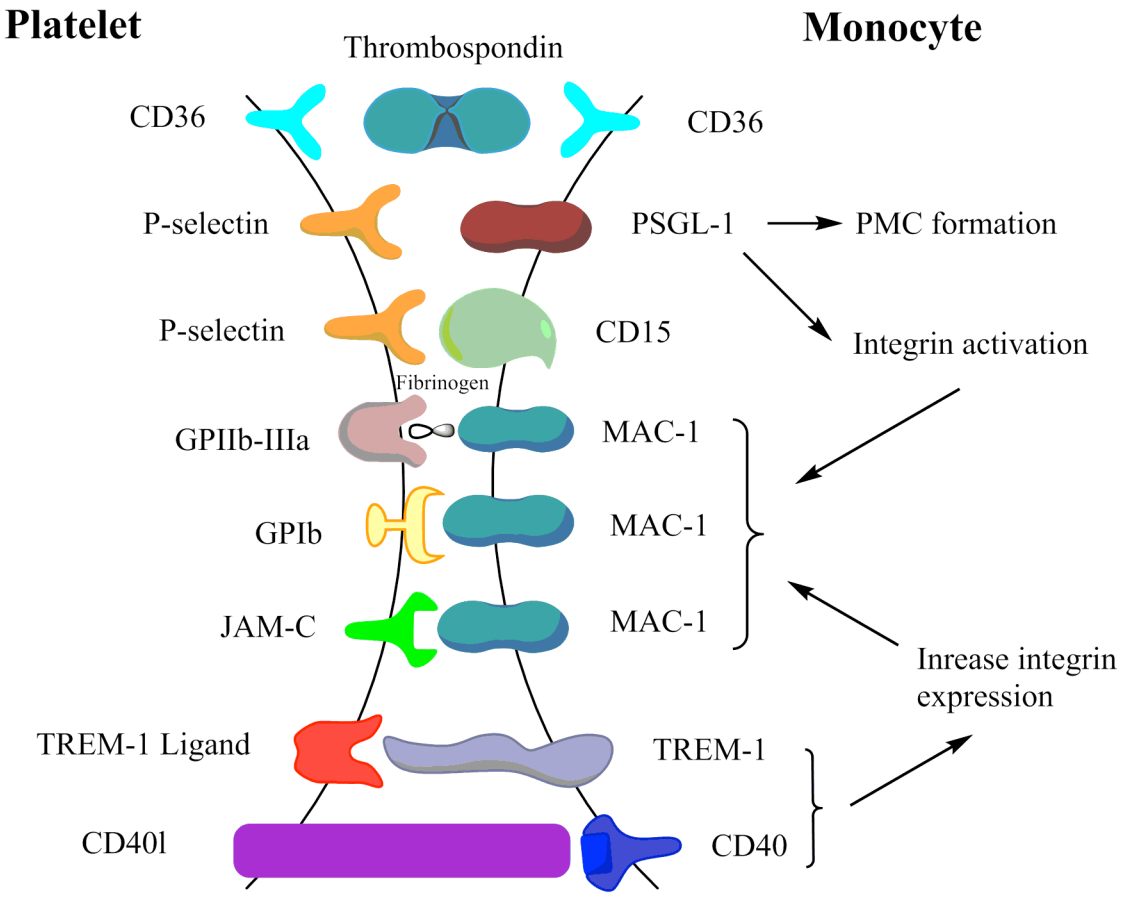

Figure 1.7: Interactions involved in monocyte platelet aggregate formation

Representative diagram showing the interactions formed between platelet and monocytes after activation. The primary interaction is mediated through the P-selectin•PSGL-1 proteins that lead to platelet monocytes aggregate formation and integrin activation. After this the other receptors act as secondary interactions to stabilise the aggregate and promote intracellular signalling. Adapted from van Gils et al., 2009b.

The P-selectin•PSGL-1 interaction has been implicated in the activation of the monocyte integrin macrophage-1 antigen (MAC-1) (Evangelista et al., 1996), which is able to bind to platelet GPIb (D. I. Simon et al., 2000) and junctional adhesion molecule C (JAM-C) (Santoso et al., 2002) directly as well as forming a bridge to GPIIbIIIa with

fibrinogen (Gawaz et al., 1991). Other interactions between CD40•CD40L and the triggering receptor expressed on myeloid cells 1 (TREM-1)•TREM-1 ligand can also stabilise the aggregate and increase MAC-1 activation (van Gils et al., 2009a).

The binding of platelets to monocytes is important in thrombus formation as platelets selectively incorporate monocytes and regulate monocyte function. For example platelets are able to induce monocyte TF expression (Celi et al., 1994; Lindmark et al., 2000), nuclear factor kappa B (NF-κB) activation (Weyrich et al., 1995) and plasminogen-activator inhibitor-1 (PAI-1) expression, all of which could increase clot stability.

1.9 Monocytes in thrombosis

Monocytes are nucleate cells derived from a common myeloid precursor in the bone marrow that also gives rise to neutrophils (Gordon and P. R. Taylor, 2005). Monocytes circulate in the blood for several days (Whitelaw, 1966), where they constitute 5-10% of peripheral blood leukocytes, before entering into tissues to replenish resident macrophage and dendritic cell populations or are cleared by the spleen. The differentiation of monocytes into macrophages is highly dependent on external factors, with at least 4 different populations identified so far (M1-M4) (Gleissner et al., 2010; Mantovani et al., 2004; Zhou et al., 2010). Even though monocytes are not terminally differentiated, they are important in the progression of atherosclerosis (section 1.3) and thrombosis as well as their key roles in immune responses such as phagocytosis and antigen presentation.

In the circulation, monocytes are found as a heterogeneous population, classified into at least 3 subsets depending on the cell surface expression of CD14 and CD16. These are $CD14^{hi}/CD16^{low}$, $CD14^{+}/CD16^{+}$ and $CD14^{low}/CD16^{+}$ (Grage-Griebenow et al., 2001; Passlick et al., 1989). The reason for the different subsets is not completely understood, but reports suggest heterotypic roles in atherothrombosis (Hristov and C. Weber, 2011). Differences between the subsets have been identified at the transcriptomic level (Martinez, 2009). In a study by Zhao et al, 521 genes were differentially expressed between the $CD16^{low}$ and $CD16^{+}$ subsets with 305 and 216 characterising each respectively. The same study also carried out proteomics and found 235 differentially expressed proteins with 112 characterising $CD16^{low}$ and 123 $CD16^{+}$ (Zhao et al., 2009). There has been a number of studies looking at the role of subsets of monocytes in atherosclerosis that associated increased $CD14^{+}/CD16^{high}$ monocytes with an increase in

CAD (for reviews (Hristov and C. Weber, 2011; Woollard and Geissmann, 2010)). However, the roles of monocyte subsets in thrombosis are still poorly understood.

Within a thrombus monocytes have been shown to play a number of important roles in thrombus growth and stabilisation. The platelet monocyte interaction through P-selectin•PSGL-1 induces TF expression in monocytes (Celi et al., 1994; Lindmark et al., 2000). Monocytes mediate TF dependent platelet-thrombus formation (Barstad et al., 1995) and secretion of PAI-1 in response to transforming growth factor β (TGFβ) (Chan et al, in preparation) that stabilise the thrombus. In addition, monocytes are also able to activate factor (F) V and secrete enzymes that cleave prothrombin to thrombin (Kappelmayer et al., 1993; Le Guyader et al., 2004; Shantsila and Lip, 2009). Monocytes are also able to regulate thrombus formation by internalising and degrading fibrin(ogen) (D. I. Simon et al., 1993) and inactivate the procoagulant activity of thrombin through thrombomodulin expression (Satta et al., 1997).

1.10 Background to the study

The hypothesis for this study was formed through observations from two separate studies carried out by former members of this laboratory. These were based on an experimental model in which monocytes were activated by platelets in whole blood using the platelet specific GPVI agonist cross-linked collagen related peptide (CRP-XL) before isolation using immune-magnetic beads. The first compared RNA expression from stable ST-elevated MI (STEMI) patients and age/gender-matched controls using genome wide expression (GWE) profiling. Of the >3000 genes measured, a number were differentially expressed in monocytes after incubation with activated platelets including those involved in regulation of coagulation, namely tissue factor pathway inhibitor (*tfpi*), endothelial protein C receptor (*procr*) and thrombomodulin. Of particular interest, all 3 genes were significantly lower in the STEMI patients compared to controls after platelet activation. For this project it was decided to focus on 2 of these; *tfpi* and *procr*.

A second GWE study that included a number of probes for transcription factors, found differential expression profiles between inflammatory-stimulated and platelet-stimulated monocytes. Of interest, the nuclear transcription factor PPARγ was found to be upregulated in response to platelet but not inflammatory stimulation in monocytes whereas NF-κB was preferentially upregulated by the inflammatory stimuli.

In the first study, monocyte gene expression was analysed after 4h incubation with activated platelets whilst in the second study gene expression was measured after 2h. This led to the hypothesis: Are monocyte anti-coagulation genes regulated by activated platelets through the PPARγ nuclear transcription factor pathway?

The next sections will describe the roles of TFPI and EPCR in coagulation and the role of PPARγ, including crystallisation trials, to date.

1.11 The coagulation cascade

Coagulation is the sequential proteolysis of inactive zymogens to their active forms and can be separated into 2 pathways, intrinsic and extrinsic, that converge into a common endpoint. The intrinsic or contact pathway of coagulation is initiated through high molecular weight kininogen, prekallikrein and FXII forming a complex on collagen causing downstream events and will not be discussed here (Gailani et al., 2015). The transmembrane TF protein initiates the extrinsic pathway. Both lead to the formation of thrombin and fibrin.

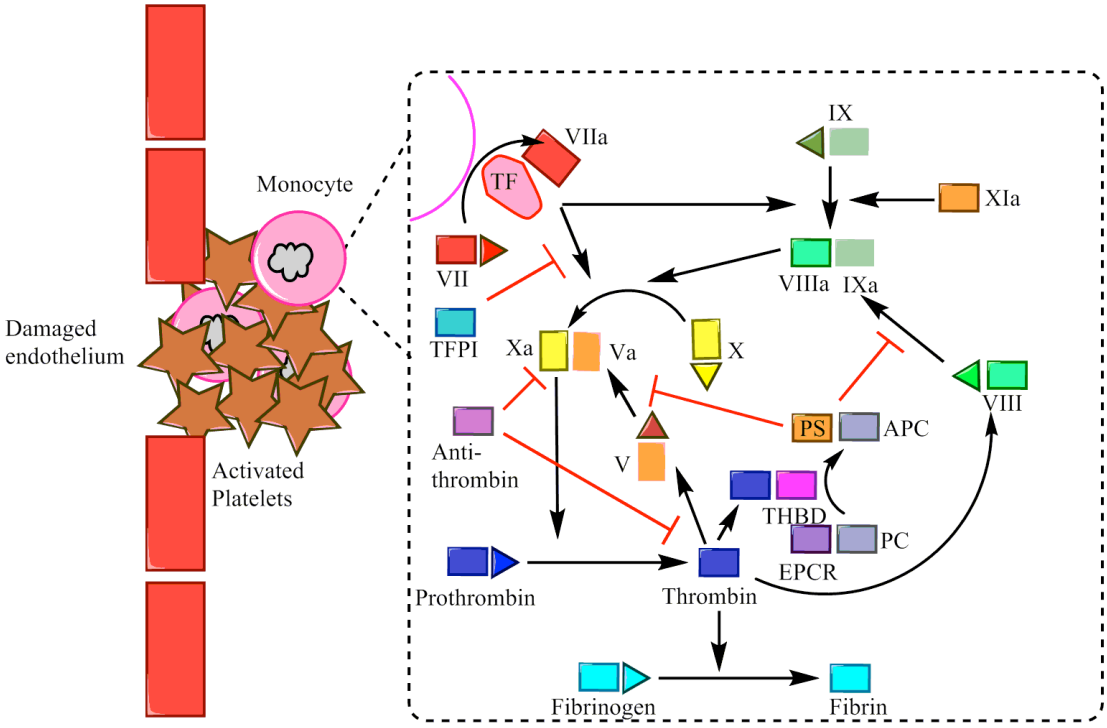

Figure 1.8: Extrinsic coagulation cascade

Extrinsic coagulation is initiated when membrane bound, active tissue factor becomes exposed to the circulation. The resulting cascade of sequential zymogen cleavage results in positive feedback and the formation of both thrombin and fibrin that activate platelets and stabilise clots respectively. Coagulation is regulated at various point as shown be the red arrows.

In the absence of damage or stimuli, TF remains spatially separated from the circulation and its binding partner FVII. TF is expressed constitutively at the cell surface of fibroblasts and SMC's that are present in the vessel wall (Drake et al., 1989) so following damage, coagulation is rapidly initiated. TF can also be synthesised by EC's and monocytes and remains associated with the Golgi and endosomes until an external stimulus is received, e.g. tumour necrosis factor α (TNFα) mediates TF translocation to the apical surface of EC's (Narahara et al., 1994; Osterud, 1998; Tremoli et al., 1999). TF is also present on circulating cells, including monocytes, in an encrypted form where activation may be dependent on phosphatidylserine (PS) translocation or disulphide bond formation through the action of protein disulphide isomerase (PDI) (V. M. Chen and Hogg, 2013). Upon decryption and/or activation, TF binds to FVII/VIIa to form a complex able to cleave FX to FXa that leads cleavage of prothrombin to thrombin and fibrinogen to fibrin. Thrombin and fibrin are important for platelet activation and clot stabilisation respectively. In addition FXa is also able to cleave FVIII and FV to FVIIIa and FVa, which form the Xase complex and cleave more FX (Gomez and McVey, 2006).

Activation of platelets enhances coagulation through activation of a calcium dependent scramblase (TMEM16F) that transfers negatively charged phospholipids, including PS, from the inner to the outer leaflet (Lhermusier et al., 2011). The negative charge associated with the platelet outer membrane allows coagulation factors to bind through gamma carboxyglutamic acid (GLA) residues (Zwaal et al., 1998). For factors that lack a GLA domain, binding to platelets is mediated through the GPIb-V-IX complex (Lisman, 2009). The importance of platelets in coagulation is highlighted in Scott's syndrome, a rare disease characterized by increased bleeding due to the failure of platelets to transfer negative phospholipids to the outer membrane (Zwaal et al., 2004).

Like most signalling cascades, coagulation does not proceed without regulation. There are a number of proteins that can specifically inhibit steps of coagulation. Regulation of extrinsic coagulation is mainly by 3 proteins / complexes. The first, TFPI, inhibits the initial step of FX conversion to Xa that is itself FXa dependent (section1.12). The mechanism of action of TFPI means that its ability to inhibit coagulation is dependent on the levels of TF and FXa (Osterud et al., 1995). Anti-thrombin (AT) is important in the inhibition of FIXa, FXa, FXIa and thrombin. AT is a so-called 'suicide inhibitor' as it is activated by cleavage from thrombin, the molecule it inhibits. For AT to function maximally heparinoids or heparin are also required, which has been shown to increase

the rate of inhibition 1000-fold (Blajchman, 1994). The last is the protein S (PrS)•activated protein C (APC) complex that prevents production of FVa and FVIIIa by thrombin. This inhibition is dependent on interaction of thrombin with thrombomodulin, which converts protein C to APC with the aid of EPCR (F. B. Taylor et al., 2001a).

1.12 Tissue factor pathway inhibitor (TFPI)

The *tfpi* gene is located on chromosome 2, contains 9 exons and 8 introns and spans more than 10 kilobases (Girard et al., 1991). The majority of TFPI protein is localised to EC's but has also been shown in platelets, monocytes / macrophages and SMC's (Maroney and Mast, 2008; WERLING et al., 1993). There are low levels (<2nM) of TFPI in the plasma associated with LDL and high density lipoprotein (HDL) (Broze, 1995; Lesnik et al., 1993). Upregulation of *tfpi* mRNA has been shown within a thrombus and is dependent on haemostatic stimuli, as pro-inflammatory molecules such interleukin (IL) 1β, TNFα and lipopolysaccharide (LPS) fail to upregulate *tfpi* (Piro and Broze, 2005) although fluid flow has also been implicated in *tfpi* expression in EC's (Westmuckett et al., 2000).

TFPI is expressed as two isoforms; alpha and beta. The *tfpi* mRNAs are directed to the ER via the N-terminal signal sequence where it is translated (Wun et al., 1988). As TFPI progresses through the trans-golgi network it becomes N- and O- glycosylated; TFPIβ contains more glycosylation than TFPIα (Piro and Broze, 2005). TFPIβ then undergoes glycosylphosphatidylinositol (GPI) attachment and trafficking to the plasma membrane. Although lacking a GPI signal sequence, TFPIα is thought to associate with a partner GPI anchored protein in the golgi through its third kunitz-like protease inhibitor (KPI) domain and C-terminus (Piro and Broze, 2004). Evidence for this is comes from the release of TFPI from the membrane upon phosphatidyl inositol-specific phospholipase C (PI-PLC) treatment (Sevinsky et al., 1996). Importantly, the third KPI domain contains a binding site for PrS, a co-factor for TFPI that increases the rate of TFPI-dependent FX inactivation 10-fold (Hackeng et al., 2006) (figure 1.9). One possible scenario is that TFPIα associates reversibly with the GPI-anchored proteins, leaving a pool of free TFPIα that is secreted and unable to re-associate (Cunningham et al., 2002). At the membrane, TFPI associates with lipid rafts that are important in caveolae formation (Lupu et al., 1997).

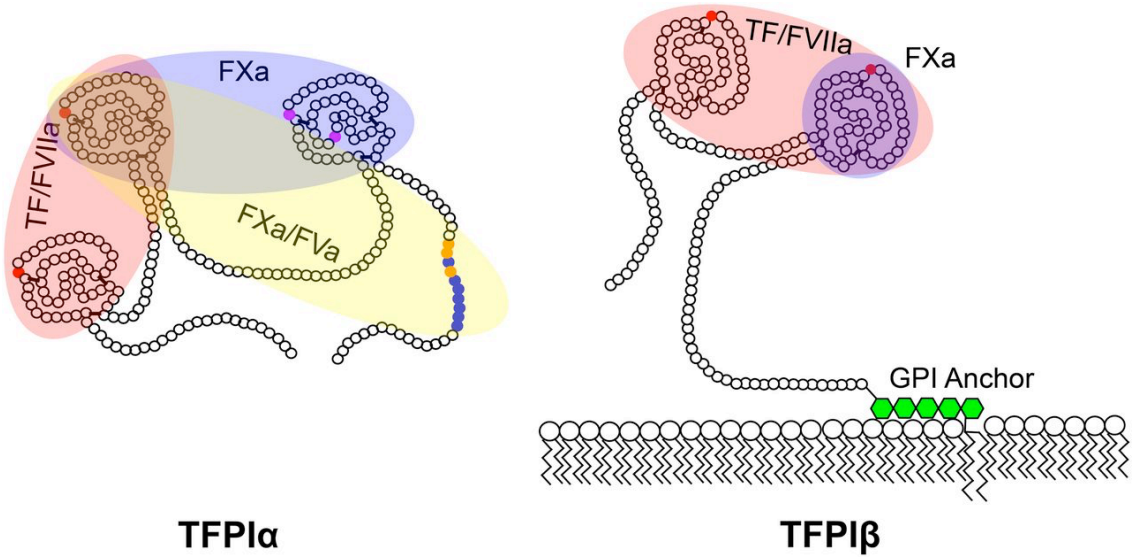

Figure 1.9: Organisation of TFPI protein domains

The TFPIα protein is composed of an N-terminal signal sequence followed by 3 kunitz-like inhibitory domains of which domain 2 is important for TF•FVII(a) inhibition and domain 3 is important for PS binding and binding to the membrane. TFPIβ contains only KPI domains 1 and 2 and is anchored to the membrane through a GPI moiety. Taken from Wood et al., 2014.

TFPI inhibits coagulation by either binding directly to FXa in the plasma or by binding to the TF•FVIIA•FX/FXa complex (Broze, 1992). TFPI may also inhibit the intrinsic pathway in a FX dependent way by inhibiting FIX (Broze, 1995). Once bound to the TF•FVIIa•FXa complex on the membrane TFPI can act to modulate TF signalling within the cell (Ahamed et al., 2005) and cause the internalisation of the complex through caveolae (Hamik et al., 1999) sequestering the pro-coagulant activity. Whilst it is apparent that TFPIα accounts for ~80% of TFPI it seems likely that its primary role is not the inhibition of the TF•FVIIa•FXa complex, as selective knockdowns of TFPIα and TFPIβ indicated that TFPIβ is responsible for most of the inhibition (Piro and Broze, 2005).

Usually involved in the degradation of extracellular matrix components, some MMPs, such as MMP-7, MMP-1, MMP-9 and MMP-12, can degrade TFPI, regulating its activity. MMP12 is produced from lipid laden macrophages and could act to inactivate TFPI on the surface of EC's allowing coagulation to progress (Belaaouaj et al., 2000). The cleavage of TFPI occurs at the C-terminal domain, which is necessary for FXa binding and the cleaved C-terminal may act as a competitive inhibitor to the full length TFPI (Cunningham et al., 2002).

The importance of TFPI is evident from KO mice where the lack of TFPI is embryonically lethal, and by the absence of cases of TFPI deficiency in humans (Z. F.

Huang et al., 1997), although low levels of TFPI are associated with an increased risk of DVT (Dahm et al., 2003).

1.13 Endothelial protein C receptor (EPCR)

EPCR was initially identified in EC's (Fukudome and Esmon, 1994) and is implicated in the increased rate of cleavage of protein C (PC) to activated protein C (APC). PC is found in the form of an inactive zymogen in the blood (Griffin et al., 2007). The EPCR gene *procr* is located on chromosome 20 and gives rise to a 46kDa type 1 trans-membrane protein that consists of an extracellular domain, a trans-membrane domain and a short cytoplasmic tail (Simmonds and Lane, 1999). A soluble form of EPCR (sEPCR) is also found circulating in plasma (Kurosawa et al., 1997) and is thought to arise from shedding at the membrane brought about by an ADAM family enzyme, namely ADAM17, as a result of inflammatory mediators such as thrombin (Qu et al., 2007). It has also been shown that pro-inflammatory mediators such as TNFα decrease the transcription and translation of thrombomodulin and EPCR resulting in a decreased production of APC and therefore reduced anti-coagulative effect (Nan et al., 2005).

It is thought that EPCR can bind to both PC and APC with roughly the same affinity and when bound to APC it sequesters its ability to inhibit FVa and FVIIIa (Regan et al., 1996). However, upon binding of protein C, EPCR presents the protein to the thrombin•thrombomudulin complex and increases the conversion to APC approximately 5 fold (Stearns-Kurosawa et al., 1996). This process is necessary and relevant *in vivo* as shown by the fact that plasma concentrations of APC are higher than the proposed Km for PC of the thrombin:thrombomudulin complex alone (F. B. Taylor et al., 2001b).

Evidence also suggests that whilst EPCR allows APC to be produced and inactivate FVa and FVIIIa, EPCR may itself bind to FVII and FVIIa, due to the close homology of FVIIa and PC Gla domains (Preston et al., 2006), and aid in its internalisation and inactivation (Ghosh et al., 2007) (figure 1.10).

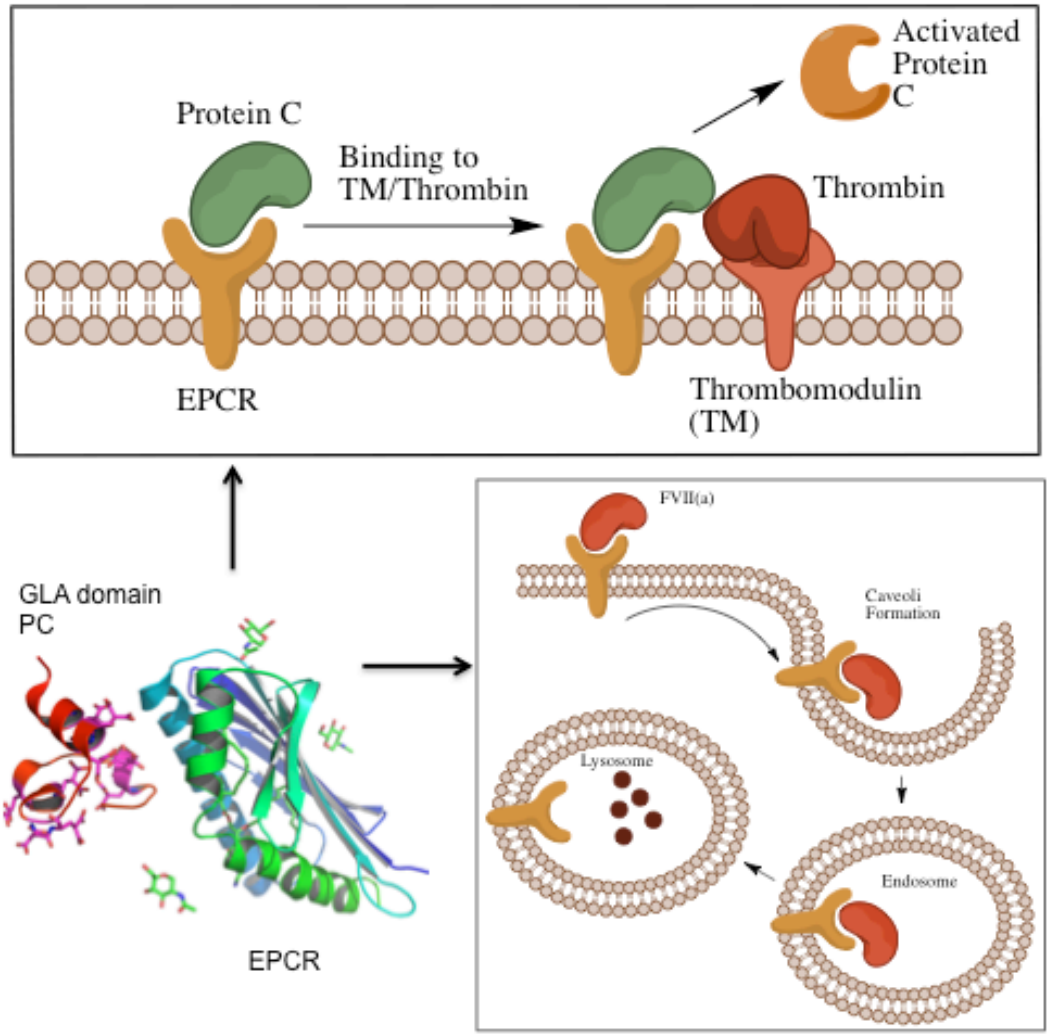

Figure 1.10: Role of EPCR in coagulation

Figure showing the mechanism of action of EPCR. Top, EPCR binds to protein and presents it to the thrombomodulin • thrombin complex, which is able to activate PC. Bottom right, similarly, EPCR is thought to be able to bind to and internalise FVII(a) due to homology between FVII(a) and PC. Bottom left, EPCR is membrane bound with fatty acids coordinating its position. Binding of EPCR to PC occurs via the GLA domain of PC. Protein data bank (PDB) 1LQV (Oganesyan et al., 2002).

EPCR KO mice show embryonic lethality around day 10 while higher levels of sEPCR (due to higher rates of cleavage) are associated with an increased risk of thrombosis (W. Li et al., 2005).

Whilst a large proportion of the literature has focused on EPCR and its role in EC's, EPCR has also been reported to be present on a number of other cell types including monocytes (Galligan et al., 2001), suggesting that whilst the EPCR effect maybe largely

attributable to endothelial cells some important contributions may come from other cell types.

1.14 Introduction to nuclear receptors (NR's)

Gene expression is a process by where the DNA code is read by polymerases to produce, mostly, single stranded RNA molecules. Gene expression is controlled at the level of i) transcription, which in eukaryotes is particularly controlled by chromatin structure, ii) splicing and mRNA stabilisation and iii) translation. NR's largely control remodelling of chromatin and initiation of gene expression through recruitment of protein complexes.

The NR family comprises 48 proteins that regulate both specific and overlapping gene sets (Mangelsdorf et al., 1995). The first NR's were cloned in 1985 (human glucocorticoid receptor) and 1986 (human estrogen receptor) (Evans, 2013). NR's play an important role in a number of diseases, with an estimated 10-20% of the worlds pharmaceuticals aimed at regulating these proteins (Ottow and Weinmann, 2008). Perhaps the best recognised of these is the inhibition of the estrogen receptor by tamoxifen in the treatment of breast cancer (Shiau et al., 1998), but others target NR's in liver disease (Wagner et al., 2011) and the androgen receptor in prostate cancer (Heinlein and Chang, 2013).

Almost all of the NR's have been cloned and structural studies have revealed shared domain architecture. NR's consist of a N-terminal variable region followed by a conserved DNA-binding domain (DBD), a variable hinge region, a 12-helix ligand-binding domain (LBD) and a variable C-terminal sequence. Binding of NR's is exclusively mediated through the DBD (Green and Chambon, 1987) and whilst conserved in overall structure, specificity is achieved through binding to specific partners and on the number of nucleotides between repeats (Rastinejad et al., 2013). NR's are divided into retinoid X receptor (RXR)-heterodimers, homodimers, monomers and steroid NR's. NR LBDs are also conserved but attain specificity through the size of the LBD, which has been shown to be between 0 and 1500Å (Y. Li et al., 2003).

In the absence of ligand, NRs recruit co-repressors such as silencing mediator for retinoid and thyroid hormone receptor (SMRT) and nuclear receptor co-repressor 1 (N-CoR1) through the sequence motif (LxxH/IIXXXL/L) (X. Hu and Lazar, 1999). These co-repressor complexes have associated histone deacetylase (HDAC) proteins that de-acetylate lysine residues on histones (P. J. Watson et al., 2012). De-acetylation

tends to lead to chromatin folding and repression of gene expression. On ligand binding, co-repressors are replaced with co-activators that are recruited via the sequence motif LxxLL (the NR box) (Heery et al., 1997). Co-activators usually have associated histone acetyl transferases (HATs) that tend to acetylate histone residues, leading to chromatin un-folding and expression (Glass and Rosenfeld, 2000). There are two mechanisms of co-activator recruitment, the first is the mousetrap model, whereby helix 12 is positioned away from the LBD in the absence of ligand and moves proximal to the LBD upon ligand binding (Wurtz et al., 1996). Whilst this is true for certain NR's, the current model of dynamic stabilisation, suggests in the absence of ligand, helix 12 is in a mobile conformation and when ligand binds this is stabilised through structural changes (Nagy and Schwabe, 2004).

1.15 Peroxisome proliferator activating receptor gamma (PPARγ)

PPARγ, PPARα and PPARβ/δ, are transcription factors and members of the nuclear hormone receptor superfamily. The PPAR isoforms differ in expression, ligand recognition and gene regulatory network. PPARα is involved in lipid catabolism and is expressed mainly in brown adipose tissue but also in the kidney, liver and heart. PPARβ/δ is the least studied with little information relating to function, but is expressed in multiple tissues (J. Berger and Moller, 2002). PPARγ can be subdivided into 2 major isoforms, PPARγ1 and PPARγ2. Expression of PPARγ1 has been localized to a number of tissues and cells including platelets (Ray et al., 2008), monocytes / macrophages, liver, skeletal muscle, EC's and SMC's (Fajas et al., 1997; Ricote et al., 1998). PPARγ2 is almost exclusively expressed in differentiating pre-adipocytes and is essential for adipogenesis (Tontonoz et al., 1994). Platelets have been shown to release PPARγ in MPs upon activation, which can be endocytosed by THP-1 monocyte cells (Ray et al., 2008).

The PPARγ gene is located on chromosome 3p25.2, spans 1.5kb and contains 9 exons. In addition to the 2 isoforms mentioned above, other isoforms of PPARγ have been detected that differ at the N-terminus, namely PPARγ3 and more recently PPARγ4, although PPARγ1, 3, and 4 encode the same polypeptide irrespective of alternative initiation start codons (Aprile et al., 2014; Fajas et al., 1998). There are also an additional three transcripts, designated γ1ORF4, γ2ORF4 γ3ORF4 that have been described in colorectal cancers that lack the LBD and act in a dominant negative manner (Aprile et al., 2014; Sabatino et al., 2005) (figure 1.11).

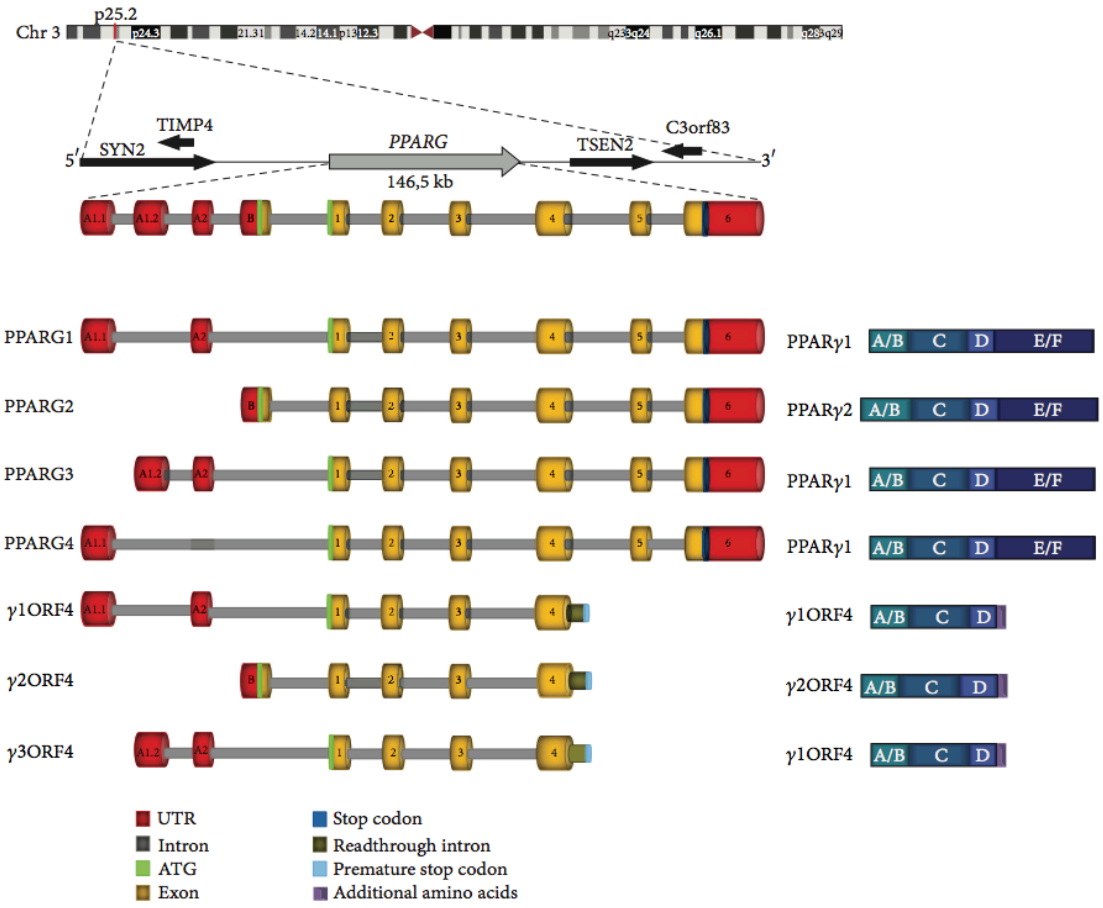

Figure 1.11: Alternative isoforms of PPARγ

Location of the pparγ gene and its introns and exons associated with splice variants. From Aprile et al., 2014.

Information regarding the regulation of *pparγ* gene expression is not well defined but there is some evidence suggesting regulation via nuclear factor-like 2 (NRF2) (Cho et al., 2010), CCAAT/enhancer binding protein (C/EBP) β (Wu et al., 1995) and sterol regulatory element binding protein (SREBP) (Fajas et al., 1999) as well as positive regulation by PPARγ itself (Steger et al., 2010; Wu et al., 1999). miRNA-540 has been shown to act as a negative regulator and targets the PPARγ mRNA for degradation via the RNA-induced silencing complex (RISC) (L. Chen et al., 2015).

Within cells PPARγ is predominantly found in the nucleus. In the absence of an activating signal such as a ligand, PPARγ is prevented from initiating expression of target genes through interaction with co-repressors SMRT / NCoR. PPARγ can undergo a number of post-translational modifications including acetylation via HDAC3 (X. Jiang et al., 2014), which also suppresses its activity and polyubiquitination for targeted degradation by the 26s proteasome, a process potentiated by interferon gamma (IFNγ)

and phosphorylation (Z. E. Floyd and Stephens, 2002). Activation of PPARγ occurs through binding of a ligand in the LBD. Conformational changes reduce binding affinity of co-repressors and increase affinity of co-activators; including PPARγ Co-activator 1α (PGC1α). In order for PPARγ to activate transcription it binds DNA as a heterodimer with RXR (J. Berger and Moller, 2002). The PPARγ•RXR heterodimer recognizes a direct repeat (DR) of DNA termed the peroxisome proliferator response element (PPRE) with consensus sequence AGGTCA separated by 1 base. PPARγ binds to the 5' DR and RXR binds to the 3' (Temple et al., 2005) (figure 1.12).

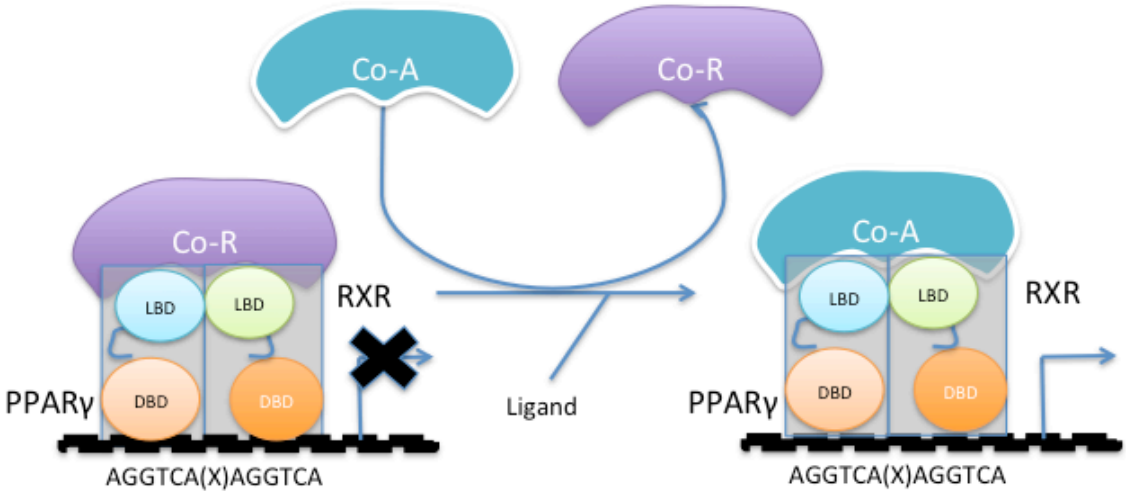

Figure 1.12: Mechanism of PPARγ activation

In the absence of ligand PPARγ is inactive through interaction with associated co-repressors such as NCoR and SMRT. Binding of ligand results in a conformation change in helix 12. This allows binding of co-activators such as PGC1a and transcriptional activation.

There are a number of ligands that can activate PPARγ that can be classified as oxylipins and include AA and linoleic acid (LA) and derivatives thereof such as 9- and 13-hydroxyoctadecaenoic acid (HODE) (Itoh et al., 2008; Nagy et al., 1998) and 15-deoxy-$\Delta^{12,14}$-prostaglandin J_2 (15d-PGJ2) (Kliewer et al., 1995). 15d-PGJ2 is a potent PPARγ agonist that can be synthesized by platelets and monocytes but its relevance *in vivo* has been controversial due to the fact that it is thought to be present at too low a concentration to be able to stimulate PPARγ (Nosjean and Boutin, 2002). Other AA derivatives such as 15-HETE (Nagy et al., 1998) and 12-HETE (Q. Li et al., 2004) have also been reported to serve as PPARγ ligands.

There are also a group of synthetic ligands, collectively known as thiazolinediones, which include rosiglitazone, piaglitazone and farglitazar that activate PPARγ (J. Berger et al., 1996). Since the late 1990's, these have been in widespread use in patients with

type II diabetes where they are used to activate PPARγ and reduce insulin resistance (Moller and Greene, 2001). Rosiglitazone was at one point the world's best selling anti-diabetic drug. However, a study in 2007 suggested rosiglitazone increased the risk of cardiovascular events, which resulted in restrictions and its use sanctioned by the US Food and Drug Administration (FDA) in 2010, although this was overturned in 2013 upon re-analysis of the data (Nissen and Wolski, 2007; Stone et al., 2015; Tucker, 2013).

1.16 Structural characterisation of PPARγ

The structure of the PPARγ-LBD was first solved in 1998 using isomorphous replacement (IR) (Nolte et al., 1998). In the study, Nolte et al crystallised the PPARγ-LBD without ligand (apo) to 2.2Å and with the synthetic ligand rosiglitazone and co-activator steroid receptor co-activator 1 (SRC-1) to 2.3Å. The structure revealed 13 helices and a 4 stranded β-sheet, with Hx3 to the C-terminus similar to other NR LBDs (figure 1.13a).

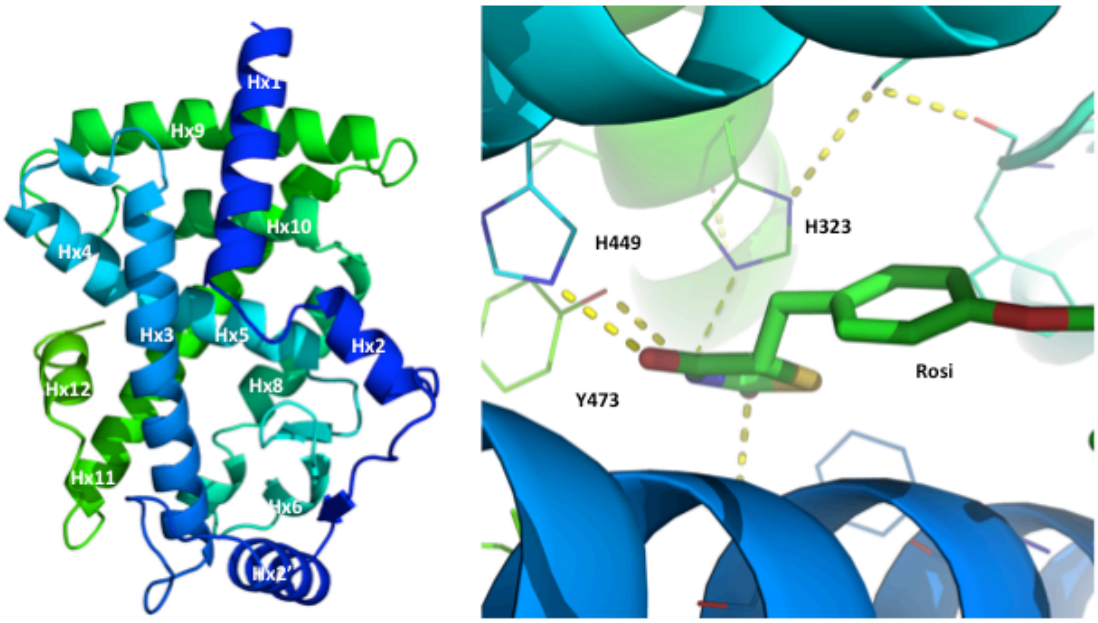

Figure 1.13: Structure of first PPARγ-LBD and in complex with rosiglitazone

The first published structures of PPARγ. A) The apo PPARγ-LBD showing overall fold. The LBD is composed of 13 helices designated 1-12 and a 4-stranded β-sheet. The fold from Hx3 to the c-terminal is similar to that of other nuclear receptors (PDB 1PRG). B) Rosiglitazone positioned around Hx3 in the LBD with the polar head group making contacts with several polar side chains from the main chain (PDB 2PRG) (Nolte et al., 1998).

The identified ligand binding pocket was estimated at ~1300Å^3 and formed a t-shaped cavity from the C-terminus, around Hx3 and Hx6 to the β-sheet. Rosiglitazone occupied only 40% of this cavity making specific contacts at a number of residues in Hx3, Hx4, Hx10 and Hx12 to stabilise the head group, as well as with residues in a hydrophobic pocket (figure 1.13b). Interaction with the co-activator was shown to be dependent on the conserved LXXLL motifs within the SRC-1 peptide, with one motif binding to one molecule and the second binding to the second yielding a 2:1 ratio of PPARγ:SRC-1 (Nolte et al., 1998).

Since the first structure in 1998, a number of PPARγ structures deposited in the PDB (http://www.rcsb.org/pdb/home/home.do) in complex with ligands, both activating and inhibitory, and with co-repressors and co-activators. Of note is the 2000 paper by Gampe Jr et al, which showed the crystal structure of the PPARγ-LBD•RXRα-LBD heterodimer with their respective ligands and co-activators. This revealed the molecular basis for RXR binding with many NR's and, importantly, showed that the PPARγ-LBD was rotated ~10° from the C2 symmetry of the RXR-LBD, a deviation not seen in the homodimers (Gampe et al., 2000). In 2008 Itoh et al determined the crystal structure of the PPARγ-LBD in complex with oxidised fatty acids likely to relevant *in vivo*. They also showed that the PPARγ-LBD was able to accommodate more than one ligand and that oxidised fatty acids can couple covalently to cysteine (Cys) 285 in the LBD (Itoh et al., 2008). Finally, another 2008 paper by Chandra et al showed the structure of full-length PPARγ in complex with RXRα, ligands, co-activator and DNA (figure 1.14). This was the first to consolidate and verify information on the PPARγ-LBD and DBD that had been determined using isolated domains and showed that the PPARγ-LBD made contacts with multiple domains including the RXR-DBD (Chandra et al., 2008). The combined information from crystal structures has allowed the mechanism of heterodimerisation, interaction with co-repressors and co-activators and basis of ligand binding to be determined.

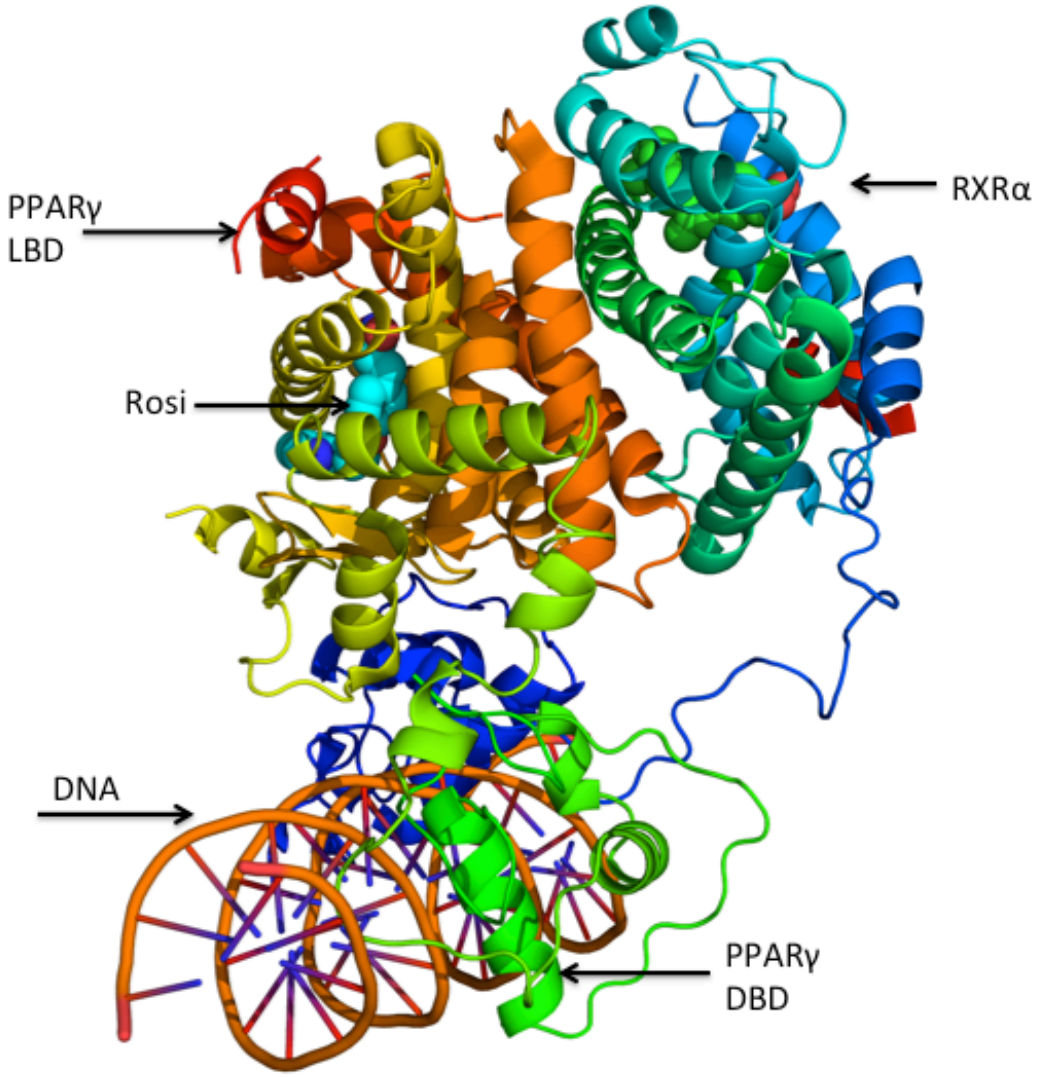

Figure 1.14: Full length PPARγ in complex with RXRα bound to DNA

PPARγ binds to RXRα through conserved residues in H10/11 within the LBD. The LBD of PPARγ has a flexible region that attaches it to the DBD. The DBD binds upstream of the RXRα DBD that has a similar overall architecture. PDB 3DZY (Chandra et al., 2008).

1.17 Hypothesis and aims

Based on the evidence presented in section 1.10, it was hypothesised that activated platelets are able to regulate the expression of two key anti-thrombotic genes; *tfpi*, and *procr* in monocytes through the effects of soluble mediators released into the extracellular medium; and that this regulation is modified by the effect of aspirin, and through activation of the NR PPARγ.

Chapter 3 explored the effect of activated platelets on the expression of the two anti-thrombotic genes and of *pparγ*, using RT-qPCR and specific inhibitors of COX-1 and 12-LOX. The following specific questions were addressed:

1. Is the increase in monocyte gene expression dependent on platelet activation?
2. Is the increased monocyte gene expression due to endogenous transcription or transfer of mRNA?
3. Is monocyte gene expression dependent on direct contact between platelets and monocytes or mediated through platelet-derived soluble mediators, and if so, what types of molecules present in the platelet releasate are regulating expression?
4. Do inhibitors of AA metabolism effect gene expression in monocytes?

Chapter 4 aimed to demonstrate that the increase in *tfpi, procr and pparγ* gene expression in the monocytes could also be seen at the protein level.

Chapter 5 aimed to identify the molecules released from platelets that were responsible for increasing both *tfpi* and *procr* expression in monocytes. MS based approaches and inhibitors of COX-1 and 12-LOX were used to dissect out the potential AA metabolites (oxylipins) or proteins that could be responsible for regulating the three genes of interest.

In Chapter 6 oxylipins identified from chapter 5 were used in transactivation and structural (X-ray crystallographic) studies to demonstrate that platelet-derived oxylipins are able activate and interact with PPARγ. Two specific oxylipins were selected based on their relative abundance in platelet supernatants and the effects of COX-1 and 12-LOX inhibitors on their levels.

Chapter 2: Materials and Methods

Unless otherwise stated, materials were purchased from Sigma Aldrich Ltd, Dorset, UK. Buffer recipes will be described within the relevant sections.

2.1 Blood collection

Blood was collected, with informed consent, from healthy volunteers, who claimed not to be on medication. All studies were conducted under Ethical approval from the University of Leicester Ethics Committee. An experienced phlebotomist collected blood from the antecubital fossa, without use of a tourniquet to avoid activation of monocytes and platelets, via a 21-gauge needle into Vacutainers (Becton Dickinson, Oxford, UK). The first 3ml was collected into an ethylenediaminetetraactic acid (EDTA) tube (5.4mg) and analysed using a Beckman Coulter AcTdiff haematology analyser (Beckman Coulter UK Ltd, High Wycombe, UK) to obtain a whole blood count. Unless stated otherwise, all subsequent blood was collected into 4.5ml tri-sodium citrate (0.105M) tubes and processed within 20min of being taken.

2.2 Sample preparation

2.2.1 Platelet poor plasma (PPP)

Whole blood was centrifuged at 1800xg for 30min with the brake on. The resulting platelet poor upper layer was removed in one operation using a Pasteur pipette.

2.2.2 Platelet rich plasma (PRP)

Whole blood was centrifuged at 160xg for 20min with the brake off. The resulting platelet rich upper layer was removed in operation using a Pasteur pipette, and used within 20min.

2.2.3 Washed platelets

Whole blood was first inhibited with 1/6 volume of acid citrate dextrose (ACD) (0.085M tri-sodium citrate, 0.071M citric acid, 0.11M glucose, pH 6.3) to inhibit platelet aggregation during centrifugation. PRP was prepared as above and centrifuged at 600xg for 15min. The resulting platelet pellet was resuspended in acidic HEPES-buffered saline (HBS) (10mM HEPES; 150mM NaCl; 5mM LiCl; 1mM $MgSO_4$; pH 6.0), re-centrifuged and the pellet resuspended in HBS pH 7.4. Platelets were re-centrifuged, and the resulting pellet resuspended in an appropriate buffer (as

detailed in subsequent sections) at $400x10^3/\mu l$ unless stated otherwise. Prostacyclin (0.57μM) was added before each centrifugation to minimise platelet activation.

2.2.4 Preparation of platelet releasate

Platelet releasate was prepared using washed platelets ($200\text{-}600x10^3/\mu l$ depending on the downstream application) stimulated with 0.5μg/ml CRP-XL for 15min at 37°C. The platelets were then pelleted by centrifugation at 1500xg for 15min. The resulting supernatant was centrifuged for 2min at 13000xg before being transferred to clean eppendorf tubes and centrifuged at 20000xg for 30min to pellet platelet MPs. The releasate from each individual was aspirated and used immediately, or stored in aliquots at -20°C.

2.2.5 Separation of high and low molecular weight proteins

Platelet releasates were separated into high and low molecular weight fractions using Amicon Ultra molecular weight cut off (MWCO) filters (Merck Millipore, Feltham, UK). Briefly, platelet releasate was added to the filters that were then centrifuged at 4000xg for 20min. The concentrated high molecular weight proteins were aspirated from the filter cartridge and stored at -20°C, or diluted back to the original volume in RPMI (Gibco). The low molecular weight fraction was collected as the flow through from the concentration and stored at -20°C.

2.2.6 Extraction of oxylipin metabolites

Oxylipin metabolites were extracted from platelet releasates using a hexane method (C. P. Thomas et al., 2010). Briefly, 2.5ml extraction solvent (1M acetic acid: propan-2-ol: hexane (2/20/30 v/v/v)) was added per 1ml releasate in borosilicate glass tubes with 12mm plastic lids containing polytetrafluoroethylene (PTFE) seals (all Fisher Scientific) and the sample vortexed briefly. An additional 2.5ml of hexane was then added to each sample, which was again vortexed and centrifuged at 500xg for 5min at 4°C. The upper hexane layer containing the oxylipins was aspirated and the resulting aqueous fraction was re-extracted by the addition of an equal volume of hexane, mixed and centrifuged again at 500xg for 5min at 4°C. The resulting hexane layer was combined with the first fraction and evaporated either under nitrogen gas or using a vacuum centrifuge. Oxylipins were redissolved using a small volume of hexane (to ensure collection of material that had attached to the sides of the tubes). This was

evaporated and the sample resuspended in an appropriate solvent for downstream analysis. Metabolites were stored at -80°C if required.

2.2.7 Isolation of monocytes from blood

Three different methods were used to isolate monocytes from whole blood depending on the starting material, incubation conditions and downstream application. When incubations were carried out in whole blood and the downstream application was RT-qPCR (section 2.8), CD14 Dynabeads® (Life Technologies Ltd, Paisley, UK) were used due ease of use and quick isolation protocol. If isolation of monocytes was required prior to incubation for use in RT-qPCR and flow cytometry (section 2.9), CD14 microbeads (Miltenyi Biotech, Surrey, UK) were used. Finally, if monocytes were to be used for western blotting analysis (section 2.11) a pan monocyte negative isolation method (Miltenyi Biotech) was used.

2.2.7.1 Monocyte isolation using CD14 Dynabeads®

CD14 Dynabeads® were used to isolate monocytes from whole blood for real time PCR and nuclear protein extraction. CD14 Dynabeads® at a volume of 25µl/ 1ml whole blood were pipetted from the vial and 1 volume phosphate-buffered saline (PBS) (137mM NaCl; 2.7mM KCl; 10mM Na_2HPO_4; 1.8mM KH_2PO_4) pH 7.4 / 5mM EDTA added. The beads were washed once in PBS pH 7.4 / 5mM EDTA using a magnetic particle concentrator (MPC; Life Technologies Ltd) before being resuspended to the original sample volume in PBS pH 7.4 / 5mM EDTA. Blood samples were centrifuged at 600xg for 10min and the supernatant aspirated to remove any soluble CD14. The pellet was resuspended in PBS pH 7.4 / 5mM EDTA to the original volume before addition 25µl/ml washed CD14 Dynabeads®. Samples were incubated on a Dynal rotary mixer (Life Technologies Ltd) for 20min at 4°C, then placed in the MPC for 2min and the supernatant discarded. The beads were washed 3 times in PBS pH 7.4 / 5mM EDTA.

For monocyte depletion, 50µl/ml CD14 Dynabeads® were added and incubated for 30min at 4°C on the rotary mixer. The samples were then placed in the MPC for 2min and the supernatant transferred to a new tube leaving the monocytes behind.

2.2.7.2 Peripheral blood mononuclear cell (PBMC) isolation

PRP was first removed from the haematocrit to reduce platelet contamination. The remaining blood cells were resuspended in PBS pH 7.4 / 5mM EDTA to the original

volume, then diluted 1:1 with PBS pH 7.4 / 5mM EDTA before being layered on top of Lymphoprep (Axis Shield, Dundee, Scotland) at a ratio of 2 parts sample to 1 part Lymphoprep. Following centrifugation at 800xg for 25min (low acceleration and deceleration), monocytes and lymphocytes were removed from the Lymphoprep-plasma interface and washed twice in PBS pH 7.4 / 5mM EDTA at 300xg for 15min. PBMCs were resuspended in 2ml PBS pH 7.4 / 5mM EDTA and counted before further centrifugation at 300xg for 15min. Finally, PBMCs were resuspended in appropriate media at a predefined concentration dependent on the experimental conditions.

2.2.7.3 Positive Monocyte isolation using CD14 microbeads

The method used was adapted from a previously described method (Miltenyi et al., 1990). PBMCs were prepared and the resulting pellet resuspended at $1.25x10^8$leukocytes/ml in PBS pH 7.4 / 5mM EDTA before the addition of CD14 microbeads at a concentration of 20µl per 10^7 nucleated cells. The sample was incubated at 4°C for 15min and centrifuged at 300xg for 10min before being resuspended in PBS pH 7.4 / 5mM EDTA (50µl per 10^7 nucleated cells). Monocytes were isolated either manually using an LS column (Miltenyi Biotech) following the manufacturer's instructions, or using the AutoMacs Pro cell isolation system (Miltenyi Biotech). Isolated monocytes were centrifuged at 300xg for 15min and resuspended in the appropriate buffer for the application required. The scheme for the method is illustrated in figure 2.1.

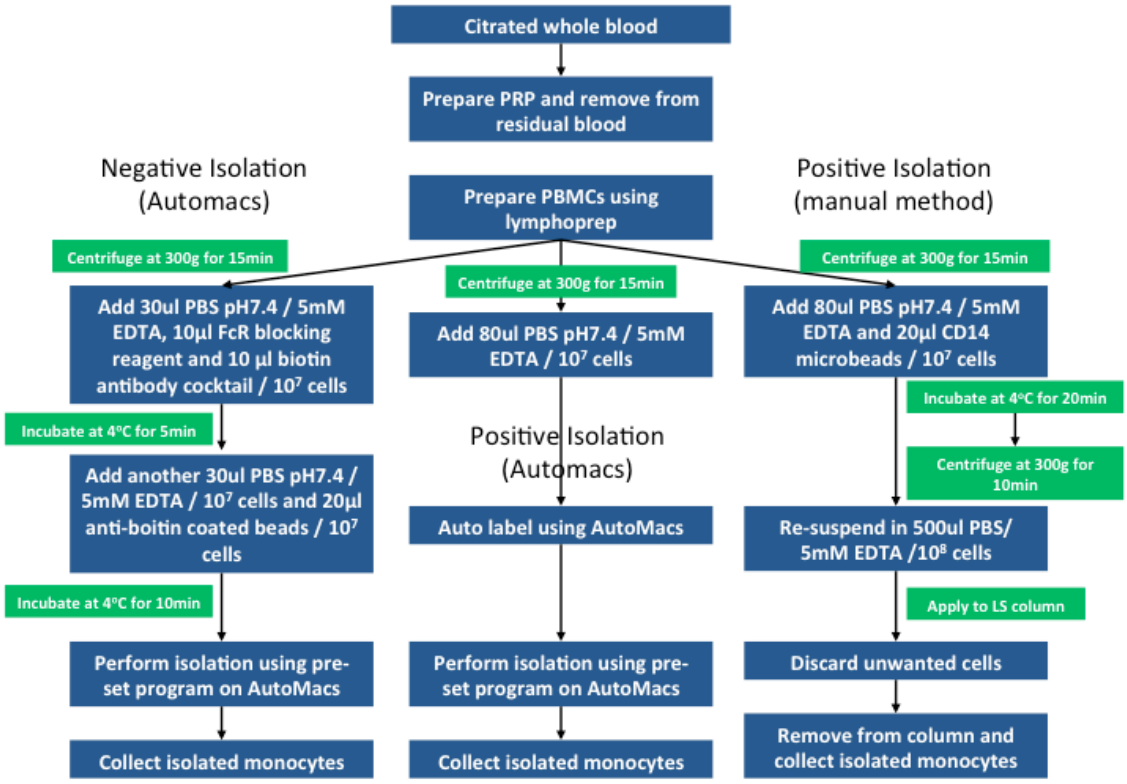

Figure 2.1: Methods for monocyte isolation

PBMCs were prepared from whole blood and incubated with either the CD14 microbeads or with the pan monocyte reagents according to the manufacturers instructions. Monocytes were then isolated using either LS columns or an Automacs cell isolation system.

2.2.7.4 Negative isolation of monocytes (Pan monocyte isolation)

PBMCs were prepared and the resulting pellet was resuspended at $3.33x10^8$leukocytes/ml in PBS pH 7.4 / 5mM EDTA before the addition of 10µl FcR blocking reagent (human Ig) and 10µl biotin antibody cocktail (directed against: CD235a; CD3; CD7; CD15; CD19; CD56; CD66abce; CD123; CD335; Aimee Tyler, personal communication) (both from Miltenyi Biotech) per 10^7 leukocytes. The sample was incubated at 4°C for 5min before the addition of a further 30µl PBS pH 7.4 / 5mM EDTA and 20µl anti-biotin coated beads (Miltenyi Biotech) per 10^7 nucleated cells. Samples were incubated for a further 10min at 4°C before monocytes were isolated using the AutoMacs cell separation system.

2.3 Culturing monocytes

Monocytes, either from PBMCS (section 2.2.7.1) or after isolation with CD14 microbeads (section 2.2.7.2) were cultured in 6 well plates.

PBMCs were resuspended in macrophage serum free media (M-SFM) (Life Technologies Ltd) at a concentration of $2.5x10^6$/ml and 2ml added to each well. The monocytes were left to adhere for 2h at 37°C in 5% CO_2/air atmosphere. The non-adherent lymphocytes were removed by 3 gentle washes in warm PBS and the monocytes cultured in M-SFM for 24h.

Isolated monocytes were centrifuged at 300xg for 10min and resuspended in M-SFM at $0.5x10^6$/ml. The required number of monocytes were then added to each well and made to a final volume of 2ml using M-SFM. After 24h in culture, M-CSF (50ng/ml) was added to the cultures. After 4 days the media was changed. Monocytes were cultured up to a maximum of 7 days and harvested using TRIzol (Life Technologies Ltd) at various time points.

An overview of monocyte and platelet isolation methods and preparation of platelet-derived material is shown in figure 2.2. Once isolated, monocytes were reconstituted with washed platelets or platelet-derived material at a concentration and ratio that reflected that found in the circulation.

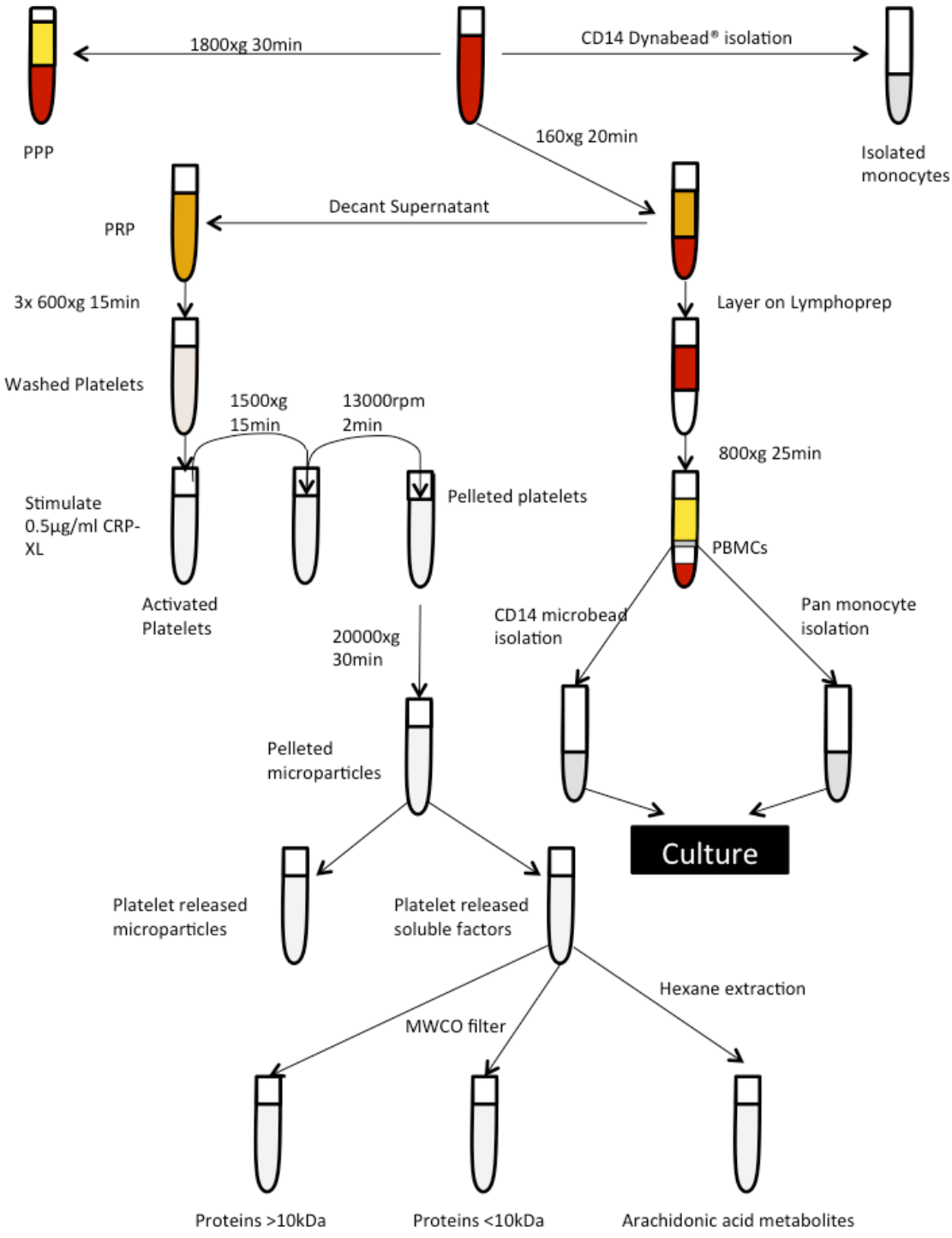

Figure 2.2: Overview of sample preparation

A summary of protocols used to isolate platelets and their associated fractions and monocytes using a number of immunomagnetic methods.

2.4 Cell culture

2.4.1 EA.hy926 cells

EA.hy926 cells (a somatic cell hybrid made by fusion of primary human umbilical vein cells with a thioguanine resistant clone of A549) were obtained from the American Type Culture Collection (ATCC; Middlesex, UK). The cells were grown in Dulbecco's modified eagles medium (DMEM) (Life Technologies Ltd) supplemented with 10% (v/v) foetal calf serum (FCS) (Life Technologies Ltd) and 5% penicillin (100IU (base/ml)) / streptomycin (100µg/ml) (Pen/Strep) (PAA Laboratories Ltd, Yeovil, UK), herein referred to as complete medium. They were seeded in T75 flasks in 20ml complete medium at a concentration of $1.5x10^6$ total cells. When confluent, medium was removed and the cells washed for 10s with 1ml trypsin (0.25µg/ml) then incubated with 3ml trypsin for 5min to detach the cells. The trypsin was inactivated by addition of 7ml complete medium. The cells were removed into a clean, sterile Falcon flask, counted using a haemocytometer, centrifuged at 500xg for 5min and resuspended at $1x10^6$cells/ml in complete medium. When 6 well plates were used, cells were seeded at a concentration of $0.5x10^6$ total cells.

To prepare cells for use in experiments, trypsin was avoided as this digests proteins on the surface. The medium was removed and the cells washed twice in 5ml Dulbecco's PBS (DPBS). An appropriate amount of DPBS was added and the cells removed by scraping. Once the cells had been suspended in DPBS they were removed from the flask and counted. The cells were then centrifuged at 500xg for 5min before being resuspended in HBS pH 7.4 at a final concentration of $1x10^6$cells/ml.

2.4.2 THP-1 Cells

THP-1 cells, a myelo-monocytic cell line derived from an acute monocytic leukaemia patient (ATCC), were seeded at $1.5x10^6$ total cells in T75 flasks in RPMI1640 medium (Life Technologies Ltd) supplemented with 10% FCS and 5% Pen/Strep. THP-1 cells grow in suspension and were subcultured every 3 days. The media with the cells was removed, counted and $1.5x10^6$ THP-1 cells were added to a new T75 flask containing 20ml of fresh medium.

For transformation into adherent macrophage-like cells, phorbol myristate acetate (PMA) at a final concentration of 1µg/ml was added directly to the medium. The cells were then cultured for 24h to become adherent.

2.4.3 293T cells

293T cells are a transfectable derivative of human embryonic kidney 293 cells containing the SV40 antigen (ATCC). Cells were cultured in complete medium. When confluent, cells were washed once with DPBS before being detached using 5ml 0.25µg/ml trypsin. The cell suspension was then removed, counted and seeded at $1.5x10^6$ total cells in new culture flasks.

2.5 Chandler loop

This experimental model was used to generate thrombi *in vitro* that resemble arterial thrombi. Saline (150µl) was added to 900µl citrated whole blood before recalcification with 11mM $CaCl_2$. Aliquots of 1ml of the mixture were immediately injected into polyvinyl chloride (PVC) tubing 45cm long, 3mm internal diameter, 4.2mm external diameter. The ends were joined with a connecter 5mm long, 4mm internal diameter and the loop incubated at 37°C for 6h at 36rpm, unless otherwise stated. The dimensions and speed were chosen to represent the shear stress found within arteries *in vivo*. The average shear rate is calculated from equation 1 where r is the internal radius of the tube, R is the total radius of the Chandler loop and ω is speed of the loop. Equation 1: Average shear rate= $(4\pi R/45r)\ \omega$. The shear stress is then calculated by equation 2 where µ is the viscosity of whole blood (0.04 poise). Equation 2: Shear stress = shear rate x µ. Substituting the values above into these equations gives a value of 19.2dynes/cm^2 which is at the lower end of the shear stress found in normal arteries. However, as the thrombus forms in the tubing, blood flow is restricted and shear stress is increased eventually mimicking that seen in pathological conditions (115-350 dynes/cm^2).

Resulting thrombi were removed from the tubing, washed in Hank's buffered salt solution (HBSS) and used for RNA extraction (see section 2.6).

2.6 Sample preparation for PCR reactions

2.6.1 Total RNA isolation

Monocytes, positively isolated using CD14 Dynabeads®, were lysed in 1ml TRIzol and the TRIzol containing the RNA separated from the beads using the MPC.

Cells isolated using the CD14 microbeads and Pan monocyte methods were centrifuged for 5min at 1500rpm before the supernatant was aspirated and the cells resuspended in TRIzol reagent at 1ml per 10^7 total nucleated cells.

Thrombi that had been generated in Chandler loops were washed in 1ml HBSS and added to 1ml TRIzol and left to incubate for 10min at room temperature before being homogenised.

For all preparations the TRIzol lysate was added to a sterile 1.5ml eppendorf and left to incubate at room temperature for 5min (to disaggregate protein•nucleic acid complexes) before chloroform was added at 200µl per 1ml TRIzol. The samples were shaken vigorously for 15s by hand to mix. The samples were then left for 2-3min at room temperature before centrifugation at 12000xg for 15min at 4°C. The upper aqueous phase containing the RNA was removed for extraction. After isolation, all RNA was quantified using a NanoDrop™8000 (ThermoScientific, Hampshire, UK) and samples were stored at -20°C until reverse transcribed.

2.6.1.1 RNA isolation using TRIzol method

Total RNA extracts were mixed with 0.5ml propan-2-ol / ml TRIzol used and incubated at room temperature for 10min to precipitate the RNA. The RNA was then pelleted at 12000xg for 10min at 4°C. The supernatant was aspirated and 1.5ml 75% ethanol / ml TRIzol used added. The sample was mixed by vortexing for 10s and the RNA pelleted by centrifugation at 7500xg for 5min at 4°C. The supernatant was aspirated and the pellet allowed to air dry for 10min before resuspension in 30µl RNase free water. RNA solubilisation was aided by incubation for 10min at 60°C.

2.6.1.2 RNA isolation using the RNeasy Minikit

Samples diluted 1:1 in 70% ethanol were loaded onto an RNeasy column and total RNA extracted using the RNeasy mini-kit (Qiagen, GmbH, Germany) according to the manufacturer's instructions. Briefly, a maximum of 700µl of sample was added to an RNeasy spin column and centrifuged at 9300xg for 30s until the entire sample was loaded. The column was washed with 350µl RWI buffer by centrifugation at 9300xg for 30s before 80µl DNase 1 (30 Kunitz units; Qiagen) added and incubated for 25min at room temperature. The column was again washed with 350µl RWI buffer before 2 washes in 500µl RPE buffer (5min incubation followed by centrifugation at 9300xg for 2min). The column was transferred to a clean collection tube and centrifuged at 16200xg for 3min to remove any remaining ethanol. Finally, the RNeasy column was transferred to a clean eppendorf and 25µl RNase free, DNase free water was added to the centre of the column, which was centrifuged for 2min at 9300xg. The sample was then passed through the column again to maximise RNA yield.

2.6.2 Reverse transcription

Reverse transcription was carried out using avian myeloblastoma virus (AMV) reverse transcriptase (RT) (Life Technologies Ltd).

Prior to reverse transcription, any residual DNA was eliminated from the samples using DNase 1. For this step, 1µl 10x DNase buffer solution and 1µl DNase (1unit/µl) were added to 8µl of total RNA and incubated at room temperature for 15min. The reaction was terminated with the addition of 1µl stop solution (50mM EDTA) and incubated at 70°C for 10min. The samples were then chilled on ice before reverse transcription.

DNase treated samples were incubated with 1µl oligo$(dT)_{20}$ primers (2.5µM final concentration) (Life Technologies Ltd) and 2µl 10mM deoxyribonucleotide triphosphate (dNTP) mix (10mM each dNTP, 1mM final conc) (Life Technologies Ltd) at 65°C for 5min, to prevent RNA secondary structures inhibiting the reaction, and then placed on ice. Next, 4µl 5x cDNA synthesis buffer (250mM Tris-Acetate pH 8.4, 375mM potassium acetate, 40mM magnesium acetate), 1µl 0.1mM dithiothreitol (DTT), 1µl AMV-RT (15units/µl) (all from Life Technologies Ltd) and 1µl Riboblock RNase inhibitor (40units/µl) (ThermoScientific) were added to the RNA samples. The samples were gently mixed and incubated for 1h at 45°C in a thermal cycler and the reaction terminated by heating at 85°C for 5min. The samples were stored at -20°C until use.

2.7 End-point polymerase chain reaction

End point PCR is usually a qualitative rather than quantitative method used to identify the expression of mRNA, miRNA or other NTP in a particular system. This method, like real time PCR (see next section), utilises polymerase enzymes from archaea bacteria (thermophiles) that have optimal activity at high temperatures. A cDNA sample is added to specific primers for the region of interest along with the hot start polymerase. Amplification of the target sequence is achieved by repeating three temperature stages up to 45 times. The first stage (annealing) is ~60°C to allow specific primers to bind, the second stage (extension) is ~90°C to allow the polymerase to extend the sequence from the primers and the third stage (dissociation) is ~70°C to cause the dissociation of newly formed double stranded DNA into single strands for the next round. After the cycle has finished the products are separated by agarose gel electrophoresis.

This method can be used for quantitative analysis if 2 products are amplified in the same reaction and then separated e.g. exon/intron incorporation in mRNA.

2.7.1 Primer design

Primer design was carried out using the publically available Primer3 program (http://primer3.ut.ee). The target mRNA sequence was sourced and its complementary cDNA strand formed (to allow a forward and reverse primer pair to be created). Primers were selected by choosing an ~18-22 nucleotide stretch that had 40-60% GC content, less than 4 runs of the same nucleotide or dinucleotide repeats (e.g. ACCCC or ATATAT), minimal secondary structure formation, minimal potential to form primer dimers, and for which both primers have similar melting temperatures between 60-70°C. Primers were ordered from Eurofins Genomics (Eurofins Genomics, Germany).

2.7.2 End-point PCR for analysis of *tfpi* mRNA

RNA samples were extracted from isolated monocytes as described in sections 2.6.1.1 and 2.6.1.2 and cDNA prepared as described in section 2.6.2. Each 0.2ml sample tube contained template cDNA, 2µl 10x CoralLoad PCR buffer, 2mM MgCl2, 0.2mM dATP/CTP/TTP/GTP, 0.625µM forward and reverse primers, 0.1µl HotStarTaq plus DNA polymerase to a total volume of 20µl (all reagents from Qiagen). The samples were then amplified using the following program: 95°C for 5min; 35-45 cycles at 94°C for 30s, 57°C for 30s and 72°C for 90s; the reaction finished by 10min incubation at 72°C (Ellery et al., 2014).

PCR products were separated using a 2% agarose gel. Briefly, 6g agarose was dissolved in 300ml 1x Tris-acetate-EDTA (TAE) buffer (40mM Tris, 20mM glacial acetic acid, 1mM EDTA pH8) by heating until fully dissolved. Once dissolved the agarose solution was allowed to cool for 5min before the addition of 30µl GelRed™ (Life Technologies) and the gel cast. Once set (~40min) the comb was removed and 10µl of PCR product loaded into each well. No loading buffer was needed as CoralLoad PCR buffer acts directly as a loading buffer without effecting the PCR reaction. The gel was run at 130v for 3-4h and bands visualised using the UV light setting on the ImageQuant Las4000 (GE Healthcare). Densitometry was calculated using the ImageQuant 8.1 program (GE Healthcare).

2.8 Real-time polymerase chain reaction

The real time polymerase chain reaction (RT-qPCR) is a quantitative method for measuring the levels of a specific mRNA transcript within a sample. There are 2 methods used to carry out the RT-qPCR reactions, these are SYBR green and TaqMan®. SYBR green dyes detect all double stranded DNA formed during the reaction. As the amount of product increases the fluorescence increases proportionally. This method has two main advantages in that it is cost effective and can be used to measure amplification of any double stranded DNA so is useful when designing primers. Its main disadvantage is that it binds to all double-stranded DNA and so will detect primer dimers, although this can be checked by including a melt curve in the analysis. The TaqMan® method uses fluorescent probes that are specific for the target. In the absence of the target sequence the quencher on the probe prevents fluorescence. When the target is present the probe binds and is cleaved by the polymerase, releasing the quencher and allowing fluorescence resonance energy transfer (FRET). Due to the number of reactions to be carried out over the course of the project and the availability of primers to the genes of interest, the SYBR green method was used to detect amplification of specific targets. This study used a 96 well plate format that simultaneously measured the housekeeping gene and gene of interest in the experimental conditions.

As the reaction progresses through cycles of PCR, the fluorescence is measured during each cycle and an amplification plot produced. This is used to set a threshold during the exponential stage where the amount of PCR product is increasing fastest. The C_T (cycle threshold) value is the cycle at which the fluorescence emission exceeds the set threshold in that sample. The higher the copy number of a transcript at the start the sooner the fluorescence will cross the threshold and the lower the C_T value (figure 2.3).

Quantitative PCR can be used to calculate both the actual amount of a particular mRNA and its relative expression compared to a housekeeping gene. In this study the relative expression method was employed to calculate the fold change of the genes of interest under different conditions relative to the house keeping gene β-2 microglobulin (B2M), as this was found to show least variation in monocytes in previous studies from this group.

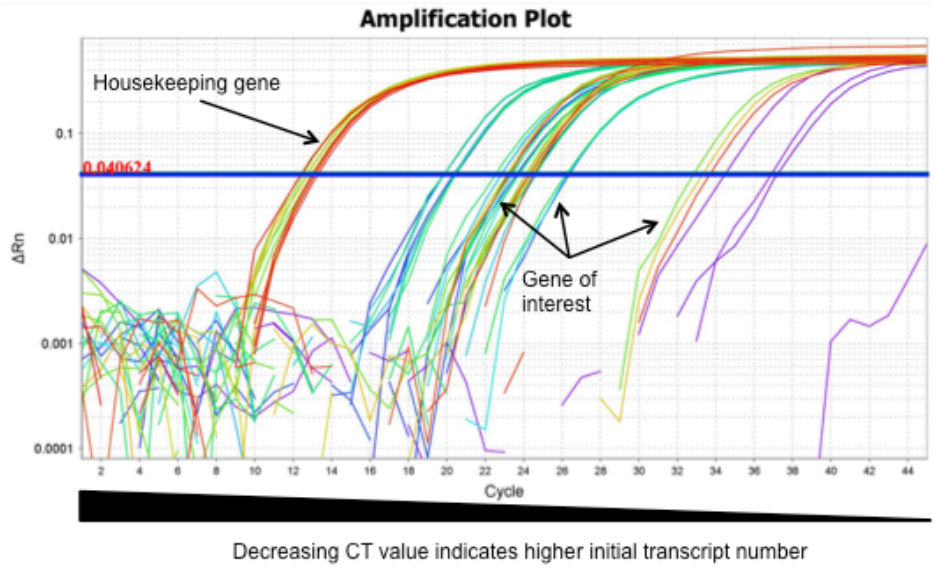

Figure 2.3: Representative example of CT values

Traces indicate the fluorescence reading of each well. As the number of cycles increases the fluorescence increases proportionally, The cycle threshold (red line) is set where the fluorescence is increasing maximally

2.8.1 Sample preparation and cycle conditions

RT-qPCR was carried out in 96 well plates using 2x QuantiFast SYBR green master mix (Qiagen) (12.5µl/well), QuantiTect primer solution (Qiagen) (2.5µl/well) and RNase, DNase free water (Qiagen) (8µl/well) along with the cDNA sample. The details of primers used are given in table 2.1.

Table 2.1: Quantitect primers used for RT-qPCR reaction

Primer	Detected Transcript	Ensembl transcript ID	Length of detected Transcript	Amplified Exons	Amplicon Length
B2M	NM004048	ENST00000349264	987 bp	1/2	98 bp
TFPI	NM006287	ENST00000233156	3927 bp	3/4/5	121 bp
PROCR	NM006404	ENST00000216968	1483 bp	2/3	149 bp
PPARγ	NM005037	ENST00000309576	1818 bp	6/7	113 bp

Reactions were carried out in triplicate to ensure the reproducibility and accuracy of the PCR reaction. A no-template control was also included in which the cDNA was replaced with RNase-free, DNase-free water. The PCR reaction was carried out using either a 7900HT PCR machine or a ViiA™ 7 Real-Time PCR machine (both from Applied Biosystems, Life Technologies Ltd). The reaction conditions were carried out

according to the manufacturer's instructions; briefly samples were heated to 50°C for 2min and then 95°C for 5min before 40 cycles of: 95°C for 10s followed by 60°C for 30s. After the last cycle a melt curve was produced and the reaction terminated. Primers were assessed upon reconstitution for efficiency, reproducibility and coefficient of determination (R^2) to determine if the assays were optimal. For this, cDNA samples from 6h stimulated monocytes were used as these preparations generally showed the highest expression of the genes being studied. A 10-fold serial dilution was set up and the PCR reaction carried out as described above. The CT was plotted in triplicate and the slope and R^2 calculated using linear correlation (figure 2.4). Assay conditions are considered optimal when the R^2 value is >0.98, which also indicates closeness of replicates and the PCR efficiency is between 90-105%.

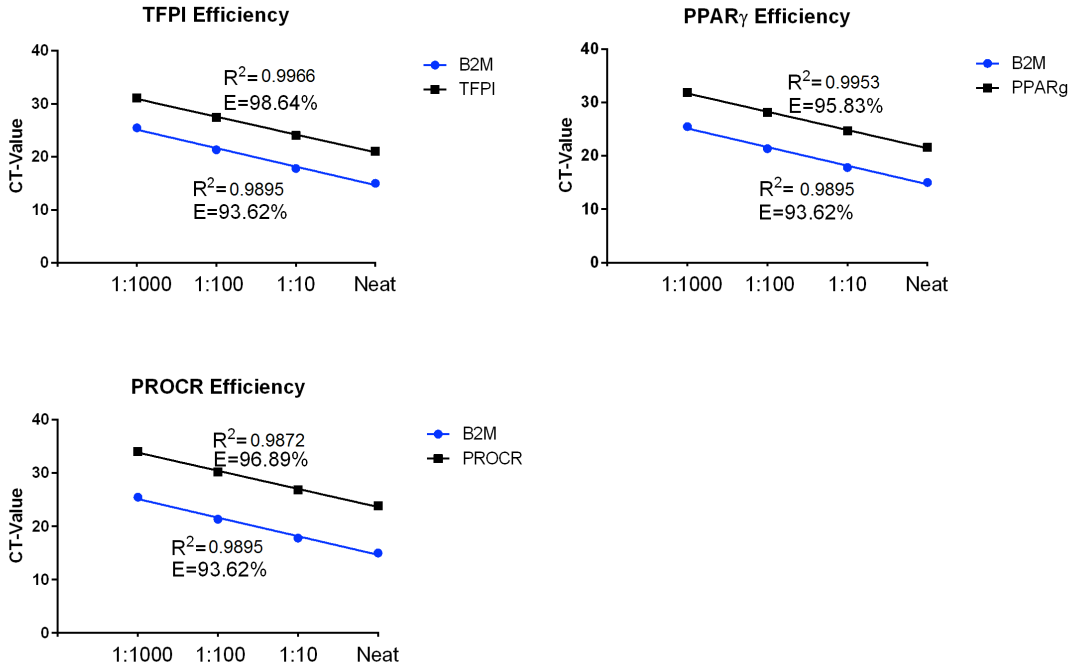

Figure 2.4: Efficiency and reproducibility of reconstituted primers

cDNA prepared from 6h CRP-XL stimulated monocytes was used to prepare a 10-fold dilution series and RT-qPCR reactions set up using reconstituted primers. Resulting CT values were averaged and plotted Vs. dilution factor to calculate primer efficiency and reproducibility.

2.8.2 Statistical analysis of RT-qPCR data

The CT values were used to calculate the fold change of the gene of interest under the different conditions compared to the housekeeping gene using a variation of the $2^{-\Delta\Delta CT}$ equation. Briefly, the T0 triplicate values for the housekeeping gene were averaged for

each donor and then an average T0 calculated between all donors. This was repeated for the gene of interest T0 values. Once these had been calculated, the fold change for the gene of interest was calculated for each individual donor using equation 1 (table 2.2). By incorporating the overall average at time 0, the inherent variation seen between donors is normalised. The results were then plotted using GraphPad Prism and appropriate T-tests carried out to determine the P-value.

Equation 1: Fold Change=$2^{-((CT(GOI)-CT(HK))TimeX-(CT(GOI)-CT(HK))Time0)}$

Where CT is cycle threshold, GOI is gene of interest, HK is housekeeping gene, timeX is CT values at incubation time and time0 is CT values at time 0.

Table 2.2: Calculated fold change using modified ΔΔCT method

Data shown for 2 genes, each tested in 2 donors in duplicate (CT1, CT2), calculated using equation 1.

Donor	**Gene**	**Time Point**	**CT1**	**CT2**	**CTavg**	**Combined average**
1	B2M	0h	14.76179	14.33358	14.54768	15.16501
2	B2M	0h	16.02596	15.5387	15.78233	
1	TFPI	0h	30.91259	31.18597	31.04928	31.14646
2	TFPI	0h	31.17098	31.3163	31.24364	
Donor	**Gene**	**Time point**	**CT_{avg} sample**	**CT T_0 avg all donors**	**2^-ΔΔCT (fold change)**	
1	B2M	0h	14.5476845	15.16500625		
1	B2M	6h	15.15361833	15.16500625		
1	TFPI	0h	31.049278	31.14646075	0.697304646	
1	TFPI	6h	22.447509	31.14646075	412.3037673	
2	B2M	0h	15.782328	15.16500625		
2	B2M	6h	14.898715	15.16500625		
2	TFPI	0h	31.2436435	31.14646075	1.434093413	
2	TFPI	6h	23.77088267	31.14646075	138.0729439	

2.9 Flow Cytometry

Flow cytometry is a technique that is used to measure the size and granularity of cells and the expression of macromolecules on the surface or within cells, fixed or alive. The sample is injected into the flow machine and, through hydrodynamic focusing, is forced into a single stream of cells. These pass through lasers (whose number can vary between 1 and 4 depending on the instrument) and the signal is converted from

analogue to digital and the results depicted as a dot plot or histogram. The laser light that reflects off at narrow angles (forward scatter (FSc)) is collected and reflects the size of the cells; the light that deflects at 90° (side scatter (SS)) represents the granularity. This allows populations of cells to be distinguished from within a complex mixture, such as blood. Macromolecules are detected using fluorescently conjugated antibodies and proteins. These are excited by, and emit fluorescence at, specific wavelengths that are detected by photomultipiers (PMTs). For example Fluorescein Iso-ThioCyanate (FITC) is excited by a blue laser at 488nm and emits at 519nm, these two values represent 100% excitement and 100% emission, in reality fluorophores will emit to varying degrees over a wide range a wavelengths (figure 2.5).

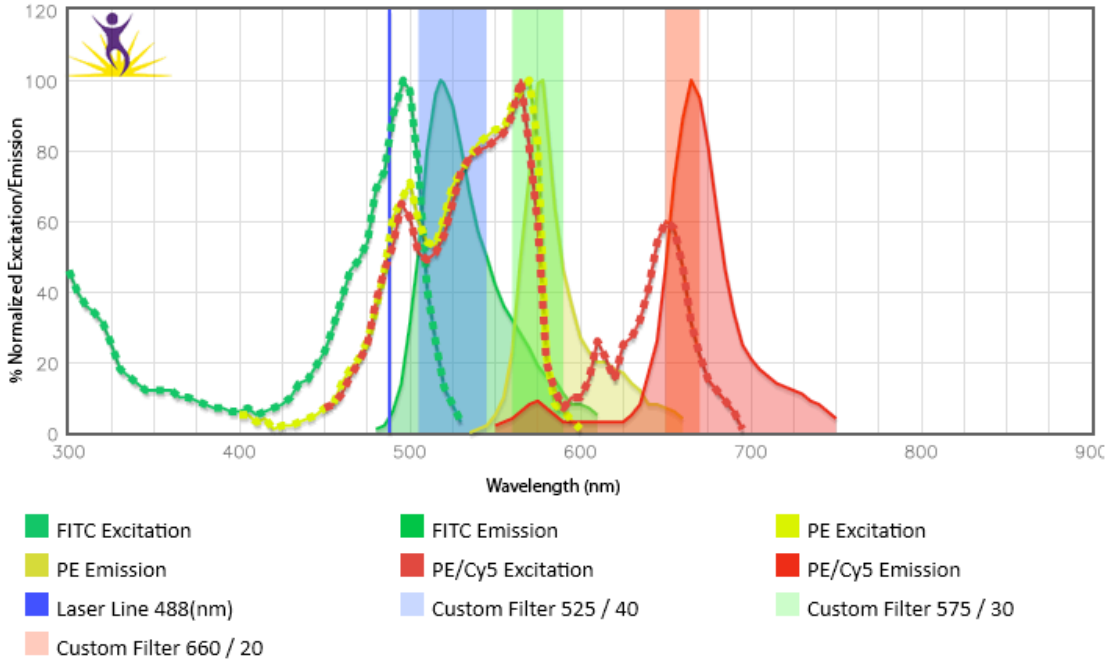

Figure 2.5: Absorption and emission spectra of common fluorophores

Fluorophores are able to absorb and emit fluorescence over a range of wavelengths that can be utilised by flow cytometrists to measure combinations of different fluorophores. Figure obtained from www.biolegend.com/spectraanalyzer.

Fluorescent filters are used to allow particular wavelengths of light pass. A combination of filters and separate PMTs allows multiple fluorophores to be detected simultaneously allowing for analysis of multiple molecules (figure 2.6).

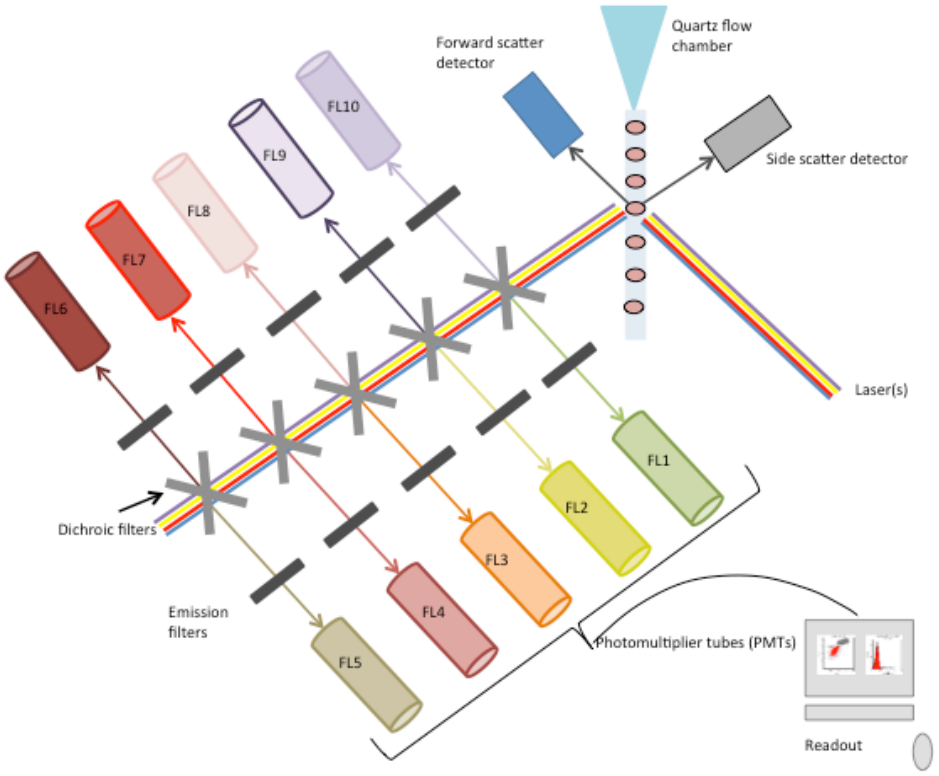

Figure 2.6: Representative layout of a flow cytometer

By using a combination of dichroic mirrors and emission filters, flow cytometers have developed to simultaneously detect up to 10 different fluorophores in a single sample.

A common problem in flow cytometry is spill over of the emission from one fluorophore into another channel. This can be seen from figure 2.5; the emission covers a range of wavelengths so spectra from two fluorophores can overlap. This spill over is only a problem if using more than two fluorophores whose emission wavelengths are not well separated. To correct for this, flow cytometer users have to carry out the process of colour compensation to ensure the results they obtain are true. Compensation can be carried out as the spillover from one fluorophore is a linear function and can be corrected for by aligning the population medians. An example of this can be seen in figure 2.7, the left panel shows uncompensated phycoerythrin (PE) spilling over into the FITC channel, however, after compensation this is a no longer an issue and we can be confident any fluorescence we see in the FITC channel is not coming from PE-labelled fluorophore

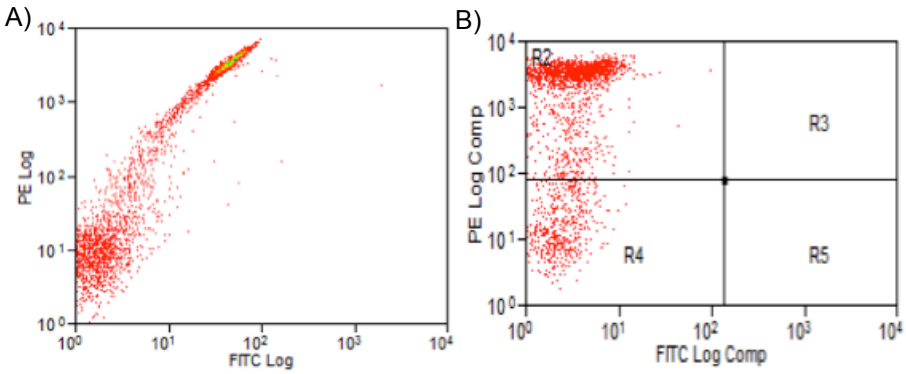

Figure 2.7: Representative examples of uncompensated (A) and compensated (B) data

The figure on the left represents the uncompensated PE-labelled fluorophore spilling into the FITC channel. The figure on the right represents the data after compensation. The PE positive cells are no longer also positive for FITC.

In this study three flow cytometers were used to carry out platelet and leukocyte analysis; an EPICS profile XL-MCL, a Gallios and a CYAN ADP (all from Beckman Coulter).

All antibodies were used at pre-determined optimal concentrations.

2.9.1 Determination of optimal antibody concentrations

All antibodies were titrated in the same way using the same protocols that would be used in the experiment, i.e. incubation times, method of erythrocyte lysis etc. Briefly, 5 concentrations were chosen around the manufacturers recommended concentrations (2 below the recommended and 2 above). Corresponding isotypes were also set up at the same concentration as the primary antibody to account for non-specific binding. Results were plotted as percent positive and median fluorescence (Md X) vs. concentration. A concentration was then selected based on maximal % positive and Md X fluorescence. Figure 2.8 shows a representative titration of a CD14-VioBlue antibody. From the graphs a concentration of 200ng was selected, as there was no further increase in percent positive cells or Md X at higher concentrations.

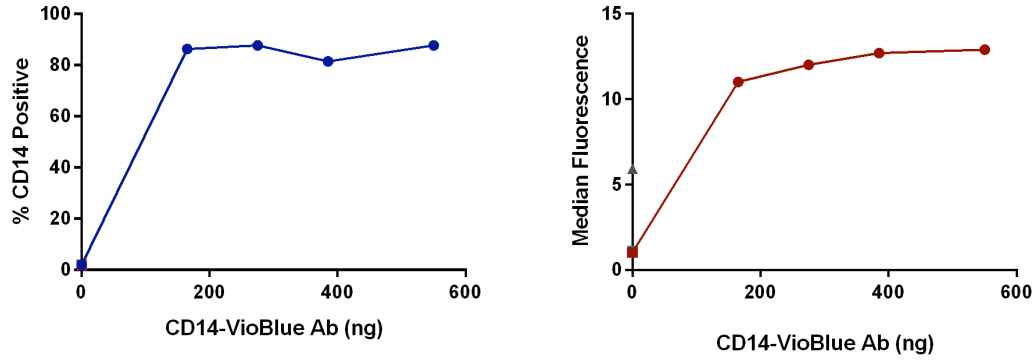

Figure 2.8: Representative example of a primary antibody titration

5 concentrations of primary antibody were chosen based on the manufacturer's guidelines along with concentration matched isotype controls. Titrations were conducted under conditions identical to that of the experiments.

A summary of antibodies used, fluorophore, source and volume added per 50µl whole blood is shown in table 2.3.

Table 2.3: Summary of fluorescently labelled molecules used for flow cytometry

Antibody	Fluorophore	Amount (µl) /50µl whole blood	Source
CD45	RPE	5	BD Biosciences
	PE-Vio770	5	Miltenyi
CD14	RPE-Cy5	5	AbD Serotec
	VioBlue	2	Miltenyi
CD42b	RPE	1	Biolegend
P-selectin	FITC	5	R&D Systems
Protein			
Annexin-V	Alexa Fluo® 647	5	Biolegend
Dye			
7-AAD	N/A	10	Biolegend

Non-specific binding of antibodies was controlled for using isotype matched non-specific antibodies.

2.9.2 Monocyte Platelet Aggregation

To study the interaction of platelets with monocytes, whole blood was stimulated with a predetermined concentration of CRP-XL for 10min at 37°C prior to 1:1 dilution with HBS pH 7.4 containing 5µl anti-CD14-RPE-Cy5 antibody (AbD Serotec, Kidlington, UK; Miltenyi Biotech) to label monocytes and an anti-CD42b-RPE (Biolegend, London, UK (1µl); Miltenyi Biotech (5µl)) antibody to label platelets. After 30min incubation at room temperature, erythrocytes were lysed with either Optilyse C (Epics

XL-MCL and Gallios) or Versalyse (Cyan ADP) (both Beckman Coulter) according to the manufacturer's instructions. Each lysing solution altered the refractive index of the sample so that they were only compatible with the laser configuration of the indicated flow cytometer. Samples were then run on the flow cytometers and the CD14 positive monocyte population gated for CD42b fluorescence (figure 2.9). Gates were set at 2% based on the fluorescence of matched isotype controls.

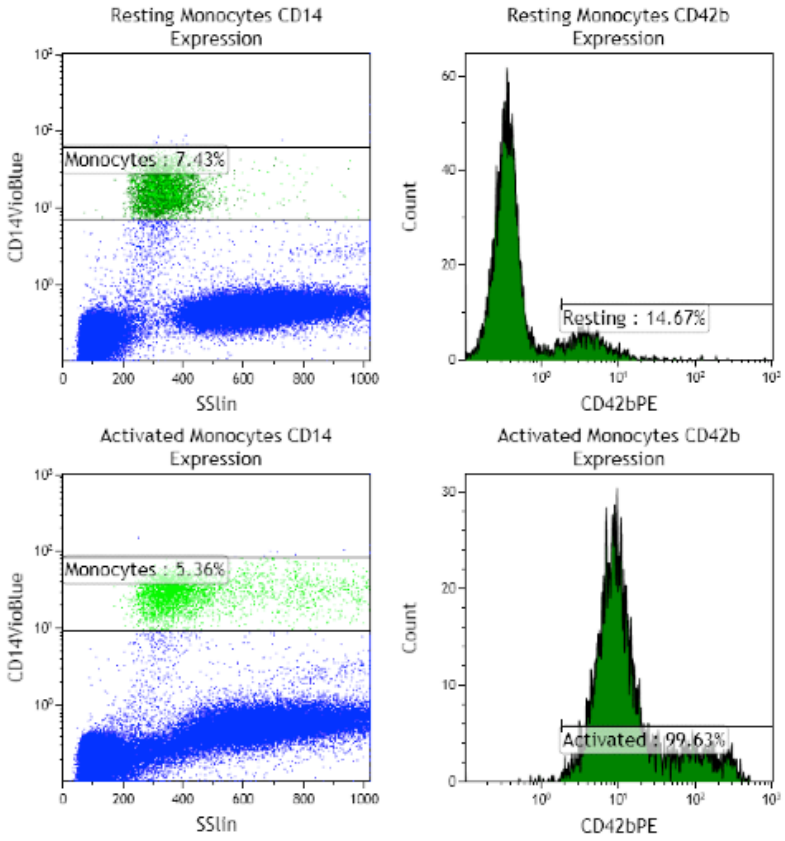

Figure 2.9: Representative example of monocyte platelet aggregation

Whole blood was incubated with fluorescently-conjugated CD14 antibody and CD42b in the absence (top panel) or presence (bottom panel) of 0.5µg/ml CRP-XL.

2.9.3 Platelet P-Selectin Expression

To detect the transfer of P-selectin from platelet α-granules to the membrane as a marker of their activation, platelets either in whole blood, in PRP or after washing were diluted 1:10 with HBS pH 7.4 and incubated with 5µl anti-P-selectin-FITC (R&D Systems, Minnesota, USA) antibody for 20min at room temperature. Samples were then further diluted 1:10 with 0.2% formyl saline (FS) (0.2% v/v formaldehyde, 0.85% w/v saline solution), incubated for 10min at room temperature to allow equilibration of antibody, before a final 1:10 dilution with 0.2% FS. Samples were analysed on the flow

cytometer within 2 hours, gating the platelets on size (FSc) and granularity (SS) and assessed for P-selectin expression, as illustrated in figure 2.10.

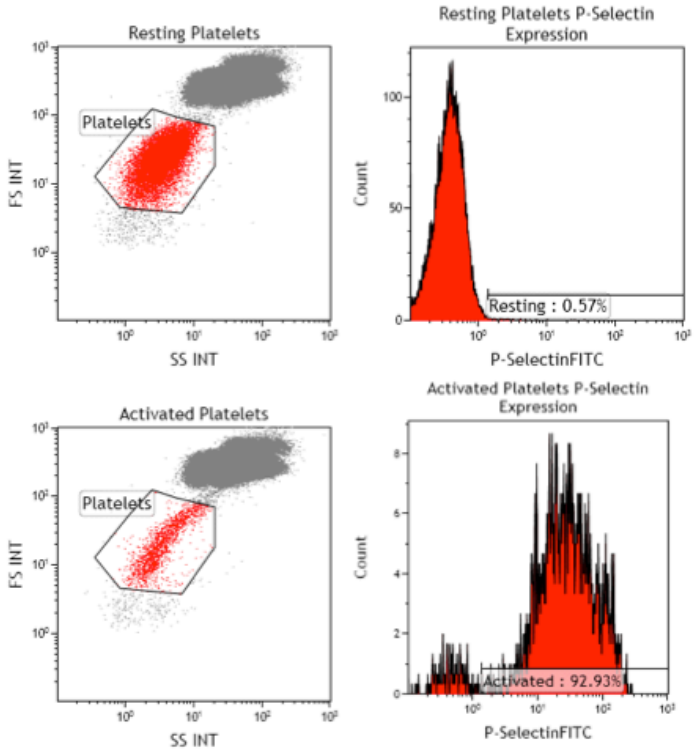

Figure 2.10: Representative example of platelet P-selectin expression

Whole blood was incubated with the fluorescently-labelled P-selectin antibody in the absence (top panel) or presence (bottom panel) of 0.5µg/ml CRP-XL. Note the shape change of platelets in the first histogram reflecting the change from discoid to sphere.

2.9.4 Monocyte purity after isolation

To assess the purity of isolated monocytes with respect to other leukocytes after isolation, whole blood or isolated monocytes were incubated with the pan monocyte marker anti-CD45-RPE (BD Biosciences, Oxford Science Park, UK (10µl); Miltenyi Biotech (5µl)) and the monocyte-specific marker anti-CD14-RPE-Cy5 (5µl) for 30min at room temperature. Erythrocytes were lysed with either Optilyse C or Versalyse before analysis by flow cytometry. Leukocytes were gated on CD45 expression and then total CD14 fluorescence (figure 2.11).

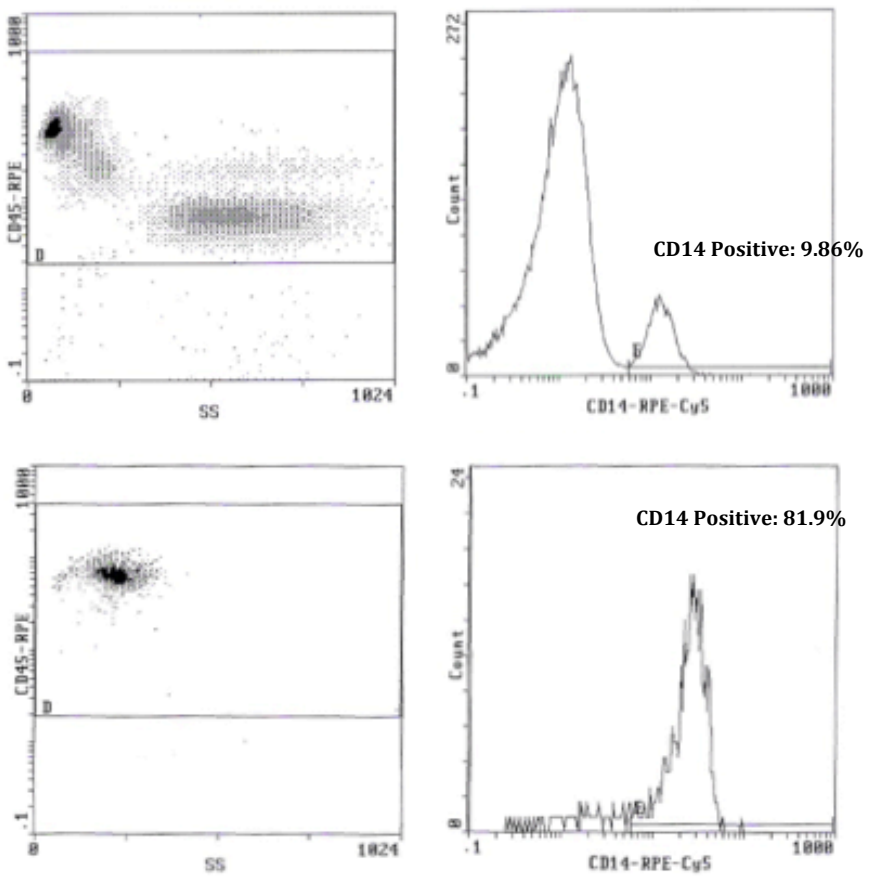

Figure 2.11: Representative example of monocyte purity after isolation

Whole blood or isolated monocytes were incubated with the pan monocyte marker CD45 and the monocyte specific marker CD14. The top panel shows the % of monocytes in whole blood and the bottom panel shows the % of monocytes after isolation.

2.9.5 Monocyte apoptosis and death

To confirm that monocytes were still viable after incubations they were assayed for apoptosis and cell death. Following incubation of whole blood, monocytes were labelled using CD14VioBlue (Miltenyi Biotech) for 30min at room temperature. Cells were centrifuged at 500xg for 10min and resuspended in 1ml Annexin-V binding buffer (HBS pH 7.4 with 2mM Calcium). Samples were then incubated with Alexa Fluor® 647 Annexin-V (Biolegend) for 10min followed by 7-aminoactinomycin D (7-AAD) (Biolegend) for 5 min before analysis. Controls for Annexin-V (without calcium) and 7-AAD (without 7-AAD) were used to set fluorescence to 2%. Apoptosis and cell death were analysed using a two-dimensional dot-plot for Annexin-V vs. 7-AAD (figure 2.12). Annexin-V binds to phosphatidylserine, which is normally present on the inner-leaflet of the plasma membrane but is translocated to the outer-leaflet during apoptosis.

The DNA binding dye, 7-AAD, is unable to enter intact live cells but can enter dead cells. This allows live, apoptotic and dead cells to be discriminated.

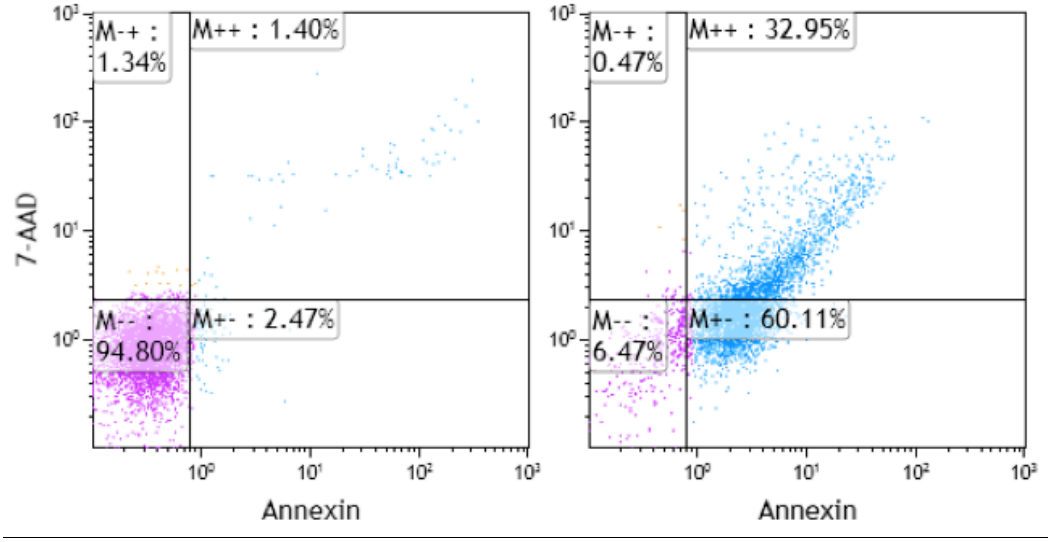

Figure 2.12: Representative example of monocyte cell death and apoptosis

Whole blood or isolated monocytes were incubated with CD14, Annexin-V and 7-AAD before analysis by flow cytometry. Monocytes were gated based on CD14 fluorescence and analysed for Annexin-V and 7-AAD on a dot plot. Shown are representative examples of healthy (A) and apoptotic (B) monocytes.

2.10 Platelet Aggregometry

Developed in the 1960's (Yáñez-Mó et al., 2015b), platelet aggregometry is used to measure platelet aggregation in response to different agonists and inhibitors. The principle of platelet aggregometry is relatively simple and based on light transmission. If platelets are present in a single suspension then they are dispersed in the solution and light transmission is low, however, if stimulated the platelets aggregate into clumps, allowing light to be transmitted through. The transmission of light through each sample is recorded continuously over a set period of time (normally 5-10min). Aggregation was analysed using a PAP8E Platelet Aggregation Profiler (Bio/Data Corporation, Horsham, PA, USA). Whole blood was collected and PRP and PPP prepared as described in sections 2.2.1 and 2.2.2. PPP was used to set the 100% aggregation value and an unstimulated PRP sample used to set the instrument at 0% (no aggregation). Samples of PRP were incubated for 10min at 37°C, with stirring, in the presence or absence of inhibitors (aspirin, $5x10^{-4}$M; esculetin 150µM; baicalein 100µM) before being transferred to the test wells. After incubation, a predetermined concentration of ADP was injected into the PRP sample and recording started immediately. Aggregation was measured over 6min.

Before carrying out experiments, the optimum concentration of ADP to be used with each donor was determined by titration. Five concentrations were used (400nM-4μM) and a dose was chosen that gave the characteristic biphasic response seen with ADP (figure 2.13, lines 3 and 4); most often this was 2μM. To titrate inhibitors, PRP was incubated for 10min with 5 inhibitor doses before activation with the selected ADP concentration.

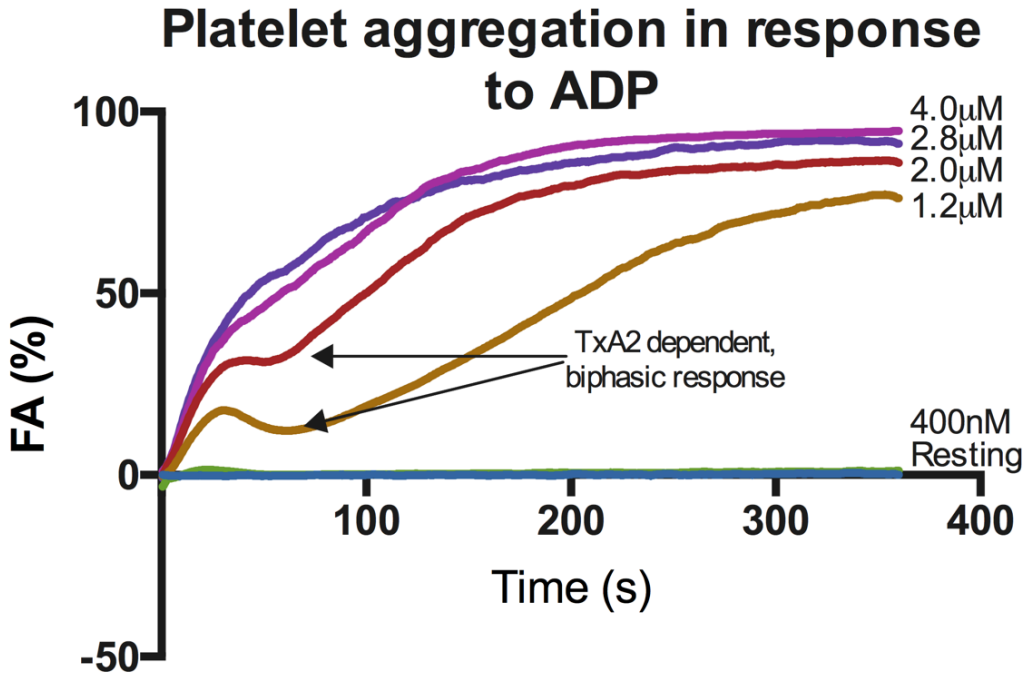

Figure 2.13: Representative PAP8 trace for an ADP titration

PRP was incubated in test wells before the addition of increasing concentrations of ADP. Traces show aggregation in response to increasing ADP concentration: 1) resting, 2) 0.4μM, 3) 1.2μM, 4) 2μM, 5) 2.8μM, 6) 4μM.

2.11 Western Blotting

Western blotting (Towbin et al., 1979) is a technique adapted from Southern blotting, (Southern, 1975). Whereas Southern blotting is used to analyse DNA, Western blotting allows the detection and quantification of the relative expression of proteins in a complex mixture by the use of antibodies. The mixture of protein is first separated by polyacrylamide gel electrophoresis before being transferred onto a nitrocellulose or polyvinylidene fluoride (PVDF) membrane. The membrane is incubated with antibodies to the protein of interest and then with a secondary antibody that recognises the immunoglobulin type of the primary antibody, and is typically conjugated to an enzyme such as horseradish peroxidase (HRP). The signal is visualised using a

chemi-luminescence instrument and if the protein of interest is present in the sample then a band or bands should be identifiable at the predicted molecular weight(s).

2.11.1 Protein extraction

2.11.1.1 Protein extraction using RIPA buffer

Isolated cells were adjusted to $2x10^6$/ml and centrifuged at 500xg for 5min. The supernatant was removed and cells re-suspended in 1ml RIPA buffer (150mM NaCl; 50mM TRIS pH 7.4; 0.5% sodium deoxycholate; 0.1% sodium dodecyl sulphate (SDS); 1% IGEPAL CA630) containing 1 cOmplete Ultra protease inhibitor cocktail tablet (Roche Diagnostics Ltd, West Sussex, UK) (Cat. No. 05-892-988-001) per $2x10^6$ cells. The samples were sonicated for 30s using a Soniprep 150 manual sonicator (MSE Ltd, London, UK) and left on ice for 30min before centrifugation at 16200xg for 10min, to pellet cell debris and insoluble material. The supernatant was transferred to sterile eppendorf tubes and stored at -20°C.

2.11.1.2 Protein extraction using the TRIzol method

Initially, samples were treated as in 2.6.1 but the aqueous upper layer was removed and 0.3ml 100% ethanol added to the organic phase per 1ml TRIzol. After several inversions the samples were left at room temperature for 2-3min before a 5min, 4°C centrifugation at 2000xg to pellet DNA. The supernatant containing the protein was transferred to sterile tubes and 1.5ml isopropanol added per 1ml TRIzol used initially. After incubation for 10min at room temperature the samples were centrifuged at 12000xg for 10min at 4°C to pellet the protein. The protein pellet was washed 3 times in 0.3M guanidine hydrochloride in 95% ethanol (20min incubation followed by centrifugation at 7500xg for 5min at 4°C). After the third wash 2ml of 100% ethanol was added per 1ml TRIzol used initially and vortexed. After 20min incubation at room temperature the samples were centrifuged at 7500xg for 5min at 4°C. The pellet was air dried for 5-10min and 50-200µl 1% SDS added to solubilise the protein. Samples were heated to 55°C to aid solubilisation.

2.11.1.3 Nuclear protein extraction

To study the NR PPARγ, monocyte nuclear proteins were isolated using the NucBuster™ Protein Extraction Kit (Novagen, Merck Millipore) according to the manufacturer's instructions. Briefly, monocytes were isolated using CD14 Dynabeads as described in section 2.2.7.3 and 75µl NucBuster Reagent 1 added per 15ml initial

whole blood used. The suspension was vortexed at high speed for 15s and then left on ice for 5min before a further vortex. At this stage the Dynabeads were removed by two sequential incubations in the MPC. The monocyte lysate was then centrifuged at 16000xg for 5min at 4°C to pellet nuclei. The cytoplasmic fraction was removed and the nuclear pellet washed once with 500µl PBS. The washed pellet was then resuspended in 1µl Protease Inhibitor cocktail, 1µl 100mM DTT and 37.5µl NucBuster Reagent 2 per 15ml whole blood used initially. The sample was then vortexed at high speed for 15s, incubated for 5min on ice and vortexed again before centrifugation at 16000xg for 5min at 4°C. The resulting supernatant contained monocyte nuclear proteins and was stored at -80°C until further use.

2.11.2 Determination of protein concentration

2.11.2.1 Bio-Rad DC protein assay

The DC protein assay (Bio-Rad Laboratories Ltd, Hertfordshire, UK) was used to determine the concentrations of proteins in samples in detergent based solutions. Bovine serum albumin (BSA) standards (0.000, 0.125, 0.250, 0.500, 1.000mg/ml) were prepared by serial dilution using the same detergent based solution used to extract the protein samples. The protein samples were also diluted 1:3 in the same buffer. Standards and samples were pipetted (5µl) in triplicate into a 96 well vinyl disposable plate. The working solution A′ was made by adding 20µl reagent S per 1ml reagent A and 25µl added to each well. After this 200µl reagent B was added to each well and mixed before being left for 15min. The absorbance of the samples was measured at 650nm using a NOVOstar microplate reader (BMG Labtech Ltd, Buckinghamshire, UK). The mean absorbance's of the standard BSA samples were plotted using GraphPad Prism and the unknown sample concentrations interpolated from the standard curve using a least fit squares model.

2.11.2.2 Bicinchoninic acid (BCA) assay

This method of protein determination was used to assay samples for use in mass spectrometry. BSA standards (0.000, 0.025, 0.125, 0.250, 0.500, 0.750, 1.000, 1.500 and 2.000mg/ml) were prepared by diluting the stock BSA solution (2000µg/ml) in the same diluent as the samples (ammonium bicarbonate pH 7.4). The working reagent (WR) was made by adding 50 parts reagent A (sodium carbonate, sodium bicarbonate, BCA and sodium tartrate in 0.1M sodium hydroxide) with 1 part reagent B (containing

4% cupric sulphate) (50:1 v/v). Standards or samples (25µl) were incubated with 200µl WR in a 96 well plate for 30min at 37°C (or 2h at room temperature) before absorbance was measured at 562nm using the NOVOstar microplate reader. The mean absorbance of the standard BSA samples were plotted using GraphPad Prism and the unknown sample concentrations interpolated from the standard curve using a least fit squares model.

2.11.3 Preparation of samples for electrophoresis

To load samples for electrophoresis, 10-50µg of total protein was added (determined from sample concentration) to an appropriate amount of reducing 5x loading buffer (10% SDS; 250mM Tris HCl pH 6.8; 20% glycerol; 0.02% bromophenol blue; 10mM DTT) and Milli-Q water. The samples were then incubated at 100°C for 5min before centrifugation at 9300xg for 30s, and stored on ice until needed.

2.11.4 Sodium Dodecyl Sulphate Polyacrylamide Gel Electrophoresis (SDS-PAGE)

SDS-PAGE allows separation of proteins on the basis of size alone as the SDS binds the protein at approximately 1.4g SDS per gram protein. This masks the natural charge and gives all proteins the same mass: charge ratio. A 10% resolving gel (0.375M Tris/HCl pH8.8, 33.35% Bis/Acrylamide, 0.1% SDS, 0.05% ammonium persulphate (APS), 0.05% tetramethylethylenediamine (TEMED)) was cast in the Mini-PROTEAN 3 gel casting system (Bio-Rad). A layer of propan-2-ol was pipetted onto the resolving gel to remove bubbles and ensure an even gel edge and was left for 40min to set. Once set, the propan-2-ol was removed and the gel washed 3 times with milli-Q water before a 4% stacking gel (0.125M Tris/HCl pH6.8, 13.2% Bis/Acrylamide, 0.1% SDS, 0.05% APS, 0.1% TEMED) was pipetted onto the resolving gel. A 10 well comb was placed into the stacking gel and allowed to set for 30min.

Once set the glass plates were removed from the casting stand and assembled in the electrophoresis tank. A 1x tris-glycine-SDS (TGS) running buffer was prepared from a 10x stock (0.25M Tris pH 8.6, 1.92M glycine, 1% SDS) (Affymetrix UK Ltd, High Wycombe, UK) and poured into the chamber. The combs were removed and the samples loaded into the wells along with a protein ladder (Thermo Scientific) for MW determination. The gel was then run at a constant voltage of 100v for 15min then 120v for 90min.

2.11.5 Western Blotting

After electrophoresis, the stacking gel was removed and each resolving gel placed in transfer buffer (20.5mM Tris, 150mM glycine, 20% methanol) for 20min to equilibrate. A PVDF transfer membrane was prepared by incubation for 10s in methanol followed by 5min in milli-Q water before being placed in transfer buffer for 10-15min. Western blotting cassettes were then assembled white side down in the following order: sponge, filter paper, membrane, gel, filter paper, sponge (all pre-soaked in transfer buffer). The cassettes were then closed and placed in the holder in the correct orientation. The wet transfer was run at 115v for 72min. The cassette was then dismantled and the membrane used immediately for immuno-detection.

2.11.6 Protein Detection

To block non-specific binding, membranes were incubated in tris-buffered saline (TBS) (137mM NaCl; 25mM Tris; 2.7mM KCl; pH 7.4) containing 1% Tween-20 (TBS/T) and 5% (w/v) non-fat milk powder (Marvel) for 1h at room temperature with gentle agitation. The primary antibody solution was then made up in TBS/T with 5% milk powder and incubated overnight at 4°C. Membranes were washed 3 times for 5min in TBS/T and secondary antibodies added in TBS/T with 5% milk unless otherwise stated (table 2.4) and incubated for 1h at room temperature. The membranes were washed 3 times for 5min in TBS/T before being developed using a 1:1 ratio of solutions A and B from the ECL prime chemiluminescent western blotting developing kit (GE Healthcare Life Sciences, Buckinghamshire, UK). The membranes were allowed to develop for 5min before excess solution was removed and the membranes visualised using the ImageQuant Las4000 (GE Healthcare).

Actin was used as a loading control as it was thought to be the most stable and is commonly used for western blotting normalisation. All secondary antibodies were conjugated to HRP.

Table 2.4: Primary and secondary antibodies used for western blotting

Antibody	Dilution	Company	Secondary	Dilution	Company
TPFI (pAb)	1:2000	R&D systems	Anti-goat	1:5000	R&D systems
EPCR (mAb)	1µg/ml	Abcam	Anti-mouse	1:5000	Abcam
PPARγ (mAb)	1:500	Santa Cruz	Anti-rabbit	1:10000	Abcam
Actin (mAb)	1:5000	Abcam	Anti-mouse	1:5000	Abcam
TBP (mAb)	1µg/ml	Abcam	Anti-mouse	1:5000	Abcam

2.11.7 Multiple Antibody analysis and stripping and re-probing membranes

In some cases it was necessary to probe membranes for multiple proteins. If this was the case, membranes were stripped and re-probed.

To strip membranes for re-use they were first washed 3 times in TBS/T (30s each) before two 10min incubations in mild stripping buffer (200mM glycine, 0.1% SDS, 1% Tween20, pH2.2). Stripping buffer was removed by two 10min washes in PBS followed by two 5min washes in TBS/T. The membrane was then ready to be blocked and re-probed.

2.12 Quantification of platelet-derived proteins and oxylipins by LC-MS/MS

Mass spectrometry (MS) can trace its roots back to the late 1910's when the work of Thomson, Aston and Dempster built early mass spectrometers for the identification of elemental isotopes. Aston identified 212 of the 278 naturally occurring isotypes whilst Dempster is credited with creating the first modern MS. During the first half of the 20th century the capabilities of MS was recognised and played important roles in the Manhattan project as well in the petroleum industry. It wasn't until the second half of the century though until the potential of MS was seen for protein and lipid analysis (http://www.chemheritage.org/research/institute-for-research). Now MS is able to analyse complex mixtures of proteins, lipids, oligosaccharides, oligonucleotides and detect a number of post-translational modifications such as phosphorylation.

Early MS approaches had been severely limited due to the lack of techniques to ionise molecules and transfer them into the gas phase without fragmentation. This changed with the development of electrospray ionisation (ESI) and matrix assisted laser desorption/ionisation (MALDI). These catalysed the production of more sophisticated

analysers and spearheaded the field of proteomics and lipodomics. Before this, MS had mainly been used to determine the amino acid sequence of known polypeptides and provide structural information on known molecules (Domon and Aebersold, 2006).

The principle of ESI is based on molecules being dissolved in a volatile solvent that is forced through a capillary. At the end of the capillary a large electric charge disperses the solvent into an aerosol of charged droplets that are directed by a nebulising gas. The solvent evaporates with the aid of a warm drying gas and the resulting ions pass into the analyser (Fenn et al., 1989). MALDI on the other hand uses a laser and matrix. The sample is dissolved in a volatile solvent and mixed with a solution with a vast of excess of matrix e.g. sinapinic acid. An aliquot is added to the sample target and allowed to dry before placement in the high vacuum of the MS. A laser is directed at the sample/matrix mixture and the matrix transforms the laser energy to excitation energy for the sample, which is then dispersed from the surface and can be detected (Karas and Hillenkamp, 1988). MALDI is most commonly coupled to time-of-flight (ToF) analysers.

There are a number of different analysers available to researchers that each have their own advantages and disadvantages discussion of which is beyond the scope of this thesis. ToF analysers determine post-translational modifications and the mass charge ratio of peptides based on the time taken for the charged peptide to travel the length of a tube with specified length under vacuum. Ion trap (IT) analysers trap ions in the device allowing accumulation over time. IT analysers have good sensitivity and high throughput capabilities but low ion-trapping capacity and mass accuracy but this has been somewhat overcome with the introduction of linear IT (Domon and Aebersold, 2006). Another type of IT analyser is the Fourier transform-ion cyclotron resistance (FT-ICR) that require a magnet (usually a superconductor), ion trapping cell, high vacuum and sophisticated data system, similar to nuclear magnetic resonance (NMR). These have proved very useful in terms of resolving power and mass accuracy resulting in better data quality (Scigelova et al., 2011). Most recently, the orbitrap mass analyser, based on a number of the already described analysers, has been introduced. The orbitrab MS is new generation and gives enhanced sensitivity and mass accuracy compared to other machines (Q. Hu et al., 2005). Most of these analyses are used in combinations with 1-4 quadropules that select specific M/Z charges, provide collision and further selection, all with the hope of increasing sensitivity and accuracy.

Even with the impressive advances in MS over the past 3 decades the ultimate goal of being able to detect the full proteome or lipodome of a cell is far off. This is mainly due

to the complexity of the material being analysed, with more than several thousand proteins spanning up to 10 orders of magnitudes in each cell. For example there are over 1000 lipid entities present in macrophages (Dennis et al., 2010) spanning 6 orders of magnitude, so detecting these remains elusive (Murphy and Gaskell, 2011).

2.12.1 Quantification of platelet-derived proteins by LC-MS/MS

The preparation of the platelet releasates was done by myself, digestion of peptides, running of the samples and peptides assigned by Jatinderpal Sandhu, statistical analysis was carried out by Amirmansoor Hakimi and interpreting the data and analysis carried out by myself.

Platelet releasate was prepared in HBS pH 7.4 as in section 2.2.4 to obtain released proteins. Platelet released proteins were exchanged into 100mM ammonium bicarbonate pH 7.4 buffer using 10kDa MWCO filters (samples were concentrated then diluted in ammonium bicarbonate). Protein concentration was determined by adding 1% sodium deoxycholate and carrying out the BCA assay (section 2.11.2.2). Following protein determination, proteins were reduced by addition of 15mM DTT for 30min at 50°C and alkylated with 20mM iodoacetic acid (IAA) for 30min at room temperature. Proteins were then digested with 1µg trypsin per 25µg protein at 37°C overnight, and digestion was stopped with the addition of 0.1% formic acid (FAc). The resulting peptides were purified using solid phase extraction and concentrated, firstly by evaporating volatile liquids by speed vacuum centrifugation for 2h at 14000rpm followed by rapid freezing of the sample in liquid nitrogen, and then freeze drying at 1mbar and -50°C to lyophilise the peptides. Dried pellets were re-constituted in 10µl of 0.1% FAc + 10µl of 50fMol alcohol dehydrogenase (ADH) as an internal standard, enabling absolute quantitation of the proteins post-analysis.

Tryptic peptides were separated on an Ultimate 3000 RSLC nano high performance liquid chromatography (HPLC) system (Dionex/ThermoFisher Scientific, Bremen, Germany). Samples were loaded onto a Cartridge based trap column, using a 300µm x 5mm C18 PepMap (5µm, 100Å) and then separated using the Easy-Spray pepMap C18 column (75µm x 50cm) with a gradient from 3-10% B in 10min, 10-50% B in 37min, 50-90% in 9min and 90-3% in 26min, where mobile phase A was 0.1% FAc in water and mobile phase B, 80%/20% acetonitrile/water in 0.1% FAc. Flow rate was 0.3µL/min. The column was operated at a constant temperature of 45°C.

The nanoHPLC system was coupled to a Q-Exactive mass spectrometer (ThermoScientific, Bremen, Germany). Separated peptides were ionised using the heated electrospray ionisation source (HESI II) and transported through the ion transfer tube to the S lens, a radiofrequency device that focuses the ions into a tight beam. Ions were then injected into the bent flatapole before they enter the quadrupole mass filter where specific masses are selected. The selected ions travel into the octapole and into the nitrogen filled C-trap collision cell where they are bunched into small packets before being injected into the orbitrap mass analyser (figure 2.14). The orbitrap consists of a barrel like outer electrode and an inner electrode running through the middle. Injected ions become trapped due to the balance between their attraction to the inner electrode and centrifugal forces. This means the ions orbit around the inner electrode as well as along the electrode producing helical travel paths. The trapped ions frequency signal is converted to an m/z spectrum by the Furrier transform.

The Q-Exactive was operated in the data-dependent top10 mode; full MS scans were acquired at a resolution of 70000 at m/z 200 to 2000, with an ACG (ion target value) target of 10^6, maximum fill time of 50ms. MS2 scans were acquired at a resolution of 17500, with an ACG target of 1e5, maximum fill time of 100ms. The dynamic exclusion was set at 30s, to prevent repeat sequencing of peptides.

The raw data files were processed and peptides were assigned to proteins using Proteome Discoverer 1.4. All searches were performed against the UniProt human database (http://www.uniprot.org), with the precursor mass tolerance set at 10ppm with a maximum of 2 missed cleaveages. Carbamidomethyl of cysteine was set as a static modifications and oxidation of methionine was set as a dynamic modification. All analysis was filtered using a 1% FDR (false discovery rate).

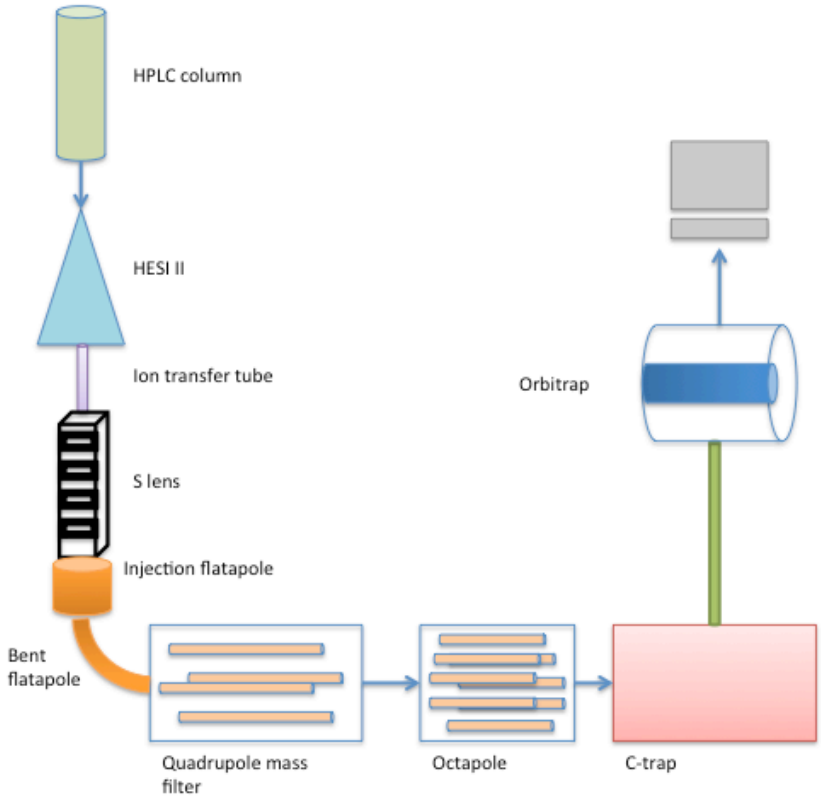

Figure 2.14: Schematic of Q-Exactive mass spectrometer

Digested proteins are separated by HPLC and ionised by electrospray ionisation. After focusing, ions are selected based on m/z and detected by the orbitrap mass analyser.

2.12.2 Quantification of platelet-released oxylipins by LC-MS/MS

Platelet releasate samples were prepared as in 2.2.4, oxylipins were extracted as in 2.2.6 and resuspended in 100µl 70% ethanol. Samples were stored in small glass vials with 200µl glass inserts and lid with PTFE seal (all from Kinesis, St Neots, UK) at -80°C until used for analysis. A standard curve for each analyte as well as quality controls and blanks were extracted alongside the samples. Each sample also contained internal controls (deueterated AA, 15-HETE and PGD2) to account for variation in the extraction, and the anti-oxidant butylated hydroxytoluene (BHT).

Samples were analysed by Katrin Sander using a by a 4000 QTRAP® system (AB SCIEX, Framingham, USA) with a Turbo V™ Ion source with a TurbolonSpray probe (AB SCIEX) coupled to a high performance liquid chromatography system (Shimatsu). The 4000 QTRAP® is a triple quadrupole system allowing tandem mass spectrometry coupled to liquid chromatography (LC-MS/MS). Analysis was in negative ion mode as oxylipins have a weakly acidic group (OH) that can lose its proton and become negative. Each sample (20µl) was injected onto an HPLC column (ACE 3 C18

150x2.1mm) and analytes were separated according to their chemical properties using mobile phase A (deionised water/0.02% FAc) and mobile phase B (acetonitrile:methanol (4:1) with 0.02% FAc) at 300µl/min. Ionisation was induced by the nebulizer gas (30psi), heater gas (30psi) and curtain gas (10psi) at 450°C (ESI). Molecules of a specific m/z were selected using the first quadrupole mass analyser which uses electric currents to stabilise ions of a particular m/z, directing them through the analyser whilst all other ions are lost (figure 2.15).

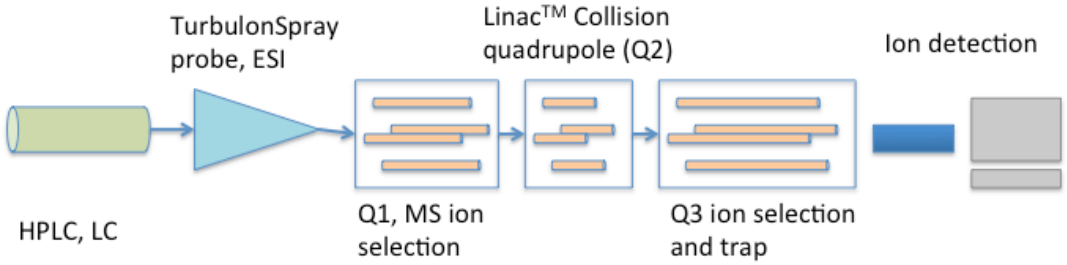

Figure 2.15: Schematic of a 4000 QTRAP® mass spectrometer

Extracted oxylipins were separated by HPLC and ionised before entering the triple quadrupole of the QTRAP. After ion selection and collision, the ions are trapped and detected based on characteristic m/z peaks.

After selection, ions travelled into the LINAC™ collision cell, where the high pressure accelerated the ions through the collision quadrupole and were fragmented into characteristic smaller ions through collision with gas molecules. Each analyte was analysed under a set of pre-specified conditions (table 2.5) obtained by analysing analytes individually.

Table 2.5: Ion pairs and analytical parameters for oxylipin LC-MS/MS

Analyte	Precursor ion (m/z value)	Production (m/z value)	Depolarising potential (eV)	Collision energy (eV)	CXP (eV)
8-HETE	319.24	155.07	-65	-20	-9.89
9-HETE	319.24	123	-70	-23	-6.6
11-HETE	319.24	166.9	-65	-22	-11
12-HETE	319.24	178.9	-75	-20	-3
15-HETE	319.24	301.1	-55	-18	-13
20-HETE	319.24	301	-85	-22	-19
8,9-EET	319.24	155.08	-72	-17	-9.74
9-HODE	295.23	171.102	-60	-30	-10
13-HODE	295.23	195.138	-60	-28	-10
9-OxoODE	293.21	185.12	-85	-28	-12
13-OxoODE	293.21	113.1	-75	-28	-8
PGD/E2	351.22	271.21	-40	-25	-20
TXB2	369.23	169.09	-50	-25	-10
6-KetoPGF1a	369.1	162.8	-31	-36	-12
Linoleic acid	279.23	279.23	-75	-10	-7
AA	303.23	259	-85	-22	-7
AA-d8	311.28	267.29	-50	-20	-10
PGD2-d4	355.24	193.15	-45	-29	-10
15(s)-HETE-d8	327.29	226.25	-67	-20	-3.97

The fragmented ions then travel to the third quadrupole where the ions are prevented from exiting by applying a voltage to the exit lens. After a predefined time period a voltage is applied to the entrance lens and the ions are trapped in the third quadrupole with no other ions entering. The voltage is then increased from low to high until a voltage is reached that causes masses to resonate at the same frequency as the quadrupole. This gives them enough velocity to overcome the exit barrier voltage where they are detected.

Collected ion spectrum data were analysed using the Analyst software (AB Sciex UK Ltd, Warrington, UK) by both myself and Katrin Sander. Firstly, internal standards were analysed to calculate the standard deviation across all the samples extracted. If the standard deviation was below 15% in all internal controls, analysis continued. Internal control values were integrated into the results for each analyte and the peak area for the analyte and internal control calculated using the software. Table 2.5 indicates which IC was used for each oxylipin.

Table 2.6: Internal control used for each oxylipin

Oxylipin	IC
AA, LA	AA-d8
8,9,11,12,15,20-HETE, 8,9-EET, 9,13-oxoODE, 9,13-HODE	15-HETE-d8
TXB2, PGD/E2, 6-keto-PGF1a	PGD2-d4

The peak area fraction for each analyte in the sample was calculated (= analyte peak area / internal standard peak area), correcting for variation between the samples due to the matrix effect, extraction efficiency and variations in the injection volume. The standard curve for each analyte was plotted as peak area fraction (of standards) vs. concentration (nM). Unknown concentrations were interpolated using either linear regression or the hyperbola (where X is concentration) methods.

Concentrations of analytes in samples were corrected for volume:

= (Concentration (nM) / volume of sample extracted (0.8ml)) x final volume of extracted material (1.09ml),

Converted to ng/ml:

= (Concentration (M) x MW) x $1x10^{6}$

Then normalised to 600 x 10^{9} platelets. L^{-1}:

= Concentration (ng/ml) / (platelet concentration ($10^{9}.L^{-1}$*) (before activation) /* $600x10^{9}. L^{-1}$*)* (table 2.7).

Table 2.7: Representative calculation of concentrations of AA in LC-MS/MS samples

Interpreted concentration (nM)	Corrected concentration based on volume extracted	Conversion of nM to ng/ml (MW AA 304.47)	Normalisation to 600 x 10^{9} platelets. L^{-1}
356.94	486.33	148.07	195.26
420.87	573.44	174.60	215.12
433.31	590.38	179.75	216.14
324.98	410.87	134.82	180.96

2.13 Transactivation

Transactivation assays can be used to measure the activity of a transcription factor in response to agonists or antagonists. Called a one-hybrid system, the assay is derived from the mammalian two-hybrid system, which is designed to see if two proteins interact. In the conventional two-hybrid system a bait protein is fused to the Gal4-DBD and a potential interaction partner is fused to VP16. These are expressed in a mammalian cell along with a plasmid encoding a reporter gene (e.g. luciferase) downstream from the Gal4 response element. If the two proteins interact VP16 will be

brought into close proximity and will be able to initiate transcription of the reporter (figure 2.16a), if they do not interact than there will be no transcription (figure 2.16b). Transactivation only requires the transcription factor to be bound to the Gal4-DBD. Mammalian cells, as opposed to yeast or bacteria, express the co-repressors, co-activators and other regulatory proteins that control the activity of most transcription factors, although the levels of these may vary between cells leading to different results between cell types. To investigate the effects of ligand binding to nuclear receptors in this assay, the plasmid containing the nuclear receptor ligand binding domain (NR-LBD) fused to the Gal4-DBD is expressed in a mammalian cell line and the endogenous regulatory proteins act to control transcription of the reporter gene and reference gene (figure 2.16c), upon addition of a ligand the regulatory proteins associated with the LBD change and transcription rate is either increased or decreased (figure 2.16d).

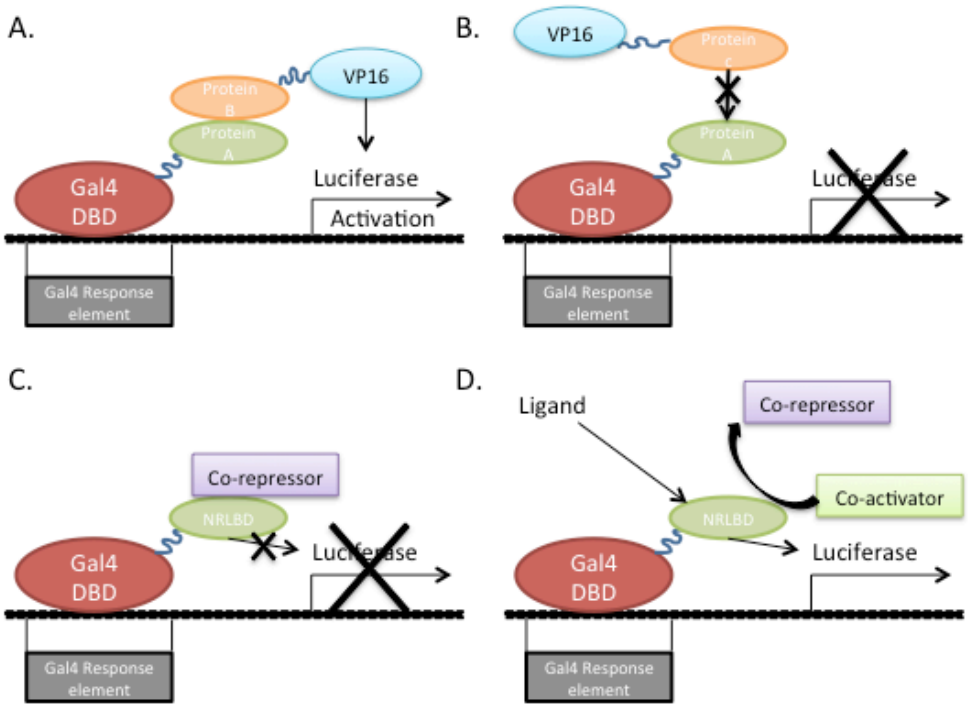

Figure 2.16: Schematic of mammalian one and two-hybrid assays

Mammalian two-hybrid system representing when 2 proteins interact (a) and do not interact (b) and the one-hybrid system showing without (c) and with (d) ligand.

2.13.1 Method of transactivation

Trypsinised 293T cells were adjusted to $5x10^5$cells/ml in complete medium before $1x10^5$ cells were seeded into a 48 well plate and cultured for 24h. Plasmid mixes were prepared containing:

- 0.18µg β-Gal plasmid (transfection control)
- 0.23µg TK-Luciferase plasmid (reporter)
- 0.1µg of plasmid encoding the PPARγ-LBD fused to GAL4-DBD.

Plasmid mixes were incubated at room temperature for 20min with DPBS (50µl) containing 0.25mM Polyethenimin (PEI) before being diluted 1:1 with DMEM without serum and vortexed. 293T cells were washed twice with DPBS and incubated for 6h at 37°C in 5% CO_2 with 100µl of the freshly prepared plasmid mix. Then 100µl DMEM with 10% FCS was added and the cells cultured overnight. PPARγ ligands (rosiglitazone, 15d-PGJ_2, 12-HETE, 15-HETE) were added the following morning and the cells cultured for a further 24h. Cells were washed once with DPBS and incubated for 2h at room temperature in lysis buffer (1.25mM Tris pH7.8, 2mM EDTA, 10% Glycerol, 1% Triton-X-100, 2mM EDTA) with gentle rocking, and placed at -80°C for at least 30min to lyse the cells. β-Galactosidase expression was used as a transfection control and for calculating normalised luciferease expression and was measured by adding 100µl β-Galactosidase substrate (0.1M Na_2HPO_4, 1M KCl, 0.1M $MgCl_2$, 0.1M NaH_2PO_4, 0.2% ortho-Nitrophenyl-b-galactoside (ONPG), 50µM β-mercaptoethanol) with 80µl lysed cells in a 96 well plate and incubating at 37°C for 10min. The appearance of a yellow colour indicated successful transfection and absorbance was measured at 420nm using a VICTOR™ X5 Multilabel Plate Reader (PerkinElmer, Cambridgeshire, UK). Reporter activity was measured using a luciferase assay (BioVision, Inc. Headquarters, California, USA) according to the manufacturer's instructions. Lysed cells (20µl) were added to an opaque 96 well plate and 100µl reagent A (containing CoA, ATP, Mg^{2+}) added. The plate was placed in the VICTOR™ X5 Plate Reader and, within 15min, 100µl reagent B (containing Luciferin) was injected, the sample was mixed and luminescence measured within 10s (figure 2.17). Transactivation was calculated using the equation: transactivation = luciferase luminescence / β-galactosidase absorbance. Each experiment was carried out in triplicate.

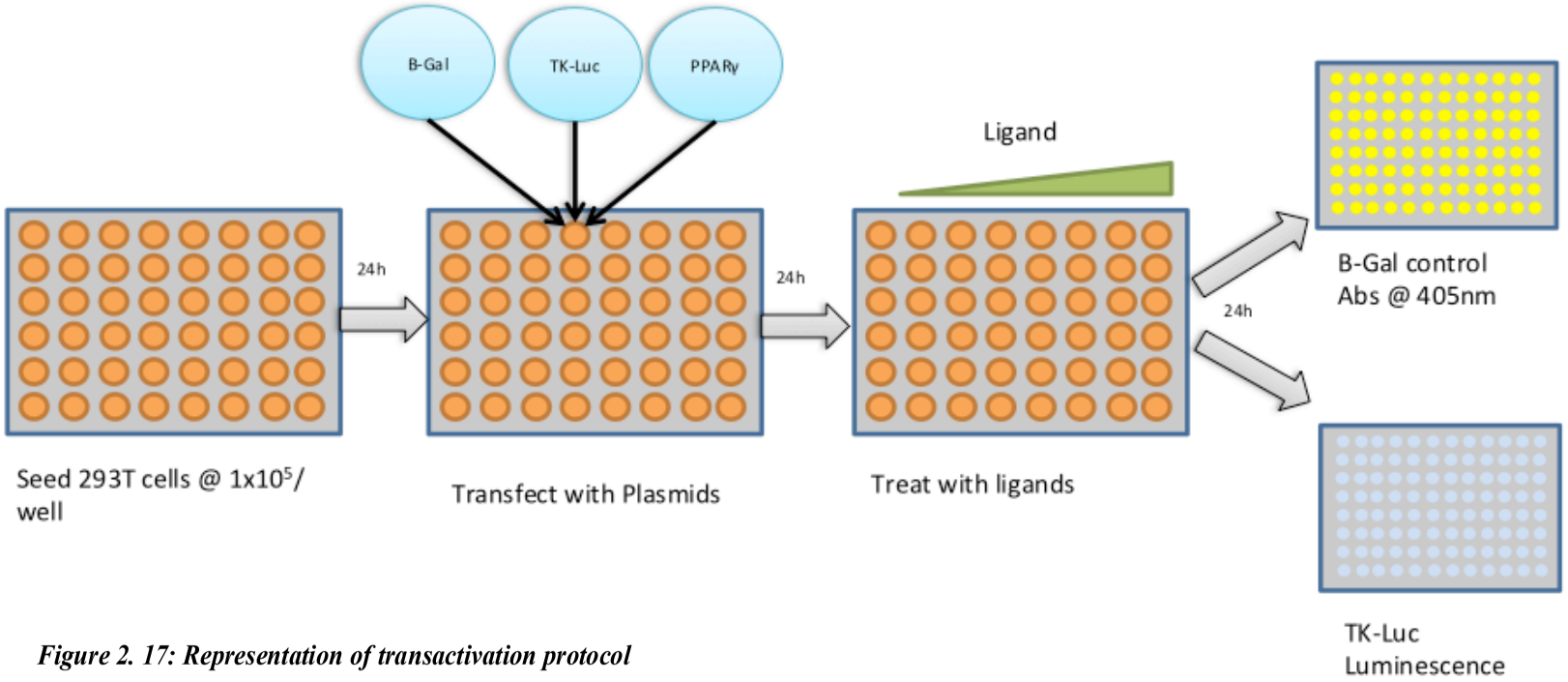

Figure 2. 17: Representation of transactivation protocol

293T cells were seeded in 48 well plates for 24h before transfection with plasmids encoding β-gal, TK-Luc and the PPARγ-LBD-Gal4DBD fusion proteins. After a 6h incubation in serum free medium, an equal volume of complete medium was added and cells incubated for 16h. Agonists were added to the cells and incubated for a further 24h before lysis and measurement of β-galactosidase and TK-luciferase.

2.14 Introduction to X-ray crystallography

The diffraction of X-rays by a crystal was first identified in the early 20th century by Max Laue and pioneered by Lawrence and William Bragg, the later formulating Bragg's law, a fundamental tool for the determination of crystal structures. William Bragg went on to solve the structure of many inorganic molecules and was part of the group that produced the diffraction pattern of the first protein crystal, myoglobin, and solve the first protein structure, lysozyme, from its diffraction pattern.

The basis of crystallography involves the expression of a protein or part of a protein at high purity in solution. The purified protein is then mixed with a buffer containing a precipitant and sealed beside / above a reservoir of the same buffer. As the concentration of the buffer / protein solution is lower than the reservoir, evaporation occurs, concentrating both the buffer and the protein to the point where nucleation occurs and crystals start to form. Protein crystals contain, on average, between 10^{13} and 10^{15} molecules.

The crystals are composed of regularly repeating units called unit cells that make up the lattice of the crystal. Within each of these unit cells there are a number of protein molecules, with each one representing an asymmetric unit.

Once a crystal has formed the most common practice is to soak the crystal in the original buffer with the lowest possible concentration of cryoprotectant to prevent ice from forming and damaging crystals during freezing. The crystal is then scooped and placed directly into liquid nitrogen (N_2) or into a stream of N_2 gas at 100K. The crystal can then be used to collect data points for structure determination.

Data is collected using a monochromatic beam of X-rays (X-rays are used as they have a wavelength of 1Å, equivalent to the distance between atoms) aimed at the crystal, which is mounted on a goniometer. The x-rays are reflected off reciprocal unit cell vertices throughout the lattice and if the waves are in phase, amplify and produce a reflection or spot on the collection device, usually a charged couple device (CCD) camera. Data usually has to be collected through 180°C rotation of the crystal to maximise resolution and completion of a structure.

The resulting diffraction patterns are then used to solve the structure of the protein. This is difficult as both the amplitude and phases are needed to solve a structure and only the amplitudes are measurable. There are number of ways to solve the phase problem including using electron dense atoms (IR), e.g. seleno-methionine, multiwavelength

anomalous scattering (MAD), and molecular replacement (MR) using an already solved similar structure.

2.14.1 Co-crystallisation of PPARγ with 12/15-HETE

The nuclear receptor PPARγ was crystallised with 12- and 15-HETE using a construct coding the PPARγ ligand-binding domain (residues 204-477) as in Itoh et al., 2008 (figure 2.18).

204 LNPESAD LRALAKHLYD SYIKSFPLTK AKARAILTGK TTDKSPFVIY DMNSLMMGED KIKFKHITPL QEQSKEVAIR IFQGCQFRSV EAVQEITEYA KSIPGFVNLD LNDQVTLLKY GVHEIIYTML ASLMNKDGVL ISEGQGFMTR EFLKSLRKPF GDFMEPKFEF AVKFNALELD DSDLAIFIAV IILSGDRPGL LNVKPIEDIQ DNLLQALELQ LKLNHPESSQ LFAKLLQKMT DLRQIVTEHV QLLQVIKKTE TDMSLHPLLQ EIYKDLY 477

Figure 2.18: Amino acid sequence of the PPARγ ligand-binding domain

Crystallisation trials were carried out using the sitting drop method and any crystals that formed were harvested in their original buffer with up to 20% glycerol and flash cooled in 100K N_2 gas. Crystals were subsequently transferred to liquid nitrogen and X-rayed at Diamond or SLS (see later). The structures were solved using molecular replacement.

2.14.1 Transformation of PPARγ plasmid into *E. coli*

The Rosetta strain of E. Coli (originally Life Technologies but now maintained in house), resistant to Chloramphenicol, were transformed with a plasmid encoding (i) the PPARγ-LBD with a His-tag and TEV cleavage site (TEV: protease encoded by the tobacco etch virus), (ii) a gene for Kanamycin resistance to allow selection and (iii) the LacI repressor gene to prevent transcription in the absence of ligand (figure 2.19). Cloning was carried out by Louise Fairall and Kush Amin into a vector based on PET30a that was made at the University of Cambridge.

Competent Rosetta were incubated for 30min on ice with 0.5µl of plasmid before a 1:5 dilution with 2x TY buffer (1.6% (w:v) Tryptone (Melford Laboratories Ltd, Bildeston Road, Ipswich); 1% (w:) yeast extract (Melford Laboratories Ltd); 85mM NaCl; pH 7.0) and 1h incubation at 37°C, shaking at 120rpm. Cells were pelleted by centrifugation at 12000g for 1s, plated on agar containing 30µg/ml Chloramphenicol and 50µg/ml Kanamycin (Melford Laboratories Ltd) and grown overnight at 37°C.

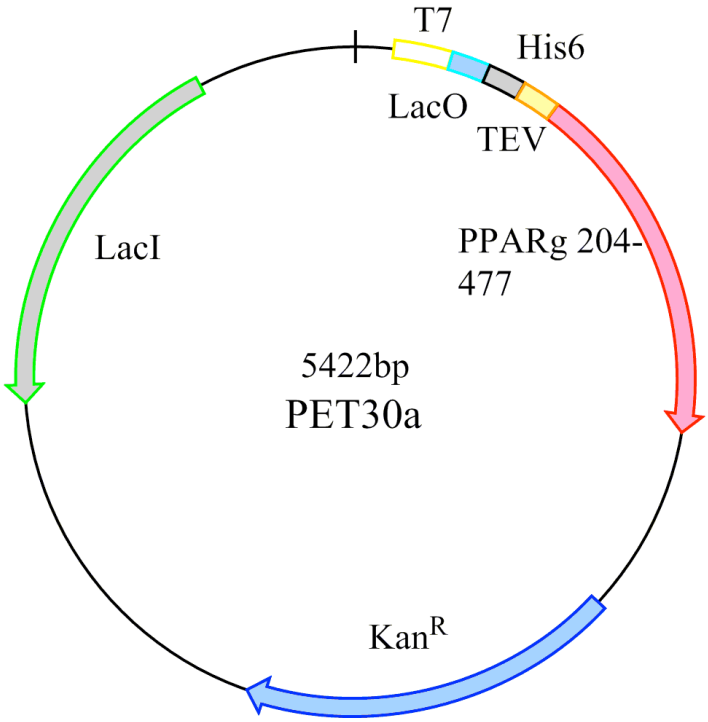

Figure 2.19: Plasmid construct used for expression of PPARγ LBD

The plasmid used encoded the PPARγ-LBD with an encorporated His-tag and TEV cleavage site, a gene for kanamycin resistance and lacI to repress expression in the absence of ligand.

2.14.2 Protein isolation and purification

A single transformed Rosetta colony was grown in 2x TY buffer supplemented with 30µg/ml Chloramphenicol and 50µg/ml Kanamycin for 4-6h (or an optical density (OD) at 600nm of 0.1) at 37°C and 120rpm. Protein expression was induced by the addition of 40µM isopropyl β-D-1-thiogalactopyranoside (IPTG) (Melford laboratories) for 20h at 20°C and 120rpm.

Cells were pelleted at 4000g for 20min at 4°C and disrupted in lysis buffer (50mM Tris pH8.0, 500mM NaCl, 10% glycerol, 1mM DTT, 1% Triton X-100, with 1 tablet of EDTA free protease inhibitor cocktail (Roche)) by sonication (3 x 30s) using a Soniprep150. Insoluble material was pelleted by centrifugation at 30000g for 20min at 4°C. The supernatant was poured on to Ni-NTA beads (Qiagen) (1.5ml slurry/1l culture) that had been prewashed in lysis buffer and incubated for 30min at 4°C. Beads were pelleted at 4000g for 2min at 4°C and washed 4 times in wash buffer (50mM Tris/HCl pH8, 500mM NaCl, 10% Glycerol, 1mM EDTA, 20mM Imidazole pH8) before the addition of elution buffer (50mM Tris/HCl pH8, 500mM NaCl, 10% Glycerol, 1mM EDTA, 300mM Imidazole pH8) and the protein eluted from the beads

by incubation for 15min at 4°C. The Ni-NTA was pelleted and the supernatant filtered through a 0.22µm filter (Millipore).

Protein concentration was determined by blanking a spectrophotometer at 595nm with 1 part Biorad protein assay solution (Biorad) and 4 parts deionised water and then adding 2µl of the protein solution before reading absorbance. Protein concentration was calculated from the measured absorbance using a standard curve from known concentrations of BSA. The His tag was removed from the protein by addition of TEV protease (made in house) (1mg TEV / 100mg protein), while dialysing the protein into 50mM Tris pH8, 50mM NaCl, 1mM DTT, 5% glycerol overnight at 4°C.

The protein sample was further purified using ResourceQ and Superdex S75 (S75/200) columns (both from GE Healthcare) coupled to an AKTA gel purification system (GE Healthcare). The sample was loaded on to the ResourceQ column in low salt buffer (20mM Tris/HCl pH 7.4; 50mM NaCl; 1mM TCEP (tris(2-carboxyethyl)phosphine)) and eluted using an increasing salt gradient (high salt buffer: 20mM Tris/HCl pH 7.4; 500mM NaCl; 1mM TCEP). The resulting protein sample was concentrated to 0.5ml using an Amicon ultra 10kDa MWCO filter (4000xg at 4°C until the desired volume was reached) and filtered using a 0.22µM filter. The sample was then injected onto the Superdex S75 column that had been pre-washed in gel filtration buffer (30mM Tris/HCl pH 8.0; 50mM NaCl; 5% glycerol; 1mM mercaptoethanol; 0.5mM EDTA) and 0.5ml fractions collected. The fractions with the highest concentration of pure protein were pooled and concentrated to 8mg/ml using an Amicon ultra 10kDa MWCO filter at 4000g, 4°C.

SDS-PAGE gels (Life Technologies) were run at every stage to monitor protein purity.

2.14.3 Crystallisation trials

The purified protein was used to set up crystallisation trials with potential ligands. For each trial 20µl of protein was used and incubated with increasing ratios of ligand : protein or a vast excess (1mM) of ligand (12-HETE (Cambridge Bioscience) or 15-HETE (Toshimasa Itoh)). Crystallisation trials were set up using a pre-determined NR-LBD screen (Molecular Dimensions Ltd, Suffolk, UK) containing 96 buffers of varying salt, pH and precipitant (appendix 1) optimised for the crystallisation of nuclear receptor ligand-binding domains. Crystallisation was set up using the sitting drop method with 80µl of each buffer in a reservoir well of a crystallisation plate (MRC plate). The plate was then set up using a Cartesian robot (Genomic Solutions Ltd.,

Huntingdon, UK) which aliquots 100nl of each buffer into 2 wells designated A and B (figure 2.20) and then aliquots 100nl of the protein sample into the buffer.

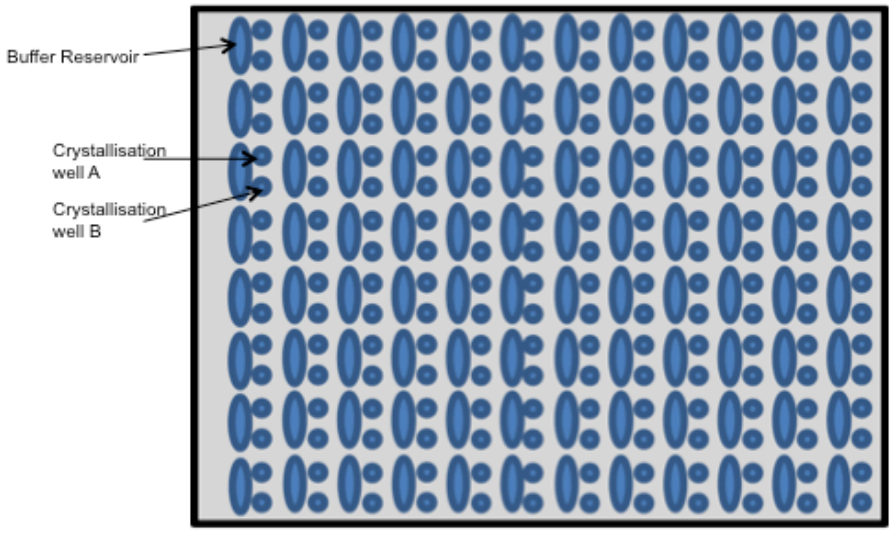

Figure 2.20: Crystallisation plate layout

The large oval wells represent the buffer reservoirs and the 2 small circular wells represent where the crystallisation occurs. Each buffer reservoir has 2 associated wells allowing for 2 different conditions e.g. with and without ligand.

The 2 wells allow 2 different protein conditions to be set up with the same buffer (e.g. with varying protein concentration or ligand concentration). Once finished the plate was sealed and left at room temperature for 3-7 days to allow crystal nucleation and growth (figure 2.21).

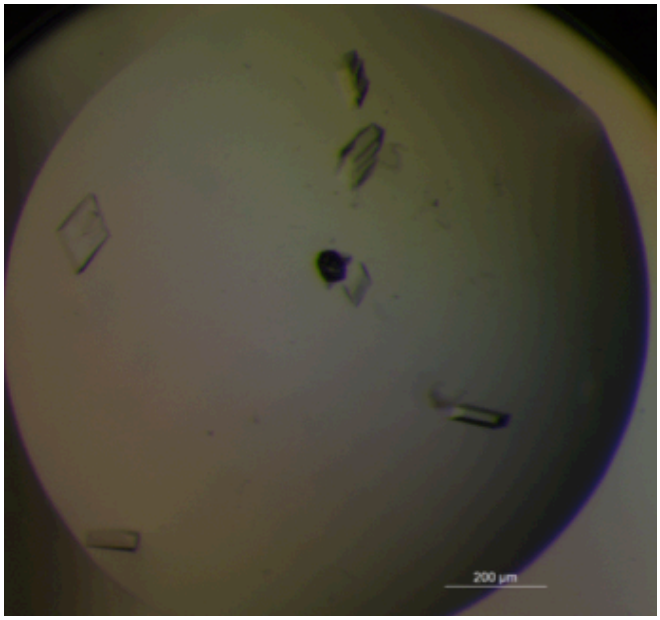

Figure 2.21: Crystal development

Image of well with buffer droplet and protein crystals. Taken after 5 days.

2.14.4 Crystal collection

Once crystals had formed they needed to be collected and stored in liquid nitrogen prior to X-ray analysis. Firstly a cryo-protectant was made that was identical to the buffer in which the crystals had formed, but with the addition of the lowest concentration of glycerol that prevents ice forming when frozen. This was determined by placing cryo-loops with cryo-protectant in a stream of N_2 gas at 100k, checking for a glass like appearance with no ice formation and no ice rings when X-rayed. The cryo-protectant buffer was added onto the crystals (2µl) and individual crystals scooped into cryo-loops and frozen under a stream of N_2 gas before being transferred to liquid N_2.

2.14.5 Data collection and structure determination

Crystals were X-rayed at either the Diamond (Oxford) or SLS (Villigen, Switzerland). The cryo-loop containing the crystal was mounted on the goniometer and centred so as always to be in the X-ray beam path when rotated through 360°. The crystal was first X-rayed to determine diffraction and if promising a complete data set was collected. The data were indexed and integrated using iMosflm (Leslie, 2006) and scaled using the CCP4 programs (Collaborative Computational Project, Number 4, 1994). The structure was solved using molecular replacement using Phaser (Rossmann, 1990; Rossmann and Blow, 1962; Scapin, 2013) based on an already solved structure of PPARγ (PDB: 2VSR (Itoh et al., 2008)). The resulting structure was rebuilt using C*oot* (Emsley and Cowtan, 2004) (http://www2.mrc-lmb.cam.ac.uk/personal/pemsley/coot/) before a simulated

annealing omit map was created using Phenix, which removes model bias by rebuilding the structure in discrete sections ((Adams et al., 2010); http://www.phenix-online.org). Structures were refined using Refmac5 (Murshudov et al., 1997). Potential PPARγ ligands were built in Marvin Sketch and merged with the protein structure if density was observed. A more comprehensive outline of structure determination is provided in section 6.2.

6.15 Statistical analysis

Since for most experiments there were less than 10 replicates, a frequency distribution test was not appropriate as advised by the departmental statistician. Instead, a parametric test was carried out if the data had a similar mean and median value, indicative of normally distributed data (most commonly a paired Student's t-test or ANOVA). If the median and mean were different or there was an obvious outlier a non-parametric test was performed (most commonly a Wilcoxon or Friedman test). Where data had been normalised to the control to create a ratio, a one-sample t-test was performed.

Chapter 3: Anti-thrombotic gene expression in monocytes induced by platelets activated through GPVI

3.1 Introduction

As described in section 1.10, data from a previous study had shown that platelet-activated monocytes from stable STEMI patients had lower mRNA levels of a number of anti-thrombotic genes compared to controls. These samples were taken from the patients in a stable state, more than 3 months after their cardiac event so the differences were unlikely to be due to the acute effects of the MI (Unni Krishnan et al., manuscript in preparation). One hypothesis for the observed difference was that the anti-thrombotic and/ or anti-coagulant therapies the patients were taking were affecting gene expression. The patients were taking a number of different medications but the one universal drug was aspirin. A parallel study also found that mRNA for the transcription factor *pparγ* was highly upregulated in platelet-activated monocytes (Rosienne Farugia et al., manuscript in preparation).

The aim of the work described in this chapter was to explore these findings in more detail, firstly by investigating the expression profiles of *tfpi*, *procr* and *pparγ* in platelet-activated monocytes over 8h and to determine whether this was through direct contact or mediators released from platelets. Following this the affect of aspirin on monocyte gene expression was analysed and it was established whether the effect was being mediated through its action on platelets or through a direct effect on monocytes. Next the effect of inhibiting 12-LOX, the alternative pathway of AA metabolism in platelets, on the relative expression of these three genes was analysed, and finally, the contribution of monocyte gene expression in an *in vitro* thrombus model was investigated to determine whether it may be of relevance *in vivo*.

A whole blood *in vitro* model was employed, as had been used in the earlier studies, in which platelets were selectively activated via the GPVI collagen receptor using CRP-XL, a collagen-mimetic peptide, and allowed to interact with monocytes, which were then isolated with immune-magnetic beads, and gene expression quantified by RT-qPCR. The isolation of monocytes from whole blood was achieved using either the same immune-magnetic beads as in previous studies; namely CD14 Dynabeads (section 2.2.7.1), or, in later experiments that required isolation of monocytes from whole blood

prior to incubation with platelets, using CD14 Miltenyi immune-beads (section 2.2.7.3). The principle of these two methods is the same.

3.2 Do activated platelets induce monocyte *tfpi*, *procr* and *pparγ* gene expression?

3.2.1 Determination of optimum CRP-XL concentration

To identify a concentration of CRP-XL that caused maximum degranulation with minimum microparticle release, whole blood was incubated for 10 minutes at 37°C with concentrations of CRP-XL ranging from 0.125-2.00µg/ml. Samples were then analysed by flow cytometry to measure P-selectin expression and Annexin-V binding as markers of degranulation and MP formation respectively.

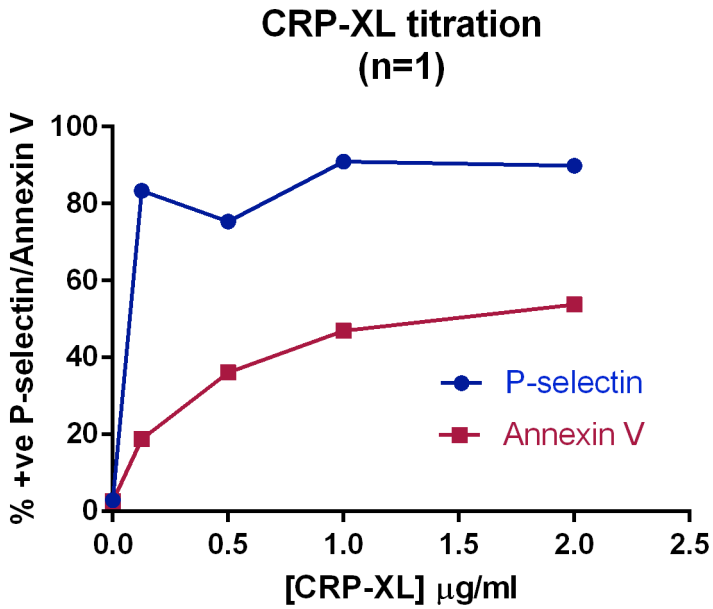

Figure 3.1: Determination of optimal CRP-XL concentration

Whole blood was incubated with increasing concentrations of CRP-XL (0.000, 0.125, 0.500, 1.000 and 2.000µg/ml) and either P-selectin-FITC or Annexin-V-FITC. The platelet population was identified based on FSc and SS and analysed for either P-selectin-FITC or Annexin-V-FITC, (n=1).

For this batch (batch 2), the lowest concentration of CRP-XL used (0.125µg/ml) induced maximal platelet P-selectin expression, increasing from 2.9% in the unstimulated blood to 83.3% and remained >75% at all other concentrations. The percentage of Annexin-V platelets, an indicator of MP generation, showed a dose-dependent increase with increasing CRP-XL concentration. At the lowest concentration of CRP-XL (0.125µg/ml), Annexin-V binding was 18.7% and rose to a maximum of 53.8% at 2.00µg/ml (figure 3.1). From this titration, 0.125µg/ml CRP-XL was selected on the basis of maximal degranulation (P-selectin binding) with minimal

PS translocation to the outer leaflet (Annexin-V binding). Another batch (batch 1) that had been titrated by another member of the group was used at 0.5µg/ml.

3.2.2 Time course of monocyte gene expression for *tfpi*, *procr* and *pparγ* following activation with CRP-XL

To confirm that platelet activation can induce monocyte gene expression, and to determine the most appropriate time point for RT-qPCR analysis of the genes of interest, whole blood was incubated at 37°C for up to 8h with and without 0.5µg/ml CRP-XL (batch 1). Monocytes were isolated using CD14 Dynabeads® and gene expression analysed by RT-qPCR. To confirm that the platelets were activated in these samples, monocyte platelet aggregation was assessed at each time point using flow cytometry (figure 3.2).

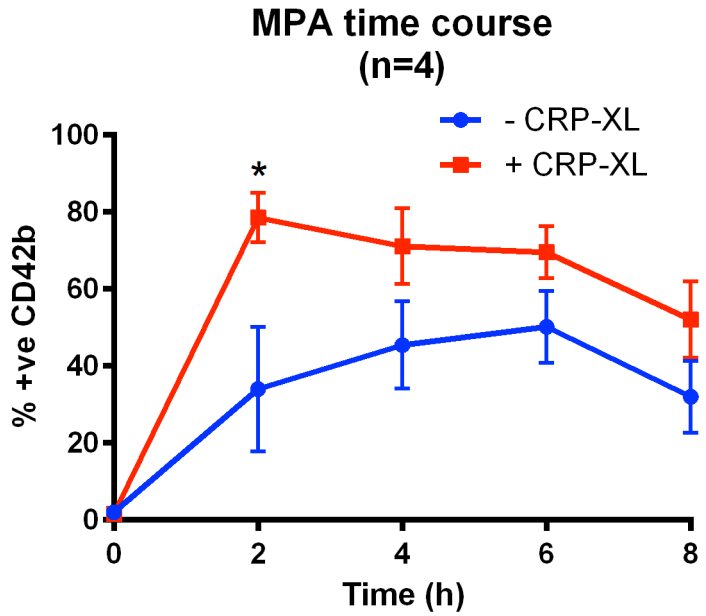

Figure 3.2: Monocyte platelet aggregation over 8h

Whole blood ±CRP-XL was incubated at 37°C for up to 8h. At each time point an aliquot was incubated with the monocyte specific anti-CD14-RPE-Cy5 antibody and the platelet specific anti-CD42b-RPE antibody and analysed by flow cytometry. CD42b positive monocytes have platelets bound. P-values calculated using multiple t-tests (=<0.05; n=4). Data show mean±SEM.*

The percentage of monocytes with bound platelets increased after addition of CRP-XL to nearly 80% at 2h, falling slightly at subsequent time points to ~60% at 8h (figure 3.2). This is in line with previous observations, and reflects loss of P-selectin from the platelets ((Dole et al., 2007)). The control samples, without CRP-XL also showed some increase in MPA formation over time but this was significantly less than that seen in the

CRP-XL-stimulated samples at all time points (p=<0.0001 for 2, 4 and 6h and p=<0.001 for 8h; n=4).

In whole blood stimulated with CRP-XL, monocyte *tfpi* gene expression increased in a time-dependent manner from 2.9±1.6 at T0 to 3408.1±951.5 at 6h, reaching a plateau at 8h (3624.46 ±983.11) (p=<0.01 for both) (figure 3.3a, red line). In the absence of CRP-XL there was a comparatively small increase in *tfpi* expression over the 8h, reaching a maximum (170.6±53.5) at 6h (figure 3.3a, blue line). There was a significant difference between stimulated and non-stimulated samples at all time points (p=<0.05) apart from at rest (0h).

In CRP-XL stimulated blood, monocyte *procr* expression had not occurred by 2h but after that it increased to 7.6±2.7 at 4h, with a further small increase at 6h and at 8h reaching 19.0±7.3 (p=<0.01) (figure 3.3b, red line). In the absence of CRP-XL, monocyte *procr* gene expression was low, and similar at 2h, 4h and 8h compared to baseline. There was a small but significant increase at 6h compared to baseline (p=<0.001) (figure 3.3b, blue line). The differences between stimulated and unstimulated samples were not significant at any time point.

Monocyte *pparγ* gene expression in the presence of CRP-XL showed a large increase at 2h (99.0±18.7) compared to T0 (1.2±0.3) (p=<0.001) after which expression decreased to 32.6±6.1 at 4h, rising slightly at 6h and 8h (figure 3.3c, red line). Without CRP-XL, *pparγ* expression increased slightly with time from 1.1±0.2 at baseline to 36.3±24.5 at 8h, but the rise was not significant (figure 3.3c, blue line). Expression was higher in the stimulated compared to unstimulated samples at all time points but this was only statistically significant at 2h (p=<0.05).

These results show that activated platelets are able to induce monocyte *tfpi* and *pparγ* gene expression and suggest a trend towards increased *procr* expression, although this did not reach significance. Based on the time course of all 3 genes, subsequent measurements of gene expression by RT-qPCR were carried out at 6h. In some later experiments *pparγ* expression was measured after 2h.

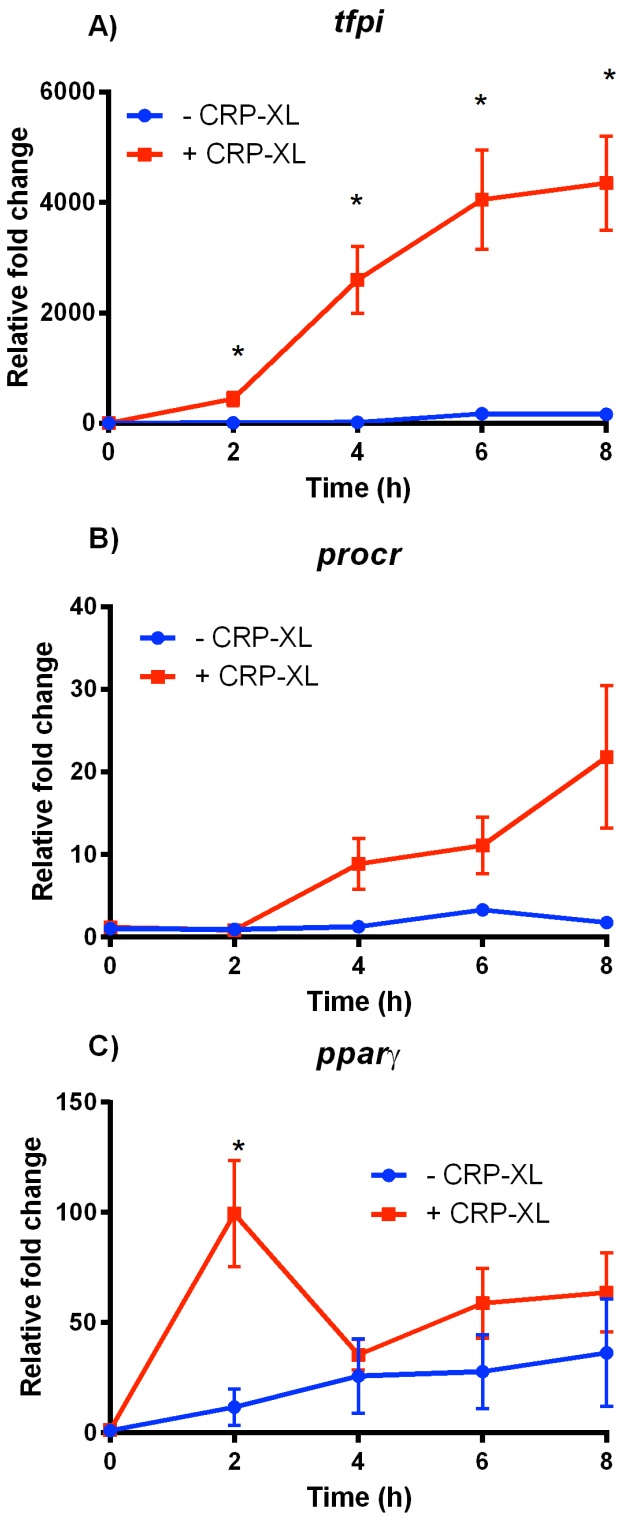

Figure 3.3: Platelet-induced monocyte gene expression over 8h

Whole blood was incubated ±0.5µg/ml CRP-XL for 0-8h before monocyte isolation using CD14 Dynabeads®, RNA extracted using RNeasy columns and RT-qPCR using QuantiFAST SYBRgreen master mix for tfpi A), procr B) and pparγ C). P-values calculated using multiple t-tests (=<0.05). Data show mean±SEM; n=4.*

3.2.3 Effect of actinomycin on the expression of *tfpi, procr and pparγ in* platelet-activated monocytes

To demonstrate that platelet-induced expression of these three genes was due to endogenous transcription, and not transfer of mRNA from platelets, whole blood was pre-incubated at 37°C for 10min with and without 10mM actinomycin (to inhibit RNA polymerase) before adding 0.5µg/ml CRP-XL (batch 1) and incubating for 6h at 37°C. Monocytes were isolated using CD14 Dynabeads®, and gene expression analysed by RT-qPCR (figure 3.4).

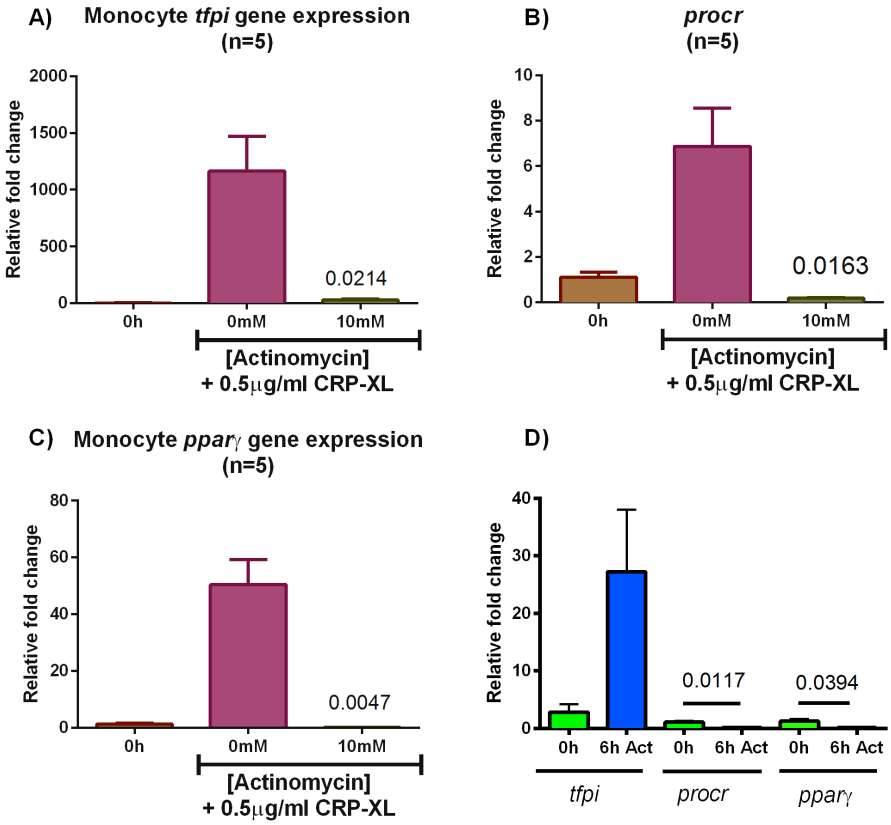

Figure 3.4: The effect of actinomycin on platelet-induced monocyte gene expression

Whole blood was incubated ±10mM actinomycin for 10min at 37°C prior to simulation with CRP-XL (0.5µg/ml) for 6h at 37°C. Monocytes were isolated using CD14 Dynabeads® and total RNA extracted using RNeasy columns. After reverse transcription, RT-qPCR was carried out using QuantiFAST SYBRgreen master mix for tfpi A), procr B) and pparγ C). D) Comparative fold change in tfpi, procr and pparγ between resting and 6h CRP-XL and actinomycin treated samples. P-values were calculated using a Student's paired t-test. Data show mean±SEM; n=5.

Before gene expression analysis, the effect of actinomycin was tested on platelet activation and MPA formation and found not to effect either (data not shown). Actinomycin D effectively blocked expression of all 3 genes compared to non-treated

platelet-activated samples. Actinomycin caused a 96.8±1.4%, 96.4±1.0% and 99.7±0.1% reduction in monocyte *tfpi, procr* and *pparγ* expression, respectively (figure 3.4a-c). These results indicate that gene expression is induced by platelets and is endogenous to the monocytes rather than being a result of transfer of mRNA from extracellular sources such as platelets or platelet-derived MVs.

Interestingly, expression of *procr* and *pparγ* in the samples pre-treated with actinomycin were negligible compared to the levels in resting samples, while *tfpi* expression was still 27.3±10.8 fold higher. This could represent transfer of a small amount of mRNA from platelets or platelet-derived MVs as platelets have been shown to express *tfpi* mRNA and to contain TFPI protein (Maroney et al., 2007). This is shown more clearly in figure 3.4d, where just the data for the unstimulated and actinomycin D treated samples are shown, allowing the scale of mRNA expression to be adjusted to show these differences.

3.3 Regulation of monocyte *tfpi*, *procr* and *pparγ* genes by platelet-derived factors

3.3.1 Effect of blocking MPA formation on monocyte gene expression

To determine whether direct cell-cell contact between activated platelets and monocytes is required to induce gene expression, the P-selectin blocking monoclonal antibody 9E1 (20μg/ml) was included in CRP-XL-stimulated blood samples to prevent platelet monocyte aggregation.

To confirm 9E1 blocked platelet monocyte aggregation, whole blood incubated with and without 9E1 for 5min and activated with 0.125μg/ml CRP-XL (batch 2) at 37°C for 10min was analysed by flow cytometry for MPA formation (figure 3.5a). In the absence of 9E1, 85.8±0.94% (mean±SEM; n=3) of monocytes were detected as MPA's. However, when 9E1 was present there was a significant decrease in MPA formation to 8.6±1.2% (p=<0.0001), confirming 9E1 blocks MPA formation.

To test the effect of direct cell-contact on gene expression, whole blood was incubated in the absence or presence 9E1 for 5min before activating platelets with 0.125μg/ml CRP-XL (batch 2) and incubating the blood for 2/6h at 37°C.

Monocyte *tfpi* and *procr* gene expression followed a similar profile; both increasing after 6h stimulation compared to resting (figure 3.5b and c). When 9E1 was present to block monocyte platelet aggregation there was a small, non-significant decrease in expression for both *tfpi* and *procr* from 2713±1829 to 1533±229.9 and 24.3±8.7 to 15.4±0.53 (mean±SEM; n=3) respectively, a difference that likely reflects both

experimental variation and the data for both genes being skewed by the same very high responder, however this will need to be confirmed.

Monocyte *pparγ* expression showed an increase at 2h between the stimulated and resting samples as previously described (figure 3.5d). However, unlike *tfpi* and *procr*, there was a significant decrease in expression in the presence of 9E1 from 119.6±9.2 to 49.4±6.5 (p=0.0393).

These results suggest that molecules released from activated platelets regulate monocyte *tfpi* and *procr* gene expression, whilst *pparγ* expression is regulated by both direct contact and by molecules released from platelets.

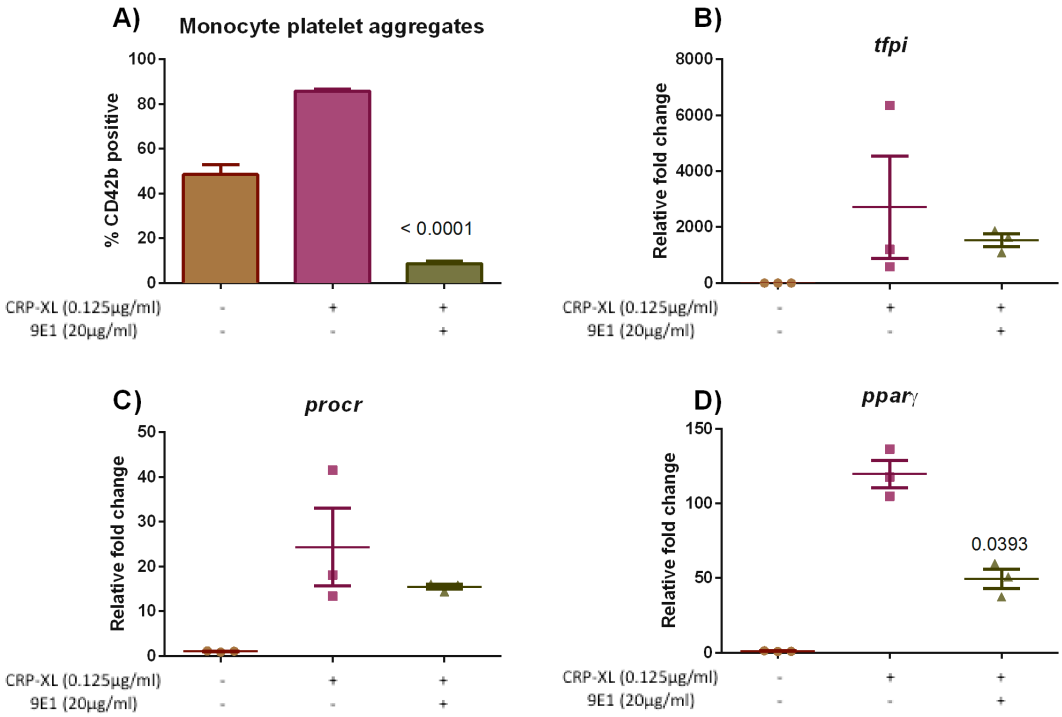

Figure 3.5: Effect of 9e1 on monocyte gene expression

Whole blood was incubated with or without 9E1 (20µg/ml) before stimulation with 0.125µg/ml CRP-XL for 2h (pparγ) or 6h (tfpi and procr) at 37°C. Monocytes were isolated, total RNA extracted and converted to cDNA. RT-qPCR was carried out using QuantiFAST SYBRgreen reagents for tfpi A), procr B) and pparγ C). P-values calculated using a Wilcoxon t-test for tfpi and procr and Student's paired t-test for pparγ. Data show mean±SEM; n=3.

3.3.2 Isolation of monocytes from whole blood

To confirm these findings and to characterise the mechanisms by which platelets induce monocyte gene expression, it was necessary to isolate monocytes prior to incubation with autologous platelets or their released factors. While immunomagnetic bead-based methods are able to isolate monocytes the challenge was to prepare monocytes that were

free of contaminating platelets. Initially, three immunomagnetic bead-based methods were tested by flow cytometry to assess the purity of the isolated monocytes and the residual platelet contamination; RosetteSep^{TM} human monocyte enrichment cocktail (StemCell Technologies); CD14 pan monocyte isolation; and CD14 microbead positive isolation (both from Miltenyi Biotech).

After isolation according to the manufacturer's instructions, monocyte purity was assessed relative to whole blood by flow cytometry. Both whole blood and isolated monocytes were incubated with the pan leukocyte marker CD45-RPE and the monocyte specific marker CD14-RPE-Cy5. The CD45 positive population was gated and analysed for CD14 expression. Samples were run in duplicate on the XL flow cytometer (figure 3.6).

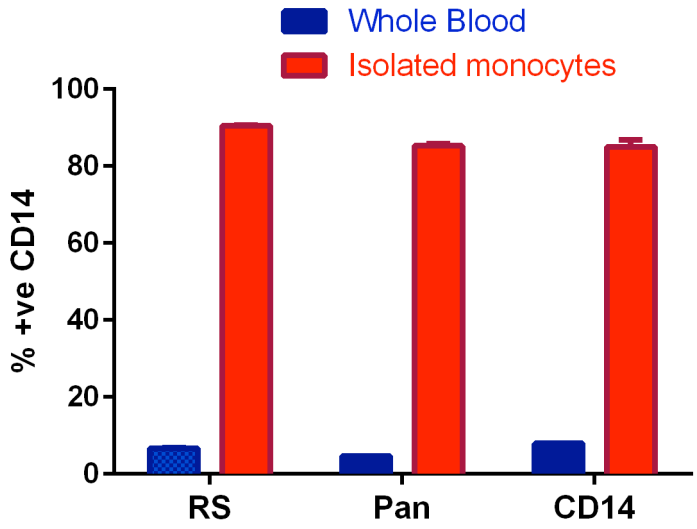

Figure 3.6: Purity of isolated monocytes.

Monocytes were isolated from whole blood using 3 different methods and assessed for purity using flow cytometry based on CD14 expression. Abbreviations are RS: RosetteSep, Pan; Pan monocyte, CD14; CD14 microbead. N=1.

After isolation, all methods increased the CD14+ve monocyte population compared to whole blood. The percentage of CD14+ve events increased from a mean (±SEM) of 6.7±0.10% to 90.5±0.1% using RosetteSep; from 4.7±0.005% to 85.3±0.7% using the Pan monocyte method and from 8.0±0.035% to 85.1±1.9% using the CD14 microbead method (mean±SEM).

Each sample was also assessed for platelet contamination by flow cytometry by measuring the time taken to reach 5000 events within the platelet gate. Both the RosetteSep and pan monocyte methods reached 5000 events in 1 second whereas the

CD14 microbead method reached 5000 events in 22 seconds. For this reason it was decided to use CD14 microbeads for monocyte isolation in all subsequent RT-qPCR experiments.

3.3.3 Effect of platelet-derived soluble material and microparticles on monocyte gene expression

To determine whether platelet-derived soluble factors or MPs were responsible for inducing monocyte gene expression, autologous monocytes and washed platelets were isolated from whole blood. The platelets were activated with 0.5µg/ml CRP-XL (batch 1) for 10min at 37°C and the releasate isolated by centrifugation. Part of the platelet-derived releasate was separated into soluble material and MPs by centrifugation at 20000xg for 30min. The soluble fraction was removed and the MPs re-suspended in RPMI-1640 medium. Autologous monocytes were incubated at 37°C for either 2h or 6h with vehicle, platelet releasate, soluble platelet material or platelet-derived MPs and gene expression analysed by RT-qPCR (figure 3.7).

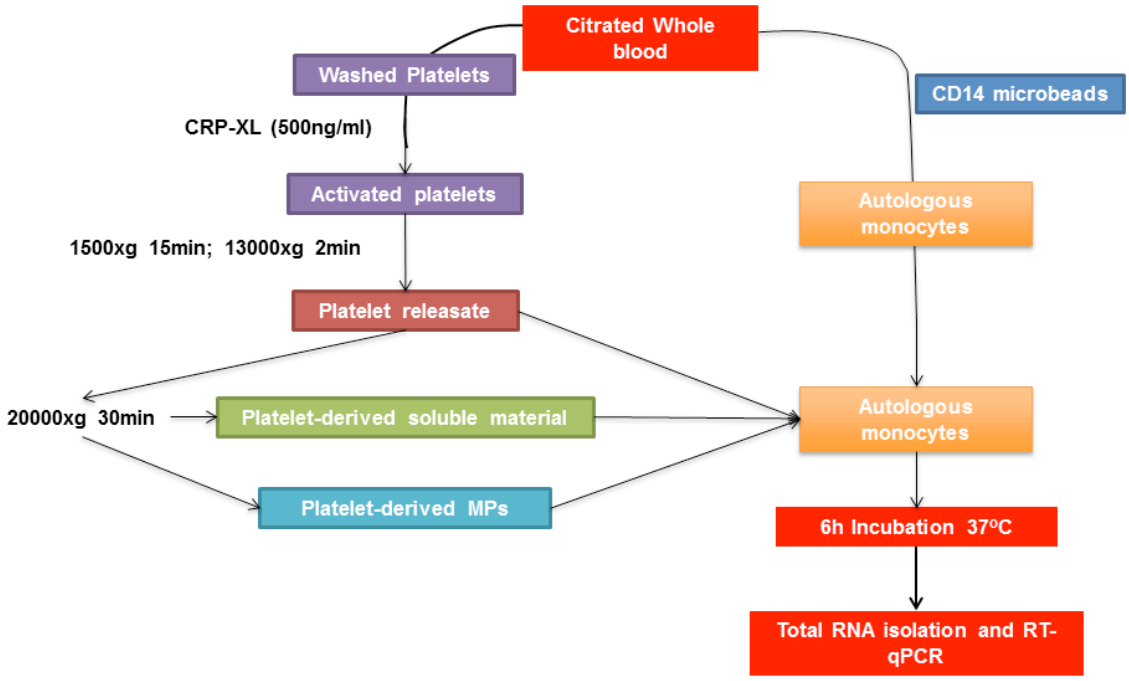

Figure 3.7: Flow chart for determining platelet-derived soluble components regulating gene expression

Washed platelets were activated with 0.5µg/ml CRP-XL and the platelet removed by centrifugation. Part of the releasate was separated into the soluble component and MPs by centrifugation before reconstitution with autologous monocytes. Samples were incubated for 2/6h before RNA extraction and RT-qPCR.

Monocyte *tfpi* and *procr* showed similar expression profiles with the different fractions. Both *tfpi* and *procr* expression was significantly increased with the platelet releasate compared to the control (monocytes incubated in media) (*tfpi* p=0.0118; *procr* p=0.0348) and similar, or even higher levels of expression were seen with the platelet soluble material. In contrast, platelet-derived MPs did not cause any significant difference in expression of either *tfpi* or *procr* between the 6h vehicle control and (figure 3.8a and b).

The effect of the different fractions on expression of monocyte *pparγ* was harder to interpret. The platelet releasate produced lower gene expression compared to control samples. Although this was slightly elevated after incubation with the platelet-derived soluble molecules again this was lower than the control samples (figure 3.8c). Platelet-derived MP's showed similar attenuation of expression compared to the releasate.

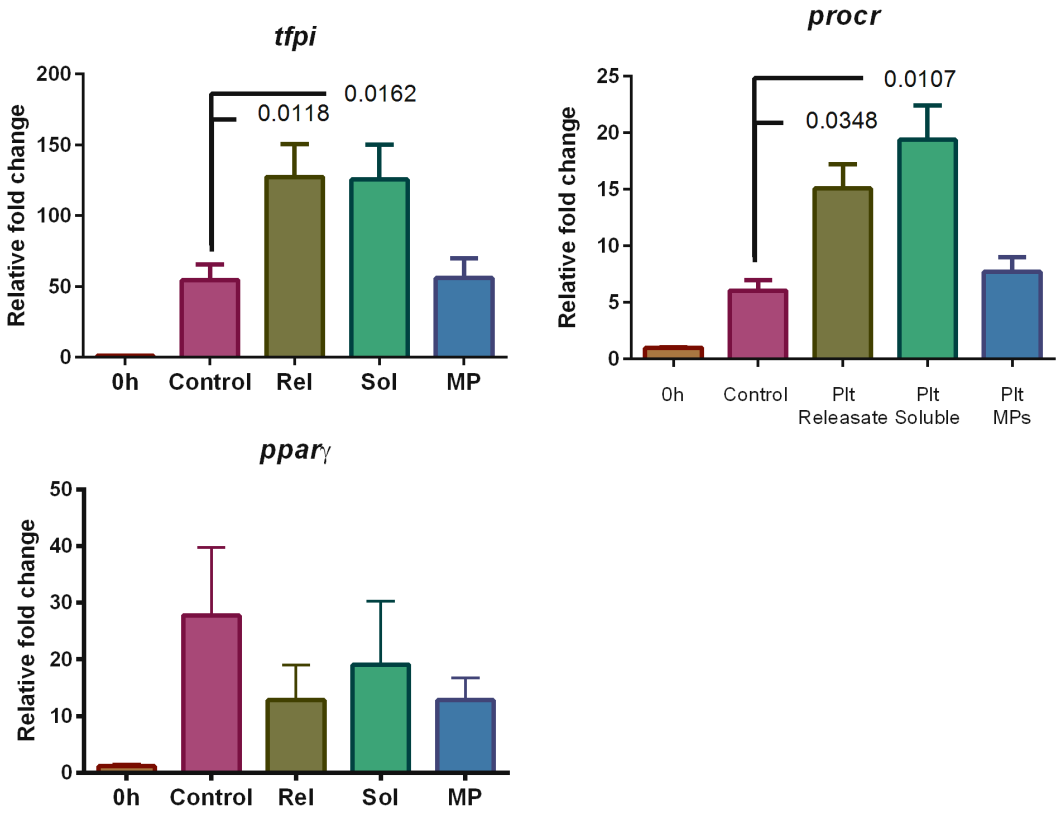

Figure 3.8: Effect of platelet-derived releasate fractions on monocyte gene expression

Washed platelets were activated with 0.5μg/ml CRP-XL before releasate was isolated and separated into soluble and MP fractions. These were incubated for 2h (pparγ) or 6h (tfpi and procr) with autologous monocytes before total RNA extraction with RNeasy columns and reverse transcription. Gene expression was measured by RT-qPCR using QuantiFAST SYBRgreen master mix for tfpi A), procr B) and pparγ C). P-values were calculated using a repeated measure one-way ANOVA for tfpi and procr and a Friedman test for pparγ. Data show mean±SEM; n=4.

These data suggest that monocyte *tfpi* and *procr* expression are mediated through soluble molecules released from activated platelets and not platelet-derived MPs. Interestingly, monocyte *pparγ* expression is attenuated by components derived from activated platelets compared to control samples and may suggest *pparγ* expression is more dependent on direct contact through MPA formation.

3.3.4 Effect of platelet-derived proteins and oxylipins on monocyte gene expression

After showing soluble factors were responsible for monocyte *tfpi* and *procr* expression the next step was to determine the nature of the released material that caused this effect. For this, isolated monocytes were incubated with platelet-derived soluble fractions; specifically molecules <10kDa, molecules >10kDa and oxylipins. Washed platelets were incubated at 37°C for 10min with 0.5µg/ml CRP-XL (batch 1) and the releasate isolated by centrifugation as in the previous section. The soluble releasate was further fractionated into proteins < and > 10kDa using 10kDa MWCO filters, and oxylipins using a hexane-based method (C. P. Thomas et al., 2010). The oxylipins were dried under nitrogen, re-dissolved in methanol and then resuspended in RPMI-1640 at a maximum methanol concentration of 2% (v/v). Each platelet-derived fraction was reconstituted with autologous, CD14 microbead-isolated monocytes at equivalent concentrations to the original blood, and incubated for 6h at 37°C before total RNA extraction and RT-qPCR.

Compared to controls (monocytes in media with appropriate vehicle), monocyte *tfpi* expression was significantly increased by 151.5±9.2% with proteins >10kDa (p=0.0005) and by 411.9±64.1% with the oxylipin fraction (p=0.0009) but there was no increase with proteins <10kDa (figure 3.9a). Conversely, monocyte *procr* expression was predominantly induced by proteins >10kDa (338.5±65.8%; p=0.0192) although there was trend towards an increase with proteins <10kDa (1.79 fold) but this did not reach significance. There was no change in expression when oxylipins were present (figure 3.9b). Interestingly, although monocyte *pparγ* expression appears to be induced mainly by direct contact, there was a significant increase with the oxylipin fraction compared to the control sample (223.2±26.3%; p=0.0008). Expression of *pparγ* was significantly reduced in the presence of proteins both <10kDa (40.2±8.8% decrease; p=0.0064) and >10kDa (21.3±5.6% decrease p=0.0066), (figure 3.9c) consistent with the observations with the whole platelet releasate shown previously (figure 3.8).

These results suggest that different types of molecule regulate platelet-mediated expression of these anti-thrombotic genes in monocytes with *tfpi* and *pparγ* mainly being induced by oxylipins and *procr* by proteins >10kDa.

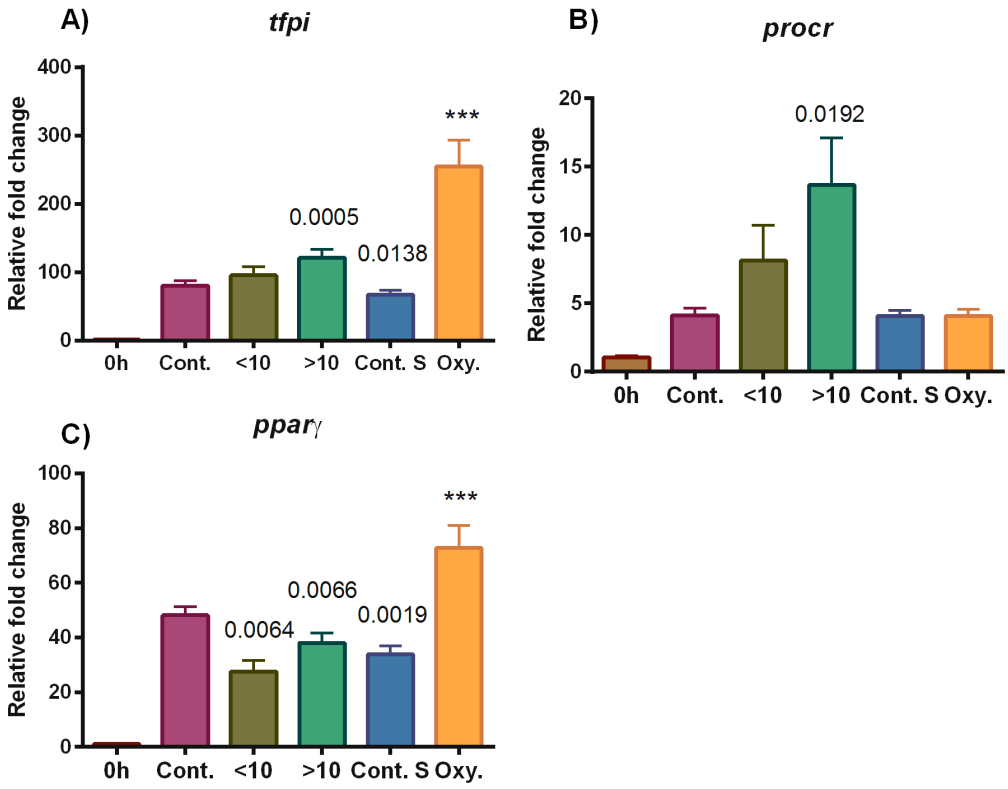

Figure 3.9: Effect of platelet-derived metabolites on monocyte gene expression

*Platelet releasate was separated into proteins < and > 10kDa and oxylipins before reconstitution with autologous monocytes and incubation at 37°C for 2h (pparγ) or 6h (tfpi and procr). Total RNA was isolated and used in RT-qPCR reactions for tfpi A), procr B) and pparγ C) expression. Data show mean±SEM. P-values calculated using a repeated measures one way ANOVA. Numerical P-values are compared to control and asterisk to the solvent control (Cont. S) (***=<0.001); n=9.*

3.4 Effect of inhibiting COX-1 on gene expression in platelet-activated monocytes

The previous experiments suggested that oxylipins might be regulating the expression of two of the three genes. The next stage was therefore to test the effect of inhibitors of the downstream metabolism of AA and LA through COX-1 and 12-LOX. Firstly experiments were conducted in which COX-1 was inhibited with aspirin.

3.4.1 Effect of aspirin on platelet aggregation

To confirm that each batch of aspirin used in this study was effective in inhibiting COX-1, aspirin was titrated against ADP using Born-type aggregometry to measure platelet aggregation in PRP. ADP was used as opposed to CRP-XL as ADP is sensitive

to the TxA2 dependent secondary wave of aggregation (figure 3.10). ADP was first titrated with each donor to determine the concentration for maximal aggregation whilst maintaining a two-phase aggregation response curve. Platelet aggregation was then measured in PRP in response to ADP following incubation with aspirin at 0-500μM. Figure 3.10 shows an example of traces from a single donor.

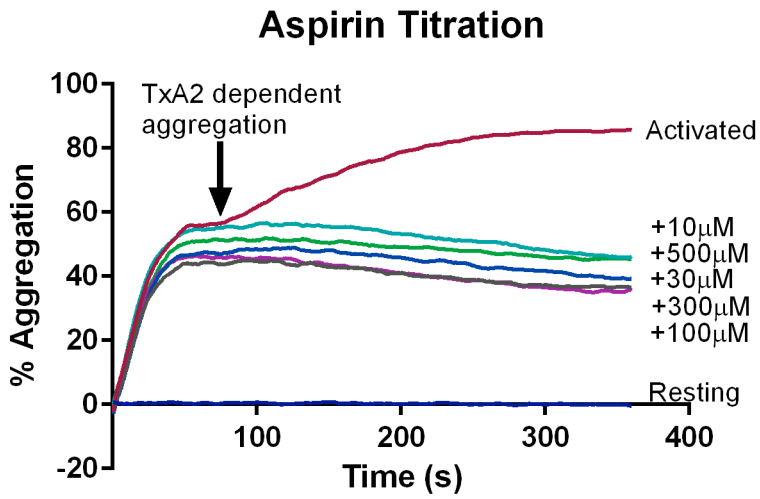

Figure 3.10: Representative aggregometry trace in response to aspirin

PRP was incubated at 37°C for 10min with increasing concentrations of aspirin (0-500μM) before activation with a concentration of ADP that produced an almost maximal two-phase aggregation (determined individually for each donor) and aggregation recorded for 6min.

A concentration of ADP was used that produced a final aggregation (FA) of 94.8±7.3% (mean±SEM; p=<0.0001; n=4) representing maximal platelet aggregation. With the addition of 10μM aspirin, the secondary phase of aggregation was inhibited so that FA decreased to 62.5±10.7% (p=<0.01). This decreased further to 36.3±6.5% (p=<0.0001) with 30μM aspirin, but there was no further effect with any of the higher doses of aspirin (all p=<0.0001) (figure 3.11a). Very similar results were seen when area under the curve (AUC) was used as a measure (figure 3.11b). This indicates that maximum inhibition by aspirin was seen at concentrations of 30μM and above.

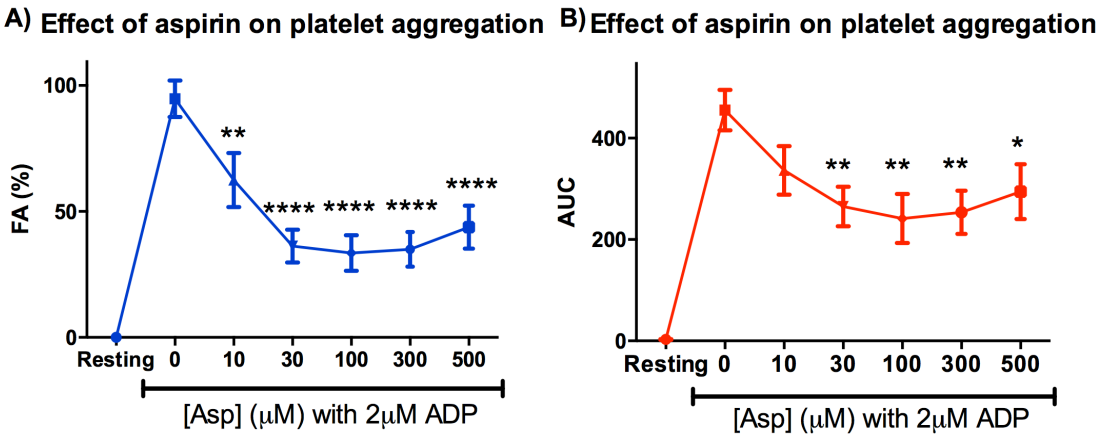

Figure 3.11: Effect of aspirin on platelet aggregation.

PRP was prepared from whole blood and incubated with increasing concentrations of aspirin (0-500μM) at 37°C for 10min before stimulation with an optimal concentration of ADP for 6min. Figures show: FA A) and AUC B). P-values calculated using an ordinary 1 way ANOVA, values compared to ADP only sample. (=<0.05; **=<0.01; ****=<0.0001). Data show mean±SEM; n=4.*

3.4.2 Effect of aspirin on platelet activation and monocyte platelet aggregation

As previous results had suggested that the increase in monocyte gene expression was through released factors for *tfpi* and *procr* and direct contact for *pparγ*, the effect of aspirin on granule release and MPA formation was measured. The effect of aspirin on platelet α-granule release was measured by labelling of P-selectin on the platelet surface after activation by flow cytometry. Washed platelets were incubated at 37°C for 10min in the presence or absence of 500μM aspirin before activation with 0.5μg/ml CRP-XL (batch 1) and incubation with an anti-P-selectin-FITC antibody. P-selectin expression was assessed by flow cytometry.

Before activation, washed platelets that had been treated with aspirin had a similar level of P-selectin expression compared to those that were untreated. Activation with CRP-XL caused a significant increase in expression for both aspirin treated and untreated samples compared to the corresponding controls, which was slightly (~5%), but significantly lower in the aspirin treated platelets (p=0.0246) (figure 3.12).

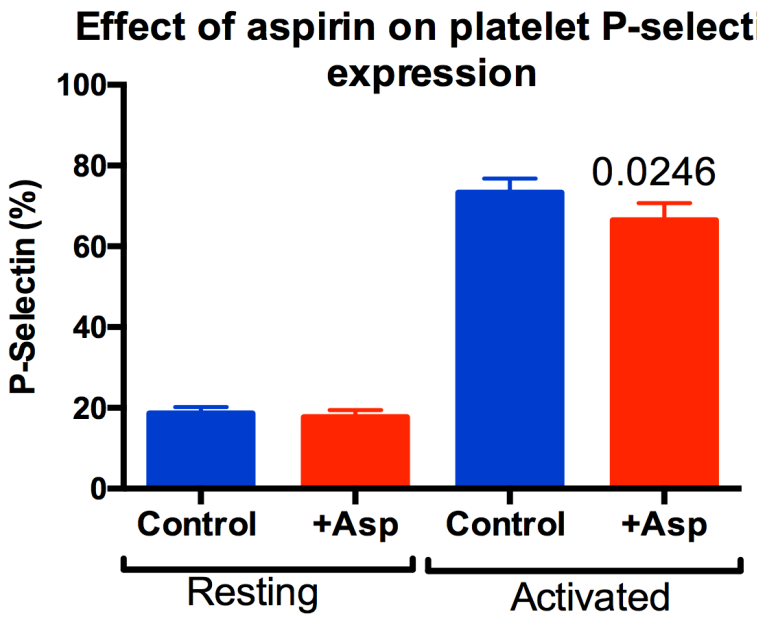

Figure 3.12: Effect of aspirin on platelet α-granule release

Washed platelets were treated for 10min at 37°C either with or without 500μM aspirin before activation with 0.5μg/ml CRP-XL. Platelets were incubated with an anti-P-selectin-FITC antibody and platelets identified based on FSc and SS using a CyanADP flow cytometer and P-selectin expression measured. P-values calculated using Student's paired t-test. Data show mean±SEM; n=6.

Due to the significant decrease in P-selectin expression seen in aspirin-treated CRP-XL-activated platelets, the effect of aspirin on platelet monocyte aggregate formation was also measured as this is dependent on platelet P-selectin. Whole blood was incubated at room temperature for 10min with aspirin (0-300μM) before incubation at 37°C for 10min with 0.5μg/ml CRP-XL. Blood samples were incubated with CD14-RPE-Cy5 and CD42b-RPE to stain monocytes and platelets respectively and analysed for MPA formation using a CyanADP flow cytometer. Each sample was analysed in duplicate.

At T0, 33.7±2.5% (mean±SEM) of monocytes were positive for CD42b (figure 3.13a) and had a median fluorescence (Md X) of 1.91±0.15 (figure 3.13b). Upon activation with 0.5μg/ml CRP-XL, MPA formation increased to 94.3±0.4%. There was no change in MPA formation in the presence of any of the concentrations of aspirin (figure 3.13a). There was, however, a trend towards an increase in Md X fluorescence with all concentrations of aspirin, although only an n of 1. This ranged from 100.8±0.45 (samples ran in duplicate) (300μM) to 107.7±4.0 (50μM), with an average increase in Md X fluorescence of 25.2±1.1 compared to activated samples without aspirin (78.7±4.9).

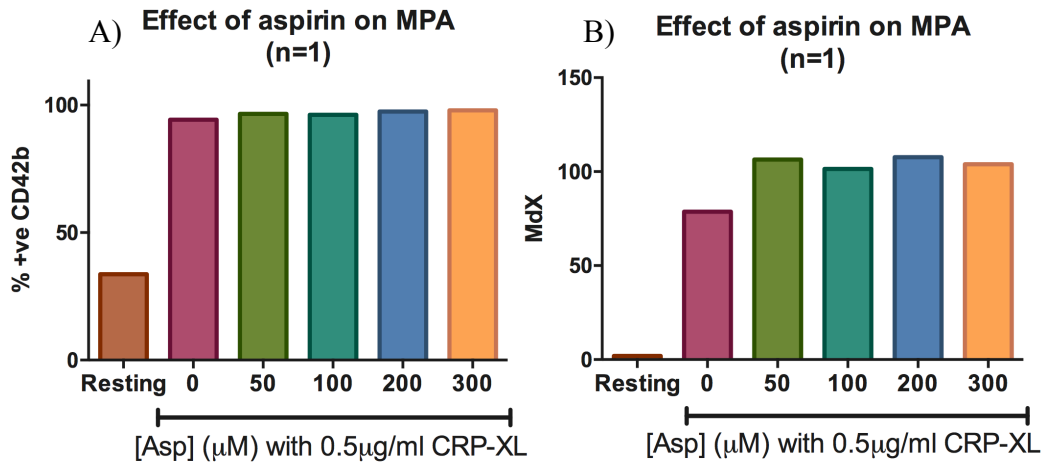

Figure 3.13: Effect of aspirin on monocyte platelet aggregation

*Whole blood was incubated with or without increasing doses of aspirin (0-300μM) prior to stimulation with 0.5μg/ml CRP-XL. Monocyte platelet aggregates were analysed using the Coulter EPICS XL flow cytometer. Monocytes were gated and analysed for expression of the platelet marker CD42b. Figures show CD42b positive expression A) and mean fluorescence intensity B). P-values calculated using an ordinary 1 way ANOVA (**=<0.001 and ***=<0.0001). Data show mean±SEM; n=1.*

These results suggest whilst aspirin slightly reduces platelet P-selectin expression, it has no inhibitory effect on MPA formation. The increase in anti-CD42b antibody fluorescence is probably as a consequence of aspirin inhibiting platelet-platelet aggregation, allowing more platelets to bind to each monocyte.

3.4.3 Effect of aspirin on gene expression in platelet-activated monocytes

In order to determine the effect of aspirin on monocyte gene expression, whole blood was incubated at 37°C with either a low ($8.3x10^{-5}$M; 75mg) or high ($5x10^{-4}$M; 450mg) dose of aspirin (equivalent to ~100mg/day or 600mg/day in man respectively) for 10min before activating the platelets with 0.5μg/ml CRP-XL (batch 1) for 6h. Monocytes were isolated using CD14 Dynabeads®, and gene expression analysed by RT-qPCR.

As previously, activation of platelets with CRP-XL caused a significant increase in monocyte *tfpi* expression after 6h compared to resting. Both low and high doses of aspirin reduced *tfpi* expression by 42.6±11.7% and 39.5±9.7% respectively, although they did not reach significance (figure 3.14a). The effect of aspirin on *procr* expression followed a similar profile; CRP-XL caused a significant increase compared to resting with the low dose of aspirin reducing this by 56.3±6.9% and the high dose by 52.3±9.6 but again these did not reach significance (figure 3.14b). Aspirin had the opposite effect

on monocyte *pparγ* expression however, with the low dose increasing expression by 50.5±15.9% (p=0.0096). The high dose by showed a similar affect (64.2±35.5%) but did not reach significance (figure 3.14c).

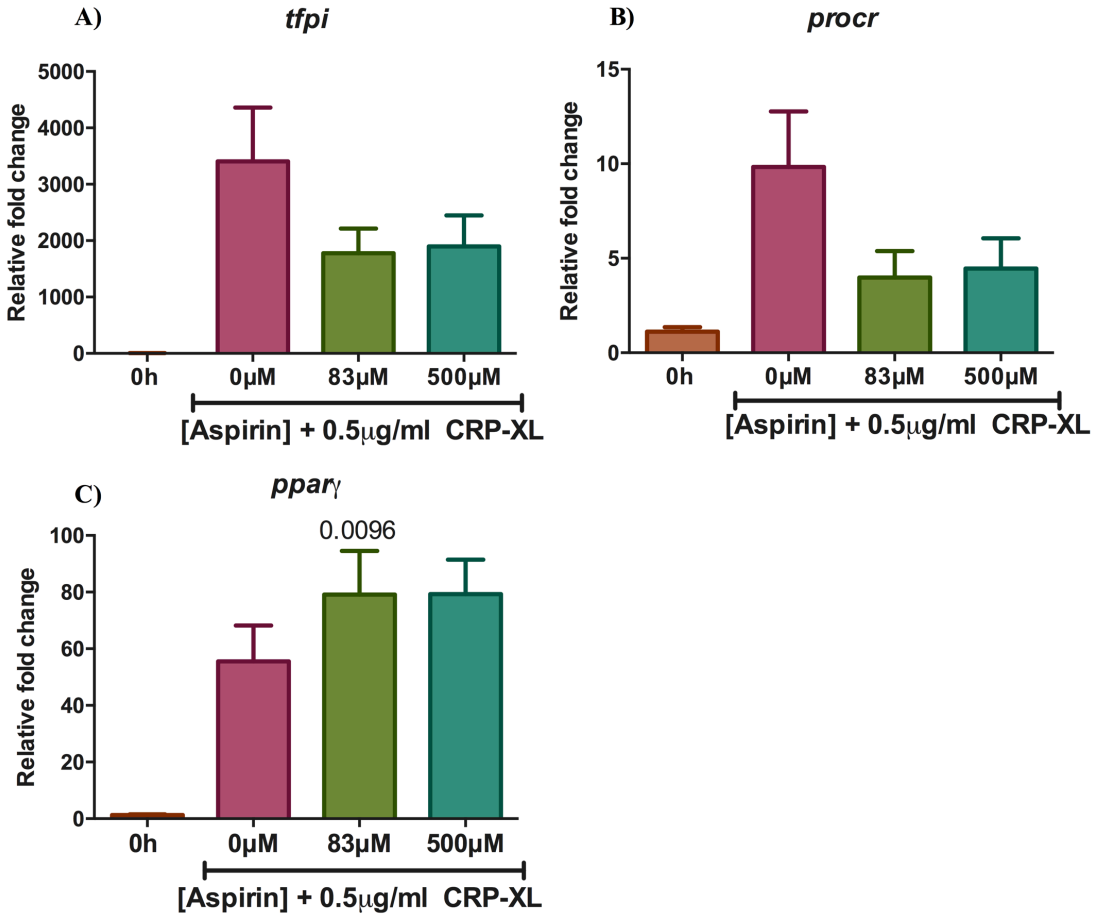

Figure 3.14: Effect of aspirin on platelet-activated monocyte gene expression

Whole blood in the absence or presence of low (83μM) or high (500μM) doses of aspirin was stimulated with 0.5μg/ml CRP-XL for 6h before monocyte isolation and RT-qPCR using a QuantiFAST SYBRgreen mastermix for tfpi A), procr B) and pparγ C). P-values calculated using a Wilcoxon test for tfpi and procr and a Student's paired t-test for pparγ. Data show mean±SEM; n=4.

The effect of aspirin on monocyte gene expression seen in these results suggests that aspirin is the likely cause for reduced monocyte *tfpi* and *procr* expression in platelet-activated monocytes from STEMI patients. The effects on monocyte *pparγ* expression is also in concordance with reports from the literature (Hua et al., 2009; Yiqin et al., 2009) illustrating the diverse roles aspirin plays in gene regulation.

3.4.4 Effect of aspirin-inhibited platelets on monocyte gene expression

After demonstrating the role of aspirin in platelet-induced monocyte gene expression in a whole blood model, the next step was to determine whether this effect was being

mediated through the action of aspirin on platelets or on monocytes. PRP was prepared from whole blood and half the platelets treated with aspirin (500µM) for 10min before being washed 3 times with HBS pH 6, the final supernatant was saved and used in platelet aggregometry to show the aspirin had been removed (figure 3.15). The remaining blood cell pellet was used to isolate monocytes using CD14 microbeads.

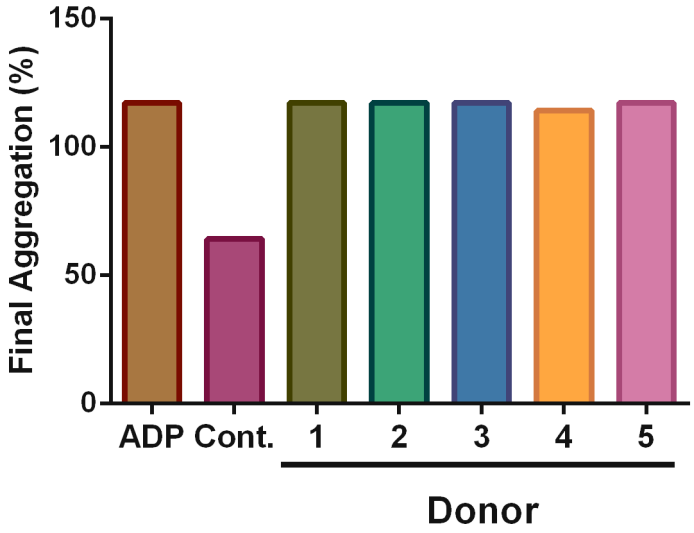

Figure 3.15: Platelet aggregometry using supernatant from aspirinated platelets

Platelets were isolated from whole blood and incubated with 500µM aspirin for 10min at 37°C before 3 washes in HBS. The supernatant from the final wash was saved and used in platelet aggregometry. Cont. is the control sample and the numbers refer to the donor.

Incubations were set up as follows: 0h, 6h platelets without aspirin and monocytes, 6h platelets with aspirin and monocytes and 6h both platelets and monocytes with aspirin before activation with 0.5µg/ml CRP-XL (figure 3.16). Total RNA was extracted using RNeasy columns and gene expression analysed by RT-qPCR.

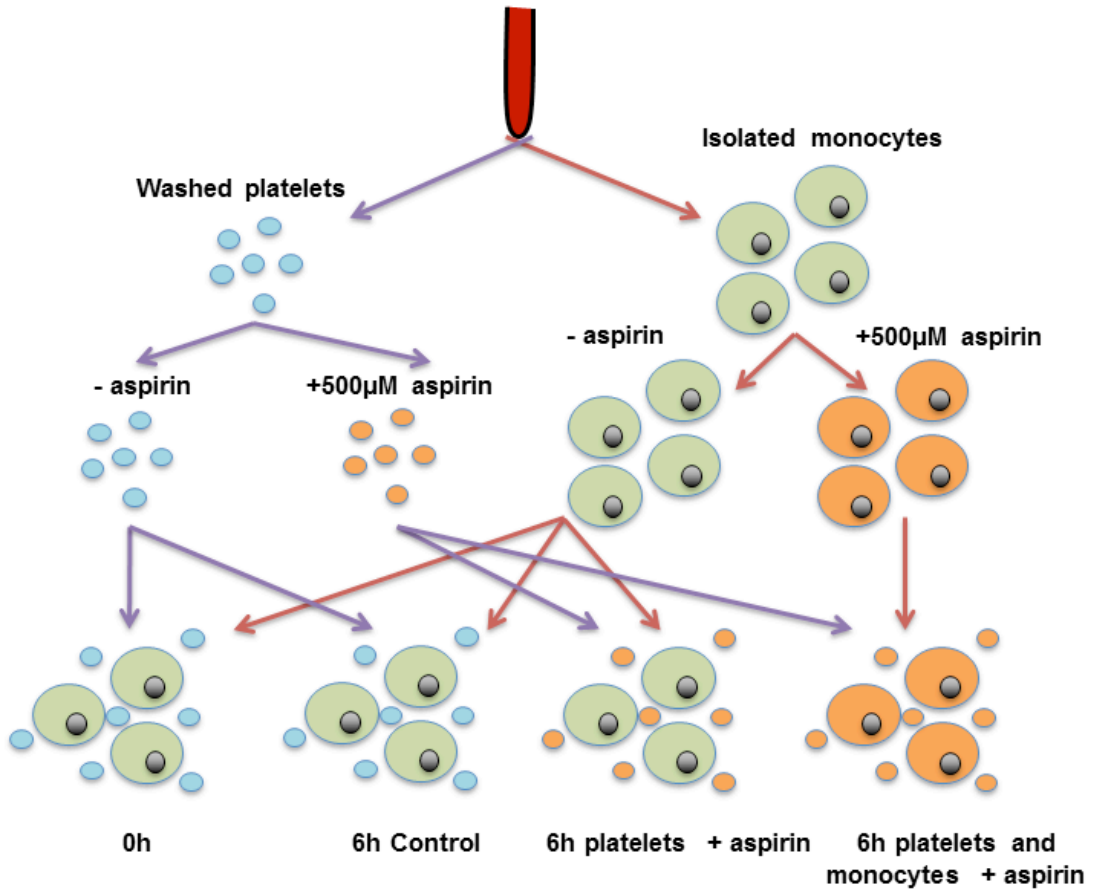

Figure 3.16: Experimental approach to identify method of aspirin action

Washed platelets were incubated in the presence of aspirin (500μM) or vehicle before reconstitution with autologous monocytes that had been incubated in the presence of aspirin (500μM) or vehicle in the indicated combinations.

Both *tfpi* and *procr* showed a similar expression profile. Expression was significantly increased between resting and activated samples (*tfpi* p=0.0190; *procr* p=0.0203; n=5). When only the platelets where inhibited with aspirin *tfpi* expression decreased by 33.5±2.7% (mean±SEM; p=0.0166) with no further decrease when both platelets and monocytes were inhibited. This result was similar for *procr*, with a 46.3±4.1% decrease in expression when only platelets were inhibited with aspirin (p=0.0098) and no further decrease when both monocytes and platelets were inhibited (figure 3.17a and b). Unlike the previous results in whole blood, there was no significant change in *pparγ* expression when either the platelet or the platelets and monocytes were inhibited with aspirin, suggesting regulation of this gene may be more complicated than first thought (figure 3.17c).

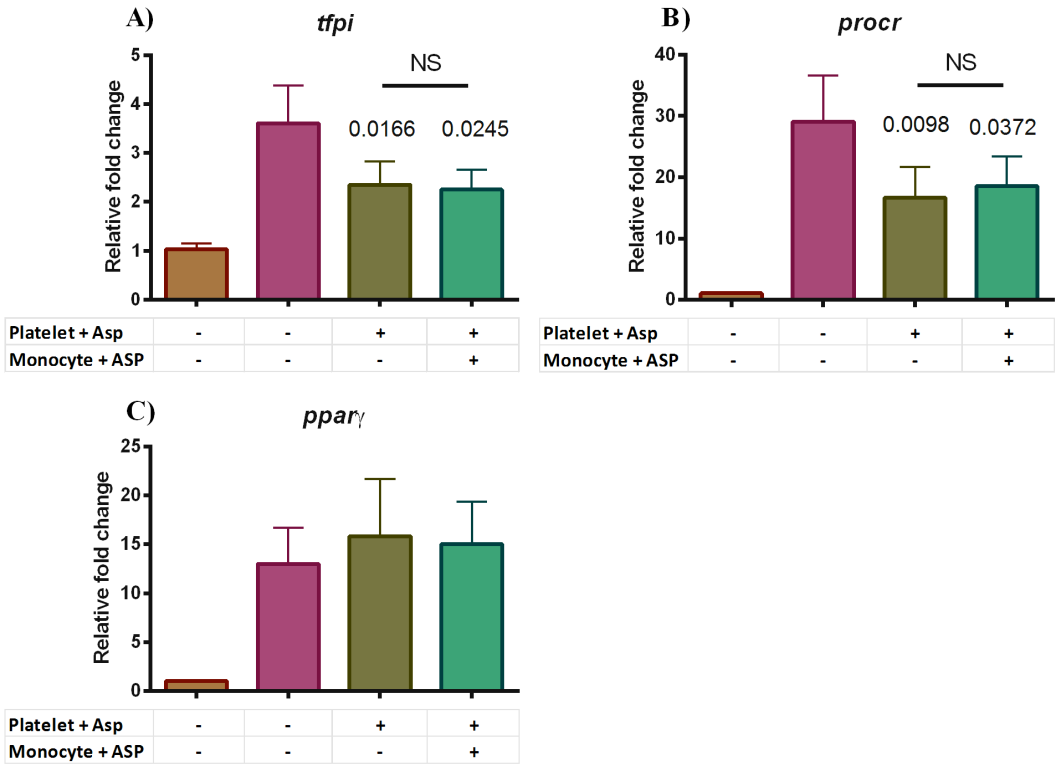

Figure 3.17: Effect of aspirinated platelets and aspirinated platelets and monocytes on gene expression *Washed platelets ±500μM aspirin were reconstituted with autologous monocytes ±500μM aspirin and incubated for 6h at 37°C before total RNA was isolated and RT-qPCR carried out using QuantiFAST SYBRgreen master mix for tfpi A), procr B) and pparγ C). P-values were calculated using a Student's paired t-test for tfpi and procr and a Wilcoxon test for PPARγ. Data show mean±SEM; n=5.*

These results indicate that the effect of aspirin on monocyte *tfpi* and *procr* gene expression seen in whole blood is a result of aspirin inhibiting COX-1 in platelets, rather than a direct effect of aspirin on monocytes. The slight trend towards increased expression of monocyte *pparγ* gene expression under both conditions suggests that aspirin may be mediating its slightly enhancing effect through platelets and not monocytes.

3.4.5 Effect of aspirin-treated platelet-derived soluble metabolites on monocyte *tfpi*, *procr* and *pparγ* expression

Previous results had shown that *tfpi* and *pparγ* expression was regulated in part through platelet-derived oxylipins and *procr* was through platelet-derived proteins. Therefore, to determine if the observed effect of aspirin was on these fractions, platelets, treated with or without aspirin, were activated and the releasate fractionated as in the method described previously (3.3.4).

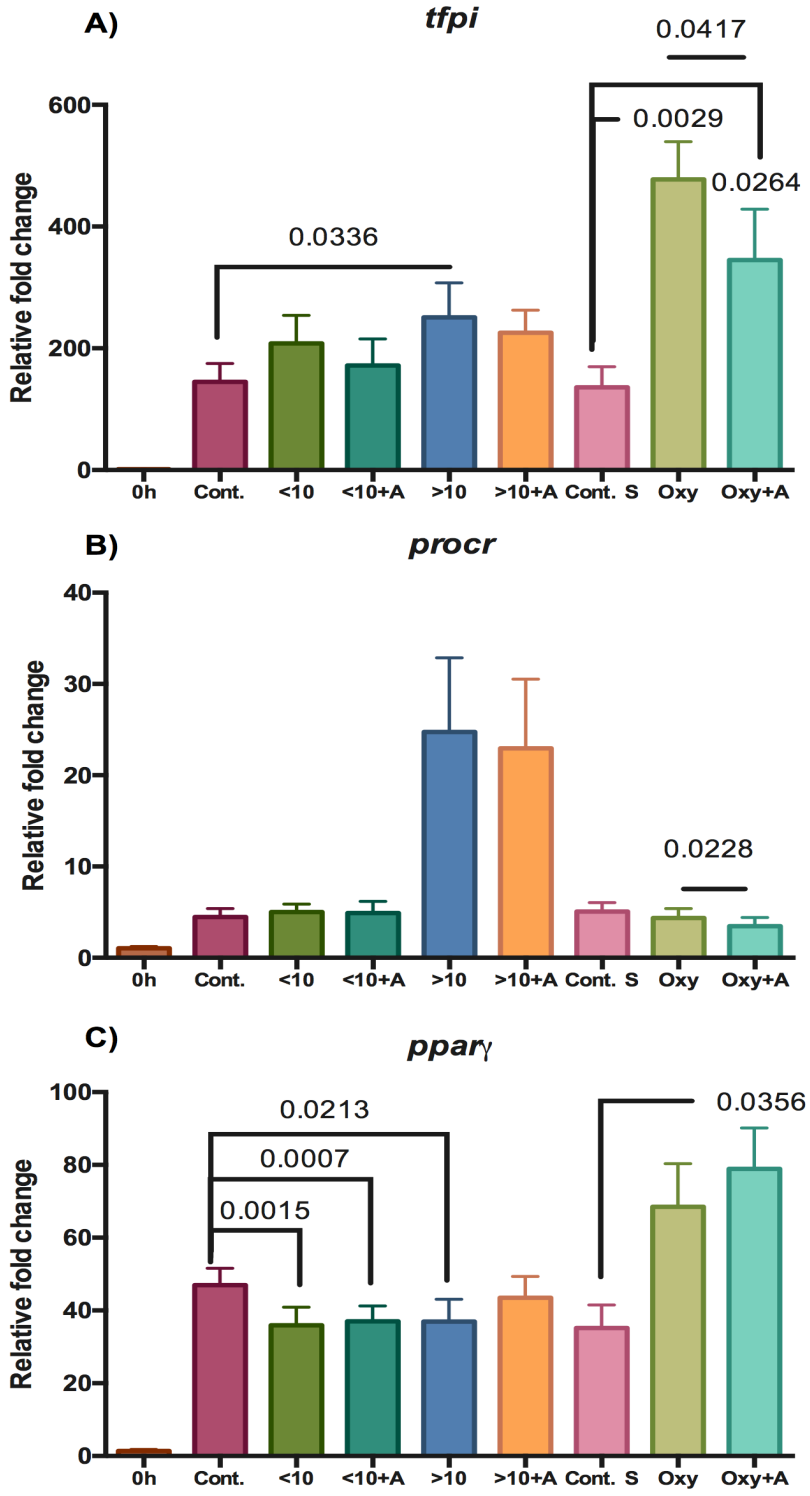

Figure 3.18: Effect of aspirin-treated platelet-derived metabolites on monocyte gene expression

Platelet-derived < and > 10kDa proteins and extracted AA metabolites pre-treated ± 500μM ASP were incubated for 6h with autologous monocytes before RNA extraction and RT-qPCR for tfpi A), procr B) and C) pparγ. Data show mean±SEM. P-values calculated using a repeated measures one way ANOVA; n=4. The '+A' represents with aspirin and 'oxy' is oxylipins.

The expression of all 3 genes was similar to section 3.3.4 (figure 3.9), with *tfpi* predominantly induced by oxylipins, *procr* by >10kDa proteins and *pparγ* by oxylipins.

There was a significant decrease in *tfpi* expression induced by the oxylipins derived from aspirin-treated platelets compared to those from non-aspirin-treated platelets (30.9±13.0% decrease; p=0.0417), similar to that seen in previous experiments (figure 3.18a). A small decrease was observed in *tfpi* expression with proteins both < and > 10kDa, but this was not significant.

There was a small decrease in *procr* expression between the aspirin and non-aspirin treated >10kDa proteins (p=0.0630). A significant decrease was observed in the aspirin-treated compared to non-aspirin-treated oxylipins (p=0.0228), although neither of these fractions produced a significant difference in gene expression compared to control (figure 3.18b).

Monocyte *pparγ* gene expression showed no change in the presence of aspirin with protein < or > 10kDa. There was a 17.2±8.6% increase in *pparγ* expression with oxylipins derived from aspirin treated platelets compared to untreated platelets although this was not significant (figure 3.18c).

3.5 Effect of inhibiting 12-LOX on gene expression in platelet-activated monocytes

3.5.1 Effect of esculetin and baicalein on platelet aggregation

Having explored the effect of inhibiting COX-I with aspirin, the effect of inhibiting 12-LOX on platelet aggregation was determined using two inhibitors; esculetin and baicalein. First each inhibitor was titrated against CRP-XL using Born-type aggregometry (figure 3.19).

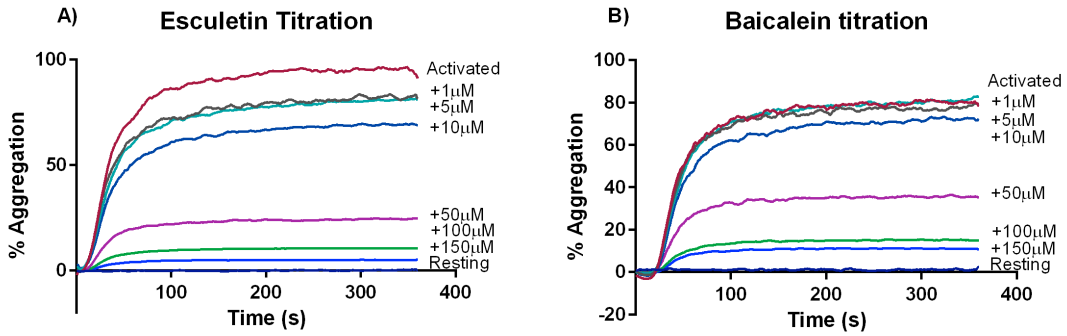

Figure 3.19: Representative aggregometry trace in response to esculetin and baicalein

PRP was incubated at 37°C for 10min with increasing concentrations of either esculetin or baicalein (10-150μM) before activation with a concentration of CRP-XL that produced almost maximal aggregation (determined individually for each donor) and aggregation recorded for 6min.

Initially both ADP and CRP-XL were used as agonists for these titrations (data not shown) however, similar results were obtained with both, suggesting the effect was not principally affecting the secondary wave of aggregation, therefore experiments were limited to CRP-XL. As previously, first a concentration of CRP-XL that gave almost maximal aggregation was determined for each donor. PRP was then incubated for 10min with increasing doses of either esculetin or baicalein (10-150µM) before activation with CRP-XL and aggregation recorded for 6min.

Stimulation with CRP-XL caused almost maximal aggregation of 86.6±4.2% (mean±SEM; p=<0.0001; n=5). The addition of 1µM and 5µM esculetin produced a small decrease in final aggregation (FA) to 79.4±2.7% and 72.4±3.3% respectively. Higher concentrations of esculetin produced a steady, concentration-dependent decrease in FA, falling to 3.6±0.4% at the highest concentration (150µM) (figure 3.20a). Baicalein, at the same concentrations showed an almost identical profile to esculetin (figure 3.20b). A similar profile for AUC was also observed with both inhibitors (data not shown). These results indicate that 150µM esculetin and baicalein completely block platelet aggregation in response to CRP-XL, with a mode of action that differs from that of aspirin in that they block primary aggregation.

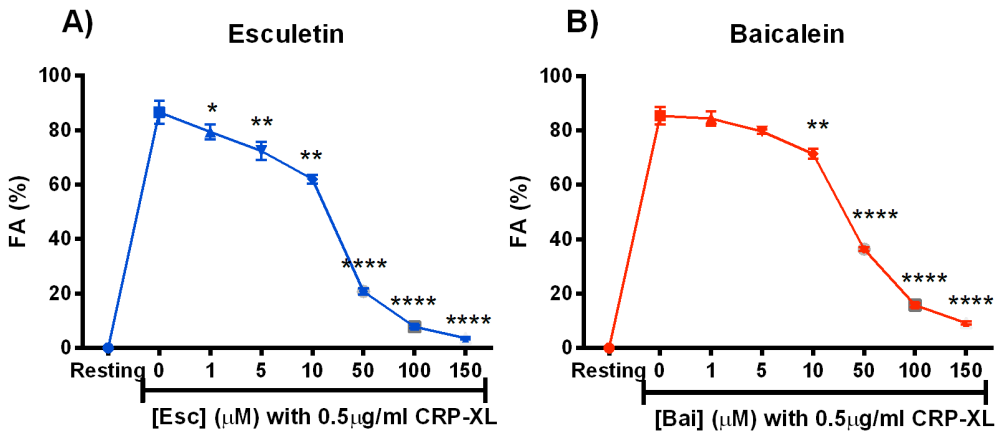

Figure 3.20: Effect of esculetin and baicalein on platelet aggregation

PRP was prepared and incubated for 10min with increasing concentrations of esculetin or baicalein (0-150µM) before activation with 0.5µg/ml CRP-XL and aggregation recorded for 6min. Figures are: FA with esculetin A) and FA with baicalein B). P-values calculated using an ordinary one-way ANOVA (=<0.05, **=<0.01 and ****=<0.0001). Data show mean±SEM; n=5.*

3.5.2 Effect of esculetin and baicalein on platelet activation and platelet monocyte aggregation

The effect of 12-LOX inhibition on platelet α-granule release, as measured by P-selectin expression, was also assessed by flow cytometry. PRP was incubated at 37°C for 10min with or without 150μM baicalein or esculetin before activation with 0.5μg/ml CRP-XL and incubation with an anti-P-selectin-FITC antibody.

P-selectin expression in platelets activated by CRP-XL was similar in the presence or absence of 12-LOX inhibitors, suggesting that 12-LOX probably does not play a role in platelet α-granule release (figure 3.21).

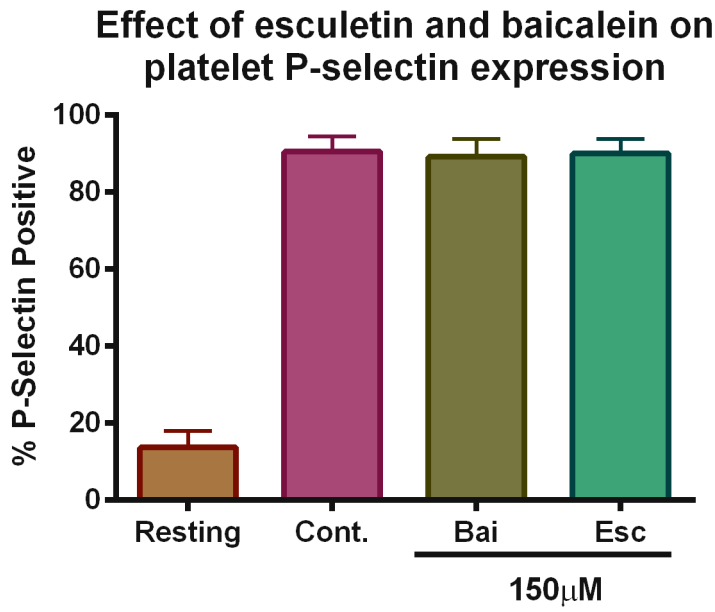

Figure 3.21: Effect of 12-LOX inhibition on platelet α-granule release

PRP was prepared from healthy donors and incubated at 37°C for 10min with or without 150μM baicalein or esculetin before activation with 0.5μg/ml CRP-XL. PRP was incubated for 20min with an anti-P-selectin-FITC antibody before analysis using a Gallios flow cytometer. Data show mean±SEM; n=3.

Although 12-LOX inhibition had no effect on platelet P-selectin expression, the effect on platelet monocyte aggregation was still measured as, like aspirin, inhibiting 12-LOX prevents platelet aggregation and may increase the amount of platelets binding to monocytes. Whole blood was incubated at 37°C for 10min with and without 150μM baicalein or esculetin before the addition of 0.5μg/ml CRP-XL (batch 1). Blood samples were incubated with CD14-RPE-Cy5 and CD42b-RPE to label monocytes and platelets respectively and analysed for MPA formation using a Gallios flow cytometer.

At rest, 33.6±12.6% (mean±SEM) of monocytes were positive for CD42b expression (figure 3.22a) and had a median fluorescence intensity (MdX) of 4.7±1.2 (figure 3.22b). Upon activation with 0.5µg/ml CRP-XL, MPA formation increased to 89.3±5.4%. There was no significant change in MPA formation in the presence of either 12-LOX inhibitor (figure 3.22a). After platelet activation, MdX fluorescence increased to 33.6±6.6. Interestingly, unlike aspirin, there was no increase in the MdX fluorescence with either 12-LOX inhibitor but a slight trend towards a decrease although not significant (figure 3.22b).

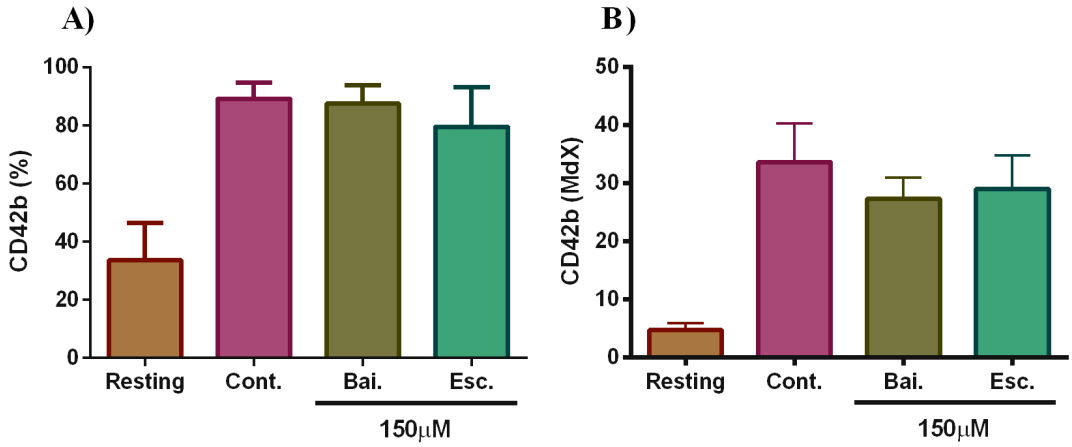

Figure 3.22: Effect of 12-LOX inhibition on MPA formation

Whole blood was incubated with or without 150µM baicalein or esculetin prior to stimulation with 0.5µg/ml CRP-XL. Monocyte platelet aggregates were analysed using a Gallios flow cytometer. Monocytes were gated and analysed for expression of the platelet marker CD42b. Figures show CD42b positive expression A) and mean fluorescence intensity B). Data show mean ±SEM, n=3.

3.5.3 Effect of 12-LOX inhibition on gene expression in platelet-activated monocytes

To explore the effect of 12-LOX inhibition on monocyte anti-thrombotic gene expression and to see the combined effect of both COX-1 and 12-LOX inhibition, whole blood was incubated at 37°C for 10min with vehicle (0.1% dimethyl sulfoxide (DMSO)), 150µM esculetin ±500µM aspirin or 150µM baicalein ±500µM aspirin before platelet activation with 0.5µg/ml CRP-XL for either 2h or 6h at 37°C. Monocytes were isolated using CD14 Dynabeads® and gene expression analysed by RT-qPCR (figure 2.23).

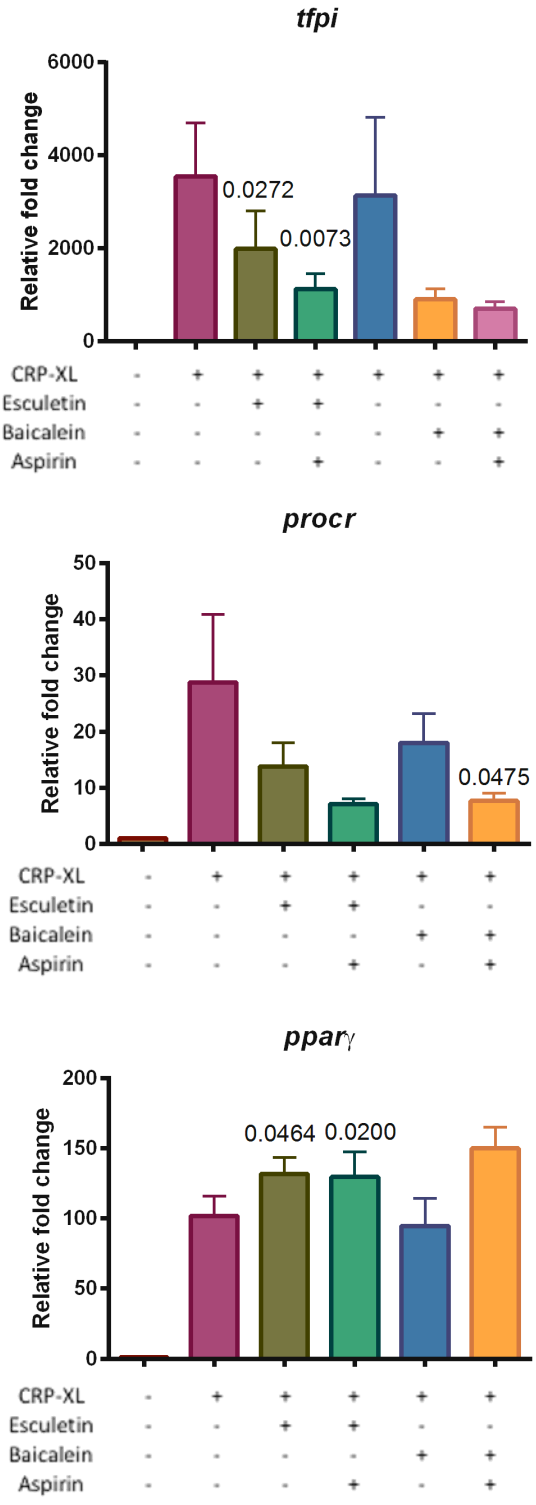

Figure 3.23: Effect of 12-LOX inhibition on platelet-activated monocyte gene expression

Whole blood was incubated at 37°C for 10min with 150μM esculetin or baicalein with or without 500μM aspirin before incubation with 0.5μg/ml CRP-XL for 2h (for pparγ) or 6h (for tfpi and procr). Monocytes were isolated and RT-qPCR carried out to assess gene expression for tfpi A), procr C) and pparg E). B), D) and F) are normalised to CRP-XL only samples for tfpi, procr and pparγ respectively. P-values calculated using an ordinary 1 way ANOVA. Data show mean±SEM, n=3.

The 6h time point was used to measure monocyte *tfpi* and *procr* expression. Both showed a similar increase after activation and exhibited similar changes in expression with 12-LOX inhibition. In the presence of esculetin, monocyte *tfpi* expression decreased by 47.4±5.9% (mean±SEM; n=3), with a further 33.7±12.7% reduction by addition of aspirin (figure 3.23a and b). In the presence of baicalein, a similar pattern was seen although to a slightly lesser extent and with more variation between donors. Monocyte *procr* expression decreased by 45.8±17.4% with esculetin and the addition of aspirin further decrease expression by 37.6±17.8. Baicalein reduced expression by 30.8±7.9% and the addition of aspirin further decreased expression by 54.2±7.3% (figure 3.23c and d).

Changes in monocyte *pparγ* gene expression in the presence of esculetin and baicalein with and without aspirin were harder to interpret. Esculetin increased expression by 31.2±7.6% (mean±SEM; n=3) with no further increase in the presence of aspirin. Interestingly, this profile was not observed with baicalein, which showed no difference in *pparγ* expression alone but a trend towards increased expression (56.2±33.3%) with the addition of aspirin, although this did not reach significance (figure 3.23e and f). The explanation for this difference in expression between the two 12-LOX inhibitors is currently unknown.

These results suggest that both the cyclooxygenase and lipoxygenase pathways of AA metabolism are important for regulating *tfpi* and *procr* gene expression in platelet-activated monocytes and the effect is additive. Suggesting products of both COX-1 and 12-LOX pathways may be involved. How these two pathways regulate *pparγ* gene expression is currently unclear but some answers could lie in the off-target effects of these inhibitors.

3.6 Monocyte gene expression in an *in vitro* model of thrombosis

The experimental model up to now has relied on the activation of platelets in the absence of thrombus formation and the measurement of monocyte gene expression. To determine if monocyte gene expression is relevant in a thrombus model the Chandler loop model was used as an *in vitro* model of thrombosis. Whole blood was incubated with CD14 Dynabeads to deplete monocytes and the blood resuspended in the original volume of autologous plasma. Chandler loop thrombi were formed with and without monocytes for 6h. Resulting thrombi were homogenised in TRIzol and the expression of *tfpi, procr* and *pparγ* genes analysed by RT-qPCR (figure 3.24).

To confirm that monocytes were effectively removed, flow cytometry was used to measure CD14+ve cells. Before depletion, 7.4±1.2% (mean±SEM) of the total leukocyte population was CD14 positive. This decreased to 0.32±0.089% after monocyte depletion (p=0.0032; n=5), representing a 95.5±1.1% reduction in CD14+ve cells (figure 3.24a).

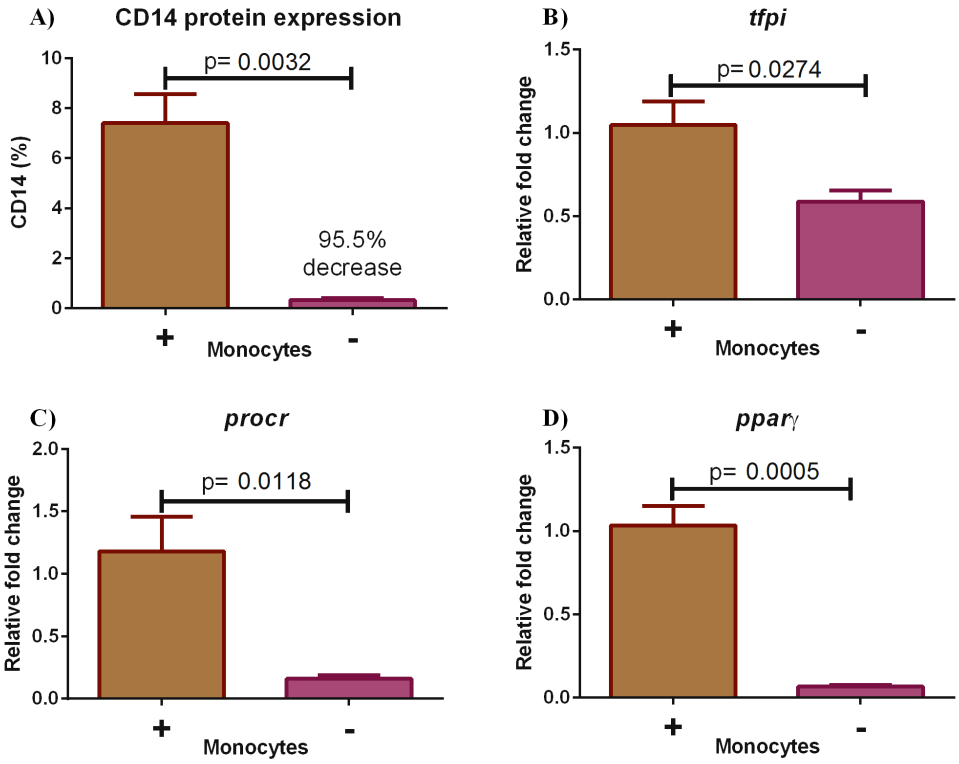

Figure 3.24: Monocyte contribution to antithrombotic gene expression within a thrombus.

A) Whole blood ±monocytes was used in flow cytometry experiments to measure CD14 expression using a XL Epics flow cytometer. Whole blood ±monocytes was re-calcified and Chandler loop thrombi formed before homogenisation, RNA extraction and measurement of or tfpi B) procr C) and pparγ D) mRNA expression by RT-qPCR. P-values calculated using Student's paired t-test. Data show mean±SEM, n=6.

Expression of all 3 genes was significantly lower in thrombi formed from blood depleted of monocytes (figure 3.24b-d). Using expression in thrombi formed with monocytes as the positive control, *tfpi* gene expression decreased from 1.05±0.14 (mean±SEM) to 0.59±0.066 in the thrombi formed with monocyte-depleted blood, representing an average decrease of 39.3±9.4% (p=0.0274; n=6). *Procr* gene expression decreased from 1.2±0.28 to 0.16±0.029 representing an average decrease of 82.7±4.8% (p=0.0118; n=6) while *pparγ* gene expression decreased from 1.0±0.12 to 0.065±0.012; an average decrease of 93.1±1.7% (p=0.0005; n=6).

These results highlight the importance of monocyte gene expression on the levels of these 3 key anti-thrombotic genes in thrombi. Almost maximal contribution of *pparγ* (~90%) and *procr* (~80%) mRNA and ~40% of *tfpi* mRNA.

3.7 Discussion

Platelets are fundamental to the processes of haemostasis and thrombosis. However, unlike nucleated cells, platelets have restricted flexibility in their response to the local environment due to limited capacity to translate protein from pre-existing mRNA pools, and are unable to transcribe genes in response to stimuli. Activated platelets can bind to monocytes in the circulation through receptor ligand interaction. The platelet-dependent recruitment of monocytes into thrombi and subsequent activation allows the potential for the synthesis of new genes and proteins to regulate thrombus growth, stability and dissolution. The way in which activated platelets switch on and regulate gene expression in monocytes and the contribution of monocytes to thrombus dynamics is a largely understudied area of research, with most focus on the induction of TF through P-selectin•PSGL-1 interaction (Celi et al., 1994; Christersson et al., 2008; Furie and Furie, 1996).

The aim of this chapter was to identify the pathway from activation of platelets to induction of monocyte *tfpi*, *procr* and *pparγ* expression and was based on the previous findings that i) *tfpi* and *procr* are increased in monocytes in response to platelet activation in stable STEMI patients and controls, ii) expression of both *tfpi* and *procr* was significantly lower in stable STEMI patients then controls and iii) PPARγ is upregulated in monocytes after platelet activation. By using RT-qPCR, the main findings from this chapter are as follows:

I. Activated platelets increase monocyte *tfpi* and *procr* expression in a time dependent manner reaching a maximum at 8h
II. Activated platelets increase monocyte *pparγ* expression maximally after 2h
III. Expression of all three genes is dependent on endogenous transcription
IV. Direct monocyte platelet interaction is not required for *tfpi* and *procr* expression but is for the majority of *pparγ* expression
V. The increase in *tfpi* and *pparγ* expression seen with soluble mediators is due to oxylipins whereas *procr* is due to proteins

VI. Treatment with aspirin attenuates *tfpi* and *procr* expression but increases *pparγ* expression. In all three cases this is likely through the effect of aspirin on platelets

VII. Similar results are also seen with the inhibition of 12-LOX

VIII. Inhibiting both 12-LOX and COX-1 has an additive inhibitory effect on expression of monocyte *tfpi* and *procr*

The current model was chosen as opposed to cultured peripheral blood monocytes or a monocyte cell line for a number of reasons. Firstly, monocytes incorporated into a growing thrombus are recruited directly from the circulation, and so by using freshly isolated monocytes we are closely replicating the phenotype of those cells. Second, thrombus formation in response to injury is rapid, and propagated by activated platelets. By using whole blood we can specifically activate platelets and incubate for short periods of time, allowing minimum genotypic and phenotypic changes in monocytes. Third, adherence to plastic can, by itself, initiate differentiation of monocytes to macrophages (Kaplan and Gaudernack, 1982) through a separate mechanism that may or may not reflect factors occurring within a thrombus. Finally, monocyte cells lines, whilst used as a comparison in some experiments, are fusions with immortal cells and do not represent true monocytes.

Activation of platelets was achieved through GPVI activation with the collagen mimetic CRP-XL (Knight et al., 1999). GPVI, as opposed to PAR1/4 or P2Y1/12, was chosen because this receptor leads to degranulation and is integral to activation of integrins through inside out signalling at sites of vascular damage in areas of high shear, such as those in the arterioles of the myocardium (Nieswandt and S. P. Watson, 2003). GPVI, unlike the ADP and thrombin receptors, is unique to platelets and therefore any changes in monocyte genotype and phenotype would be a consequence of platelet activation.

Both *tfpi* and *procr* mRNA showed small increases in expression over the 8h time course in unstimulated samples, attributed to a degree of spontaneous platelet activation in the samples. When stimulated however, there were large increases in the expression of both genes after 4h, reaching a maximum at 8h. Expression of *pparγ* in the platelet activated samples showed the largest increase at 2h. These results suggest upregulation of monocyte *tfpi* and *procr* expression is later in platelet-activated monocytes in comparison to *pparγ*. For technical reasons and costs the 6h time point was chosen to analyse expression of all 3 genes, although for some later experiments, *pparγ* expression was analysed at 2h.

Activated platelets are known to contain mRNA (Schubert et al., 2014) that can be released into microvesicles and a recent platelet transcriptomic study identified *tfpi* mRNA in platelets and placed it in the top 8 percentile of all platelet mRNA. mRNA for *procr* and *pparγ* were below the cut-off (L. M. Simon et al., 2014). The rise in monocyte *tfpi* could therefore be due to transfer of platelet mRNA to the monocyte. Gene expression was shown to be endogenous to monocytes through inhibition of transcription by actinomycin D. However, whilst *tfpi* expression showed a ~97% decrease in expression in the actinomycin treated compared to untreated samples, there was still a small 27-fold increase compared to unstimulated samples that could result from transfer of mRNA from platelet microvesicles. With the current knowledge and experimental techniques, testing this would be difficult. Some research has shown transfer of fluorescently labelled material into THP-1 cells (Risitano et al., 2012), but showing transfer of a specific mRNA molecule into peripheral blood monocytes is challenging.

Platelets interact with monocytes in a number of different ways. This can be through direct contact, the most common being the P-selectin•PSGL-1 interaction but also CD40L•CD40, CD36•CD36 homodimer complex, αIIbβ3/GPIb/JAM-C•Mac1 and others (van Gils et al., 2009b). All of these direct contacts have the potential to initiate signalling and induce gene expression with the most well studied being P-selectin-induced expression of TF in monocytes (Celi et al., 1994; Christersson et al., 2008; Ezzelarab et al., 2014; Lindmark et al., 2000). However, platelets also secrete a cocktail of proteins, small molecules and ions from their α- and dense granules, as well as oxylipins generated from AA, and vesicles containing protein, mRNA and miRNA. This means platelets have a number of ways to influence other cells.

Induction of *tfpi* and *procr* was shown likely to be dependent on released material rather than through direct contact. However, due to the increased response of one donor for *tfpi* and *procr*, further experiments are required to confirm blocking MPA formation does not affect expression levels. In addition to the method used here, incubating monocytes with a PSGL-1 activating peptide in the absence of platelet activation could also show this. In contrast, expression of *pparγ* was shown, in part, largely to be dependent on direct monocyte platelet interaction. The concentrations of CRP-XL used were shown to result in limited Annexin-V binding, an indicator of MP formation. However, as MP release was not measured directly it was possible some expression could be being mediated through monocytes interacting with platelet-derived MP's.

Removing MP's by centrifugation showed induction of *tfpi* and *procr* expression to be derived from soluble mediators. Unfortunately, small vesicles such as exosomes can only be removed using specialised kits or ultra-centrifugation for long periods of time and so an interaction between exosomes and monocytes could not be ruled out, although these are thought mainly to consist of platelet-derived miRNA. Expression of *pparγ,* although shown to be mainly through direct contact, showed a decrease in expression with the platelet releasate, soluble fraction and microparticles, suggesting expression is both positively regulated by direct contact and negatively regulated through released material.

To determine the type of molecule inducing expression, the soluble material was separated into material < and > 10kDa, assumed to be largely protein, and oxylipins. In this case monocyte *tfpi* expression was shown to be oxylipin dependent and *procr* protein dependent. Although this is highly probable, conformation is needed by treating the platelet releasate with activated charcoal to remove oxylipins and proteinase K to digest proteins. The inhibition of *pparγ* expression seen with the platelet releasate and soluble fractions was replicated with both material < and > 10kDa suggesting negative regulation may be protein in nature. There was an ~200% increase in expression seen with platelet-derived oxylipins that could suggest regulation of monocyte *pparγ* is through transfer of a labile oxylipin. This could be through PPARγ, which is present in small amounts in circulating monocytes and is known to positively regulate its own transcription through oxylipin agonists (Steger et al., 2010; Wu et al., 1999).

Of the large number of soluble mediators released from activated platelets, a number are known to affect other cells including monocytes. For example, 12-HETE has been implicated in P-selectin induced TF expression (Pellegrini et al., 1998) and the α-granule proteins platelet factor 4 (PF4) and CCL5 (also known as regulated on activation, normal T-cell expressed and secreted (RANTES)) have been shown to affect a number of monocyte functions (Hundelshausen et al., 2001; Kasper et al., 2007; Kasthuri et al., 2012; Schall et al., 1990). These two chemokines could be responsible for some of the induction of *procr* seen here and this will be discussed further in chapter 5. The upregulation of *tfpi* by oxylipins further supports the hypothesis that *tfpi* could be regulated by PPARγ as a number of PPARγ ligands have been identified as released from platelets including 9- and 13-HODE (Daret et al., 1989; Itoh et al., 2008) and 12- and 15-HETE (Q. Li et al., 2004; Nagy et al., 1998) (see section 5.2).

Activation of platelets results in liberation of AA from the plasma membrane via activation of $cPLA_{2\alpha}$. Subsequently, AA can be converted to a number of oxylipins, the two most abundant being TXA_2 produced from COX-1 and 12-HETE from 12-LOX. These two enzymes are responsible for the majority of AA metabolism and can be inhibited by aspirin (COX-1) and esculetin or baicalein (12-LOX). To extend previous preliminary findings that indicated aspirin inhibits expression of *tfpi* and *procr* expression in monocytes, the effect of inhibiting both major pathways of AA metabolism on monocyte gene expression was studied, starting with aspirin.

Platelet aggregometry confirmed doses of aspirin between 30μM (27mg) (which is lower than the common 81mg prescribed for daily use) and 500μM (450.4mg) (equivalent to a 500mg loading dose) completely inhibited COX-1 activity. P-selectin expression was slightly reduced after treatment with aspirin but MPA formation was unaffected suggesting minimal effect on platelet degranulation, in agreement with the literature (Klinkhardt et al., 2003; Storey et al., 2002). Doses of aspirin corresponding to that prescribed to patients who have recently had an MI were used (assuming maximum absorption) (table 3.1), to look at the effect on gene expression in platelet-activated monocytes.

Table 3.1: Relationship between therapeutic aspirin dose and concentration used

	Amount (mg)	**Amount (g)**	**/by MW aspirin (180.157)**	**/by volume of circulating blood (5l)**	**Concentration (μM)**
Daily Dose	75	0.075	0.0004143mol	0.00008326M	83.26
Loading Dose	450	0.450	0.00249782mol	0.00049956M	499.56

There was a ~40% decrease in *tfpi* and ~53% decrease in *procr* expression was seen in the monocytes after aspirin treatment. For *tfpi* this corresponds to the observed effect of platelet-derived oxylipins on regulation of expression, and provides an explanation for the difference seen in platelet-activated monocytes from STEMI patients compared to controls. However, this finding potentially contradicts the established premise that aspirin should be given to all patients who have had an MI to reduce the risk of a re-infarction. The use of aspirin in primary prevention has always been debated and trials show that, whilst non-fatal MI is reduced in patients taking aspirin, overall cardiovascular mortality is unaffected (J. S. Berger et al., 2006; Eidelman et al., 2003). These findings, along with the increased risk of gastrointestinal bleeds and

haemorrhagic stroke, have limited the use of aspirin in primary prevention to high-risk males and patients with diabetes (Pignone et al., 2010; Steering Committee of the Physicians' Health Study Research Group*, 1989; E. Weber, 1988). In the prevention of secondary events, numerous trials have compared aspirin to placebo for a number of different endpoints. These were summarised by the Anti-platelet Trialist's Collaboration in 2009 and show, after meta-analysis, that aspirin reduces the secondary incidence of MI by 31%, stroke by 24% and total vascular deaths by 9% with an overall reduction in all events of ~25%, equating to 40 less events per 1000 people (Antithrombotic Trialists' (ATT) Collaboration et al., 2009). Whilst 25% is a significant reduction it still means that aspirin is ineffective in 75% of subjects. As we know, the processes that lead to an MI are multifactorial and reasons for only a 25% reduction could result from genetic variation and/or the increasingly recognised problem of "aspirin resistance" or unresponsiveness (C. N. Floyd and Ferro, 2014). However, this could also be explained, at least in part, by the effect aspirin has on monocytes. If expression of antithrombotic genes such as *tfpi* and *procr* is reduced, this in turn may affect thrombus size, stability and resolution.

An increase in *pparγ* expression at both doses of aspirin was seen, which is in line with the literature (Hua et al., 2009; Xue et al., 2010; Yiqin et al., 2009).

To establish whether the effect of aspirin was platelet or monocyte mediated; isolated platelets were treated with aspirin or vehicle before reconstitution with autologous monocytes treated with aspirin or vehicle. A sample in which only monocytes were treated with aspirin was not included for two reasons; i) recovery of monocytes from whole blood was low so it was not practical and ii) it proved almost impossible to remove platelets from the monocyte samples completely. The results showed a similar 35% reduction in *tfpi* and 45% reduction in *procr* when either only platelets were inhibited or when both platelets and monocytes were inhibited, which correlates well with the effect seen in whole blood; demonstrating aspirin is inhibiting monocyte gene expression through its effect on platelets. The expression of *pparγ* showed a slight increase with aspirinated platelets and/or monocytes but this was not to the same degree as compared to the whole blood results.

Aspirin, in addition to COX-1, also inhibits NF-κB (Kopp and Ghosh, 1994), which is present in both platelets (Liu et al., 2002) and monocytes. NF-κB is more important in monocytes, where it plays a role in regulating the expression of TF (Oeth et al., 1994) and other inflammatory genes such as TNFα (Shackelford et al., 1997). In this model it

is unlikely aspirin is affecting the role of NF-κB in monocytes as it was observed the effect of aspirin was platelet-mediated. Roles in platelets include integrin αIIbβ3 activation, platelet aggregation, P-selectin expression and platelet spreading (Malaver et al., 2009; Spinelli et al., 2010). The concentration of aspirin used was unlikely to affect NF-κB in platelets NF-κB inhibitors dose dependently inhibit platelet aggregation (Malaver et al., 2009), a feature not seen with the doses of aspirin used in this study.

Having established that *tfpi* and *pparγ* expression was largely dependent on platelet-derived oxylipins and *procr* expression on proteins, and that inhibition of COX-1 reduced *tfpi* and *procr* expression whilst increasing *pparγ* expression, experiments were performed using the platelet protein and oxylipin fractions derived from control and aspirin-treated platelets. For *tfpi*, a significant decrease in expression was seen with the oxylipins derived from aspirin-treated platelets consistent with the role of COX-1 in oxylipin production and suggesting *tfpi* is regulated by these metabolites. In contrast to *tfpi*, *pparγ* expression was increased by oxylipins derived from aspirin-treated platelets. This is similar to results seen in whole blood and could be due to the increased availability of AA for 12-LOX due to the inhibition of COX-1, increasing the concentration of 12-LOX-derived oxylipins, which may be involved in regulating *pparγ* expression. For *procr,* there was a trend towards decreased expression with protein >10kDa derived from aspirin-treated platelets. The effect of aspirin could be explained by its ability to reduce the overall amount of protein released from activated platelets. In a study by Coppinger et al., proteins detected in the releasate of activated platelets were significantly affected after treatment of the platelets with aspirin. Whilst the effect varied largely depending on the protein, a number were decreased by ≥50% (Coppinger et al., 2007), which could explain the effect seen on *procr* expression in whole blood.

12-LOX has been implicated in cross-talk between platelets and other cells. However, the role of 12-LOX in platelet activation is less clear. A dose titration using either esculetin or baicalein in aggregometry showed a dose dependent decrease in platelet aggregation; with almost complete inhibition at 150μM. Other reports in the literature have shown similar results with other 12-LOX inhibitors using a range of platelet agonists (Nyby et al., 1996; Yeung et al., 2013; 2012). Similar to aspirin, neither esculetin of baicalein effected platelet α-granule release as measured by P-selectin expression, or MPA formation.

Inhibiting 12-LOX with either esculetin or baicalein resulted in ~40% reduction in both *tfpi* and *procr* expression; similar to that observed with aspirin. Dual inhibition with both aspirin and the 12-LOX inhibitors resulted in a further decrease in expression. This is likely to be an additive effect as whilst the 12-LOX inhibitors do block TxA2 production, the concentration of aspirin used completely blocks COX-1 activity, as shown by MS in chapter 5. The effect of the 12-LOX inhibitors on monocyte *pparγ* expression is harder to interpret. With esculetin, expression increased significantly compared to control, but not as much as aspirin alone and this was not rescued with the addition of aspirin. For baicalein, no increase was seen compared to control but this was rescued to some extent with the addition of aspirin. Further investigation is needed to explain the differences between the two inhibitors but one possible explanation is off-target effects. Research into platelet 12-LOX is relatively sparce, so its mechanism of action and role within platelets is not well documented, although it appears to act upstream of PKC, to play a role in activating the integrin αIIbβ3, and to have roles in intracellular calcium accumulation and dense granule secretion (Yeung et al., 2012). Whether it is these roles of 12-LOX, or an effect on AA metabolism that is influencing gene expression, remains to be elucidated.

The last set of experiments was aimed to identify the role monocytes play in thrombus formation and whether monocyte expression of the genes of interest was important. The Chandler loop model was used as it mimics the arterial environment, and thrombi formed resemble arterial thrombi found *in vivo*. The formation of thrombus in the absence of monocytes had not been reported previously. First it was necessary to confirm their removal from blood by the magnetic beads using flow cytometry. Whilst flow cytometry showed an almost complete reduction in CD14 labelling, it is unlikely all monocytes were removed. Recent reports have suggested monocyte subsets are quite plastic and can change in response to various stimuli and disease. Preliminary data from our lab suggests CRP-XL activated platelets induce CD14 protein expression in $CD14^{low}/CD16^{+}$ monocytes changing them into $CD14^{+}/CD16^{+}$ monocytes (figure 3.25). $CD14^{low}/CD16^{+}$ monocytes are likely not to be removed from whole blood using CD14 magnetic beads and so would still be incorporated into a growing thrombus, being stimulated by activated platelets to turn on CD14 expression.

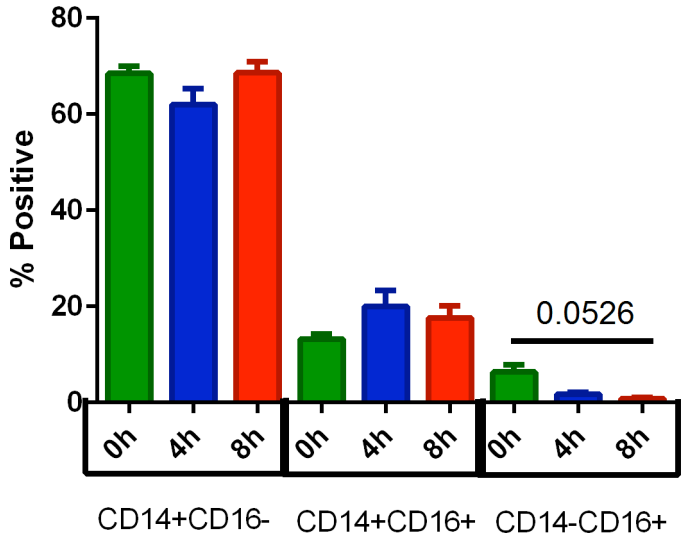

Figure 3.25: Platelet induced monocyte CD14/CD16 expression.

Isolated monocytes were incubated with activated platelets for up to 8h before flow cytometric analysis for dual CD14/CD16 expression. Data show mean±SEM.

In the present study, using this model of thrombus formation, monocytes have been shown as important for the expression of all three of the genes of interest, contributing almost 100% of *procr* and *pparγ* mRNA and 50% *tfpi* mRNA. These experiments confirmed the hypothesis that monocytes are important in thrombus formation, stability and gene expression.

In summary, this chapter has identified novel pathways of regulation of monocyte anti-thrombotic gene expression by oxylipins (*tfpi* and *pparγ)* and protein (*procr*) released from activated platelets. Aspirin was identified as the likely cause of lower gene expression of *tfpi* and *procr* in platelet activated monocytes from STEMI patients; this effect being mediated through its action on platelets. Inhibiting AA metabolism through 12-LOX also reduced *tfpi* and *procr* expression to a similar degree as aspirin.

Chapter 4: Monocyte anti-thrombotic protein expression

4.1 Introduction

Chapter 3 focused on the anti-thrombotic gene expression in monocytes induced by activated platelets and further dissected this by establishing the type of molecule released by platelets that induced these changes. Whilst the regulation of gene expression is an important indicator of cell function it does not always translate to a phenotype. The aim of this chapter was to establish whether the increased gene expression of monocyte *tfpi, procr* and *pparγ* induced by activated platelets could be replicated at the protein level. The primary method for detection of protein was western blotting but due to a number of technical problems encountered other methods were tried. As will be described in this chapter, protein expression could be detected for EPCR and PPARγ but TFPI protein expression could only be inferred from the data obtained.

4.2 Monocyte TFPI protein expression

This section aimed to determine whether platelet-induced monocyte *tfpi* gene expression correlates with an increase in monocyte TFPI protein expression. Unfortunately due to unanticipated problems with sample preparation and methodology this part of the project took longer then planned and yeilded ambiguous results. Selected results and method development will be explained in more detail below.

4.2.1 Flow cytometric analysis of TFPI on the surface of monocytes

There are a number of experimental techniques to measure protein expression from cells. In order to measure TFPI protein expression on monocytes the first method used was flow cytometry for two reasons: i) the method had been set up and partially opitimised by a previous member of the lab and ii) flow cytometry is a core technique in this laboratory with vast experience.

4.2.1.1 Experimental optimisation

Firstly, there are no available anti-TFPI antibody's validated for flow cytometry so initial experiments selected an anti-human TFPI mouse monoclonal antibody (R&D systems) and used the EA.hy926 cell line as a positive control. Secondly, there are currently no available directly conjugated anti-TFPI antibodies and therefore a

two-layer system was developed using a polyclonal goat anti-mouse-FITC conjugated secondary antibody to recognise the monoclonal mouse anti-hTFPI primary antibody.

Initially, 3 conjugated (all FITC) anti-mouse secondary antibodies were tested to identify which recognised the primary anti-TFPI antibody using $5x10^5$ EA.hy926 cells. EA.hy926 cells ($5x10^5$), in PBS pH 7.4/ 0.5% BSA/ 0.1% NaN_3, were incubated with anti-TFPI antibody (0-10µg/ml) for 30min at room temperature followed by 30min at 4°C with 10µl of each secondary antibody. Samples were then analysed using the Epics XL flow cytometer. Compared to controls, all 3 secondary antibodies recognised the anti-TFPI antibody, albeit to varying degrees. The Dako secondary antibody was best; reaching a maximum of 85.2% of cells positive for TFPI with 7.5µg/ml anti-TFPI antibody. The other two antibodies showed a similar profile with the different anti-TFPI concentrations but to a lesser extent (figure 4.1a). For this reason all subsequent experiments used the Dako secondary antibody.

To determine the effect of cell number and washing on antigen detection, $5x10^4$ and $5x10^5$ EA.hy926 cells were incubated with the anti-TFPI antibody with and without the inclusion of a washing step before incubation with the Dako secondary antibody. Using $5x10^4$ cells, cells positive for TFPI without washing was 90.0%, however, after washing this decreased to 53.4%. With $5x10^5$ cells, only 32.3% of cells were positive for TFPI, decreasing to 6.17% after washing; demonstrating that i) this system is dependent on cell number and ii) antibody binding is affected by washing between antibody incubations (figure 4.1b).

Finally, the anti-TFPI antibody (0-5µg/ml) was titrated against 5 and 10µl of the secondary antibody using $5x10^4$ EA.hy926 cells without washing. With 5µl, TFPI expression showed a bell shaped curve, increasing from 2.02% with only secondary to a maximum of 98.0% at 2.5µg/ml, decreasing to 58.3% at 5µg/ml. With 10µl of secondary antibody, TFPI antigen detection reached 89.7% with 2.5µg/ml and remained at 90% with 5.0µg/ml (figure 4.1c).

These results indicated the TFPI antibody should be used at 5.0µg/ml with 10µl of DAKO secondary antibody to detect antigen expression, with no washing step between addition of antibodies.

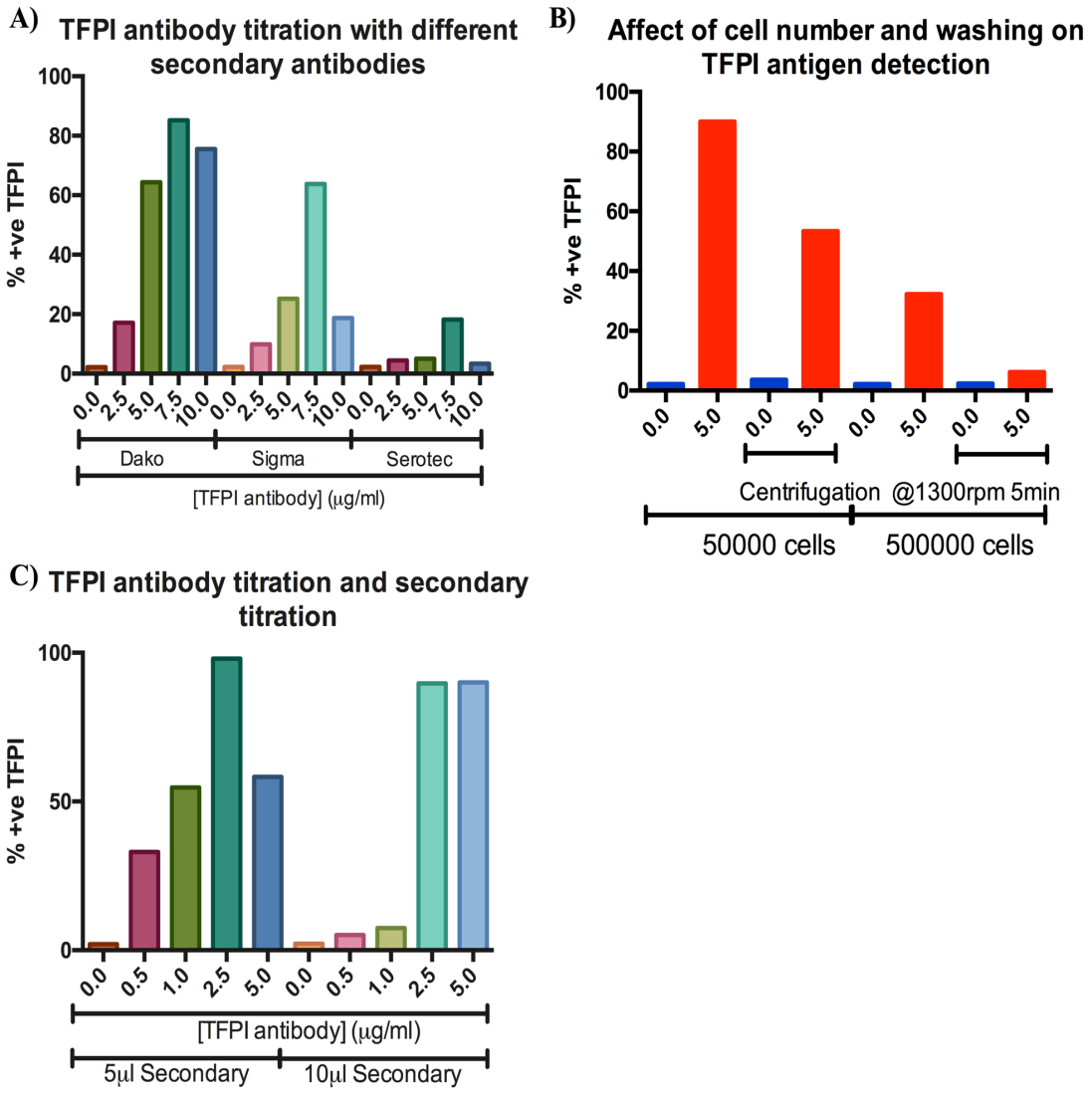

Figure 4.1: Preliminary titrations of antibodies for TFPI flow cytometry

A) Titration of TFPI antibody with set amount of each secondary, B) effect of centrifugation and cell count on TFPI labelling, C) effect of secondary concentration on TFPI detection.

4.2.1.2 Detection of TFPI antigen on the surface of platelets and monocytes

PRP or PBMCs were prepared and washed once in PBS pH 7.4/ 0.5% BSA/ 0.1% NaN_3 and resuspended at a concentration of either $5x10^4$/ml mononuclear cells or $200x10^6$/ml platelets. Platelets were reconstituted with PBMCs and incubated with 0.5µg/ml CRP-XL for 6h. Samples containing only platelets were incubated with 0.5µg/ml CRP-XL for 15min and 6h. At appropriate time points, 100µl of cells were incubated with 5µg/ml anti-TFPI antibody for 30min and then 10µl secondary antibody for 30min in the dark at 4°C. TFPI expression was analysed using the XL flow cytometer.

Monocyte TFPI expression showed a small increase of ~24% after 6h incubation with CRP-XL to 90.8±2.9% (mean±SEM; n=3) compared to resting (66.5±5.9%) but this was not significant (figure 4.2a). Platelet surface TFPI expression increased almost 2-fold compared to T0 at both 15min and 6h (from 18.9±7.9% to 35.9±3.8% and 37.7±7.4% respectively; n=3) compared to resting (18.9±7.9%) although this was also not significant (figure 4.2b). There was no further increase in platelet TFPI expression between 15min and 6h, which suggests the increase seen was from TFPI released from granule stores following activation.

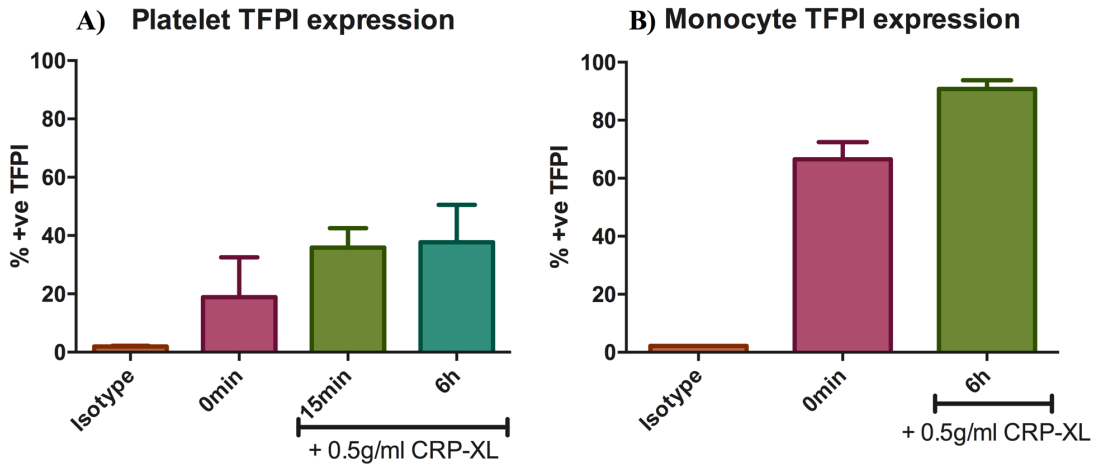

Figure 4.2: Surface expression of TFPI on monocytes and platelets

Samples were incubated with the TFPI antibody (5µg/ml) followed by the Dako secondary antibody (10µl) before analysis on the XL flow cytometer. TFPI expression on isolated monocytes reconstituted with platelets and incubated with 0.5µg/ml CRP-XL A) and washed platelets incubated with 0.5µg/ml CRP-XL B). Data show mean±SEM; n=3.

Due to the lack of availability of suitable antibodies and difficulty in experimental methods, flow cytometric detection of TFPI was not pursued further.

4.2.2 Identification of monocyte TFPI expression by western blotting

While antibodies were available suitable for western blotting, a number of unforeseen problems meant that these experiments took much longer than planned. A simplified flow chart of the problems encountered, and steps taken to overcome them, is shown in figure 4.3.

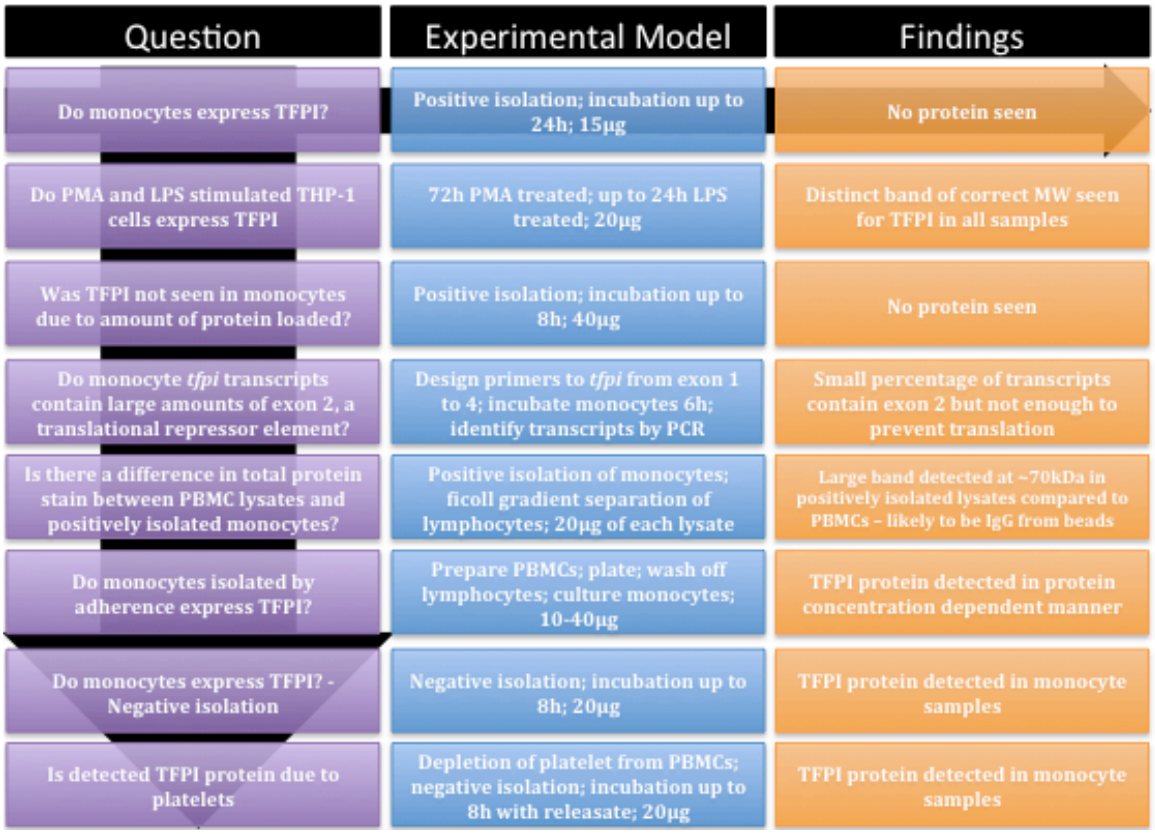

Figure 4.3: Flow table of steps to detect TFPI expression in monocytes by western blotting

Summary of approaches taken to identify TFPI expression in monocytes. The purple boxes represent the experimental questions, the blue boxes details of the experiments and the orange boxes show the findings. The down arrow indicates timeline of experiments.

4.2.2.1 Initial western blotting results

Monocytes were isolated from whole blood using CD14 microbeads and incubated at 37°C for up to 24h before being pelleted by centrifugation at 1500rpm for 5min, and then lysed in RIPA buffer. The protein concentration was determined using the DC protein assay and 15µg protein used for western blotting. Membranes were probed for TFPI and the housekeeping protein actin. Recombinant human TFPI (rhTFPI) (R&D systems) and EaHy926 lysate were used as positive controls. Secondary only controls were included to determine non-specific binding.

A band at ~45kDa was detected for both the EA.hy926 and rhTFPI samples identifying TFPI protein. No TFPI protein could be detected in the monocyte samples. Actin was detected in all samples apart from 0h and 20h – probably due to loading errors, or errors in the estimation of the protein concentration. Two different secondary antibodies were used but neither showed bands with the monocyte samples, and only faint bands with the EaHy926 positive control (figure 4.4).

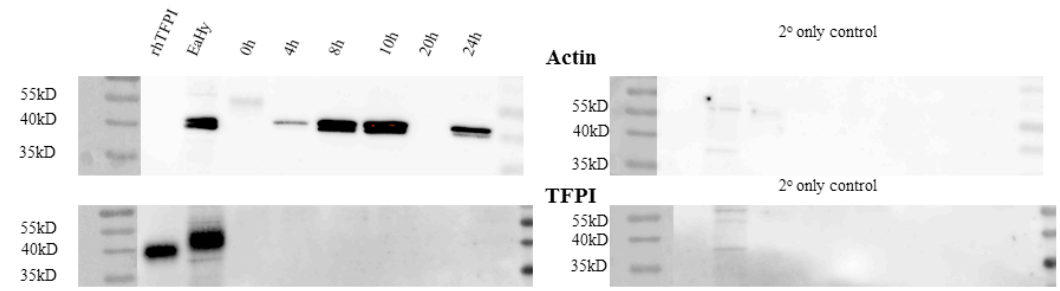

Figure 4.4: Initial western blotting for TFPI protein in monocytes

Isolated monocytes were reconstituted with washed platelets and incubated for up to 24h at 37°C with 0.50µg/ml CRP-XL. Cells were pelleted and lysed in RIPA buffer. Protein concentration was determined and subjected to western blotting for TFPI and actin.

To understand why there was no detection of TFPI in monocytes the THP-1 cell line was used to probe for TFPI protein as these cells are commonly used a model for monocytes and have been shown to express TFPI. Lysate (20µg) from untreated, 3-day 200nM PMA treated or 3 day PMA treated and 100ng/ml LPS treated (3, 6 and 24h) was used for western blotting for TFPI protein.

TFPI protein could be detected in all samples regardless of treatment (figure 4.5). The smaller MW TPFI seen in Eh.Hy926 samples could relate to differential glycosylation patterns between the two cell types. The secondary only controls show no non-specific bands demonstrating the bands seen are TFPI and that it could be detected in monocyte-like cells.

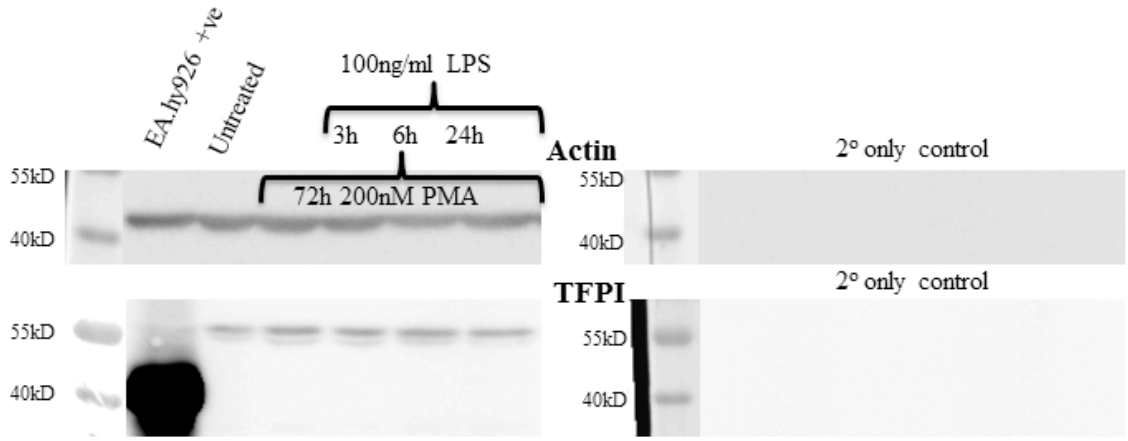

Figure 4.5: Detection of TFPI in the monocyte-like THP-1 cell line by western blotting

The THP-1 cell line was left untreated or treated with 200nM PMA for 72h before addition of 100ng/ml LPS for up to 24h to stimulate an immune response. Protein was extracted using the TRIzol method and subjected to western blotting for TFPI and actin.

Since TFPI could be detected in THP-1 cells, TFPI expression in isolated monocytes was re-examined but using more protein. Incubations were set up as before but this time

for 0, 5 or 7h. A total of 40µg monocyte lysate was used for western blotting for TFPI and actin.

TFPI protein was detected in the control EaHy926 lysate but not in the monocyte samples (figure 4.6). There was a band at a higher MW present in monocyte samples but as it was also seen in the secondary control it was classified as non-specific. A number of bands were detected in the actin blot, some of which were also present in the secondary only control suggesting non-specific binding. Non-specific binding of secondary antibodies could be occurring for a number of reasons: i) increased protein loading, ii) use of PVDF as opposed to nitrocellulose membranes, iii) experimental error.

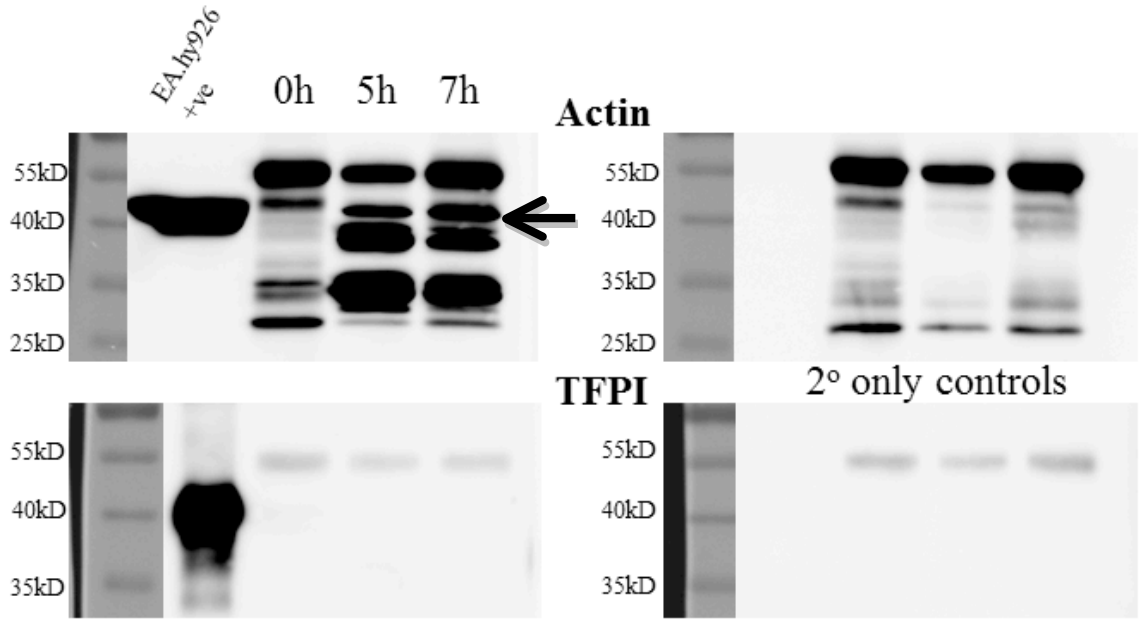

Figure 4.6: Western blot for TFPI protein in monocytes using 40µg protein

Isolated monocytes were reconstituted with washed platelets and incubated for up to 7h at 37°C with 0.5µg/ml CRP-XL. Cells were pelleted and protein extracted using TRIzol. Protein concentration was determined and subjected to western blotting for TFPI and actin.

4.2.2.2 Incorporation of exon 2 into monocyte *tfpi* transcripts

The previous western blots suggested a lack of TFPI protein in platelet-activated monocytes. Evidence in the literature for why a gene may be so highly expressed but the protein absent includes translational control, targeted degradation, and inclusion into P-bodies. However, recent work from Alan Mast's group has suggested that the incorporation of exon 2 in the *tfpi* transcript represses translation to protein (Ellery et al., 2014). Exon 2 is can be present in both *tfpi* transcripts with the relative abundance in each transcript dependent on the tissue type. Using the same primers, end-point PCR

was carried out to determine: i) the relative amounts of *tfpiα* and *tfpiβ* mRNA in monocytes and ii) the ratio of exon 2 non-containing to containing transcripts.

cDNA was prepared from monocytes isolated from whole blood incubated at 37°C for 6h with 0.5μg/ml CRP-XL. End point PCR was carried out using the manufacturer's protocol with the addition of 1μM forward primer and 1μM of either the *tfpiα* or *tfpiβ* specific reverse primers. cDNA (1.5μl for *tfpiα* and 1μl for *tfpiβ*) was added and the reaction mixture made to 20μl using milli-Q water. The reaction was as follows: 5min at 95°C; (30s at 94°C, 30s at 57°C, 90s at 72°C)x; 10min at 72°C, where x is 35 cycles for *tfpiα* and 40 cycles for *tfpiβ*. After the reaction 10μl of each reaction mixture was loaded onto a 2% agarose gel and separated by electrophoresis. Amplified DNA was visualised using gel red and a Las4000 image analyser.

No *tfpi* mRNA of either transcript was detectable at 0h but it was induced in platelet-activated monocytes after 6h, in agreement with RT-qPCR data presented in chapter 3. Both transcripts are induced after 6h and, although not quantitative, there appears to a larger amount of the alpha transcript compared to the beta transcript (figure 4.7).

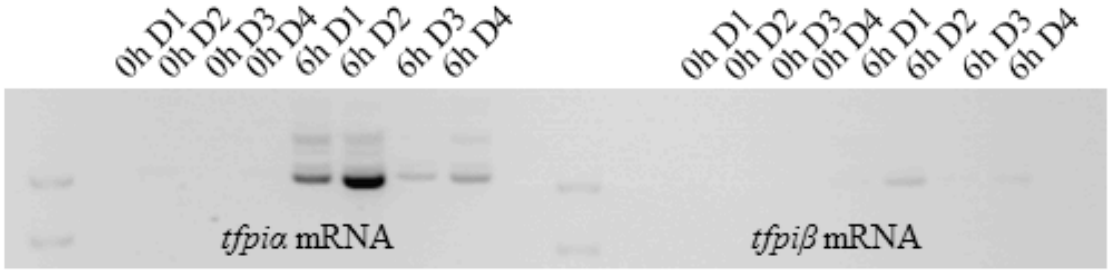

Figure 4.7: Monocyte tfpiα and tfpiβ gene expression

Monocytes from CRP-XL (0.5μg/ml) stimulated whole blood were isolated and the RNA extracted using TRIzol. After conversion to cDNA, end point PCR was carried out using a forward primer and tfpiα or tfpiβ specific reverse primers. Products were separated using a 2% agarose gel.

End point PCR is predominantly qualitative rather than quantitative and densitometry cannot normally be carried out. This case is an exception as two transcripts are formed from the same primers (with and without exon 2) and are present in the same lanes, so a comparison can be made. For monocyte *tfpiα*, there was 145413±27292DU (mean±SEM; n=5) without exon 2, and 56233±11204DU with exon 2, (figure 4.8a). For *tfpiβ*, there was 227531±38268DU (n=3) without exon 2 and 102593±15471DU with exon 2 (figure 4.8b). These results suggest that approximately 1/3rd of both the *tfpiα* and *tfpiβ* transcripts contain exon 2. Due to the donor dependent variation in *tfpi* expression

and the lack of sensitivity of PCR it was not possible to carry out densitometry on all 6 donors used (figure 4.8c).

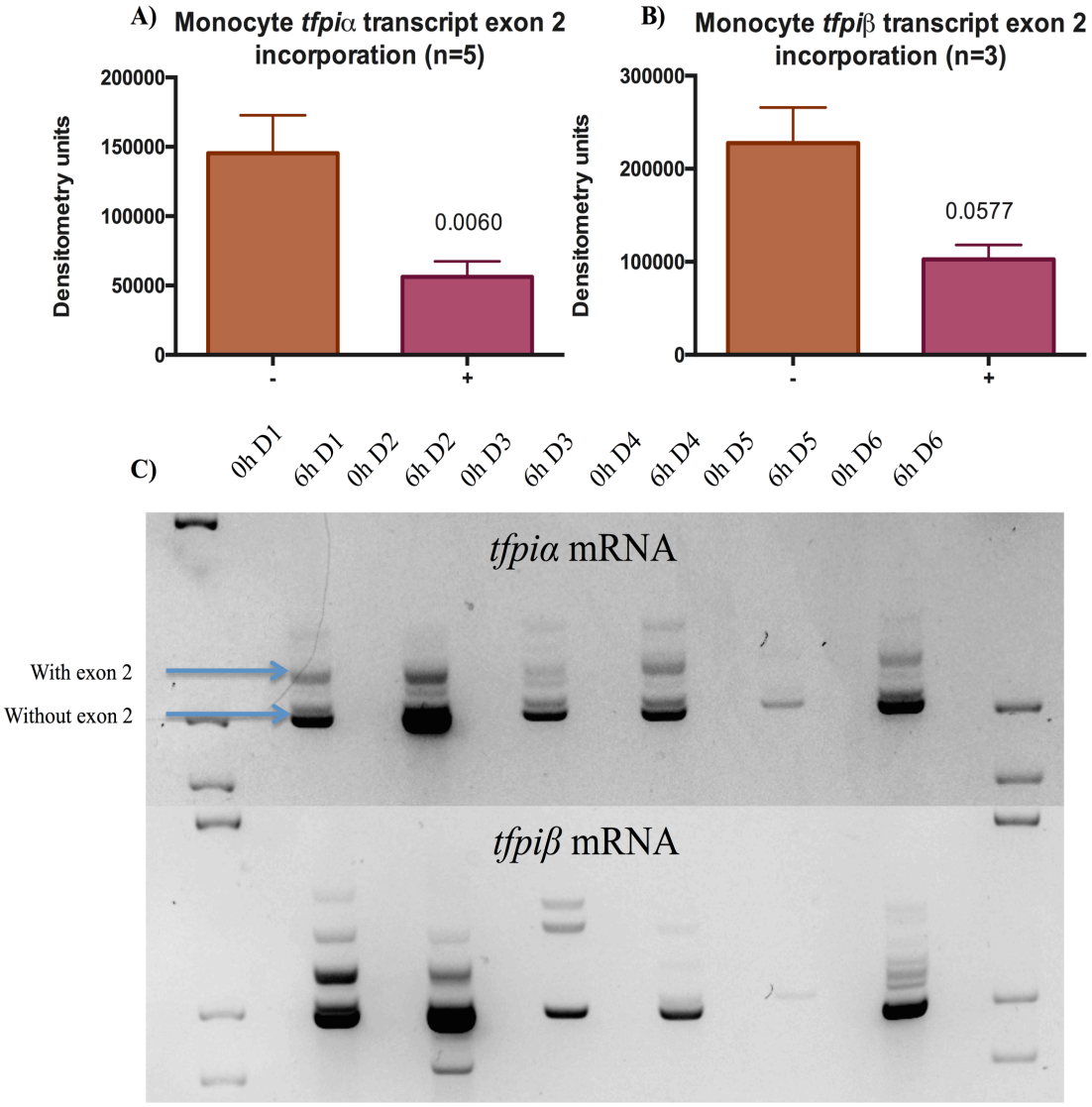

Figure 4.8: Ratio of tfpi transcripts with and without exon 2 in monocytes

Monocytes from CRP-XL (0.50µg/ml) stimulated whole blood were isolated and the RNA extracted using TRIzol. After conversion to cDNA, end point PCR was carried out using a forward primer and tfpiα or tfpiβ specific reverse primers. Products were separated using a 2% agarose gel. P-values calculated using a Student's paired t-test. Data show mean±SEM.

The results from these experiments demonstrate that monocytes do transcribe *tfpi* mRNA containing exon 2, but this only accounts for ~40% in the case of *tfpiα* and ~50% in the case of *tfpiβ*. Whilst this may inhibit translation of some *tfpi* mRNA to protein there is still a large amount present without exon 2 that should be translated.

4.2.2.3 Expression of TFPI in cultured monocytes

As results suggested monocyte *tfpi* transcripts contained some exon 2 but not all, there was still no reason why TFPI protein could not be detected by western blotting. The general consensus in the literature is that monocyte cells isolated from peripheral blood and set up in cell culture express TFPI (McGee et al., 1994). To confirm the presence of TFPI protein in human monocyte cells, monocytes were isolated by adherence and cultured for 24h to induce differentiation to macrophages. These have been shown to produce TFPI in previous studies (McGee et al., 1994), but failed to replicate in our own earlier studies using positively isolated monocytes (data not shown). Briefly, PBMCs were prepared and resuspended at $1x10^7$/ml in RPMI medium without serum, $1x10^7$ PBMCs were added per well in a 6 well plate and the volume made up to 2ml with serum free RPMI. To allow adherence, the plate was placed in the incubator at 37°C, 5% CO_2 for 2h. Lymphocytes were removed with three gentle washes with PBS and the medium replaced with macrophage serumfree medium (M-SFM). After 24h in culture the monocytes were lysed in TRIzol. After protein extraction and concentration determination volumes containing 10, 20, 30 or 40µg protein were added to SDS-PAGE gels and subjected to western blotting for TFPI.

TFPI could be detected in all lanes with lysate samples at a similar MW to the rhTFPI positive control. Band intensity increased with increasing protein loading as would be expected (figure 4.9). No bands were detected in the secondary only control indicating specific binding of the secondary antibody.

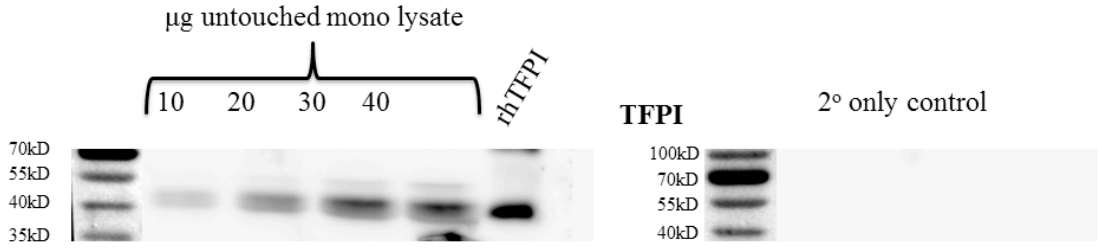

Figure 4.9: TFPI protein expression in 24h cultured primary monocytes

Monocytes were isolated by adherence from PBMCs and cultured for 24h. After 24h the cells were lysed and protein extracted using TRIzol. After quantification, protein (10-40µg) was subjected to western blotting for TFPI.

4.2.2.4 Comparison of total protein from positively isolated monocytes and PBMCs

After confirming TFPI could be detected in cultured monocytes isolated by adherence, attention was turned to the sample preparation methods; was extracting monocytes by positive isolation affecting western blotting due to release of protein from the

immune-magnetic beads? To test this, monocytes were isolated with CD14 microbeads or PBMCs prepared separately. After protein extraction using TRIzol, 20µg of protein was used for western blotting. After transfer to a PVDF membrane both the isolated monocyte and PBMC lysates were stained for total protein using Ponceau reagent.

Protein preparations from monocytes that were positively isolated using CD14 beads showed a strong and intense band between 55 and 70kDa that was not present in the PBMC lysates; this showed a band at ~45kDa probably representing actin (figure 4.10). It was hypothesised that the strong bands at 50 and 70kDa seen in the CD14 bead isolated samples could be IgG protein displaced during the lysis steps The presence of such a strong band in the monocyte samples was likely to be affecting the estimate of protein concentration resulting in insufficient cell-derived protein being loaded onto the gels.

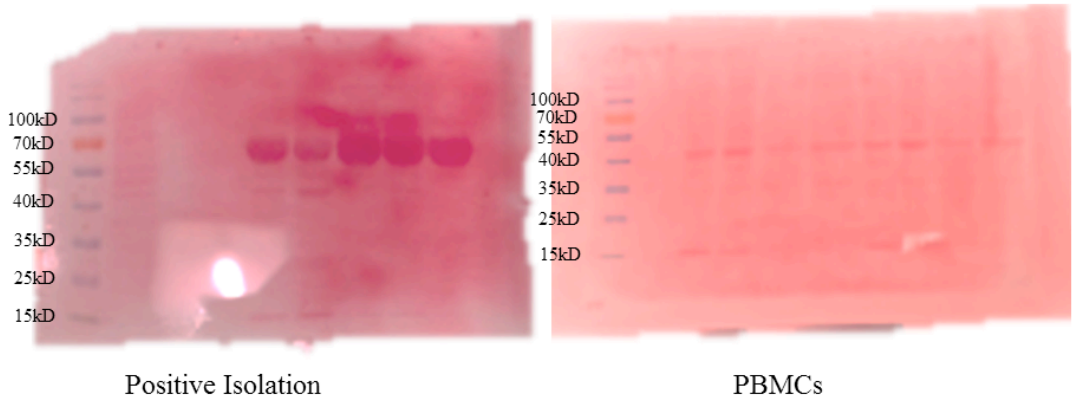

Figure 4.10: Comparison of total protein from PBMCs and positively isolated monocytes

Protein lysates from isolated monocytes A) and PBMCs B) were separated using SDS-PAGE, transferred to PVDF membranes and stained for total protein using the Ponceau reagent.

4.2.2.5 Monocyte TFPI protein expression over 8h

As the Ig from positive isolation methods was obscuring results, monocytes were isolated by a negative selection method. Using the Miltenyi pan monocyte isolation kit, autologous monocytes were reconstituted with washed platelets at a ratio similar to that found in whole blood. Platelets were activated with 0.125µg/ml CRP-XL and incubated at 37°C for 0h, 10min, 4h and 8h. These times were selected to identify TFPI released from platelets (10 minute sample), or generated by monocytes (4 and 6 hour samples). Cells were washed once with PBS, lysed in TRIzol and the protein extracted. After quantification, 20µg was used in western blotting for TFPI protein.

TFPI could be detected at the correct MW in all samples, including the 0 and 10min samples. Interestingly, densitometry analysis showed that there was a decrease in TFPI

protein between 0h and 10min post activation (figure 4.11a). However, by 4 hours TFPI expression had increased by 54.7% with no further increase seen at 8h. A representative blot from a single donor is shown in figure 4.11b.

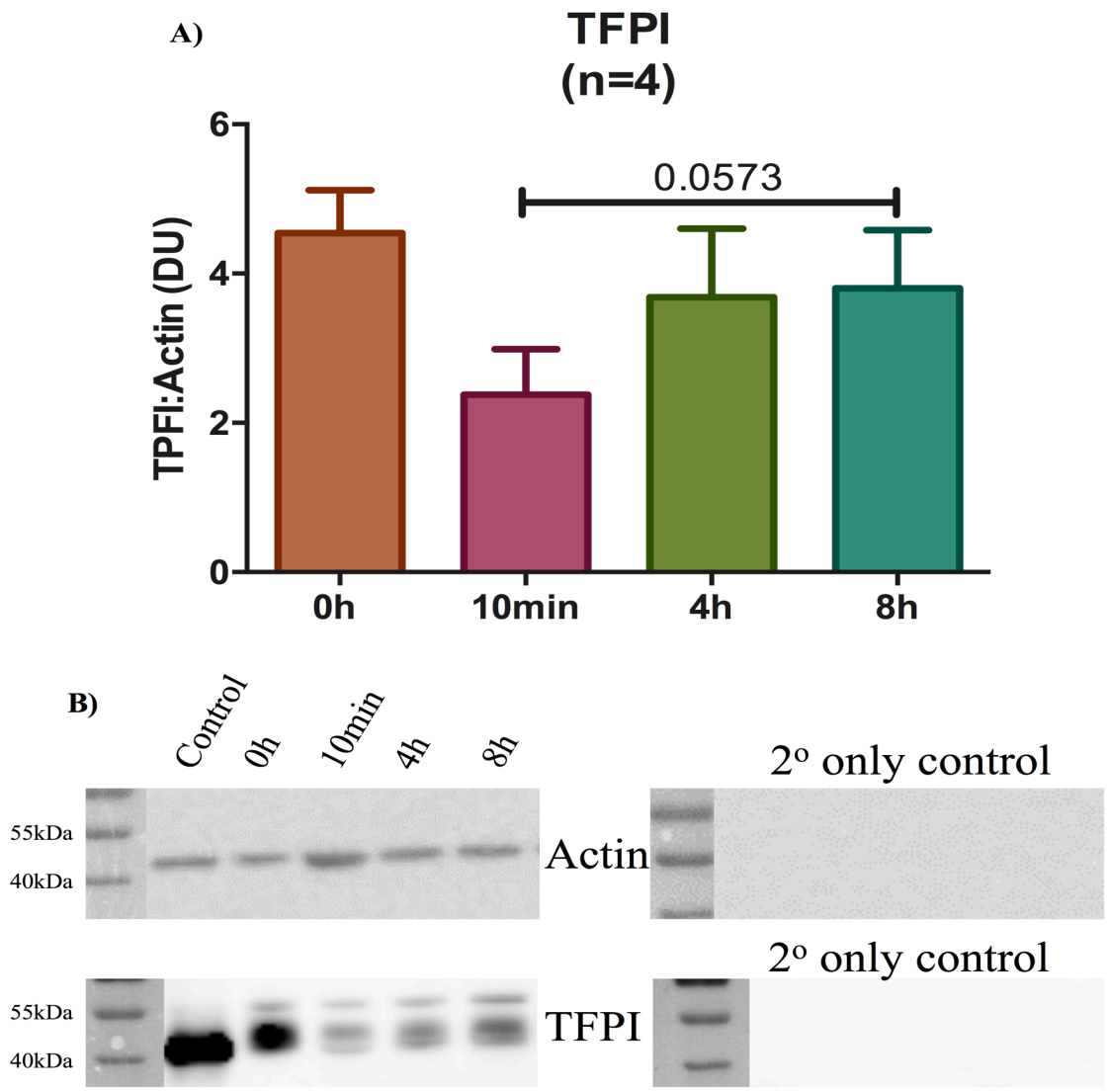

Figure 4.11: Expression of TFPI protein in negatively isolated monocytes

Monocytes were isolated using the pan monocyte isolation kit and reconstituted with washed platelets at physiological concentration before activation with 0.125µg/ml CRP-XL. At each time point, protein was extracted using TRIzol and subjected to western blotting for TFPI and Actin. The amount of TFPI was calculated relative to actin. P-values were calculated using the Students paired t-test. Data show mean±SEM; n=4.

These data suggest that TFPI protein is synthesised by the monocytes. A possible explanation for the fall in TFPI protein at 10 minutes is that platelets are known to contain TFPI (figure 4.12) and this may be released immediately on activation. This

could explain the decrease seen between 0h and 10min, however it does not rule out the possibility that monocyte could take up extracellular TFPI released from the platelets to account for the protein seen at 4h and 8h.

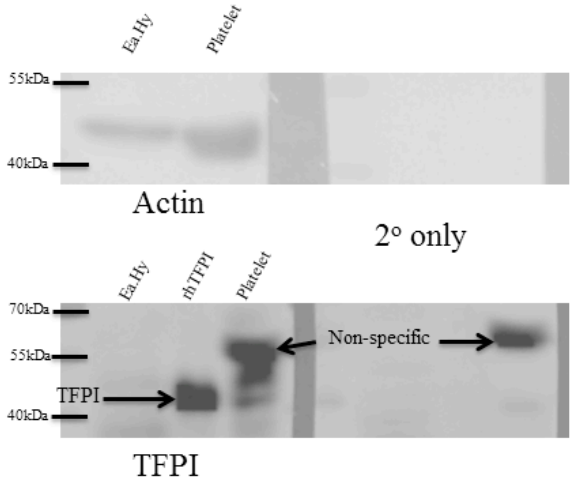

Figure 4.12: TFPI protein expression in resting platelets

Platelets were isolated from whole blood and washed before protein extraction using RIPA buffer. Protein (20µg) was loaded and subjected to western blotting for TFPI and actin.

4.2.2.6 Monocyte TFPI protein expression in the absence of platelets

It has already been shown that monocyte *tfpi* mRNA expression is induced by soluble factors released from platelets (section 3.3.3). To remove the platelet contribution of TFPI protein and any protein arising from transfer of platelet *tfpi* mRNA, a model was developed where platelets were removed from isolated monocytes and transcription inhibited using the RNA polymerase blocker actinomycin D. Whilst the majority of platelets are removed during negative monocyte isolation, a large number still remain in the final sample (figure 4.13a). In order to remove these residual platelets, an additional step in the isolation protocol was included. Prior to the isolation of monocytes, platelets were removed from the PBMC preparation using CD61 microbeads (Miltenyi Biotech). Monocytes were then removed from the resulting platelet-depleted PBMCs using the Miltenyi negative monocyte isolation kit.

Platelet contamination in the samples was analysed by flow cytometry. Without the CD61 isolation step there were large numbers of platelets in the monocyte preparation (32.5% CD42b labelling) (figure 4.13a). This could contribute to the TFPI protein expression seen in western blotting. However, the inclusion of the CD61 isolation step resulted in almost complete removal of platelets (4.0% CD42b expression) (figure 4.13b), allowing protein expression to be attributed to monocyte endogenous TFPI production.

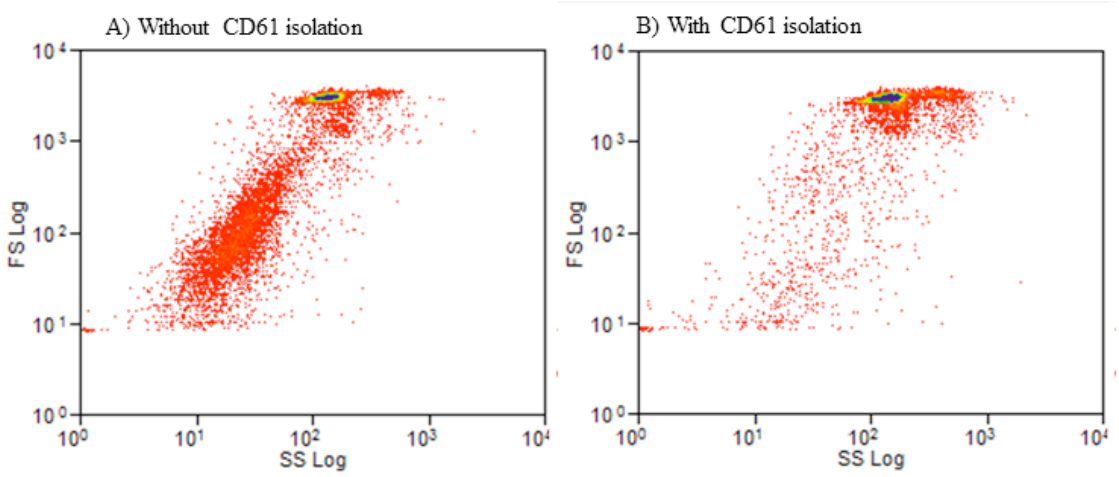

Figure 4.13: Removal of platelet using CD61 microbeads

PBMCs were prepared from whole blood and incubated with or without CD61 microbeads according to the manufacturer's instructions. After separation using the AutoMacs samples were run on the CyanADP flow cytometer and the platelet population identified based on forward and side scatter.

Platelet-depleted, negatively isolated monocytes were reconstituted with platelet-derived soluble material and incubated at 37°C for 8h in the presence or absence of 10µM actinomycin. Monocytes were washed once in PBS before lysis in TRIzol. Protein was extracted, quantified and subjected to western blotting for TFPI.

TFPI protein could be detected in all three samples of platelet-depleted monocytes. Levels of TFPI protein were high at 0h and fell significantly by 8 hours. The 8h samples both with and without actinomycin looked similar, in fact more TFPI protein appeared to be present in the sample with actinomycin, which could suggest this TFPI is derived from exogenous sources. Both 8h samples showed 2 bands, a very diffuse band of medium intensity at the same MW as the 0h band and smaller band below at the same MW as the recombinant (figure 4.14). There appeared to be more actin in the 0h sample but this was not quantified by densitometry as only one western could be run. Also due to low protein yields after isolation a secondary control could not be included, although it is unlikely the bands shown are non-specific.

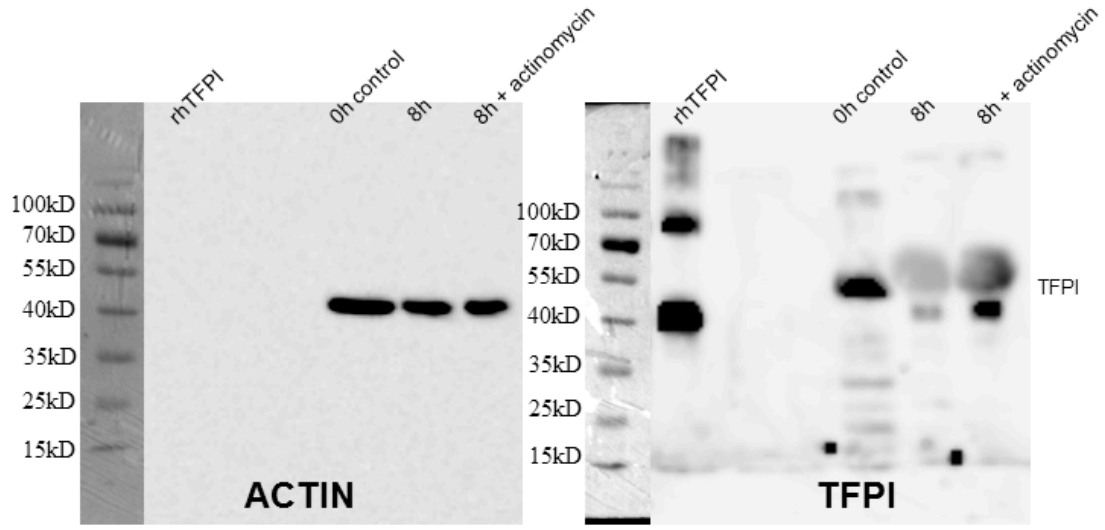

Figure 4.14: TFPI expression in platelet-depleted isolated monocytes

Isolated monocytes that had been depleted of platelets were incubated at 37°C for 8h in platelet-derived soluble material in the presence or absence of actinomycin. Extracted monocyte protein was pooled from 4 donors due to low yields and subjected to western blotting for TFPI and actin.

Unfortunately due to time constraints further experiments to determine whether or not TFPI protein is expressed in monocytes could not be carried out.

4.3 Monocyte EPCR protein expression

Expression of the EPCR protein has been shown in a number of cell types in addition to endothelial cells; including some cancer cell lines and monocytes. The aim of this section was to confirm the previous report that monocytes express EPCR. The same issues regarding monocyte isolation were also encountered in these studies but will not be discussed.

4.3.1 Measuring EPCR by flow cytometry

To determine if monocytes express EPCR, a flow cytometric method was set up using the EA.hy926 cell line as a positive control. An unlabelled EPCR antibody (Abcam) suitable for flow cytometry was acquired. No directly conjugated antibodies were available. Initial experiments used a well-established protocol set up in the laboratory. EaHy926 cells were incubated with 0.1-1µg of the anti-EPCR antibody at room temperature for 30min before the addition of a polyclonal goat anti-mouse-FITC conjugated secondary antibody (DAKO) for 20min at room temperature. The samples were analysed using an ADPcyan flow cytometer.

After setting the isotype (red line) to 2% all 3 concentrations of the anti-EPCR antibody resulted in a small shift to the right (to ~10%) suggesting positive staining for EPCR (figure 4.15).

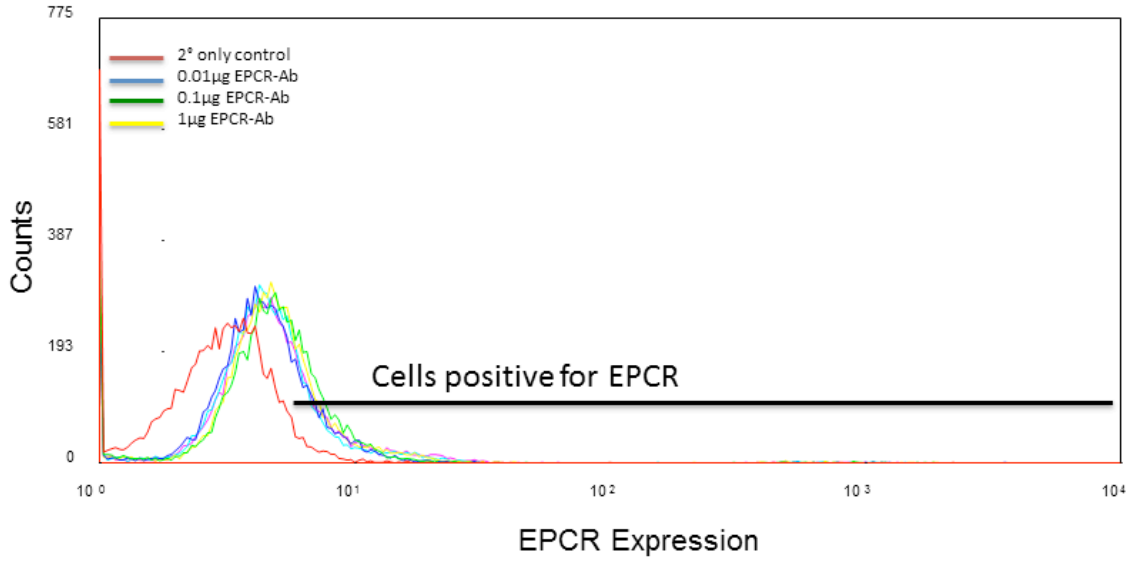

Figure 4.15: EA.hy926 cell surface EPCR expression using conventional flow method

EA.hy926 cells (5x10^4/ml) were incubated for 30min with increasing concentrations (0.1-1µg/ml) of an antibody against EPCR followed by a further 20min incubation with a FITC labelled antibody against mouse Ig's. Samples were analysed using the ADPcyan flow cytometer.

Although EPCR is accepted as an extracellular membrane protein, only a modest increase in EPCR protein could be seen on the cell surface. To explore whether larger amounts of EPCR were present within the cells, they were first fixed and permeabilised with methanol, using a method recommended by the supplier of the monoclonal anti-EPCR antibody. 1x10^6 EaHy926 cells were fixed in 80% methanol for 5min, and cells were pelleted by centrifugation and resuspended in 100µl PBS. One tube was incubated with 0.2µg of the EPCR antibody for 30min before the addition of 10µl of the secondary antibody. The secondary was also added to one tube without the EPCR antibody to act as a control. After another 30min incubation, 900µl PBS was added and the samples analysed on the CyanADP flow cytometer.

A clear shift in fluorescence with the EPCR antibody could be seen compared to the control, with the number of cells positive for EPCR increasing from 2% to 85% (figure 4.16).

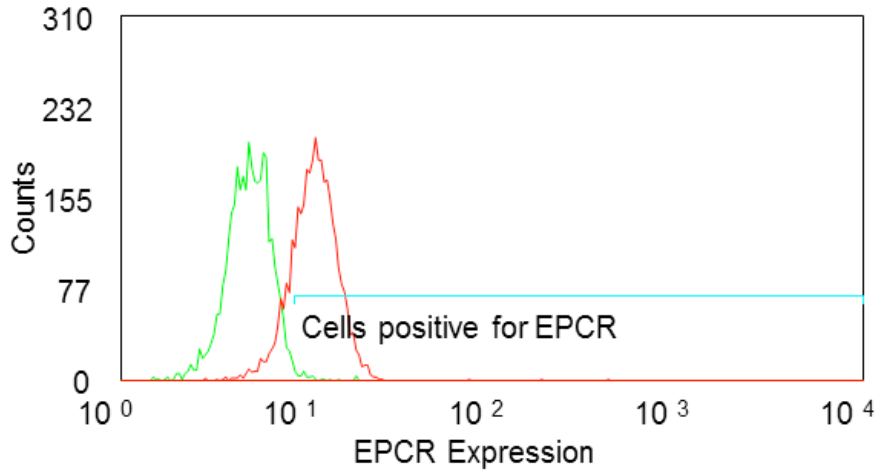

Figure 4.16: EA.hy926 total EPCR expression using flow cytometry

EA.hy926 cells (1x10^6) were fixed in 80% methanol for 5min. The cells were pelleted and resuspended in PBS with or without 0.2µg/ml EPCR antibody for 30min followed by 20min with a FITC anti-mouse antibody. Samples were analysed on the CyanADP flow cytometer.

In order to determine whether platelet-activated monocytes express EPCR protein, monocytes were negatively isolated and incubated for up to 8h at 37°C with washed platelets at physiological ratios activated with 0.5µg/ml CRP-XL. At each time point staining for intracellular EPCR was carried out as above.

No increase in EPCR expression could be seen at 0h or 8h above the secondary only control in any of the 4 donors tested (figure 4.17 shows a representative example). These results suggested either monocytes do not express EPCR, contrary to the literature, or that it could not be detected using this method, or within this time period.

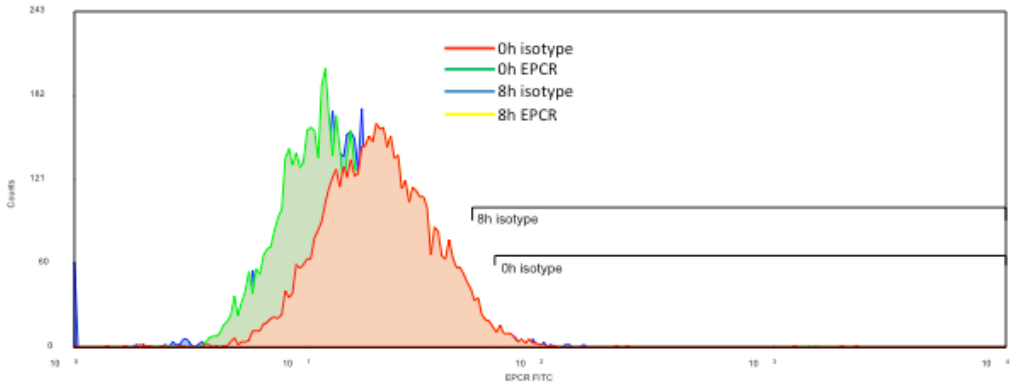

Figure 4.17: Analysis of monocyte EPCR expression by flow cytometry

Monocytes were negatively isolated from whole blood and reconstituted with washed platelets at physiological concentrations, activated with 0.5µg/ml CRP-XL and incubated for up to 8h. Samples were fixed in 80% methanol before incubation with 0.2µg/ml anti-EPCR antibody for 30min followed by 20min with a FITC-anti-mouse secondary antibody. Analysis was carried out using the CyanADP flow cytometer.

4.3.2 Measuring EPCR by western blotting

Similar problems were encountered when trying to detect EPCR by western blotting as those described for TFPI. To determine if the antibody was working and that a monocyte cell line expresses EPCR, the THP-1 cell line was treated with PMA and LPS (method identical to section 4.3.2.1) and western blotting carried out for EPCR.

Multiple bands of protein were detected in all THP-1 samples that were not present in the secondary only control (figure 4.18). The main band for EPCR is indicated on the blot and corresponds to a MW of ~32kDa, the size predicted for EPCR. Interestingly, EPCR expression appears to decrease as the monocytes differentiate into macrophages but this is restored by the inflammatory stimulus of LPS, although this needs to be confirmed.

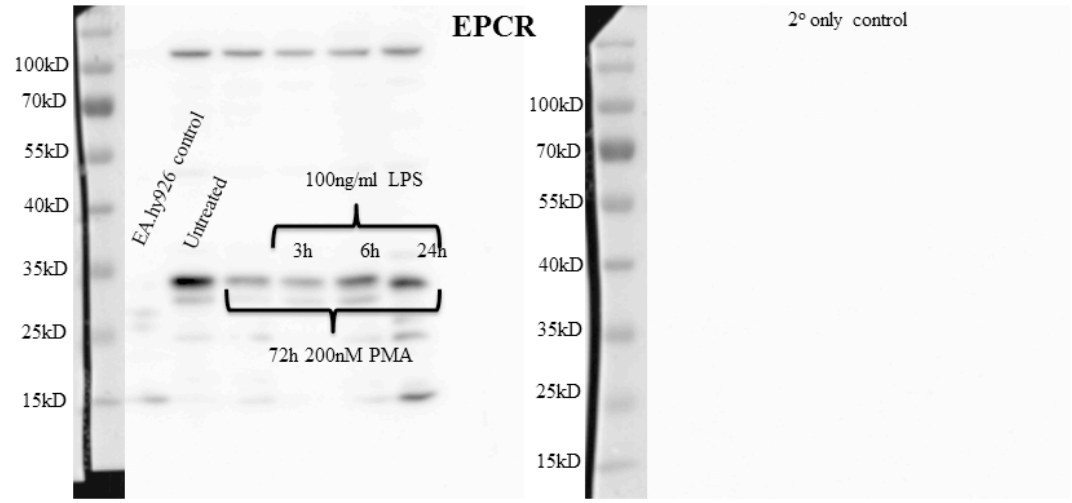

Figure 4.18: Expression of EPCR in the monocyte-like THP-1 cell line

The THP-1 cell line was left untreated or treated with 200nM PMA for 72h before addition of 100ng/ml LPS for up to 24h to stimulate an immune response. Protein was extracted using the TRIzol method and subjected to western blotting for EPCR and actin.

4.3.2.1 Monocyte EPCR expression over 8h

Using the same method of negative monocyte isolation described in section 4.3.2.4, up to 8h platelet-activated monocyte lysates were subjected to western blotting for the EPCR protein.

Similar to TFPI, EPCR protein decreased from 0h to 10min before increasing in a time dependent manner from 3.1±0.54DU at 10min to 5.5±0.36DU after 8h representing a 77.4% increase in EPCR protein (p=0.0482) (figure 4.19a). Unexplainably, of the 4 donor lysates used, EPCR was only detected in 2 donors even though actin was present

in all the samples at a visually similar level (representative example shown in figure 4.19b).

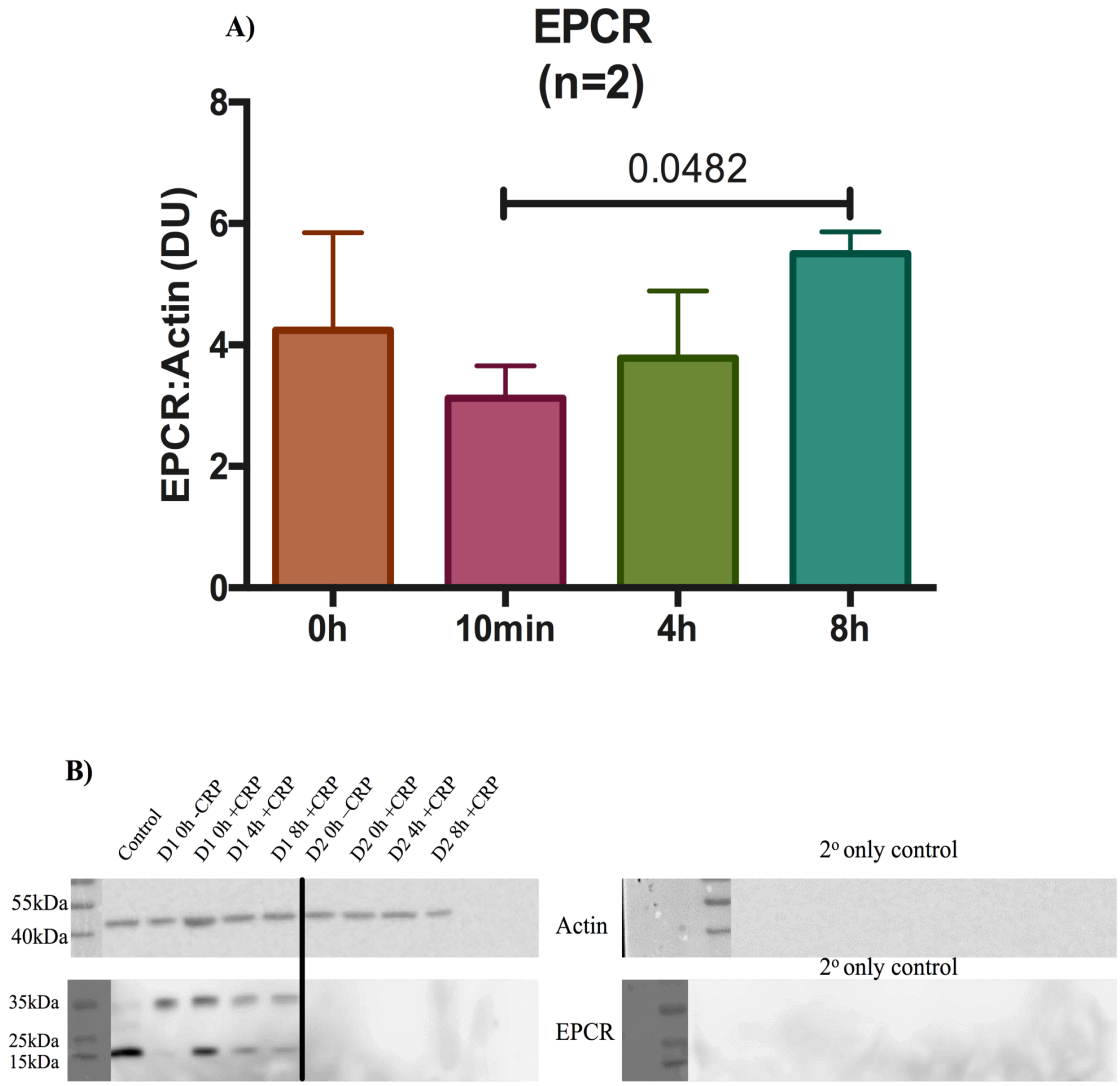

Figure 4.19: Expression of EPCR in negatively isolated monocytes

Monocytes were isolated using the pan monocyte isolation kit and reconstituted with washed platelets at physiological concentrations before activation with 0.125µg/ml CRP-XL. At each time point, protein was extracted using TRIzol and subjected to western blotting for EPCR and actin. The amount of EPCR was calculated relative to actin. P-values were calculated using the Students paired t-test. Data show mean±SEM. N=2.

4.3.2.2 Monocyte EPCR protein expression in the absence of platelets

As for TFPI, EPCR showed a decrease in protein expression between unstimulated and 10min stimulated samples. Again this could be due to EPCR protein being present in resting platelets and secreted on activation. To test this, resting washed platelet lysate was subjected to western blotting for EPCR protein (figure 4.20). From the figure,

EPCR can be seen in the positive EA.hy926 cell lysate, there appears to be a small faint band in the platelet samples that could correspond to a small amount of EPCR protein.

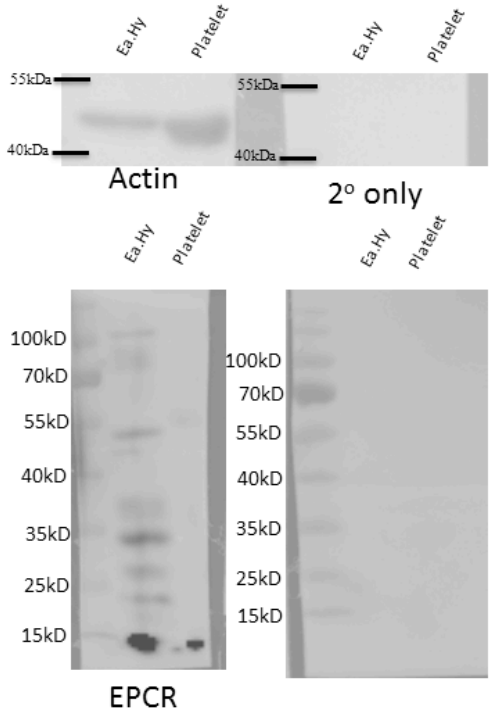

Figure 4.20: EPCR expression in resting platelets

Platelets were isolated from whole blood and washed before protein extraction using RIPA buffer. Protein (20µg) was loaded and subjected to western blotting for EPCR and actin.

As platelets may contain a small amount of EPCR, it was decided to incubate platelet-depleted monocytes with platelet-derived soluble mediators for 8h with and without actinomycin. The same method for monocyte isolation and platelet depletion was used as outlined in section 4.3.2.5 and western blotting carried out for EPCR.

EPCR was detected at both 0h and 8h as 2 bands of ~32kDa and 10-15kDa (figure 4.21). There did not appear to be an increase in EPCR protein over the 8h in this experiments, however there was less EPCR protein detectable in the actinomycin treated sample including an almost complete loss of the band at 32kDa ($p=0.0544$) (figure 2.21b). This could represent endogenous production of EPCR in monocytes. Due to low protein yields after isolation a secondary control could not be included, although it is unlikely the bands shown are non-specific.

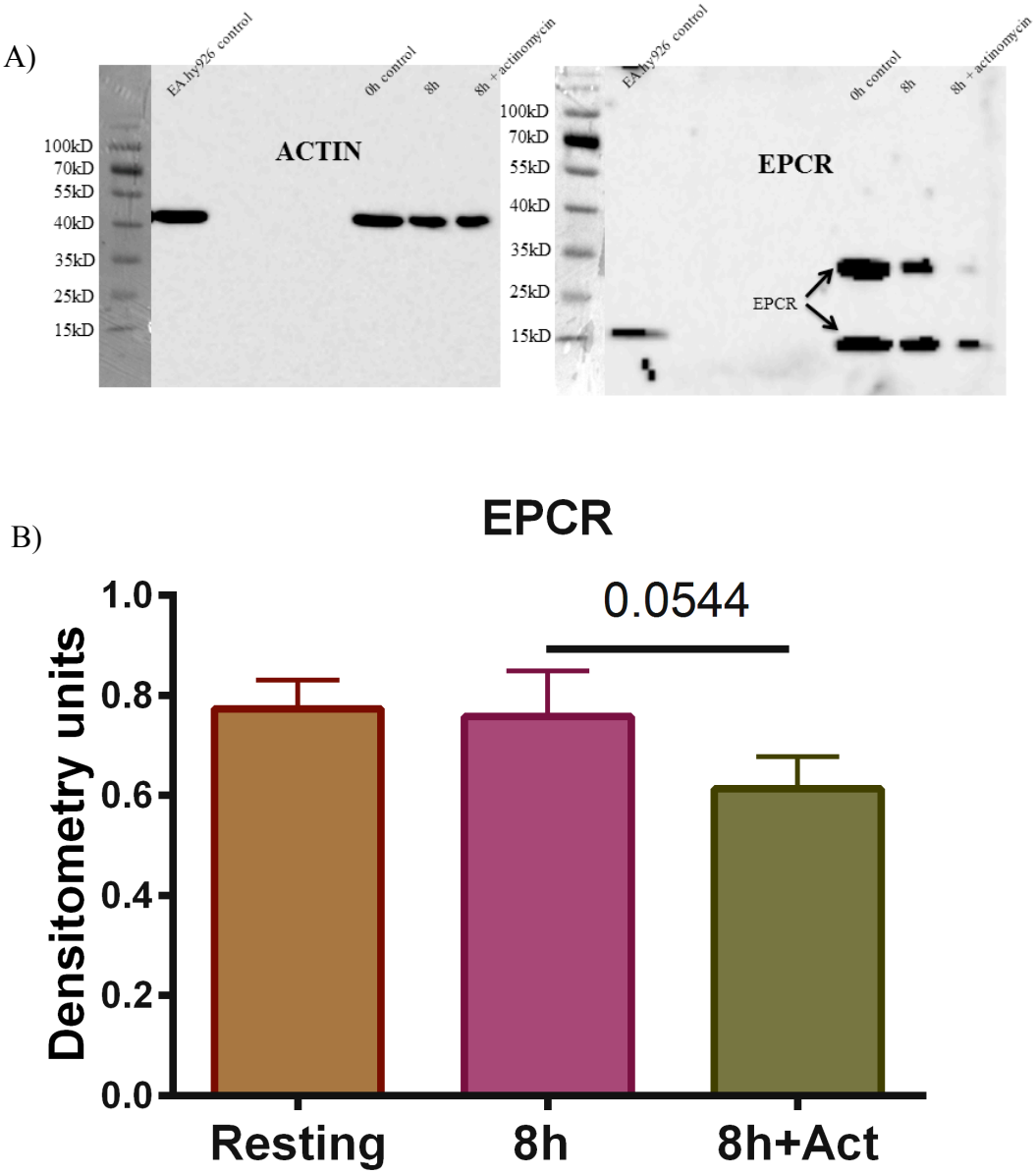

Figure 4.21: EPCR expression in platelet-depleted monocyte samples

Isolated monocytes that had been depleted of platelets were incubated at 37°C for 8h in platelet-derived soluble material in the presence or absence of actinomycin. Extracted monocyte protein from 3 donors was subjected to western blotting for EPCR and actin. A) Representative bands from a blot and B) densitometry analysis. P-value calculated using Student's paired t-test. Data show mean±SEM, n=3.

4.4 Monocyte PPARγ protein expression

Expression of PPARγ protein was only measured by western blotting. Initially PPARγ expression was measured in THP-1 cells before transformation to macrophages, with PMA and after incubation with the inflammatory stimulus LPS.

The blot shows strong expression of PPARγ in the control sample and in all the THP-1 lysates. There are no bands present in the secondary only control demonstrating recognition of PPARγ protein (figure 4.22).

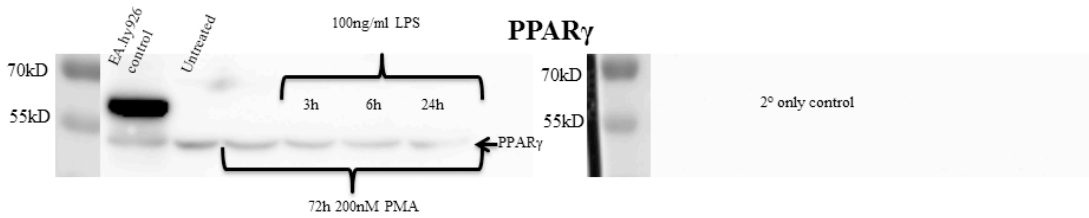

Figure 4.22: Expression of PPARγ in the THP-1 monocyte cell line

The THP-1 cell line was left untreated or treated with 200nM PMA for 72h before addition of 100ng/ml LPS for up to 24h to stimulate an immune response. Protein was extracted using the TRIzol method and subjected to western blotting for EPCR and actin.

4.4.1 Monocyte PPARγ expression over 8h

Using the same method as described in section 4.3.2.4, up to 8h platelet-activated monocyte lysate was subjected to western blotting for the PPARγ protein.

There was a noticeable decrease in the PPARγ : actin ratio between 0h resting and 10min stimulated samples (figure 4.23a). After this there was a time dependent increase in PPARγ protein up to 8h, increasing from 1.1±0.47DU at 10min after to 4.0±1.8DU at 8h, representing an increase of ~363.6%. However, it was only possible to analyse 2 out of the 4 donors due to poor antibody binding (representative example shown in figure 4.23b).

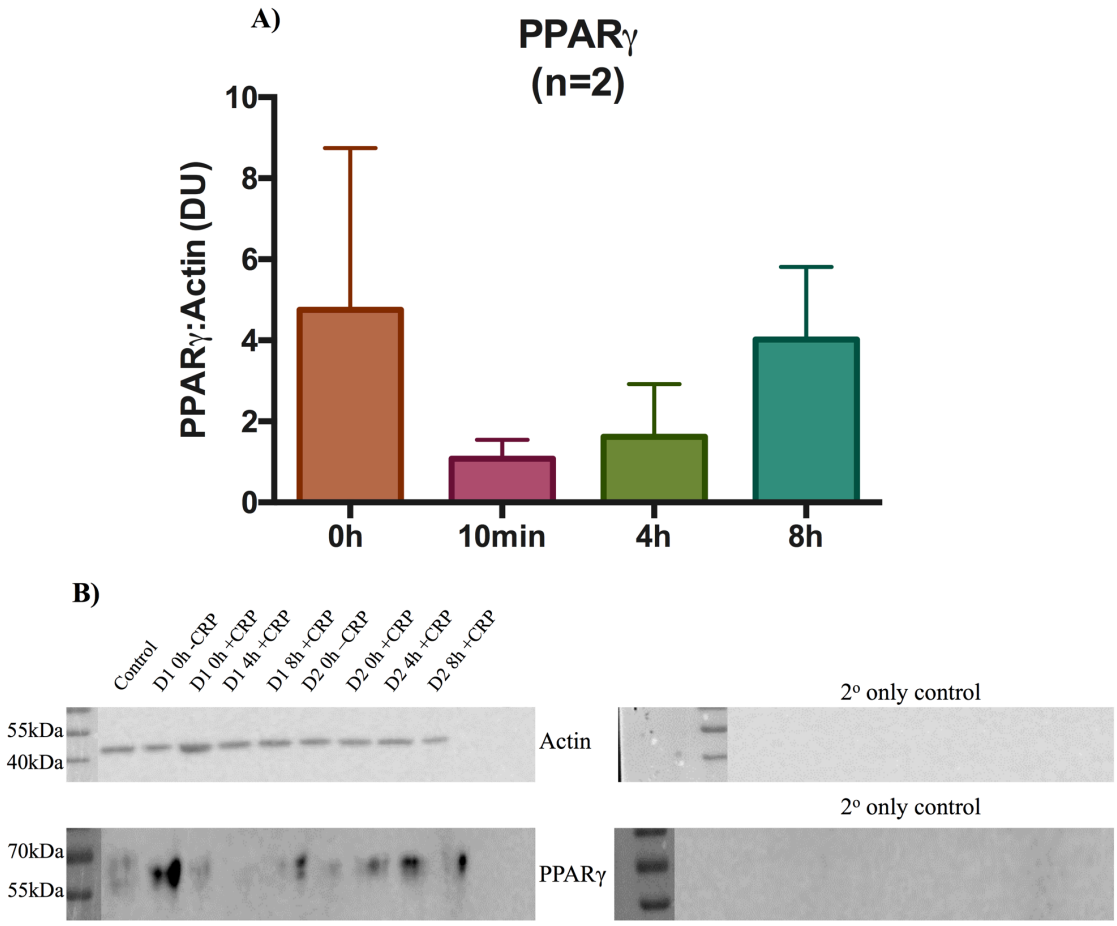

Figure 4.23: Expression of PPARγ in negatively isolated monocytes

Monocytes were isolated using the pan monocyte isolation kit and reconstituted with washed platelets at physiological concentration before activation with 0.125µg/ml CRP-XL. At each time point, protein was extracted using TRIzol and subjected to western blotting for PPARγ and Actin. The amount of PPARγ was calculated relative to actin. Data show mean±SEM.

4.4.2 Monocyte nuclear expression of PPARγ

As platelets have been shown to possess PPARγ, and as platelets are needed to induce PPARγ expression in monocytes through direct contact, monocyte nuclear protein samples were prepared using a commercially available kit. As PPARγ is mainly localised in the nucleus, by extracting nuclear protein, contamination from platelets would be minimised and positive extraction would be possible. Whole blood was incubated for 2h or 3h with 0.50µg/ml CRP-XL before monocytes extraction with CD14 Dynabeads®. Nuclear protein was extracted using the NucBuster kit as described in section 2.11.1.3. After protein quantification, 10µg nuclear protein was subjected to western blotting for PPARγ protein.

The results from this preliminary experiment appeared to show an increase in PPARγ protein from 0h to 2h and then a decrease at 3h (figure 4.24), in line with the RT-qPCR data described earlier.

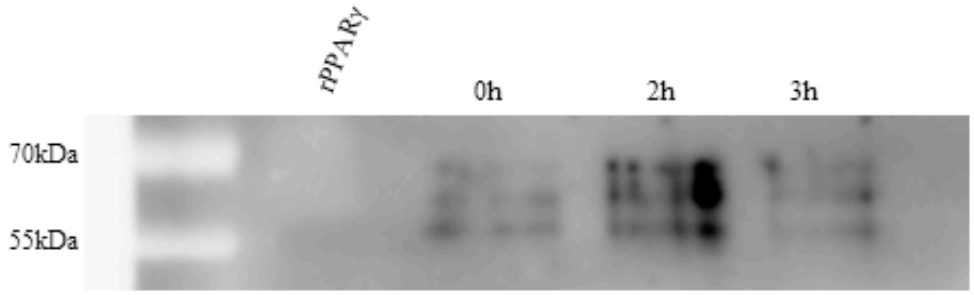

Figure 4.24: Nuclear expression of PPARγ in monocytes incubated for up to 3h

Whole blood was stimulated for up to 3h with 0.5μg/ml CRP-XL before monocyte extraction using CD14 Dynabeads®. Nuclear proteins were isolated using the NucBuster extraction kit and 10μg subjected to western blotting for PPARγ.

Unfortunately, whilst the results looked convincing, a band in the positive control could not be detected. Additionally, there was no suitable housekeeping gene and it was felt the current PPARγ antibody was not ideal.

To address these issues, a new PPARγ antibody was acquired (SantaCruz) and titrated using EA.hy926 cell lysates (figure 4.25a). PPARγ protein could be detected at all dilutions tested of primary and secondary antibody as a single band of correct MW. A dilution of 1:500 was selected and used with a 1:14250 dilution of secondary antibody. A TATA binding protein (TBP) antibody was also purchased for use as a nuclear housekeeping gene. Unfortunately when the experiment was repeated no PPARγ protein or TBP protein could be detected (data not shown). The TBP antibody was titrated using isolated 0h monocyte nuclear extract and EA.hy926 cell lysates (figure 4.25b). The results show clear detection of the TBP protein in the EA.hy926 cell lysates but not in the monocyte nuclear protein extract.

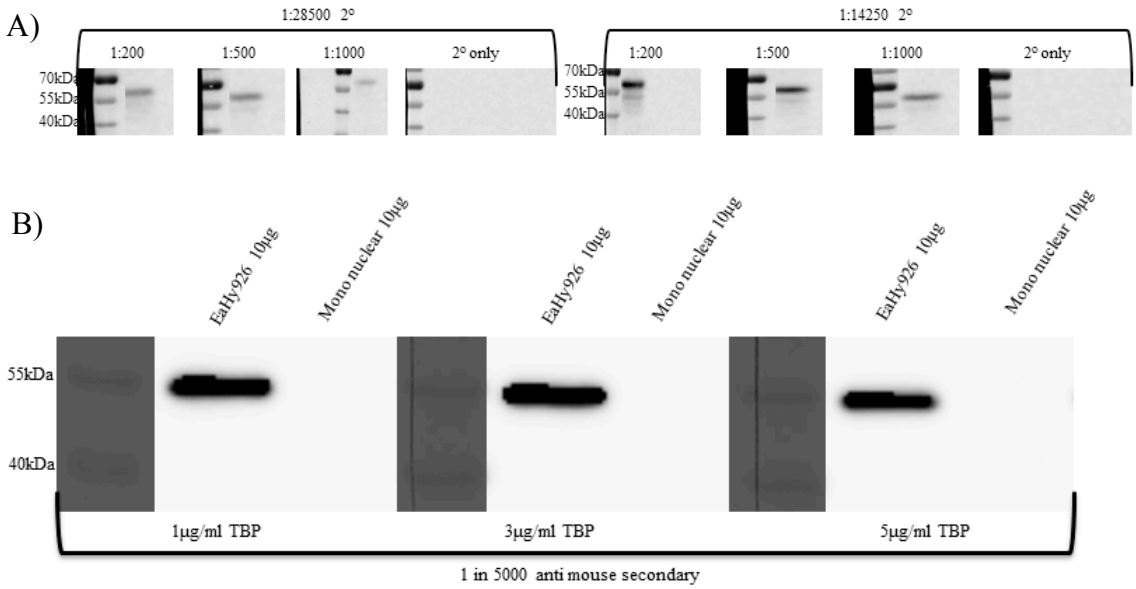

Figure 4.25: Titration of PPARγ and TBP antibodies for western blotting

EA.hy926 cell lysates where used to titrate the new PPARγ antibody A) and nuclear proteins isolated from monocytes and EA.hy926 whole cell lysate were used to titrate the TBP antibody for use as a housekeeping protein B).

As PPARγ had been detected in earlier experiments, these results were surprising as neither PPARγ nor TBP could be detected. To confirm that the NucBuster kit was still working the monocyte THP-1 cell line was used to extract both cytosolic and nuclear proteins using the NucBuster reagent and the fractions subjected to western blotting for TBP.

The blot shows clear detection of the TBP protein in both the cytosolic and nuclear fractions with no non-specific binding detected in the control (figure 4.26), suggesting that the extraction kit is still working and there may be a problem with the monocyte isolation procedure.

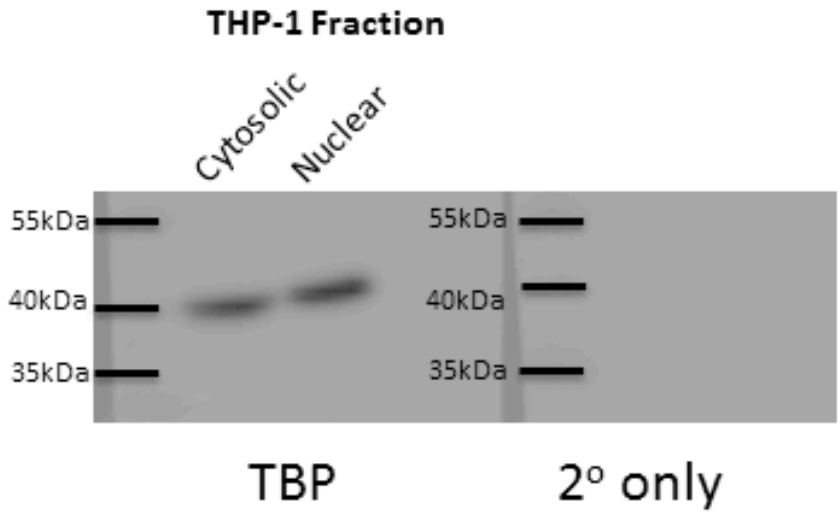

Figure 4.26: Test of NucBuster kit with THP-1 monocyte cells

Cytosolic and nuclear protein fractions were isolated from THP-1 cells ($1x10^6$) using the NucBuster extraction kit according to the manufacturer's instructions and 10μg of each subjected to western blotting for TBP.

These results suggested the nuclear extraction kit was still working. Unfortunately extraction of monocyte nuclear proteins and detection of PPARγ or TBP could not be achieved in subsequent experiments for unknown reasons.

4.5 Analysis of monocyte apoptosis, death and capacity to translate protein

The limited success of measuring protein expression in platelet-activated monocytes, and the difficulties associated with contaminating platelets, raised the question as to whether the monocytes were surviving the 8h incubation and if they were making protein. To test this, the viability of monocytes in whole blood and after isolation was measured using flow cytometry and their ability to produce proteins measured by western blotting.

4.5.1 Monocyte survival in whole blood and isolated cells

This project primarily used two methods for analysis of monocyte function; the first was to incubate whole blood prior to isolation and the second to isolate monocytes prior to incubation. Both methodologies provide different environments during the incubation period and expose the monocytes to various stresses, for this reason monocytes incubated in both ways were tested for apoptosis and cell death over an 8h time course.

whole blood or monocytes isolated using the pan monocyte isolation kit were incubated at 37°C for up to 8h with CRP-XL with and without the anti P-selectin blocking antibody 9E1. This was to block MPA formation and thereby prevent activated

platelets, which might be able to bind Annexin-V, from being attached to the surface of the monocytes and potentially giving a false positive measure of apoptosis. The isolated monocytes were reconstituted with washed platelets (both in RPMI medium) at equivalent concentrations to that seen in whole blood. Samples were incubated with CD14-VioBlue for 15min to label monocytes prior incubation for 10min with Annexin-V AlexaFluor688, to measure apoptosis, and the intercalating DNA dye 7-AAD, to measure cell death. Analysis was carried out on a Gallios flow cytometer using CD14 fluorescence as the trigger.

4.5.1.1 Apoptosis and cell death in monocytes incubated in whole blood

After platelet activation in the absence of 9E1, 40-60% of monocytes were positive for Annexin-V whilst <20% were negative for both Annexin-V and 7-AAD. Conversely, blocking monocyte platelet aggregate formation, and subsequent recognition of platelet-PS, there were significantly less monocytes in the Annexin-V positive gate and significantly more monocytes in the Annexin-V and 7-AAD negative gate (figure 4.27). In the absence of 9E1, there was significantly more monocytes dual labelled for Annexin-V and 7-AAD. The trend was similar across at all time points with little change in any of the gates over the 8h.

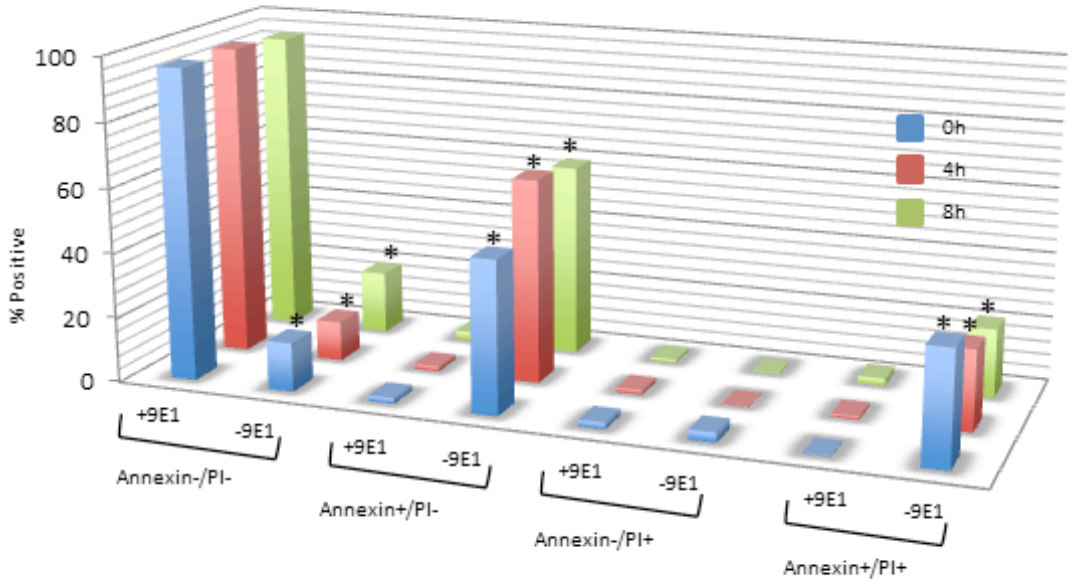

Figure 4.27: Analysis of monocyte apoptosis and death over 8h in whole blood

Monocytes were labelled using CD14-VioBlue and apoptosis and cell death measured using Annexin-V AlexaFluor 688 and 7-AAD respectively. Analysis was carried out using a Gallios flow cytometer. P-values calculated using multiple T-tests (=<0.05). The data shown represent the mean of 4 donors.*

4.5.1.2 Apoptosis and cell death in isolated monocytes incubated in medium

After isolation and in the absence of 9E1, monocytes showed a similar, high degree of Annexin-V labelling, probably due to platelets sticking to the monocytes. Monocytes labelled for Annexin-V and not 7-AAD declined slightly over the 8h as did those labelled for both Annexin-V and 7-AAD with a concomitant increase in monocytes negative for both, possibly due to platelets falling off monocytes. In the presence of 9E1 and therefore absence of monocyte platelet aggregate formation, ~50% of monocytes were negative for both Annexin-V and 7-AAD. This is maintained at 4h but decreases to <40% at 8h. Unlike in whole blood, isolated monocytes showed a time dependent increase in Annexin-V positive 7-AAD negative labelling, suggesting increased apoptosis in this isolated system. A smaller proportion of monocytes were positive for both Annexin-V and 7-AAD at 0h in the presence of 9E1 but both decreased to a similar level at 4h and 8h (figure 4.28).

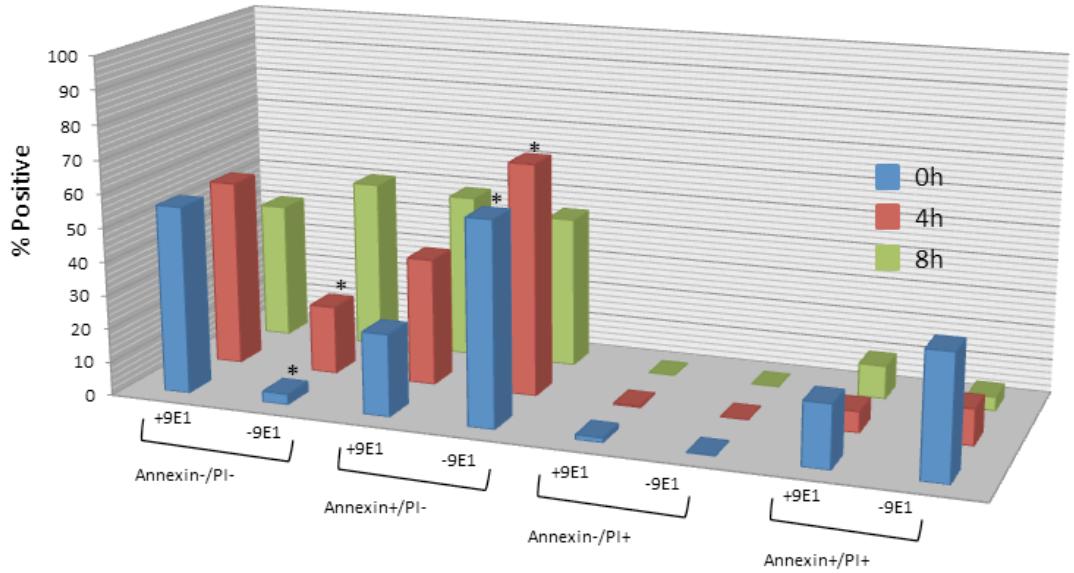

Figure 4.28: Analysis of apoptosis and death over 8h in isolated monocytes

Monocytes were labelled using CD14-VioBlue and apoptosis and cell death measured using Annexin-V AlexaFluor 688 and 7-AAD respectively. Analysis was carried out using a Gallios flow cytometer. P-values calculated using multiple T-tests (=<0.05). The data shown represent the mean of 3 donors.*

4.5.2 Monocyte protein synthesis

To confirm whether monocytes incubated for up to 8 hours in either whole blood or in medium retained their ability to translate mRNA into protein, the translation inhibitor puromycin was added to samples 30min before extraction. Puromycin inhibits protein synthesis by incorporation into the polypeptide chain during translation. The

incorporated puromycin can be detected with an anti-puromycin-HRP conjugated secondary antibody and if translation is occurring multiply bands should be detected on a western blot (Goodman et al., 2012; Traut and Monro, 1964). Whole blood was incubated at 37°C for up to 8h before monocyte isolation using CD14 Dynabeads® and protein extraction. Translation was inhibited with the addition of 25µM puromycin 30min prior to isolation. The extracted protein was subjected to western blotting and probed with an anti-puromycin primary antibody and HRP-conjugated anti-mouse secondary antibody.

From figure 4.29, multiple bands could be seen at each time point indicating the incorporation of puromycin into polypeptide chains, which reflects the occurrence of protein synthesis. As expected, there was higher intensity in the lower MW bands that shows translational arrest. There was a band of high MW in the untreated sample that suggests non-specific binding of the anti-puromycin antibody (blue arrow), no other non-specific bands were observed.

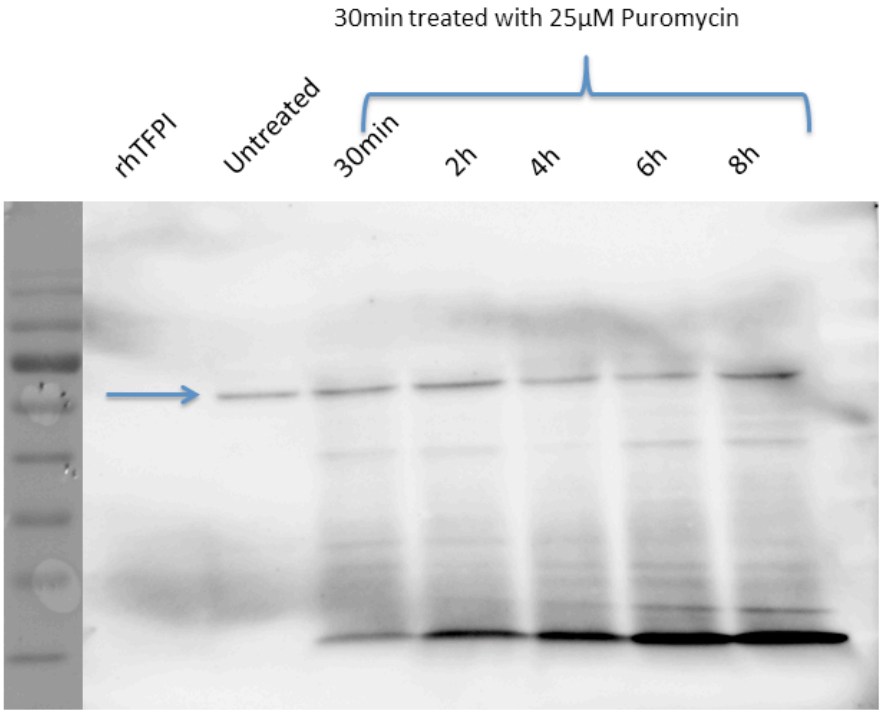

Figure 4.29: Assessment of monocyte translation using puromycin

Whole blood was incubated at 37°C for up to 8h with 0.5µg/ml CRP-XL. Before monocyte isolation using CD14 Dynabeads®, samples were incubated with 25µM puromycin for 30min. Monocytes were lysed in TRIzol and the protein extracted and quantified. Western blotting was used to detect translation via incorporation of puromycin. N=1.

4.6 Discussion

The aim of this chapter was to determine if the platelet-induced gene expression in monocytes seen in the previous chapter translates to an increase in monocyte protein expression. If this had been shown readily, this chapter would have also determined if the same effect of COX-1 and 12-LOX inhibitors was observed with monocyte protein expression as shown with the genes. Unfortunately due to difficulties in sample preparation and experimental protocols it cannot be stated unequivocally that platelets induce an increase in protein expression of the genes of interest, although their upregulation is strongly implicated. To summarise the findings of this chapter:

i. An increase in TFPI expression was seen both by flow cytometry and western blotting
ii. Monocyte EPCR protein expression could not be detected by flow cytometry but a significant increase was seen in using western blotting
iii. Monocyte PPARγ protein expression was seen to increase over 8h but was not significant and detection at 2h was hindered by experimental difficulties relating to antibodies detecting multiple bands and difficulties encountered with nuclear protein extraction and quantification.

Whilst this chapter lacks many positive findings, there are still a number of issues worth discussing. This will begin with the issues found with sample preparation and the difficulties with studying primary monocytes isolated from whole blood. The focus will then move to evidence, or lack of, in the literature for expression of the proteins of interest in monocytes.

During this chapter, major challenges arose both in terms of reagent availability, protocol development, and difficulties inherent in obtaining primary monocytes free from platelets. Firstly, primary monocytes were the necessary choice to study platelet-induced protein expression for a number of reasons: i) primary monocytes were the cell type used in the previous chapter, analysing the effect of platelet activation on monocyte gene expression; ii) during thrombus formation, it is primary monocytes that are recruited by platelets from whole blood; iii) as discussed in section 3.11, there are a number of issues with studying other forms of monocytes. With primary monocytes, the chosen protein source for the western blotting experiments, no reason was seen to change the isolation procedure used in the previous RT-qPCR experiments. However, as evidenced by numerous inconclusive results for proteins of interest, variable actin

binding and a large amount of secondary binding, it was discovered that this isolation technique was not appropriate for protein analysis by western blotting. Although not proven, it is hypothesised the protein extraction method causes the dissociation of anti-CD14 antibody from the magnetic beads into solution. The mouse-derived antibody is then extracted with the monocyte protein and causes gross underestimation of monocyte protein in samples, as well as interfering with the western blotting process. This problem has also been encountered by other colleagues (Katrin Sander; Jasbir Moore; personal communication) and suggests positive isolation techniques should not be used where protein expression is to be assessed by western blotting, at least when lysing in TRIzol or RIPA buffer. To circumvent this, the isolation method was switched to a negative method, whereby monocytes were recovered untouched using immune-magnetic beads. Positive isolation is not an issue when studying RNA expression due to the separation of protein and RNA into different phases.

Another issue when studying protein expression in primary monocytes is contamination by platelets. Platelets average ~200x10^6/ml in normal blood and therefore in 50ml there are ~1x10^{10} platelets. This is reduced by ~60% with the inclusion of a PRP step in PBMC preparation and platelets are further lost during washing steps and the isolation procedure. Nevertheless, the resulting preparations of monocytes still contain a large number of platelets, not evidenced by the blood cell counter, but obvious when using flow cytometry. Even if the platelet count is reduced to 1x10^6/ml prior to monocyte isolation, they still outnumber monocytes by 5:1. Platelets contain proteins, which will lead to the underestimation of monocyte protein in samples and, as is the case with TFPI and PPARγ, may mask any changes seen in monocytes due to the protein being present in platelets. To try and reduce this issue, platelets were removed from isolated monocyte preparations using CD61 microbeads (Schmitz et al., 1994). While this was effective in removing platelets it also caused the loss of a large number of monocytes (and other leukocytes) from the preparation meaning the amount of protein obtained was low, thereby limiting the number of samples that could be analysed by western blotting. Platelet contamination was additionally minimised by incubating monocytes with the soluble fraction derived from activated platelets, based on the evidence in chapter 3 that it is this fraction required for monocyte *tfpi* and *procr* gene induction. This could not be used to explore the production of PPARγ protein as direct contact had previously been shown to be required for induction of PPARγ. However by using a nuclear extraction method contamination by any platelet-derived PPARγ would be

reduced. Platelet contamination is also an issue with flow cytometry as the activated platelets can be bound to monocytes. This means that if platelets express the protein of interest and are bound to monocytes any increase seen could be due to proteins on the platelet rather than the monocyte.

The use of flow cytometry does circumvent the issue of positive isolation, however, due to the lack of specific antibodies this option was not developed fully.

Whilst a number of studies have reported protein expression in human peripheral blood monocytes, these have often cultured the monocytes after isolation (Gleissner et al., 2010; Kasper et al., 2007). Short incubations of up to 2h have shown induction of both TF mRNA and protein (Lindmark et al., 2000) but longer incubations are limited.

The expression of monocyte TFPI was studied using flow cytometry and western blotting. TFPI protein expression has been shown in endothelial cells (Lupu et al., 1997), macrophages (Petit et al., 1999), platelets (Novotny et al., 1988), smooth muscle cells (Caplice et al., 1998) and cancer cells (Stavik et al., 2013) but its expression in monocytes is controversial (Osterud et al., 1995). The general consensus is that monocytes express low levels of TFPI, and expression is dependent on stimuli as, for example, fibronectin-adherent, but not endotoxin stimulated, monocytes express TFPI (Bajaj et al., 2007). One study by Basavaraj et al in 2010 did show surface TFPI on monocytes in the circulation and this increased after 6h LPS stimulation (Basavaraj et al., 2010), in contrast to an earlier study showing no increase in monocyte TFPI expression in response to PMA or LPS up to 36h (van der Logt et al., 1994). Interestingly, a number of studies (Ott et al., 2001; Paysant et al., 2005; Petit et al., 1999) identifying TFPI on monocytes / macrophages and other cell types used an antibody from American Diagnostica which has since been removed for unknown reasons.

Initially, the expression of TFPI on isolated monocytes was examined by flow cytometry. Using EA.hy926 cells as a positive control it was clear that the two-layer system was dependent on the cell number and on centrifugation between antibody incubations, most likely due to low affinity binding of the antibody to the antigen. Once a method had been established, TFPI expression was analysed on isolated monocytes reconstituted with platelets in plasma and incubated for 6h with 0.5μg/ml CRP-XL. A high proportion (~60%) of monocytes were positive for TFPI at 0h, or directly after isolation. This did increase over the 6h to ~90% but the increase was not significant. Evidence from the literature, as well that presented here suggests platelets may

translocate TFPI to the plasma membrane upon activation (Maroney and Mast, 2008; Novotny et al., 1988) and as activated platelets bind to monocytes the TFPI detected could be platelet derived. Taking this into account, further experiments using this protocol would need to incorporate the inclusion of the monoclonal P-selectin function blocking antibody 9E1 to prevent the binding of platelets to monocytes.

A number of other methods were also used to identify TFPI on monocytes by flow cytometry including in-house labelling of the TFPI antibody and whole blood measurement using isotype specific secondary antibodies. Both these methods yielded largely negative results and have not been included in this chapter. Firstly, the primary TFPI antibody was labelled in house and the matched isotype control purchased commercially. In retrospect, this was not the correct approach as the isotype antibody had a much higher level of fluorescence than the labelled primary. To develop this method, labelling of both the TFPI antibody and an isotype control should be carried out in house to generate reagents with comparable fluorescence : protein ratios. The second used antibodies with different isotypes to allow dual labelling of monocytes and TFPI in whole blood. An IgG1 anti-CD14 antibody was used with the IgG2a anti-TFPI antibody to label monocytes and TFPI. The TFPI was then recognised by an anti-IgG2a labelled secondary. This method should work in principle but when trying to set up using EA.hy926 cells TFPI expression could not be demonstrated. For reasons of time and expense it was decided not to continue using flow cytometry.

Following flow cytometry, western blotting for TFPI was undertaken. As with previous reports, TFPI expression was observed in PMA and LPS treated THP-1 cells as well as in unstimulated THP-1 cells and platelet lysates. The band for TFPI detected in THP-1 cells was higher than that of the EaHy.926 cell lysates possibly due to differential glycosylation in the ER / Golgi.

Due to the early negative results from western blotting, PCR was carried out to determine if monocyte *tfpi* transcripts contained a large proportion of exon 2, as this had been show to act as a translational repressor (Ellery et al., 2014). It was found that monocytes transcribe both the alpha and beta isoforms of *tfpi* and that exon 2 could be detected in some of the transcripts but not all (3:1 alpha and 2:1 beta, without:with) suggesting that whilst some transcripts may be regulated by this mechanism a large proportion should still be translated to protein.

After the initial hurdles had been overcome with regards to sample preparation, TFPI was detected in peripheral blood monocytes after culture for 24h, supporting the

observed expression of TFPI by adherent monocytes and macrophages. When monocytes isolated by negative isolation were reconstituted with platelets prior to activation there was no difference between the resting and 8h platelet-activated samples. However, after 10min TFPI levels had decreased, suggesting platelets release TFPI into the supernatant on activation. It has been reported previously that dual-activated 'coated' platelets release TFPI either in microvesicles or as soluble protein, although it is not thought to be present in α-granules (Maroney et al., 2007). After 10min the level of TFPI protein did increase to similar levels at both 4h and 8h; an increase of ~60%. In combination with the earlier flow cytometry results this would suggest monocytes do synthesis TFPI in response to activated platelets, however it cannot be ruled out that the increase is due to monocytes taking up TFPI bearing MVs, or soluble TFPI released from platelets.

To eliminate the possibility of detecting platelet-derived tissue factor, PBMCs were depleted of platelets prior to negative isolation of monocytes and incubation with the soluble fraction released from platelets with and without actinomycin. Although soluble and exosome associated TFPI would still be present it was hoped that the actinomycin would prevent endogenous transcription of *tfpi* in the monocytes and any subtle changes could be detected. Unfortunately this did not turn out to be the case as actinomycin appeared to enhance TFPI expression.

To summarise, an increase in monocyte TFPI expression was seen by both flow cytometry and western blotting but it could not be ruled out that this was due to exogenous sources such as platelets. Future experiments would focus on showing whether or not TPFI expression on monocytes is induced by activated platelets or not. To achieve this may require a combination of flow cytometry, microscopy and western blotting and, as seen from results above, is not a trivial task.

Expression of EPCR was seen in monocytes after platelet activation by western blotting but not by flow cytometry. The flow cytometry method had been optimised using EA.hy926 cells as a positive control and EPCR labelling was clearly seen. However, when the same method was used on isolated monocytes incubated with activated platelets no protein could be detected. The reason for this is currently unknown but could be due to different binding partners of EPCR on endothelial cells and monocytes as EPCR has been predicted to have multiple binding partners (Havugimana et al., 2012). As the antibody was monoclonal and the specific antigenic region is not stated, the epitope could be masked either due to interaction with additional proteins, or by

extensive post-translational modification. These would be disrupted when using western blotting.

Similar to TFPI, untreated, PMA and LPS treated THP-1 cells were analysed for EPCR expression by western blotting. EPCR could be detected in all samples and interestingly, appeared to decrease after PMA treatment, and subsequently rescued after incubation with LPS. PMA transforms THP-1 cells to a more macrophage-like phenotype whilst LPS is an inflammatory stimulus, suggesting inflammatory stimuli switch on EPCR expression in macrophages. However, this is speculative as experiments with THP-1 cells were beyond the scope of this project.

Negatively isolated monocytes were reconstituted with platelets and incubated with CRP-XL to activate the platelets. As with TFPI, resting samples showed a high level of EPCR that decreased after 10min of platelet activation, after which, EPCR protein expression increased in a time-dependent manner. These results indicated platelet activation leads to an increase in monocyte EPCR expression. EPCR has been shown to be present on the membrane of resting monocytes (Galligan et al., 2001). Interestingly, EPCR expression was only detected in 50% of the donors even though actin binding appeared uniform. The reason for this is unknown as all the samples were on the same membrane and therefore incubated with the same solution of anti-EPCR antibody. An explanation for this could be the variability in mRNA induction. The two donors that failed to show EPCR by western blotting could have had low levels of *procr* and the protein may therefore be below the detection limit for western blotting.

The decrease in EPCR protein detection between resting and 10min stimulated samples suggested, like TFPI, platelets may contain EPCR which is released on activation. At the time of this experiment there was no record of the identification of EPCR in or on platelets. Platelet lysates were assessed for EPCR protein and there appeared to be a small amount in platelets; an observation the was recently confirmed by Fager and Hoffman (Fager and Hoffman, 2014). Whether platelets do contain EPCR remains to be validated and if so whether it is released as soluble EPCR or associated with MVs needs to be confirmed.

To rule out platelets as the source of EPCR protein detected, monocytes were negatively isolated and incubated with the soluble fraction released from CRP-XL-activated platelets with and without actinomycin to inhibit transcription. Although there was no apparent increase in EPCR protein between 0h and 8h samples there was a significant decrease in EPCR expression when actinomycin was included. The EPCR shown in the

actinomycin treated samples could be due to turnover of protein already present and is indicative of endogenous transcription in monocytes incubated with activated platelets.

To summarise, EPCR could not be detected by flow cytometry but was readily detected in western blotting samples and although some EPCR may derive from platelets, monocytes do turn over EPCR in response to platelet-derived soluble mediators.

PPARγ expression was only assessed by western blotting. Again, THP-1 cells confirmed PPARγ protein expression in this monocyte-like cell line, which appeared to decrease as the cells adopted a more inflammatory phenotype. In the same way as for TFPI and EPCR, negatively isolated monocytes, reconstituted with platelets and activated with CRP-XL for up to 8h were assessed for PPARγ expression. There was again a similar decrease between resting and samples activated for 10min, after which PPARγ protein increased in a time dependent manner. Unfortunately this was only measurable in 50% of donors due to poor band definition. As platelets are known to contain PPARγ protein (Lannan et al., 2015) and release it into microvesicles on activation (Ray et al., 2008), it was hypothesised that nuclear extraction may circumvent the problem of exogenously derived PPARγ. This was also preferred as earlier experiments had shown direct platelet monocyte contact was needed for *pparγ* expression (see section 3.3.1). The incubation times were also shortened as earlier experiments had shown induction of *pparγ* by activated platelets was maximal at 2h. Initial experiments were promising, showing an increase in PPARγ protein in 2h samples compared to resting samples and this decreased at 3h, in agreement with the RT-qPCR data (section 3.2). In this case the positive control did not show up and in addition a suitable housekeeping gene had not been purchased. A new PPARγ antibody was also purchased that identified a single band. Both these were titrated using EA.hy926 lysates and the nuclear extract from resting monocytes. Both proteins were detected in the EA.hy926 lysate but were absent from the monocyte nuclear extract. The reason for this was unknown but it was hypothesised to be down to the nuclear extraction kit. However, it was confirmed to still work using THP-1 cells. Further experiments showed both PPARγ and the housekeeping gene TBP in nuclear extracts from negatively isolated monocytes (data not shown) but no difference was seen after 2h incubation, possibly due to PPARγ segregation in the nucleus and cytosol. Future experiments would activate monocytes in whole blood with and without actinomycin before negative isolation of monocytes and extraction of total proteins.

PPARγ protein has been reported in macrophages within atherosclerotic plaques where it induces TIMP proteins to inhibit matrix degrading MMPs (Hua et al., 2009). PPARγ is also know to be present in peripheral blood monocytes and have roles in monocyte differentiation to macrophages (Bouhlel et al., 2007; Tontonoz et al., 1998) and in the regulation of monocyte cytokines (C. Jiang et al., 1998). CRP-XL has also been shown to upregulate PPARγ regulated proteins in monocytes after short incubations (Rosienne Farrugia; personal communication). It is therefore likely that the PPARγ data shown here reflects endogenous production in monocytes.

Finally, to show the lack of protein detection was not due to monocyte death or absence of translation, monocytes both in whole blood and after isolation, were tested for viability and protein translation. There are a number of viability and apoptosis assays available including caspase activation and mitochondrial dysfunction measurements. However, these methods require a large quantity of isolated cells; almost impossible to obtain for monocytes using the methods employed here. Instead, a well-established flow cytometric assay was used based on the binding of Annexin-V as a measure of apoptosis and entry of the DNA dye 7-AAD as a measure of cell death. However, even this proved hard to set up as activated platelets not only bind to monocytes but also bind Annexin-V due to the translocation of PS to the outer leaflet. To circumvent this, the monoclonal P-selectin blocking antibody 9E1 was used to prevent MPA formation. As expected, after activation monocyte Annexin-V binding increased in samples not treated with 9E1 whereas the majority of monocytes remained unlabelled in the 9E1 treated samples suggesting platelets were contributing to the Annexin-V labelling observed. A minimal amount of 7-AAD was observed in any of the samples over the time course. Isolated monocytes showed more apoptosis in the 9E1 treated samples suggesting this was not down to platelets and is most likely due to extensive manipulation during isolation. However, overall both methods resulted in a large percentage of monocytes negative for both apoptosis and cell death and therefore viable for downstream experiments. This was reflected in the translation assay, where the incorporation of puromycin was observed at all time points measured suggesting monocytes were capable of producing protein.

To provide evidence that monocytes incubated for up to 8h *ex vivo* were capable of translating mRNA to protein, translation was measured using puromycin. Puromycin is incorporated into growing polypeptide chains causing translational arrest (Goodman et al., 2012; Yarmolinsky and Haba, 1959). Puromycin was incubated with isolated

monocytes for 30min before isolation and lysis. Incorporation was detected using an anti-puromycin-HRP conjugated antibody by western blotting. At all time points up to 8h there were bands visible demonstrating the incorporation of puromycin into polypeptide chains, confirming that protein translation had occurred. These results suggested that monocytes were able to make protein throughout the duration of the time course studied.

Overall, this chapter has highlighted the difficulties in working with this model in the context of protein detection. If protein is to be associated with platelet-activated peripheral blood monocytes a method needs to be developed whereby any contributing platelet-derived proteins are taken into account. Alternatively, specific molecules released from platelets that upregulate each gene (see chapter 5) could be incubated with platelet-free monocytes (which would be a challenge in itself). To take this forward it may be necessary to try alternate techniques such as ELISAs, which are more sensitive to low levels of proteins or immunoprecipitation coupled to MS. There is also the possibility that whilst platelets induce gene expression in monocytes, this is not translated to protein. This could be for a number of reasons such as degradation signals or inclusion into P-bodies. Another possibility is that miRNA released from platelets is preventing translation of the *tfpi* mRNA. There were 31 miRNA's predicted to bind to *tfpi* using the online program miRWALK (Dweep and Gretz, 2015). When these were cross-referenced with two papers measuring miRNA released from platelets (Hunter et al., 2008; Nagalla et al., 2011), 4 miRNA's were identified; 19b, 19a, 24 and 27a. Future experiments testing whether these miRNA's can regulate monocyte *tfpi* mRNA would be very interesting.

To conclude, it is likely that platelet induce the expression of TFPI, EPCR and PPARγ proteins in monocytes but technical difficulties prevented absolute conformation.

Chapter 5: Mechanisms regulating monocyte *tfpi* and *procr* gene expression

5.1 Introduction

Gene expression (transcription) is a complex process that requires simultaneous activation of several factors. Transcription factors bind to DNA elements called promoters and initiate transcription, which can be regulated by adjacent elements called enhancers and repressors. The pathway to transcription factor activation usually begins with a small signalling molecule that either activates the transcription factor directly, or initiates a complex signalling cascade. One of the most well studied group of signalling molecules are hormones such as androgen and oestrogen and prostaglandins. These molecules can be released by the cell they affect (autocrine regulation) or act on other cells (paracrine regulation).

How cells and hormones switch on the expression of a particular gene is paramount to understanding how normal and pathological processes progress. Determining the pathway to activation and regulation of a particular gene is a challenging task, especially as regulatory pathways can differ between cell type, even for the same gene. Such research is vital, however, for the discovery of new targets for modulating disease processes.

In chapter 3 it was shown that the major stimulus for *tfpi* was oxylipins, while for *procr* it was a low molecular weight soluble protein or polypeptide. The aim of this chapter was to further dissect the factors released from activated platelets to try to identify molecules that could switch on *tfpi* and *procr* expression in monocytes. This was achieved through analysis of the platelet releasate by tandem LC-MS/MS for both platelet-derived proteins and oxylipins. The identification of platelet-derived oxylipins lead to observation that a number were potential agonists of the transcription factor PPARγ and further RT-qPCR using PPARγ agonists confirmed that this factor is able to upregulate monocyte *tfpi*. LC-MS/MS measurement of platelet-derived proteins identified a number that could regulate *procr* expression, with initial observations suggesting PF4. However, further studies revealed this was not the case and the chemokine CCL5/RANTES was a more likely candidate.

5.2 Potential mechanism of platelet-mediated monocyte *tfpi* expression

In Chapter 3 it was observed that platelet-derived oxylipins were responsible for the majority of monocyte *tfpi* gene expression. In order to further dissect the mechanism of monocyte *tfpi* gene expression this section aimed to identify the oxylipins released from activated platelets using LC-MS/MS, and to identify a pathway for *tfpi* regulation in the monocyte.

5.2.1 Identification of platelet-derived oxylipins by LC-MS/MS

A number of methods are available to identify oxylipins in samples; most are costly and only able to identify one species at a time. LC-MS/MS was selected as an accurate, cost effective method able to identify multiple targets in a single run. A major problem with identification of oxylipins by LC-MS/MS is that they have similar MWs, which makes them hard to distinguish from each other, and, due to their small size, produce a limited range of similar ion fragments. To use this method, a collaboration was formed with Prof. David Barrett's group at the University of Nottingham who were able to analyse up to 39 eicosanoids in a single sample (Zhang et al., 2007) (figure 5.1).

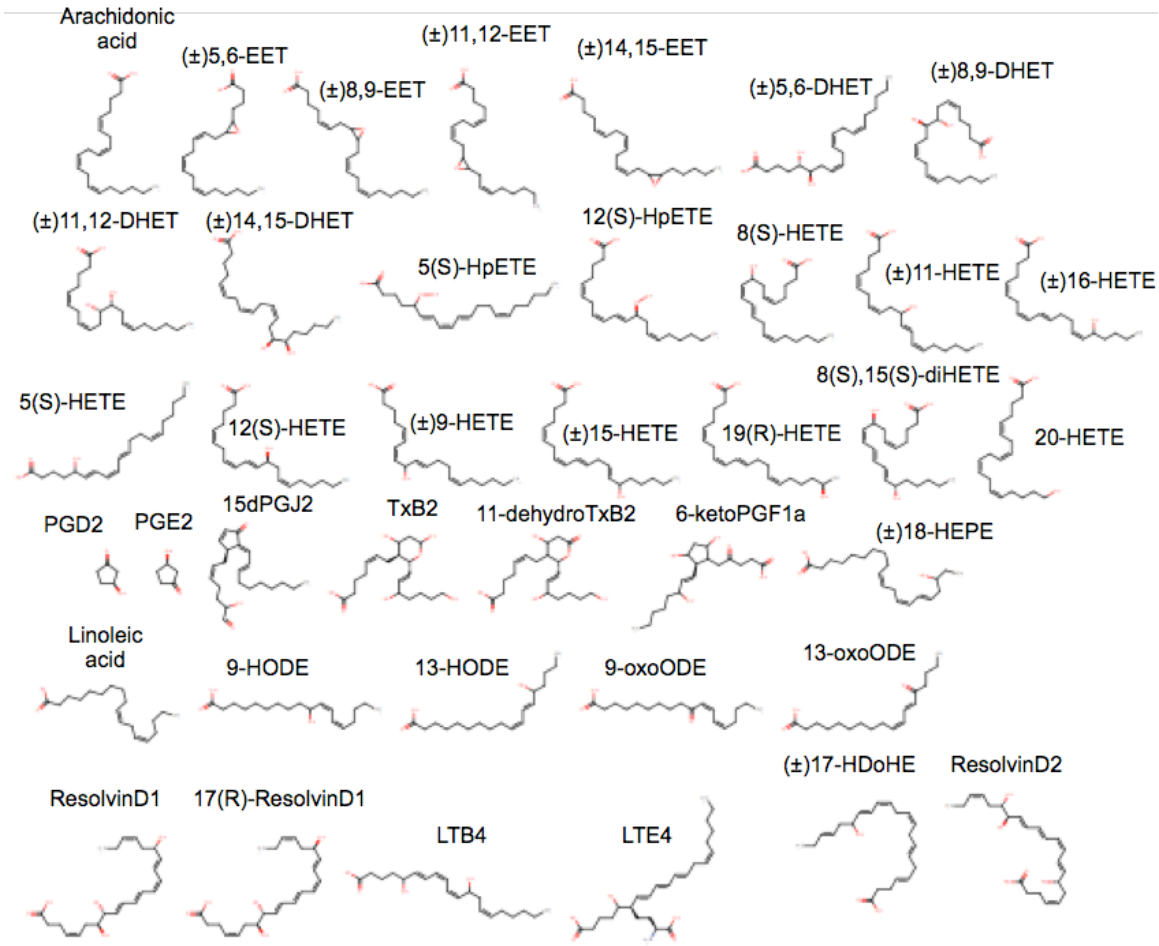

Figure 5.1: Structures of oxylipins identifiable by LC-MS/MS

Representative structures of the groups of oxylipins identifiable by LC-MS/MS.

5.2.1.1 Preliminary LC-MS/MS results

To determine if the extraction method was suitable for identification of oxylipins, a standard mixture containing known concentrations of the 39 eicosanoids was added to HBS pH 7.4 (n=6) and extracted using the previously described method (C. P. Thomas et al., 2010). The lyophilized metabolites were resuspended in 100µl 70% ethanol, analysed by LC-MS/MS and the recovery and precision of the extraction method calculated.

Table 5.1 shows the recovery (%) and precision (i.e. consistency of measured concentrations between samples) of the extraction method. Metabolites are ranked in order of recovery. A recovery of >20% is generally accepted but ideally should be >50%. Using this method, 9 of the 39 AA metabolites had a recovery below 20% (shown in red in the table).

Table 5.1: Recovery and precision of oxylipins using hexane-based extraction method

Analyte (n=6)	Precision % (RSD)	Recovery %
LTE4	27.47	0.67
6-keto-PGF1a	12.33	2.88
12-HPETE	54.54	3.21
TXB2	12.66	4.64
Resolvin D2	13.38	5.85
11-dehydro-TXB2	13.45	6.54
17-Resolvin D1	14.94	7.67
Resolvin D1	17.14	7.92
LTB4	14.75	19.41
5-HPETE	24.65	21.11
LA	12.33	25.04
8,15-DiHETE	17.79	36.75
5,6-EET	18.49	37.93
15-PGJ2	26.29	38.89
18-HEPE	21.69	40.35
19-HETE	28.35	41.12
14,15-DHET	26.32	41.41
5,6-DHET	26.58	42.11
5-HETE	16.49	45.31
16-HETE	33.90	45.45
11,12-DHET	22.68	48.50
20-HETE	23.96	49.16
8,9-DHET	20.13	49.73
9-oxo-ODE	19.08	49.85
13-oxo-ODE	17.94	50.68
AA	17.19	52.30
15-HETE	23.24	53.08
17-HDoHE	16.64	55.43
9-HETE	23.69	55.45
13-HODE	16.94	56.64
9-HODE	21.88	57.94
12-HETE	20.23	60.80
8-HETE	18.22	65.47
8,9-EET	18.22	65.47
11-HETE	27.51	70.35
11,12-EET	23.14	78.38
14,15-EET	16.61	96.43

Key: Red = outside recommended range; Black = within acceptable range; Green = within recommended range

Precision should be <15% for highly abundant metabolites and <20% for low abundance metabolites, but between 20 and 30% was deemed acceptable. Two

metabolites, 12-HpETE and 16-HETE had precision values of above 30%. This could be due to oxidation occurring during the extraction, as an anti-oxidant was not present, or to experimental error. In general good recovery did not correlate with good precision. The same extraction method was then used in a preliminary experiment to extract oxylipins from the platelet-releasates isolated from two donors. Platelets were washed 3 times in HBS pH6.0, activated with 0.5µg/ml CRP-XL, the releasate separated by centrifugation and oxylipins extracted as previously described. Platelet activation was assessed by P-selectin expression (data not shown). Extracted oxylipins were lyophilised using nitrogen gas and resuspended in 70% ethanol for analysis.

A total of 15 oxylipins were detected in both samples at concentrations ranging from ~0.8nM (8,9-EET) to ~19µM (LA) (table 5.2). Concentrations were similar between duplicates but were estimates as in these experiments standards were not included prior to extraction. However, the data supported the use of this method for further analysis of platelet-derived oxylipins.

Table 5.2: Preliminary oxylipin LC-MS/MS on platelet releasate

Oxylipin	Donor 1 (nM)	Donor 2 (nM)
Linoleic acid (LA)	22296.13	16848.59
Arachidonic acid (AA)	14236.01	11113.65
12-HETE (hydroxyeicosatetraenoic acid)	2654.792	3469.592
Thromboxane B2 (TXB2)	567.098	778.723
Leukotreine B4 (LTB4)	214.361	167.893
13-HODE (Hydroxyoctadecadienoic acid)	86.233	175.549
9-HODE	74.153	115.396
11-HETE	70.367	93.91
6-ketoPGF1α	48.648	50.304
8-HETE	7.692	11.432
13-oxo-ODE	5.787	7.479
15-HETE	4.603	4.042
9-oxo-ODE	2.905	3.244
PGE2/PGD2	2.535	2.502
8,9-EET	0.771	0.879

5.2.1.2 Identification of platelet-released oxylipins and the effect of COX-1 and 12-LOX inhibitors

These extractions were repeated in releasates from 6 donors. As well as measuring the production of oxylipins from endogenous AA and LA released during platelet activation, the effect of aspirin and esculetin (inhibitors of COX-1 and 12-LOX

respectively) on these levels was also investigated, as inhibition of both enzymes had been shown to inhibit the expression of *tfpi*.

Oxylipins were extracted from the releasate of washed, CRP-XL-activated platelets (0.5µg/ml) with and without pre-treatment with $5x10^{-4}$M aspirin, 150µM esculetin, or both (n=6). The extraction of the 24 samples was carried out simultaneously (figure 5.2) alongside standards, 4 quality control samples and 2 blanks (designated Bl- and Bl+). The anti-oxidant BHT was added to all samples and internal standards to all apart from one blank (BL-). Samples were resuspended in 70% ethanol and oxylipins measured using a 4000 QTRAP® spectrometer.

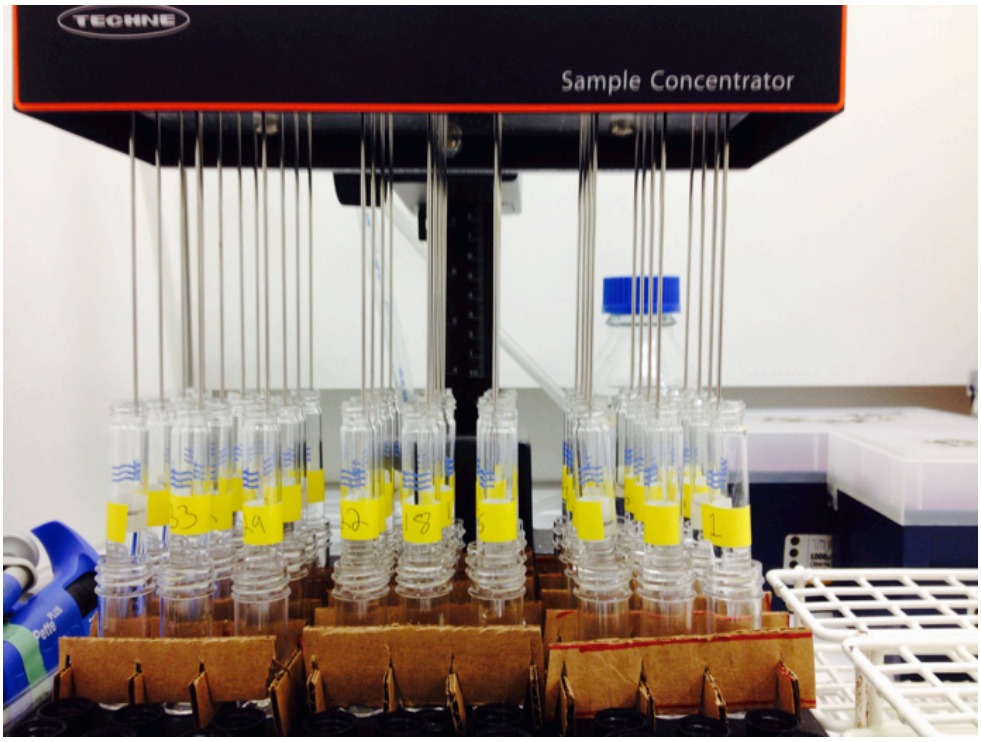

Figure 5.2: Simultaneous extraction of oxylipins from treated platelet releasate

A total of 24 samples including experimental samples, standards and controls were simultaneously extracted using a hexane-based method. Oxylipins were concentrated the setup shown in this figure.

Platelet activation was confirmed by measuring P-selectin expression on the CyanADP flow cytometer (figure 5.3). All 4 treatment groups (control, ASA, esculetin, ASA/esculetin) showed a similar level of P-selectin expression at resting of ~20%, and this increased significantly after activation with CRP-XL. While P-selectin expression was similar after activation in all samples, as found previously there was a significant reduction when aspirin was present, decreasing from 73.32±3.49 in the control to 66.44±4.30 (p=0.0246), but not with esculetin. There was a noticeable non-significant

decrease in P-selectin expression in the dual aspirin / esculetin treated samples, from 73.3±3.5% to 66.6±3.9%, probably attributable to the effect of aspirin.

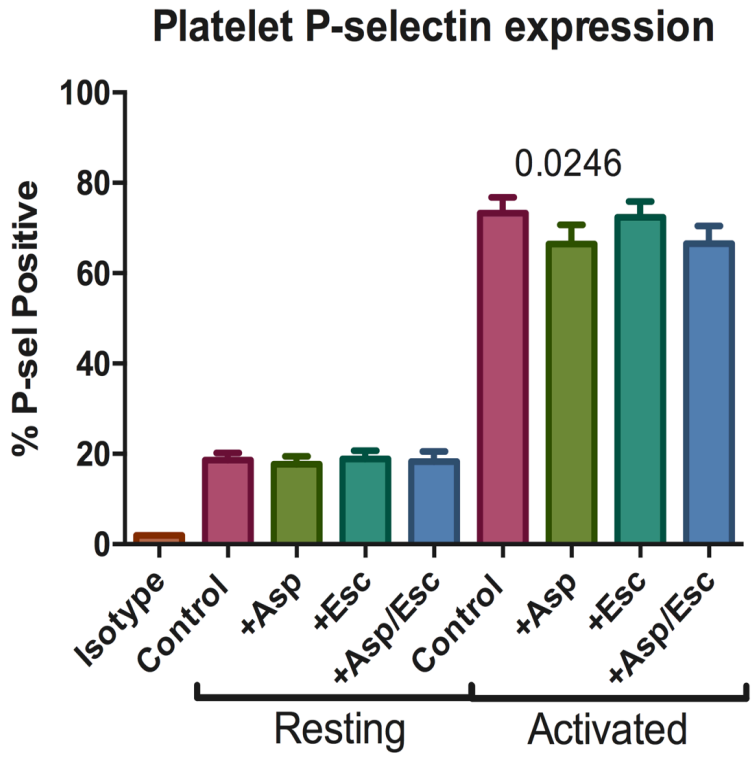

Figure 5.3: Conformation of platelet activation by flow cytometry

Washed platelets in the absence or presence of aspirin (500μM) or esculetin (150μM) were incubated at 37°C for 10min with 0.50μg/ml CRP-XL. Resting and activated platelets were analysed for P-selectin expression using the CyanADP flow cytometer. P-values calculated using the Student's paired t-test and compared to activated control samples. Data show mean±SEM; n=6.

After the samples had been processed using the 4000 QTRAP®, internal controls were used to calculate the area ratio, as described in section 2.14. Table 5.3 shows the average peak area count of each internal control across the samples. In all cases standard deviation was below 15%, which is acceptable for this analysis.

Table 5.3: Average peak area of internal controls across samples

	IC peak area		
	AA-d8	**15-HETE-d8**	**PGD2-d4**
Average peak area count QC	903780.75	8895353.50	120154.50
SDEV % QC	14.0	4.9	12.5
Average peak area count samples + QC	985525.82	8820202.25	141264.29
SDEV % samples + QC	7.8	7.6	10.3
Average peak area count EC + Bl+	1027433.23	9358087.77	124322.31
SDEV % EC + Bl+	11.7	9.1	14.5
Average peak area count all samples	998813.54	8990751.32	135892.44
SDEV % all samples	9.3	8.5	12.8

The standard deviation of each metabolite was calculated in the QC samples, giving an indication of reproducibility and variation. As before, a SD <15% indicates good reproducibility but below 20% is tolerated if the analyte is present at very low concentrations, such is the case for 8,9-EET. 9-oxoODE did show a QC standard deviation of 16.8% but as this is close to 15% the results were still included. The concentration from QC2 for LA was omitted from the calculation due to it being an outlier. No peaks for 9-HETE were observed in any of the QC's, but data was still included because the analysis gave good QC results for the other metabolites.

The area ratio for each standard was used to create a standard curve of area ratio vs. concentration for all identified metabolites. In most cases, the graph produced a straight line, however, with 4 metabolites (LA, 9-HETE, 13-oxoODE and 6-ketoPGF1a) the line was curved. For LA and 13-oxoODE the top 3 and 2 highest concentrations respectively were omitted from the standard curve as they prevented the formation of a straight line. This was most likely due to competition for the ionization source due to too high a concentration. For 9-HETE and 6-ketoPGF1α the lowest 2 concentrations were omitted because no peak was observed.

The peak area ratio was calculated for each metabolite using the internal controls and concentration determined from the standard curves. Each concentration was adjusted to take into account extraction volume, converted to ng/ml and set to amount per $600x10^9$ platelets.l^{-1}. A total of 16 oxylipins were identified in the samples. Table 5.4 represents the average concentration in ng/ml as well as the SEM for each metabolite. The most abundant metabolite was AA (184.4ng/ml) followed by TXB2 (60.75ng/ml) and 12-HETE (23.03ng/ml). There appeared to be a large amount of 6-keto-PGF1α in the samples but this is likely due to the metabolism of the exogenously added prostacyclin

during platelet washing. High concentrations of LA were also present in the samples (16.49ng/ml). The next most abundant metabolite, 20-HETE, was 16 fold lower than LA. The least abundant metabolite was found to be 8-HETE (0.00077ng/ml).

Table 5.4: Concentration of oxylipins identified in samples

Oxylipin	Av.con. (ng/ml)	SEM
AA	184.4	25.28
TXB2	60.75	19.13
12-HETE	23.03	5.767
6-keto-PGF1a	19.72	6.812
LA	16.49	2.00
20-HETE	1.086	0.2665
9-HODE	0.4621	0.1337
13-HODE	0.4383	0.1034
11-HETE	0.3239	0.1274
PGD/E2	0.2697	0.09652
15-HETE	0.1603	0.02468
13-oxoODE	0.05923	0.006143
9-HETE	0.03248	0.0146
9-oxoODE	0.0194	0.002422
8,9-EET	0.002894	0.001044
8-HETE	0.0007664	0.0001602

Concentrations were converted from nM to ng/ml and normalised to $600x10^9$ platelets / l

The effect of COX-1 and 12-LOX inhibition on the oxylipin profile was also assessed. Firstly, inhibition of COX-1 with aspirin had no effect on the release of AA, LA, 8-, 9-, 12- and 20-HETE, 8,9-EET, 9- and 13-oxoODE and 6-ketoPGF1a. As expected, aspirin completely prevented formation of TXB2 and PGD/E2 and the majority of 11-HETE and 9-HODE. There were also small but significant decreases in the release of 15-HETE and 13-HODE (figure 5.4a). Inhibition of 12-LOX by esculetin resulted in significant decreases in 8- and 11-HETE, TxB2, 9-oxoODE and 9-HODE (figure 5.4b). There was no decrease seen in 12-HETE that suggests the esculetin was not functionally effective. Dual inhibition showed a similar profile to aspirin alone (figure 5.4c).

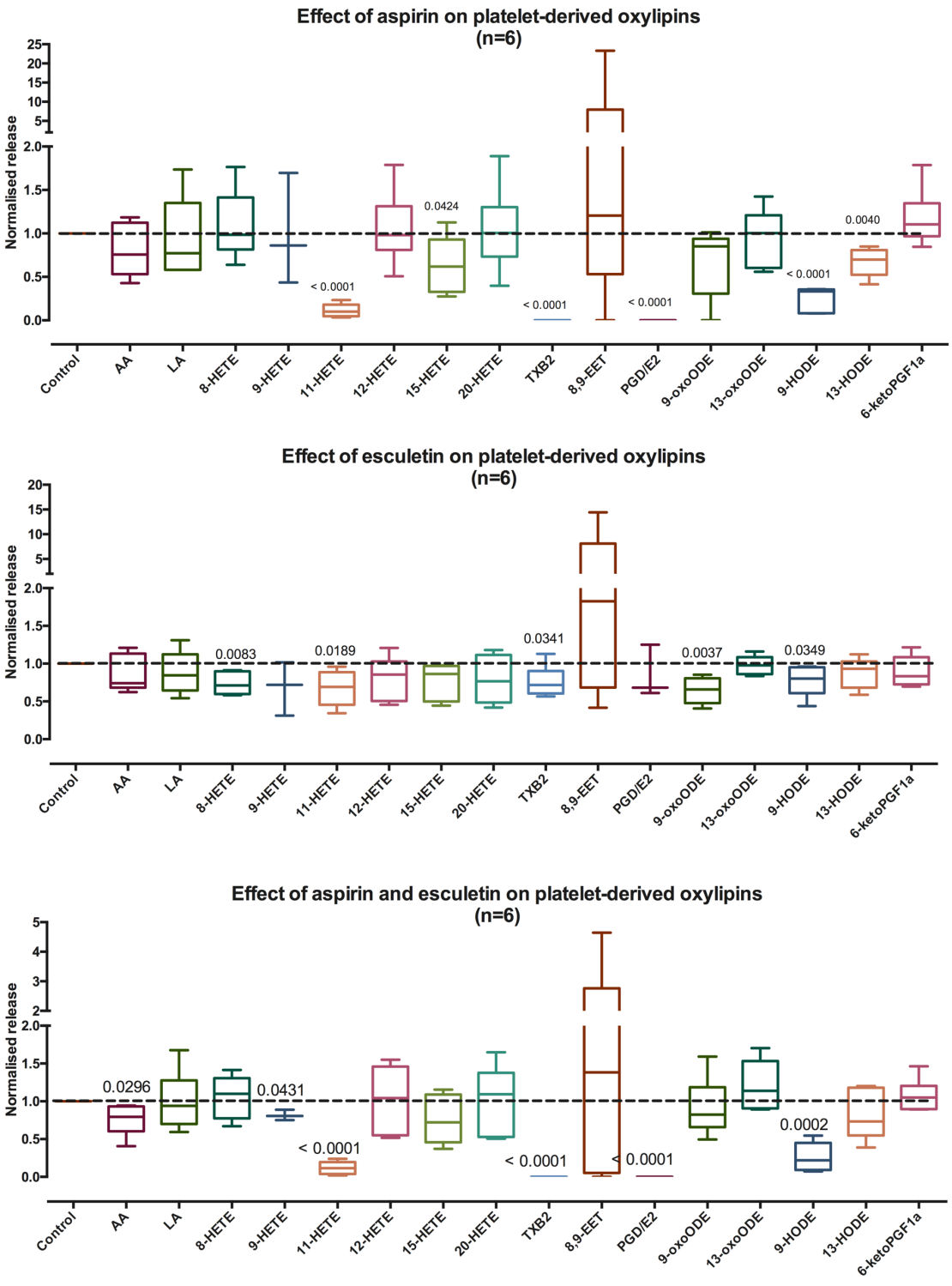

Figure 5.4: Effect of COX-1 and 12-LOX inhibition on platelet oxylipin production

Platelet oxylipins were extracted from releasate isolated from platelets treated with or without aspirin and / or esculetin and activated by 0.5µg/ml CRP-XL. P-values were calculated using a one sample t-test and are compared to control sample. Data show mean±SEM; n=6.

5.2.1.3 Effect of 12-LOX inhibition on oxylipin production from washed platelets and platelets in plasma

The previous results were as expected for aspirin but not for esculetin. On further inspection it was realised that, whilst aspirin irreversibly inhibits COX-1 through acetylation, esculetin is a non-competitive inhibitor. As both inhibitors were added prior to platelet washing, esculetin may have dissociated from 12-LOX due to the equilibrium imbalance created by washing. To test if this was the case, platelets in plasma were inhibited with esculetin (150µM) and washed up to 2 times. After each wash platelets were resuspended in normal plasma and used in platelet aggregometry. Aggregation was initiated using 1µg/ml CRP-XL. The same experiment was also carried out with baicalein, another 12-LOX inhibitor.

Without washing, esculetin (150µM) almost completely prevented platelet aggregation induced by CRP-XL. However, after the first centrifugation and resuspension in plasma, inhibition was abolished and aggregation was similar to that seen without any inhibitor and this remained true for the next washing steps (figure 5.5a and c). Identical results were seen with baicalein (figure 5.5b and c).

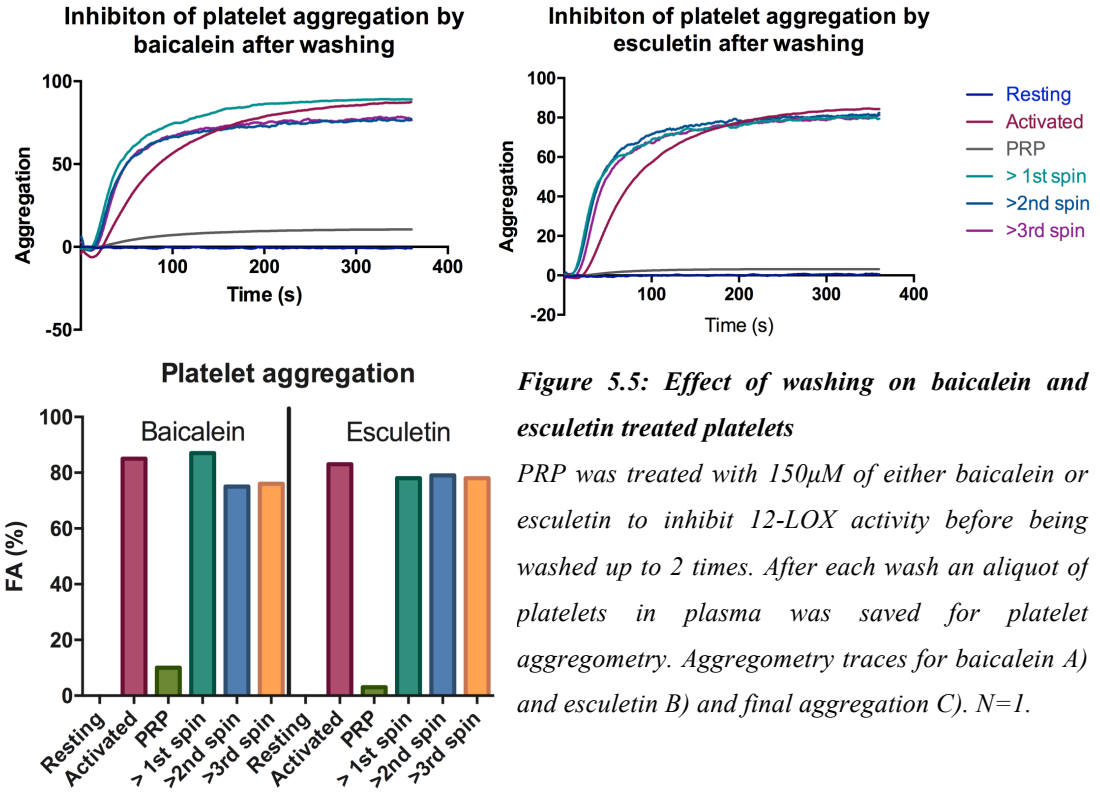

Figure 5.5: Effect of washing on baicalein and esculetin treated platelets

PRP was treated with 150µM of either baicalein or esculetin to inhibit 12-LOX activity before being washed up to 2 times. After each wash an aliquot of platelets in plasma was saved for platelet aggregometry. Aggregometry traces for baicalein A) and esculetin B) and final aggregation C). N=1.

Based on these findings, the LC-MS/MS experiment was repeated using platelets that had been washed prior to inhibition with a 12-LOX inhibitor. For this set of experiments, both esculetin and baicalein were used to inhibit 12-LOX. The method used here was the same as section 5.3.1.2 with the following modifications. Platelet rich plasma or 3 times washed platelets (resuspended in HBS pH 7.4) were incubated at 37°C for 10min with either 50 or 150μM of the 12-LOX inhibitors baicalein or esculetin, 2mM Ca^{2+} (for maximal 12-LOX activity) and Hirudin (to block any thrombin that might be formed in the PRP samples). The releasate was isolated and oxylipins extracted from 800μl of each sample alongside standards, QCs and blanks as before. Standards were prepared in milli-Q water for both sets of samples. For washed platelets, the QCs and blanks were the same as previously. For plasma samples, the QCs were pooled plasma and the blanks were milli-Q water. Due to the number of samples, after extraction the solvent was evaporated by vacuum centrifugation, which is also likely to be more efficient than using nitrogen gas. Samples were resuspended in 70% ethanol and oxylipins measured by LC-MS/MS using a 4000 QTRAP®. After measurement, the same methodology was used to calculate concentrations of analytes. In samples from washed platelets, the concentration of AA was interpreted from extrapolation of the standard curve and LA, although present, was not quantified as the QC failed.

Table 5.5 represents the absolute concentrations of oxylipins detected by LC-MS/MS in the supernatant of platelets activated in buffer and plasma. The supernatant from platelets activated in buffer identified 11 oxylipins (8-, 9-, 11-, 12- and 15-HETE, TxB_2, AA, LA, 9- and 13-HODE and PGD/E_2) ranging in concentration from 4.7fg/ml (9-HETE) to 211.9ng/ml (12-HETE) (values normalized to $600x10^9$ platelets /L). TxB_2 and AA were both shown to be at a similar concentration to 12-HETE with the next oxylipin, PGD/E_2, 47.6 fold lower. An additional 10 oxylipins (9- and 13-oxoODE, 5,6-, 8,9-, 11,12- and 14,15-DHET, 5,6-EET, 5- and 16-HETE and LTB4) were measured in the supernatant from platelets activated in plasma, along with the 11 already identified in the supernatant from platelets activated in buffer. The majority of these had concentrations well below 0.5ng/ml suggesting low plasma levels originating from sources other than platelets. The concentration of LTB4 was 1.52ng/ml but is likely to be derived from leukocytes.

Table 5.5: Oxylipins identified in buffer and plasma from activated plasma

	Washed Platelets	**Platelet Rich Plasma**
Oxylipin	**Concentration (ng/ml) (±SEM)**	**Concentration (ng/ml) (±SEM)**
12-HETE	211.9 (±79.8)	152.4 (±29.4)
TXB2	182.3 (±76.5)	254.2 (±67.4)
AA	152.0 (±53.6)	133818 (±24703)
PGD/E2	3.19 (±1.75)	6.65 (±1.73)
9-HODE	2.81 (±1.79)	6.69 (±1.88)
11-HETE	2.75 (±1.58)	5.49 (±1.60)
13-HODE	1.85 (±1.01)	4.57 (±1.07)
15-HETE	0.79 (±0.43)	8.83 (±2.61)
8-HETE	0.47 (±0.17)	0.36 (±0.077)
9-HETE	0.0047 (±0.0032)	0.056 (±0.0092)
9-oxoODE	-	0.051 (±0.019)
13-oxoODE	-	0.32 (±0.078)
LTB4	-	1.52 (±0.18)
5,6-EET	-	0.0037 (±0.0014)
16-HETE	-	0.12 (±0.015)
LA	Failed QC	16928 (±21562)
5-HETE	-	0.48 (±0.14)
5,6-DHET	-	0.16 (±0.025)
8,9-DHET	-	0.19 (±0.041)
11,12-DHET	-	0.30 (±0.053)
14,15-DHET	-	0.36 (±0.052)

For washed platelets, both 50 and 150μM of either 12-LOX inhibitor produced a similar profile for oxylipin release albeit less pronounced with the lower dose, so only results using the highest dose will be discussed. Baicalein significantly inhibited the release of all measured oxylipins excluding AA, with complete inhibition of 12-, 8- and 9-HETE, PGD/E_2 and 9- and 13-HODE and almost complete inhibition of TxB_2, 11- and 15-HETE (figure 5.6a). Identical results were seen with esculetin excluding inhibition of the formation of 9-HETE (figure 5.6b); although 9-HETE could only be detected in 50% of donors.

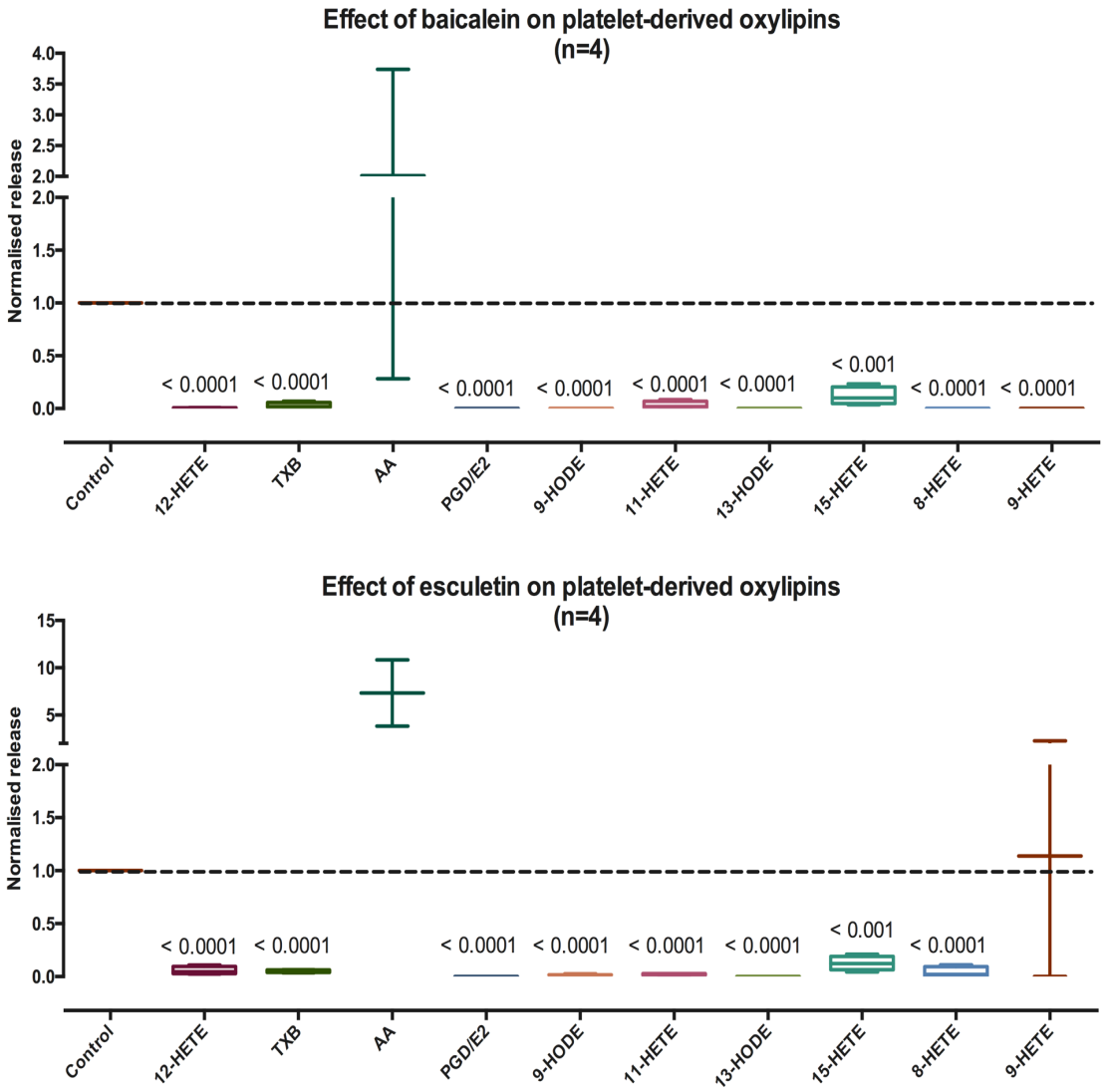

Figure 5.6: Effect of baicalein and esculetin on oxylipins released from washed platelets

Platelets, washed 3 times in HBS pH 6.0, were inhibited with 150µM of either baicalein A) or esculetin B) and activated with 0.5µg/ml CRP-XL. The supernatant was isolated, oxylipins extracted and identified by LC-MS/MS. P-values were calculated using a one sample t-test. Data show mean±SEM; n=4.

The oxylipin profile from platelets activated in plasma after inhibition with baicalein and esculetin was similar to that of washed platelets. Baicalein significantly decreased the release of 11-, 12- and 15-HETE, 13-HODE and TxB2 (figure 5.7a). Decreases were also seen with 8-, 9-HETE, 9-HODE and PGD/E2 but these were not significant. There were no significant changes seen in any of the metabolites identified only in the plasma samples. Esculetin produced similar results, with significant decreases seen in the release of 8-, 11-, 12- and 15-HETE, 9-HODE and PGD/E2 (figure 5.7b). There were also decreases in 13-HODE and 9-HETE but these were not significant. Of the metabolites only identified in plasma samples, a significant change was seen in LTB4.

Table 5.6 represents the percentage change in the baicalein and esculetin samples compared to controls.

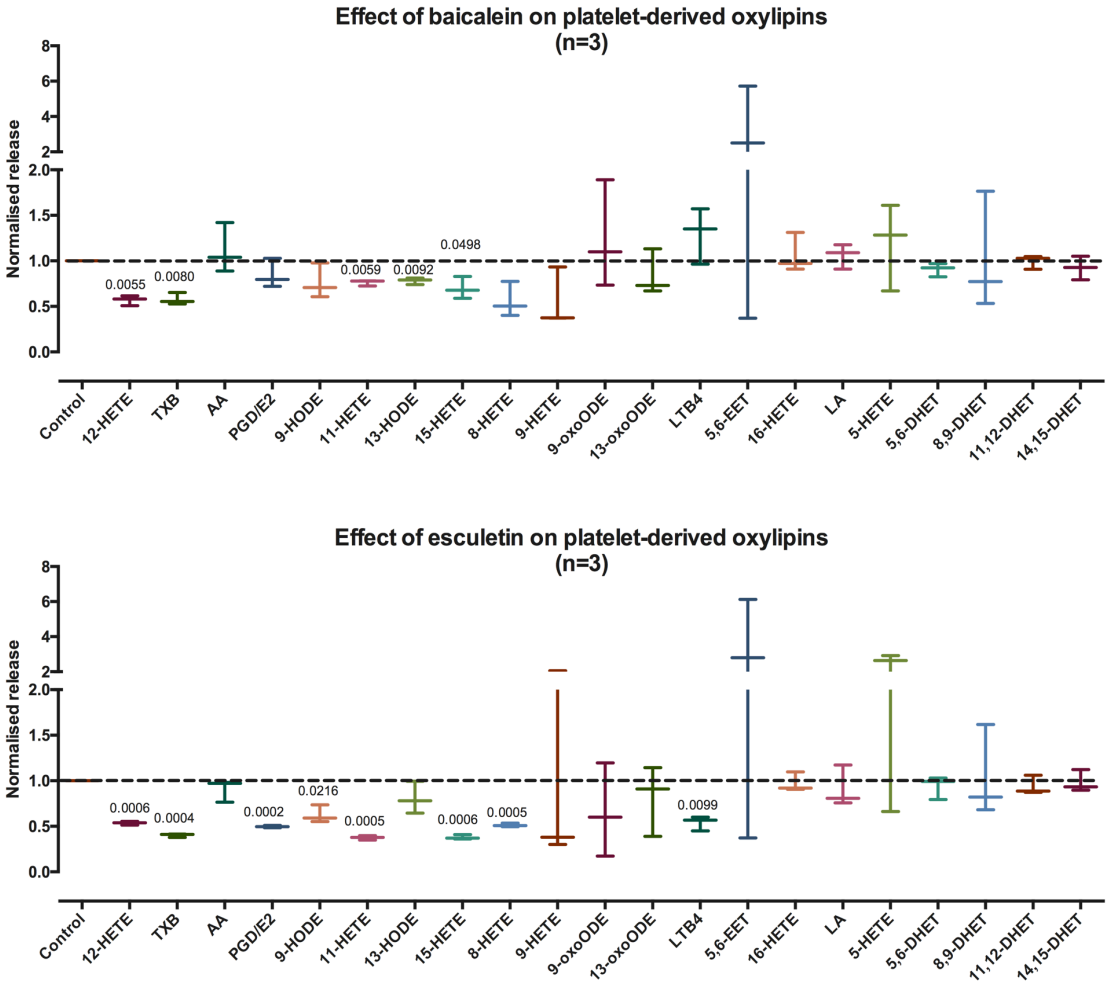

Figure 5.7: Effect of baicalein and esculetin on oxylipins released from platelets in plasma

Platelets, suspended in plasma, were inhibited with 150μM of either baicalein A) or esculetin B) and activated with 0.5μg/ml CRP-XL. The plasma was isolated, oxylipins extracted and identified by LC-MS/MS. P-values were calculated using a one sample t-test. Results are mean±SEM; n=4.

Table 5.6:Percent of oxylipin present in samples after 12-LOX inhibition compared to control samples

	% of oxylipin detected in relation to control			
	Baicalein (150µM) (mean±SEM)		Esculetin (150µM) (mean±SEM)	
Oxylipin	**Buffer**	**Plasma**	**Buffer**	**Plasma**
12-HETE	0.44±0.13	56.9±3.2	5.6±1.9	53.6±1.1
TXB	2.8±1.3	57.8±3.8	5.1±0.61	40.1±1.2
AA	201.1±72.8	111.6±15.8	733.3±350.4	90.5±7.1
PGD/E2	0.000025±0.000025	84.9±9.3	0.000025±0.000025	49.7±0.73
9-HODE	0.00017±0.00017	76.4±11.1	1.4±0.73	62.6±5.6
11-HETE	3.2±1.8	76.1±1.8	2.2±0.31	37.5±1.5
13-HODE	0.00013±0.00013	78.0±2.1	0.00013±0.00013	80.7±10.2
15-HETE	11.7±4.2	69.8±7.0	12.6±3.4	38.0±1.5
8-HETE	0.00013±7.0E-05	56.0±11.2	3.8±2.6	51.3±1.1
9-HETE	0.0043±0.0019	56.0±18.7	113.9±113.9	91.3±57.3
9-oxoODE	NA	124.2±34.1	NA	65.6±29.7
13-oxoODE	NA	84.4±14.5	NA	81.5±22.3
LTB4	NA	129.6±17.7	NA	54.0±4.6
5,6-EET	NA	286.6±155.7	NA	309.8±166.7
16-HETE	NA	106.5±12.5	NA	97.4±6.2
LA	NA	105.9±7.8	NA	91.3±13.1
5-HETE	NA	118.8±27.6	NA	207.4±71.0
5,6-DHET	NA	90.6±4.3	NA	93.9±7.3
8,9-DHET	NA	102.3±37.7	NA	104.0±29.2
11,12-DHET	NA	99.4±4.3	NA	94.1±6.1
14,15-DHET	NA	92.4±7.5	NA	98.4±7.0

5.2.1.4 Effect of platelet aggregation on oxylipin production from washed platelets and platelets in

Inhibition of COX-1 and 12-LOX also prevents platelet aggregation; to assess if oxylipin production is dependent on aggregation, PRP or washed platelets were incubated with the GPIIbIIIa blocking antibody RFGP56 (10µg/ml) prior to activation, oxylipin extraction and LC-MS/MS. Prior to use, the antibody was titrated to confirm that it prevented platelet aggregation at this concentration (data not shown).

The results in table 5.7 represent the (%) change in the amount of oxylipin detected in the supernatants from platelets activated in buffer and plasma. Inhibiting platelet aggregation in washed platelet samples had no inhibitory effect on oxylipin production after activation, and in some cases showed a trend towards an increase, although only significant for 15-HETE. Similar results were also seen in plasma samples suggesting

platelet outside-in signalling and/or aggregation is not necessary for oxylipin production through COX-1 and 12-LOX. There was a significant decrease in 13-oxoODE and a large decrease in 9-oxoODE from plasma samples, which may suggest platelet aggregation and/ or GPIIbIIIa signalling is important for the oxidation of 13- and 9-HODE.

Table 5.7: Effect of aggregation on platelet oxylipin production

	Washed platelet supernatant		Plasma supernatant	
Oxylipin	**% of control (±SEM)**	**P-value**	**% of control (±SEM)**	**P-value**
12-HETE	134.0 (±18.2)	NS	141.1 (±34.0)	NS
TXB2	137.0 (±13.5)	NS	177.5 (±64.2)	NS
AA	97.6 (±76.1)	NS	115.2 (±18.6)	NS
PGD/E2	162.7 (±51.3)	NS	206.4 (±71.3)	NS
9-HODE	189.7 (±30.3)	NS	121.9 (±26.4)	NS
11-HETE	177.4 (±44.8)	NS	193.9 (±55.2)	NS
13-HODE	171.2 (±53.7)	NS	96.1 (±15.2)	NS
15-HETE	156.0 (±14.1)	<0.05	197.7 (±63.0)	NS
8-HETE	126.9 (±20.0)	NS	155.9 (±48.8)	NS
9-HETE	122.4 (±22.4)	NS	126.2 (±24.7)	NS
9-oxoODE	-	-	9.4 (±5.8)	NS
13-oxoODE	-	-	54.4 (±11.6)	<0.05
LTB4	-	-	130.2 (±30.8)	NS
5,6-EET	-	-	144.2 (±2.4)	NS
16-HETE	-	-	105.2 (±16.3)	NS
LA	-	-	96.3 (±13.5)	NS
5-HETE	-	-	87.3 (±14.7)	NS
5,6-DHET	-	-	93.9 (±18.0)	NS
8,9-DHET	-	-	84.1 (±11.4)	NS
11,12-DHET	-	-	95.1 (±16.1)	NS
14,15-DHET	-	-	105.7 (±15.4)	NS

P-values calculated using a paired Student's t-test vs. control samples.

5.2.2 Effect of PPARγ agonists and antagonists on monocyte *tfpi* expression

Of the identified oxylipins released from platelets, at least 4 have been implicated in binding to PPARγ; 9- and 13-HODE have been crystallised with PPARγ (Itoh et al., 2008) and 12- and 15-HETE have been shown in some papers to activate PPARγ (Q. Li et al., 2004; Nagy et al., 1998). Combining these observations with the demonstration of the effects of inhibiting COX-1 and 12-LOX on monocyte *tfpi* expression, led to the hypothesis that PPARγ may regulate *tfpi* expression in monocytes.

To test this, whole blood was incubated at 37°C for 6h under 3 conditions; i) without platelet activation and in the presence of either 15d-PGJ2 (10μM) or rosiglitazone

(25μM) (PPARγ agonists), GW9662 (1μM) or T0070907 (50μM) (T007) (PPARγ antagonists), ii) with 0.5μg/ml CRP-XL and in the presence of either 15d-PGJ2, rosiglitazone, GW9662 or T007 and iii) with CRP-XL and 15d-PGJ2 and either GW9662 or T007. After incubation, monocytes were isolated using CD14 Dynalbeads® and total RNA using TRIzol. Resulting cDNA was used to measure expression of *tfpi* relative to *β2m*.

In the absence of platelet activation there was a small increase in *tfpi* expression after 6h compared to resting, which was unaffected by DMSO (0.1%). The PPARγ agonist 15d-PGJ2 showed a trend towards increased *tfpi* expression compared to the DMSO control that was similar to that induced by CRP-XL but did not reach significance (compare figure 5.8 15d-PGJ2 blue box with +DMSO red box). No change in expression was seen with the other agonist rosiglitazone or with either of the antagonists.

Platelet activation caused an increase in *tfpi* expression compared to resting samples that was unaffected by DMSO. Both rosiglitazone and 15d-PGJ2 showed a trend towards increased *tfpi* expression compared to control (+DMSO),but neither reached significance. There was, however, no change in expression with either antagonist. Expression of *tfpi* was unaffected by either PPARγ antagonist when incubated with both CRP-XL and 15d-PGJ2.

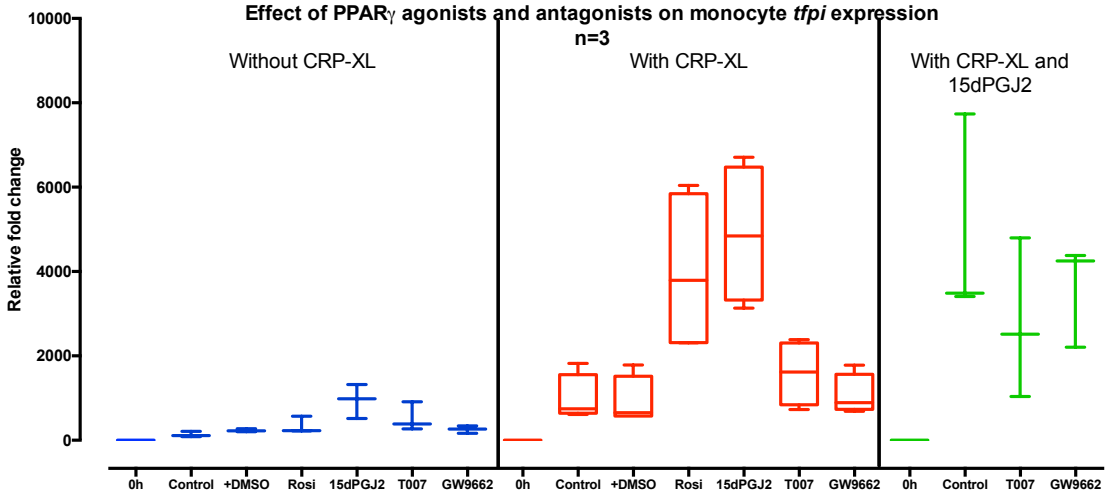

Figure 5.8: Effect of PPARγ agonists and antagonists on monocyte tfpi expression

Whole blood was incubated for 6h at 37°C with the PPARγ agonists rosiglitazone (25μM) and 15d-PGJ2 (10μM) or antagonists T007 (50μM) and GW9662 (1μM) in the presence or absence of platelet activation. Extracted monocytes were lysed and total RNA subject to RT-qPCR. P-values were calculated using a Friedman test. Data show mean±SEM; n=3/4.

These results suggest that PPARγ agonists are able to induce monocyte *tfpi* gene expression. Whilst no difference was observed with the antagonists this could be due to either too low a concentration used in whole blood or the short half-lives of these agents. In cell culture, the half life of GW9662 is ~1.9h in the supernatant and ~2.2h in cells whereas rosiglitazone is 26h in the supernatant and 54h in cells (X. Li et al., 2011). Due to time constraints the effects of PPAR inhibitors was not explored further.

5.3 Potential mechanism of platelet-mediated monocyte *procr* expression

Earlier RT-qPCR results had, in contrast to *tfpi* expression, found the monocyte *procr* expression is dependent on proteins >10kDa released from activated platelets. In order to identify potential candidates, proteins were measured in the releasate isolated from activated platelets by LC-MS/MS.

5.3.1 Preliminary identification of platelet_derived proteins by LC-MS/MS

To determine the best instrument for identification of platelet proteins, platelets from 1 healthy donor were washed once in in PBS pH 6.0 before resuspension in PBS pH 7.4 and activation with 0.5µg/ml CRP-XL. The subsequent releasate was isolated, separated into proteins < and > than 10kDa and prepared for MS. The protein samples were analysed using a SYNAPT G2-Si High Definition MS (Waters) and a Q-Exactive MS (Thermo Fisher). After analysis of peptides and identification of proteins, there were 208 and 358 proteins identified in the >10kDa sample using the SYNAPT and Q-Exactive respectively with 162 identified in both (figure 5.9a). In this run there was not enough protein in the <10kDa samples for analysis.

After analysis, a large number of proteins present in the sample were defined as plasma proteins including serum albumin. To try and reduce contamination by plasma proteins, releasate was prepared from a single donor using platelets washed 3 times in HBS pH 6.0 before resuspension in HBS pH 7.4. The extra washes significantly reduced the amount of proteins detected in the samples with 64 and 123 hits in the >10kDa sample with the SYNAPT and Q-Exactive respectively, with 54 common to both (figure 5.9b). When comparing the first run with a single wash and second run with three washes, there were 55 proteins common when using the SYNAPT (figure 5.9c) and 100 when using the Q-Exactive (figure 5.9d).

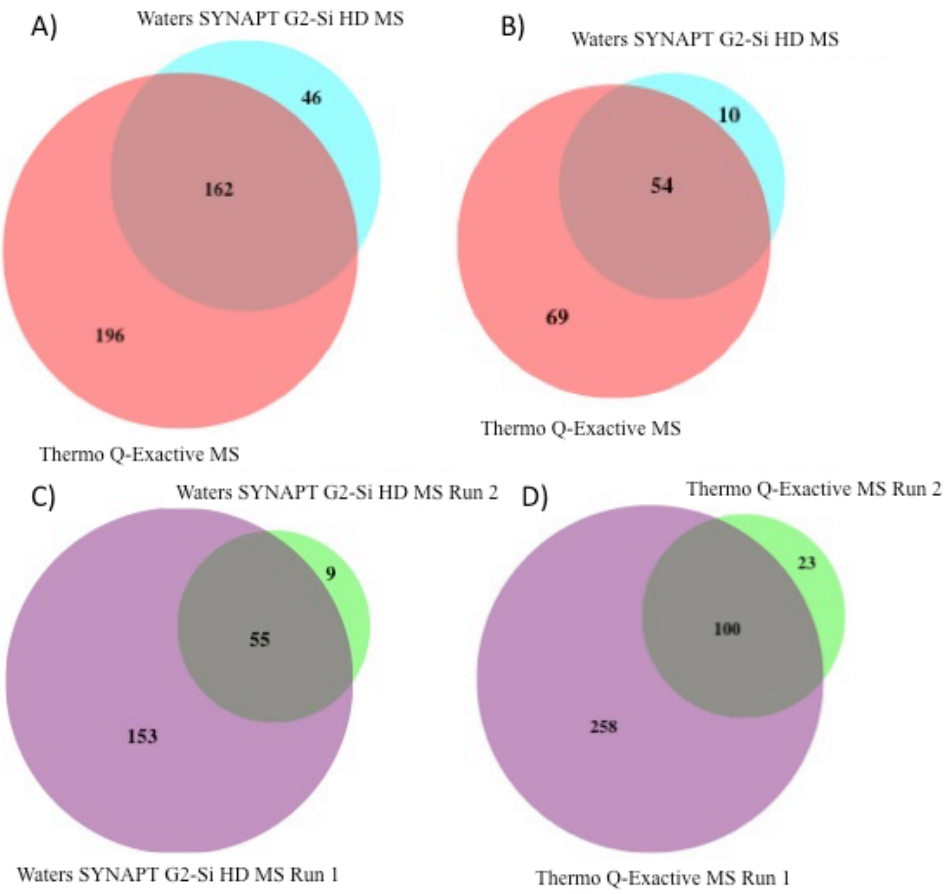

Figure 5.9: Venn diagrams comparing number of proteins identified by LC-MS/MS

Washed platelets were stimulated with 0.5μg/ml CRP-XL, the releasate isolated and separated into protein < and > 10kDa. Protein samples were prepared and protein content analysed using either a SYNAPT G2-Si HD MS or a Q-Exactive MS. The Venn diagrams compare the number of proteins <10kDa identified between the 2 machines after 1 wash A) and 3 washes B). C) and D) compare the number of proteins identified by each machine with 1 and 3 washes.

Enough protein was recovered from this preparation to run a MS analysis on proteins <10kDa. Results indicated a high proportion of keratin in samples analysed on both machines along with serum albumin and other proteins, all above 10kDa (Table 5.8). As proteins <10kDa could not be identified in the <10kDa fraction, it was felt this fractionation step was unnecessary for subsequent MS experiments.

Table 5.8: Proteins identified in the <10kDa protein fraction

Proteins identified in the <10kDa fraction	MW (kDa)
Keratin, type I cytoskeletal 10	59
Keratin, type II cytoskeletal 1	66
Keratin, type I cytoskeletal 9	62
Keratin, type II cytoskeletal 5	62
Serum albumin	69
Hemoglobin subunit beta	16
Keratin, type I cytoskeletal 14	52
Putative ankyrin repeat protein B	71

From this analysis, all future MS experiments would use the releasate from platelets that had been washed 3 times, without fractionation into proteins on the basis of MW. It was also decided to carry out all analysis on the Thermo Fisher Q-Exactive MS machine as this allows more protein to be loaded and subsequently more proteins to be identified.

5.3.2 Identification of proteins released from platelets by LC-MS/MS

To identify candidate proteins released from platelets that may up-regulate monocyte *procr* gene expression, PRP was isolated from 4 donors. Platelets were washed 3 times in HBS pH 6.0 before resuspension in HBS pH 7.4, activation with 0.5µg/ml CRP-XL and the releasate isolated and proteins prepared for MS as in 2.16.

After data analysis there were 479, 460, 523 and 524 proteins identified by MS in samples from donors 1-4 respectively. Of these, 386 were common to all 4 donors whilst a small percentage of low abundance proteins were found in individual samples (figure 5.10), most likely due to miss-identification or labelling as different isoforms.

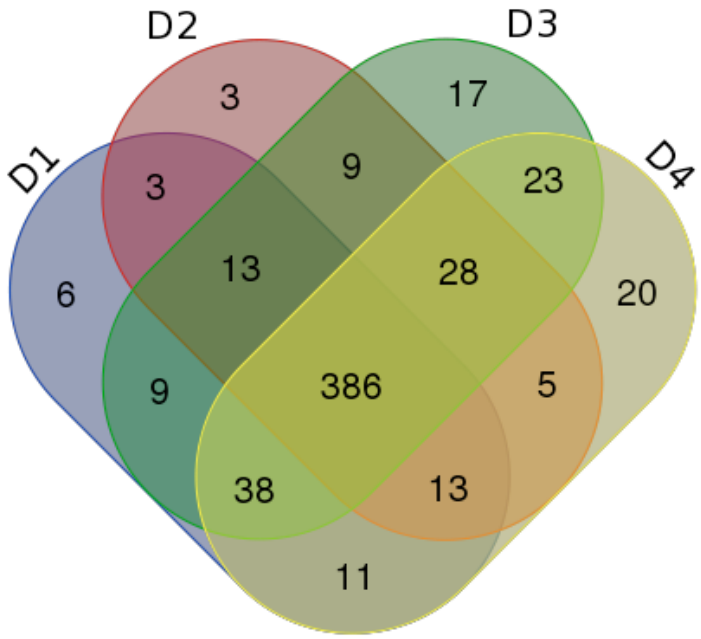

Figure 5.10: Venn diagram of proteins identified in 4 donors by LC-MS/MS

Platelets, washed 3 times in HBS pH6.0, were activated with 0.5µg/ml CRP-XL and the releasate isolated by centrifugation. After digestion with trypsin and concentration the peptides were analysed and assigned to proteins using a Q-Exactive MS and Proteome discoverer 4. Identified proteins from 4 donors were used to create a Venn diagram.

Gene ontology using Panther (P. D. Thomas et al., 2006) (http://pantherdb.org) was able to group the core proteins based on molecular function and biological processes. Proteins were assigned to 9 groups based on molecular function, with the 2 largest groups being catalytic activity (34%) and binding (28.9%). Sub-dividing the catalytic activity group further showed the majority (37.7%) of these were hydrolase associated proteins and included complement proteins, coagulation inhibitors and phosphatases. Sub-dividing the binding proteins further indicated 65.7% belonged to the protein-binding group with 54.1% involved in receptor binding including complement proteins, chemokines and fibrinogen (figure 5.11a). A total of 13 biological processes groups were identified. Here, the 2 largest were metabolic (21.9%) and cellular (19.7%) processes. Metabolic processes were further divided into 8 groups with the most prominent being primary metabolic processes (73.5%) and included a number of proteases, growth factors and protein modifying enzymes. Cellular processes were sub-divided into 7 groups with the predominant being cell communication (46.4%), following the common theme of containing chemokines, growth factors and signalling molecules (figure 5.11b).

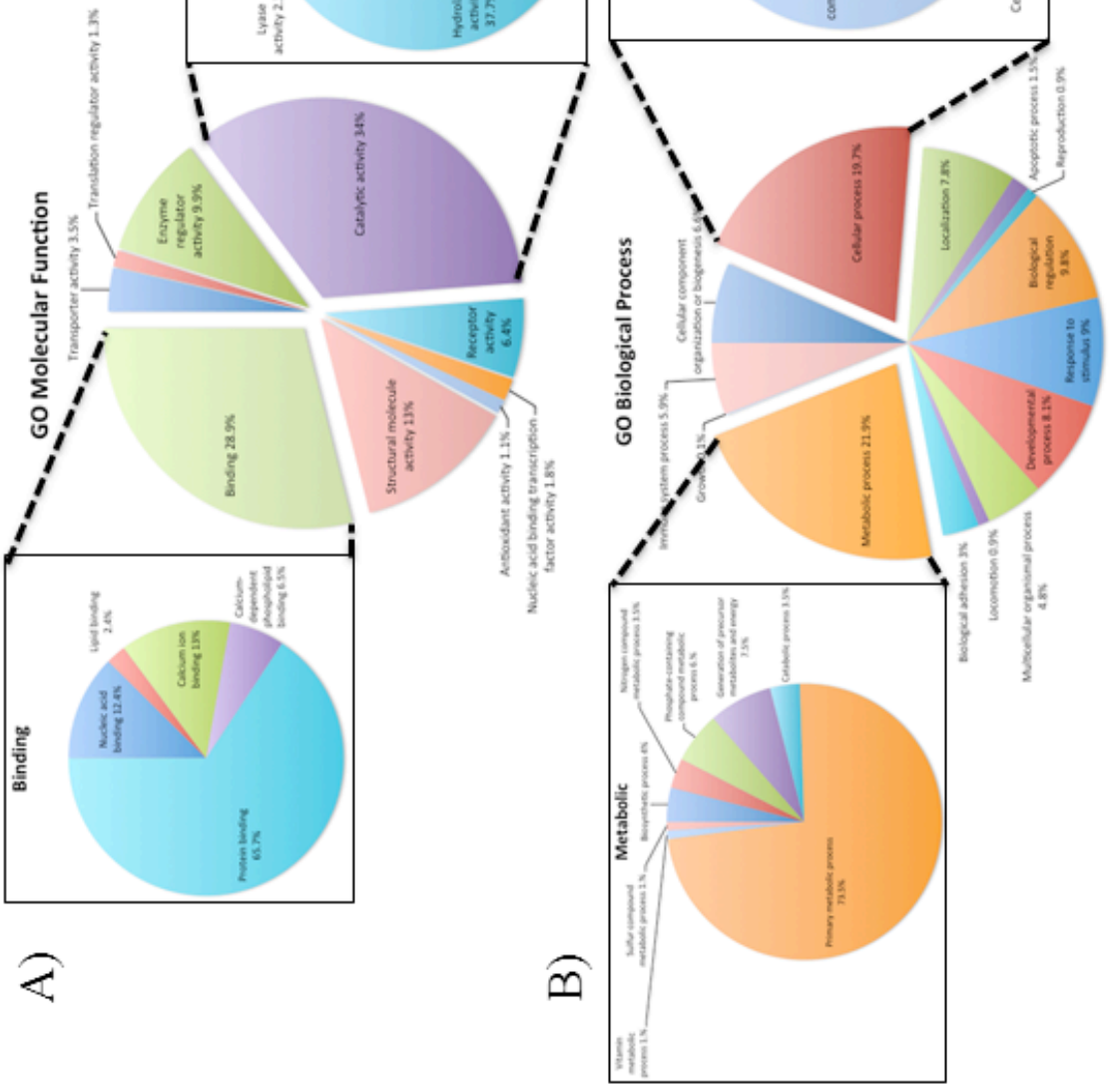

Figure 5.11: Gene ontology analysis of core proteins
Accession numbers from the core set of 386 proteins were inserted into the Panther program (Thomas et al., 2006) and gene ontology graphs for molecular function A) and biological process B) created.

A large number of proteins identified were >10kDa that could act either alone or in combination to switch on monocyte *procr* gene expression. However, rather than try to test all of the identified proteins, which would have been both costly and time consuming, prior knowledge was used to select likely candidates. This was based on the results from section 3.3.4 that identified proteins >10kDa as being the predominant species regulating *procr* expression. However, for these experiments two types of filter were used; either 15ml or 2ml 10kDa MWCO. Separating the data on the basis of the type of filter showed that a different expression pattern was seen (figure 5.12). The 4 donors whose proteins were separated by the 15ml MWCO filters had a larger fold increase in *procr* gene expression with the <10kDa proteins and a smaller (but significant) increase with the >10kDa proteins. When the 2ml MWCO filters were used there was no increase in *procr* gene expression in any of the 5 donors with the <10kDa proteins, but there was a large increase with the >10kDa proteins.

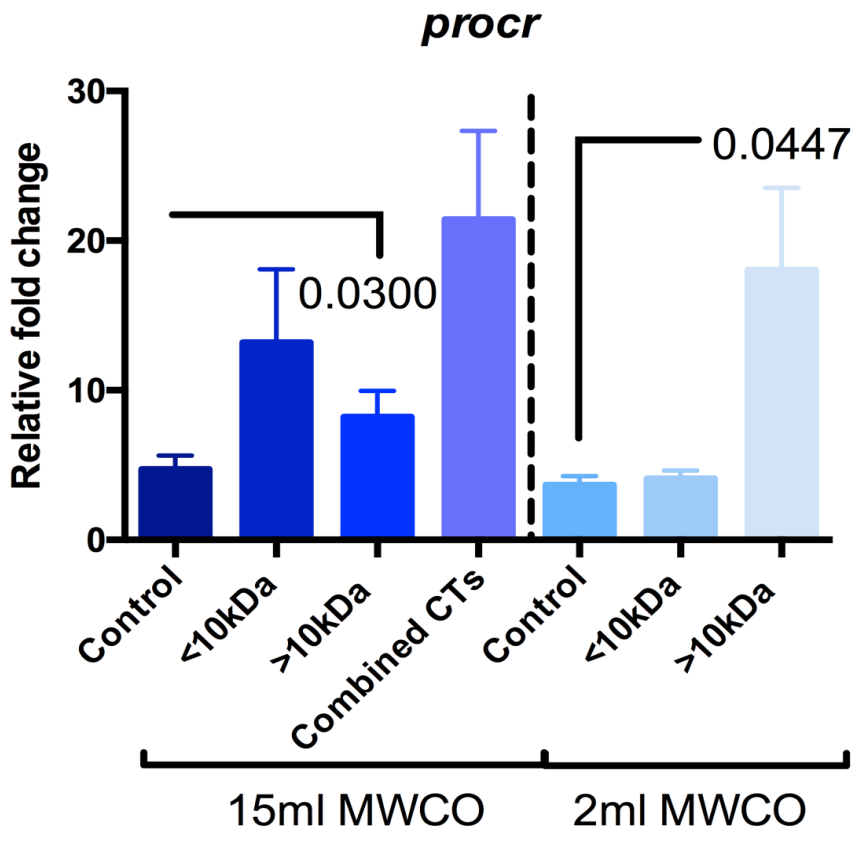

Figure 5.12: Comparison of monocyte procr expression using 15ml and 2ml MWCO filters

Autologous monocytes were reconstituted with platelet-derived proteins >10kDa and incubated for 6h at 37°C. RNA was extracted and procr gene expression calculated relative to actin using RT-qPCR. Results were plotted based in volume of separation filter and represent the mean±SEM. P-values calculated using Student's paired t-test (=<0.05).*

This data suggested the protein was ~10kDa, and that the larger filter may be more permeable to proteins that were slightly greater than 10kDa. Using an artificial cut-off of 15kDa it was now possible to reduce the large number of identified proteins to only 21 that were and present in 3 of the 4 samples (table 5.9).

Table 5.9: Proteins identified by LC-MS/MS between 10 and 15kDa

Protein	MW (kDa)
Acyl-CoA-binding protein	10
C-C motif chemokine 5	10
SH3 domain-binding glutamic acid-rich-like protein 3	10
Ig lambda-2 chain C regions	11
Platelet factor 4	11
SH3 domain-binding glutamic acid-rich-like protein 2	12
Ig lambda chain V-III region LOI	12
Ig heavy chain V-III region TIL	12
Ig kappa chain V-I region Hau	12
Peptidyl-prolyl cis-trans isomerase FKBP1A	12
Ig kappa chain V-III region SIE	12
Thioredoxin	12
Ig kappa chain C region	12
Platelet factor 4 variant	12
Tubulin-specific chaperone A	13
SH3 domain-binding glutamic acid-rich-like protein	13
Ig heavy chain V-III region BRO	13
Myotrophin	13
Platelet basic protein	14
Hemoglobin subunit alpha	15
Profilin-1	15

GO biological process analysis of these 21 proteins identified 8 groups with even distribution in the pie chart. Three of these groups, biological regulation, cellular process and response to stimuli, were considered as likely groups to contain the proteins of interest (figure 5.13a). A total of 6 proteins (Acyl CoA binding protein (CoABP), CCL5, peptodyl prolyl isomerase (PPI), PF4, PF4varient (PF4v) and platelet basic protein (PBP)) were identified but only 3 of these (PF4, PF4v and PBP) were common to all 3 groups and all three were released in reasonable amounts (figure 5.13b).

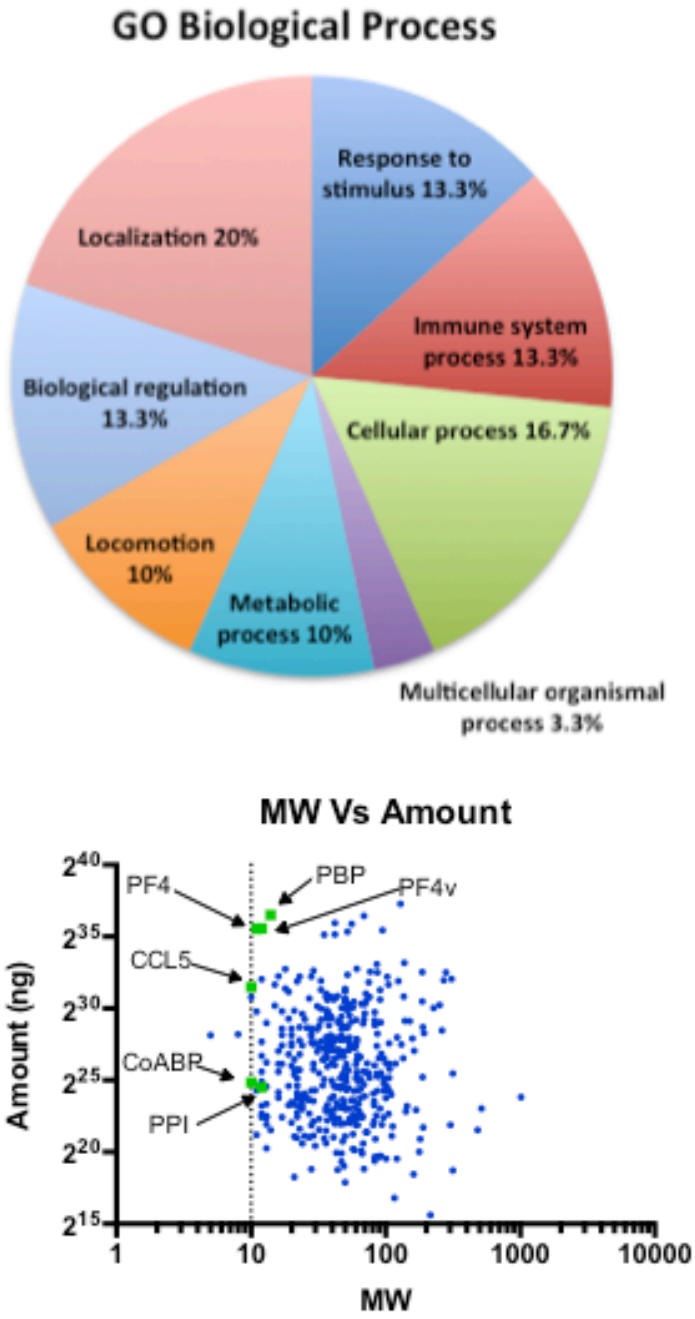

Figure 5.13: GO analysis of candidate proteins and MW vs amount of proteins identified by LC-MS/MS

A) The 21 candidate proteins accession numbers were imputed into Panther and a graph generated of biological process. B) Proteins identified by MS were plotted as MW vs. average amount and the 5 candidate proteins highlighted in green. PPI: peptidyl prolyl isomerase.

5.3.3 Is monocyte *procr* gene expression upregulated by platelet-derived PF4?

PF4 was selected above the two other candidates for a number of reasons: i) PF4 is ~11kDa and close the 10kDa cut-off described above, ii) it is present in large amounts in every sample analysed, iii) it has been shown to effect monocytes in a number of ways, including induction of differentiation into so called "m4" macrophage phenotype (Gleissner et al., 2010) and iv) aspirin has been shown to reduce the amount of PF4 released from platelets (Coppinger et al., 2007).

Monocytes do not express surface receptors for PF4 (Pervushina et al., 2004) and binding is thought to be through glycosaminoglycans (GAGs) on the surface, which meant blocking the function of PF4 through receptor antagonists would have been impossible. As an alternative, PF4 could be removed from the platelet releasate before incubation with monocytes. This was achieved using a method adapted from a recent patent (http://www.google.com/patents/US20100150892) that took advantage of the ability of PF4 to bind to heparin.

To determine if PF4 was responsible for monocyte *procr* gene expression, platelet releasate was prepared as previously described from $600x10^3$ washed platelets/µl, and autologous monocytes were isolated from the same donor using the pan monocyte isolation kit. The releasate was separated into 2 aliquots; one was treated with vehicle and the other was depleted of PF4 by incubation with heparin conjugated agarose (HA) beads (Sigma Aldrich) for 5min. The HA beads were pelleted by centrifugation at 13000rpm for 2min and the platelet releasate removed.

Incubations were set up as follows: 0h baseline, 6h autologous monocytes, 6h autologous monocytes with platelet releasate, 6h autologous monocytes with releasate incubated with HA-beads and 6h autologous monocytes with releasate incubated with HA-beads and human PF4. Total RNA was subsequently extracted and used for reverse transcription and RT-qPCR.

Control samples incubated with monocytes in media showed a ~30 fold increase in *procr* gene expression over baseline, however, this increased to ~60 fold when incubated with the platelet releasate (figure 5.14). When the platelet-derived releasate had been incubated with HA-beads prior to reconstitution with monocytes, expression was significantly reduced to levels similar to resting samples. hPF4, however, failed to rescue monocyte *procr* expression.

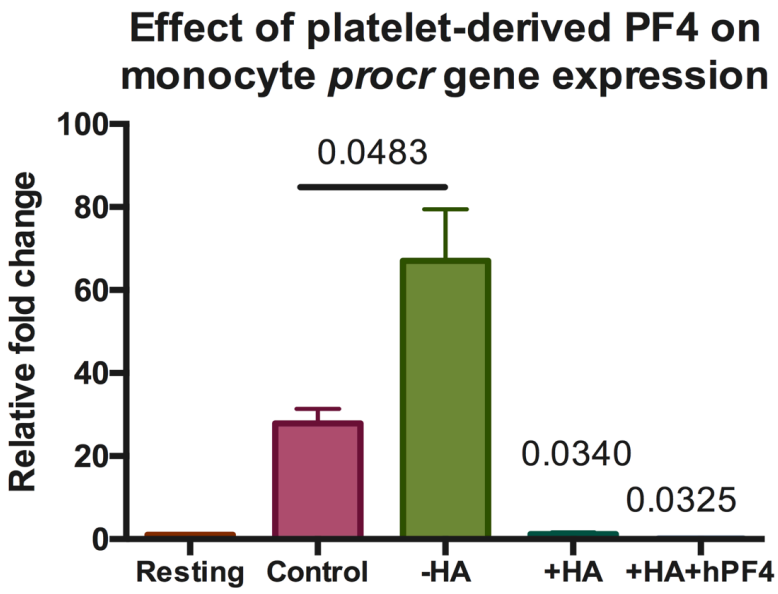

Figure 5.14: Effect of incubating platelet releasate with HA-beads on monocyte procr expression

Autologous monocytes were reconstituted with platelet-derived releasate that had been incubated with or without HA-beads to remove PF4. Incubations were at 37°C for 6h with gentle rotation. RNA was extracted using TRIzol and RT-qPCR carried for procr. P-values calculated using standard one-way Anova (p-values above the bars were calculated against –HA). Data show mean±SEM (n=3).

These results suggested that while incubation of the platelet releasate with HA-beads removed something that enhanced transcription of monocyte *procr,* the finding that hPF4 failed to rescue expression suggested this was not the active factor. However, the failure of hPF4 may have been due to it being out of date.

5.3.4 Do HA-beads remove PF4 from the releasate of activated platelets?

The results described above suggested that HA-beads removed a protein responsible for *procr* expression from the releasate of activated platelets but this could not be rescued by hPF4. To determine if the HA-beads removed PF4, the level of PF4 in control and HA-incubated releasate was measured in 3 donors by western blotting.

After transfer to the PVDF membrane, total protein was stained with Ponceau reagent (figure 5.15). The lowest observable stained protein(s) represented proteins <25kDa. Although not quantitative, there was a clear reduction in one of these proteins after incubation with the HA-beads. Due to the size of both the gel and crosslinks, proteins less then 25kDa were not separated. No other major difference could be detected at other MWs.

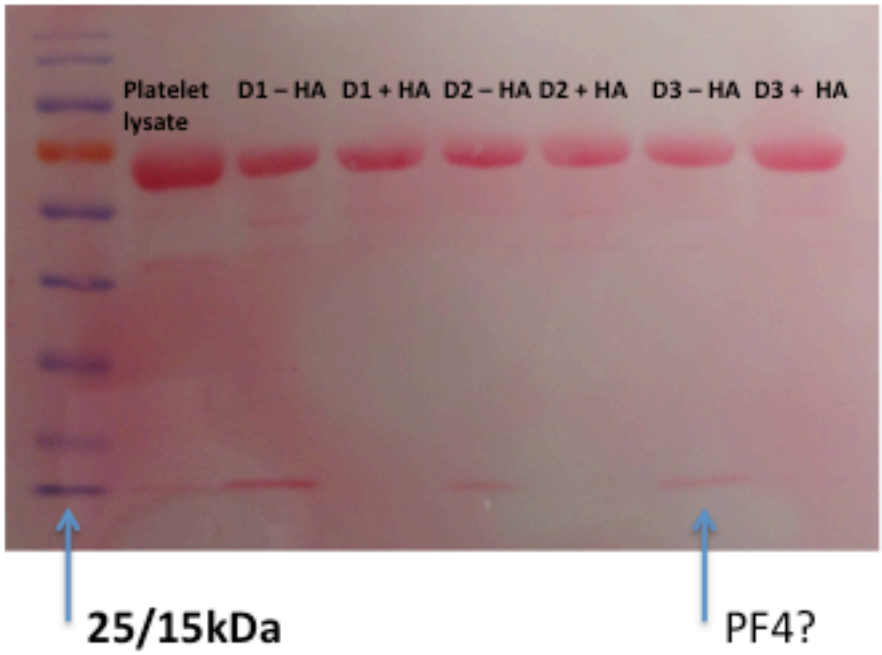

Figure 5.15: Ponceau stain of platelet releasate incubated with and without HA-beads

Washed platelets were prepared from 3 donors and activated with 0.5µg/ml CRP-XL. The releasate was isolated and incubated with or without HA-beads for 5min. The isolated releasate proteins were subjected to western blotting and the PVDF membrane stained with Ponceau reagent.

After removal of the Ponceau reagent the membrane was probed for PF4 (figure 5.16). Surprisingly, only a very small decrease in PF4 was observed in samples that had been incubated with HA-beads, suggesting the difference seen with the Ponceau reagent was due to the removal of a different protein.

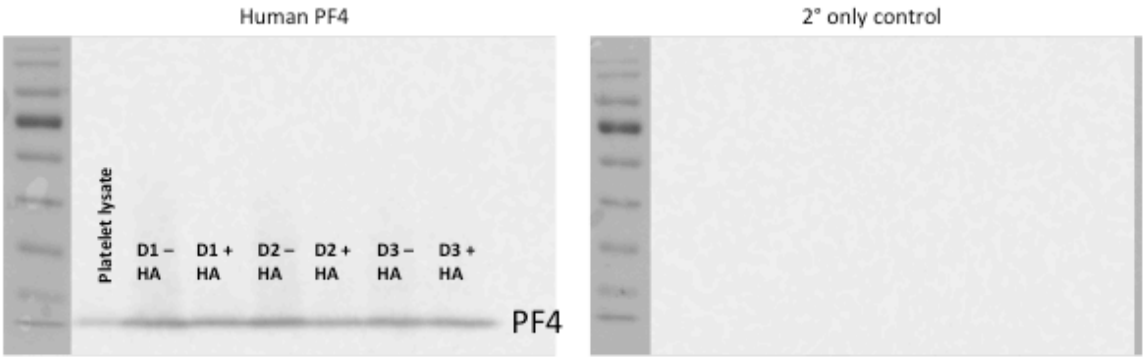

Figure 5.16: Western blot for PF4 in platelet releasate incubated with and without HA-beads

Washed platelets were prepared from 3 donors and activated with 0.5µg/ml CRP-XL. The releasate was isolated and incubated with or without HA-beads for 5min. The isolated releasate proteins were subjected to western blotting for PF4.

5.3.5 Identification of proteins removed from platelet releasates by HA-beads by LC-MS/MS

As these results suggested platelet-derived PF4 is not responsible for monocyte *procr* expression, the platelet releasates from two donors that had been incubated with and without the HA-beads were analysed by MS to identify differences in the amount of proteins.

A total of 443 proteins were identified in samples with 361 proteins common between both control and HA incubated samples (figure 5.17).

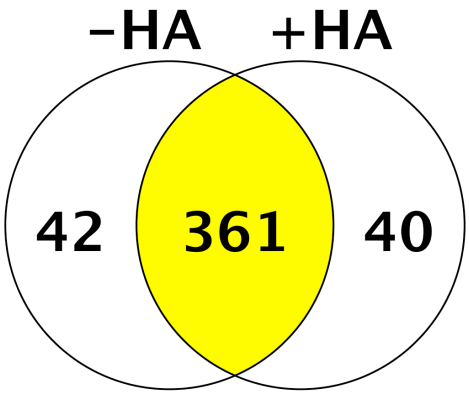

Figure 5.17: Number of proteins identified in platelet releasates incubated with or without HA-beads
Platelets were washed 3 times in HBS pH 6.0, activated with 0.5µg/ml CRP-XL and the releasate isolated. After incubation with or without HA-beads, proteins were trypsinised and concentrated ready for separation and detection using a Q-Exactive MS.

There were 42 proteins identified in the control samples that were not identified in the releasate that had been incubated with HA-beads and 40 identified in the samples incubated with HA-beads that were absent in the controls. Although the samples were matched, the apparent gain of 40 proteins after incubation probably does not reflect real results and is due to either sample contamination or identification of protein isoforms.

Absolute amounts (ng) were quantified and the control samples ranked from 1-443 with 1 being the lowest and 443 the highest amount. The average amount for the untreated samples was plotted against rank to produce a curve (figure 5.18a). By plotting the amount calculated in the samples incubated with HA-beads on the same graph, the variation could be seen between the two sets of data. As expected, this was mostly towards the low concentrations and was most likely background. There was a strong correlation between the treated and untreated samples (figure 5.18b).

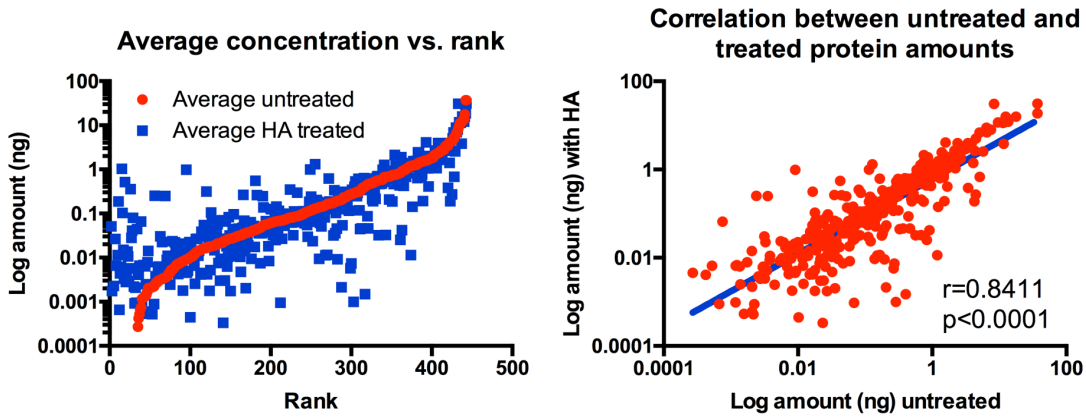

Figure 5.18: Variation and correlation between samples incubated with HA-beads and control

A) Proteins were ranked from 1-443 based on amount (ng) and plotted against log of the amount to produce curve. The amount of protein in samples incubated with HA-beads was plotted onto the graph to show the variation between samples. B) The amount of each protein in the control samples was plotted against samples incubated with HA-beads and the correlation measured using a correlation test. Amounts are an average of 2 donors.

Significant differences between the two datasets were calculated using a t-test. There was no significant change between 416 of the proteins. Of the remaining 27 proteins, 17 were significantly higher in the control compared to samples incubated with HA-beads (table 5.10). The fold changes and p-values for all the proteins can be seen from the volcano plot (figure 5.19).

Table 5.10: Proteins significantly different between platelet releasates incubated with and without HA-beads

Higher in releasates incubated without HA-beads	
Identified Proteins	**Molecular Weight**
Integrin-linked protein kinase	51 kDa
C4b-binding protein alpha chain	67 kDa
Zinc finger protein basonuclin-2	122 kDa
C-C motif chemokine 5	10 kDa
Endoplasmin	92 kDa
Alpha-mannosidase 2	131 kDa
Isoform 2 of Glia-derived nexin	44 kDa
Amyloid-like protein 2	87 kDa
Ras suppressor protein 1	32 kDa
Isoform Smooth muscle of Myosin light polypeptide 6	17 kDa
Mesencephalic astrocyte-derived neurotrophic factor	21 kDa
Complement C2	83 kDa
Moesin	68 kDa
LIM and senescent cell antigen-like-containing domain protein 1	37 kDa
IQ and AAA domain-containing protein 1	95 kDa
Isoform 7 of Nesprin-1	643 kDa
Apolipoprotein C-I	9 kDa
Higher in releasates incubated with HA-beads	
Identified Proteins	**Molecular Weight**
Rho GDP-dissociation inhibitor 1	23 kDa
Transmembrane protein 40	25 kDa
14-3-3 protein beta/alpha	28 kDa
14-3-3 protein theta	28 kDa
Fibulin-1	77 kDa
Complement component C7	94 kDa
Ig kappa chain V-II region TEW	12 kDa
Isoform 2 of Nesprin-1	380 kDa
Plectin	532 kDa
Alpha-1B-glycoprotein	54 kDa

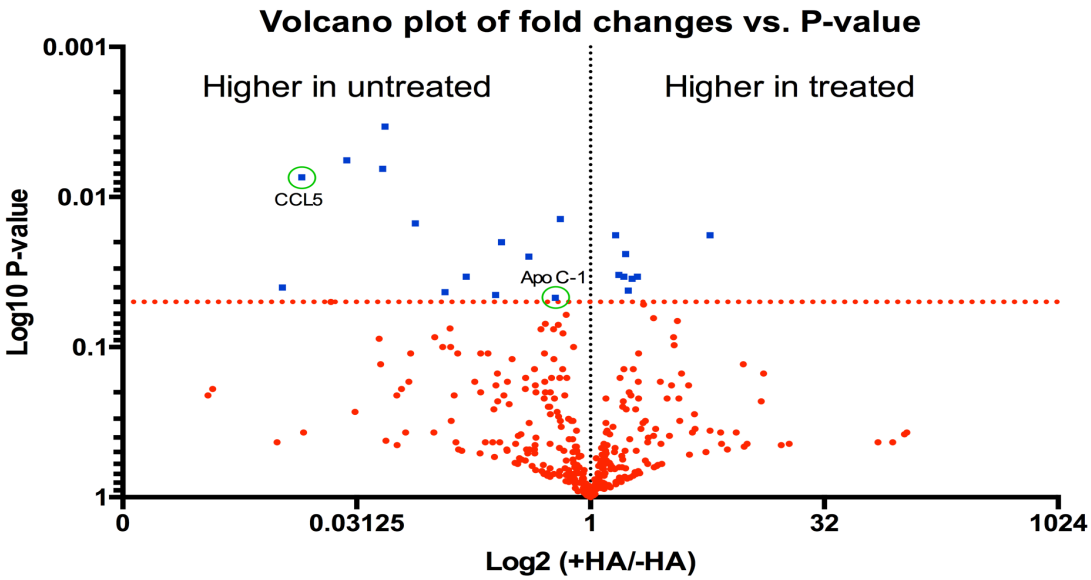

Figure 5.19: Volcano plot comparing fold change vs. p-value between proteins identified in control and after incubation with HA-beads

Proteins identified in the control and HA-incubated samples were quantified and p-values calculated using a t-test. Fold changes were calculated (+HA/-HA) and plotted against the p-value to create a volcano plot.

The proteins significantly higher in the untreated samples were identified on the amount vs. rank graph (figure 5.20) to determine if they were likely to have resulted due to background. All 17 fell within the linear region, suggesting the differences were true positives and are likely to be present at a concentration able to mediate biological processes.

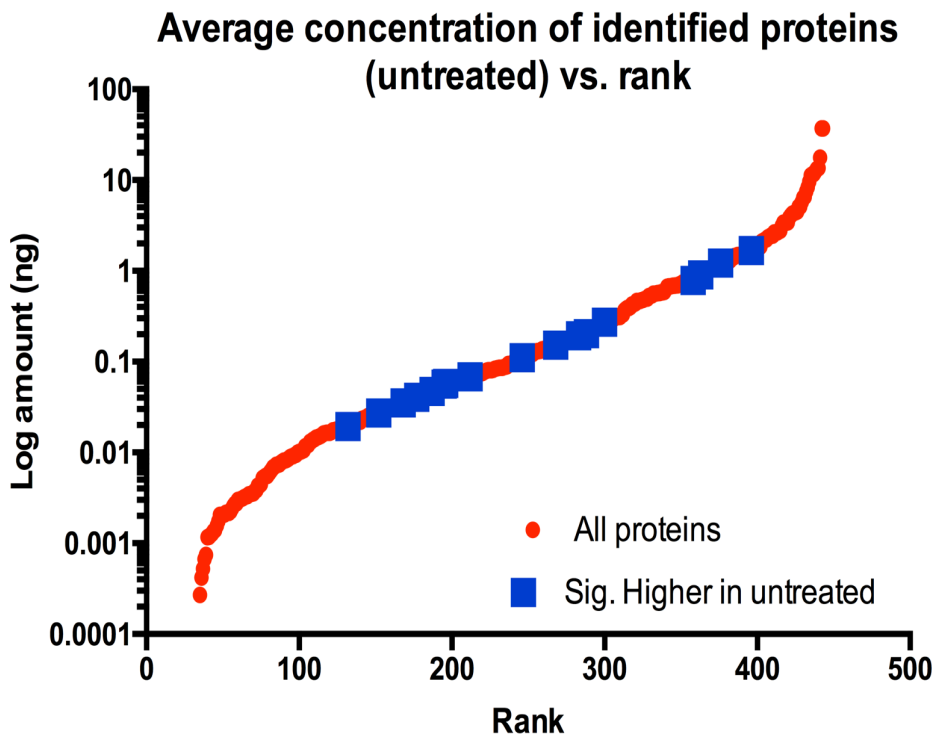

Figure 5.20: Average amount (ng) of proteins in control samples vs. rank

Proteins were ranked from 1-443 based on amount (ng) and plotted against log of the amount to produce curve. The 17 proteins identified as being significantly higher in the control compared to HA-incubated samples are highlighted blue.

The results from the LC-MS/MS confirmed previous findings that PF4 was not removed by the HA-beads (p=0.54). However, using the same criteria as before, the proteins that were significantly lower in the releasate incubated with HA-beads compared to without were inspected for proteins of ~10kDa MW. Of the 17 significantly lower in the samples incubated with HA-beads, 2 proteins were found to be ~10kDa, Apolipoprotein C-1 (p=0.047) and CCL5 (p=0.0074) (figure 5.21).

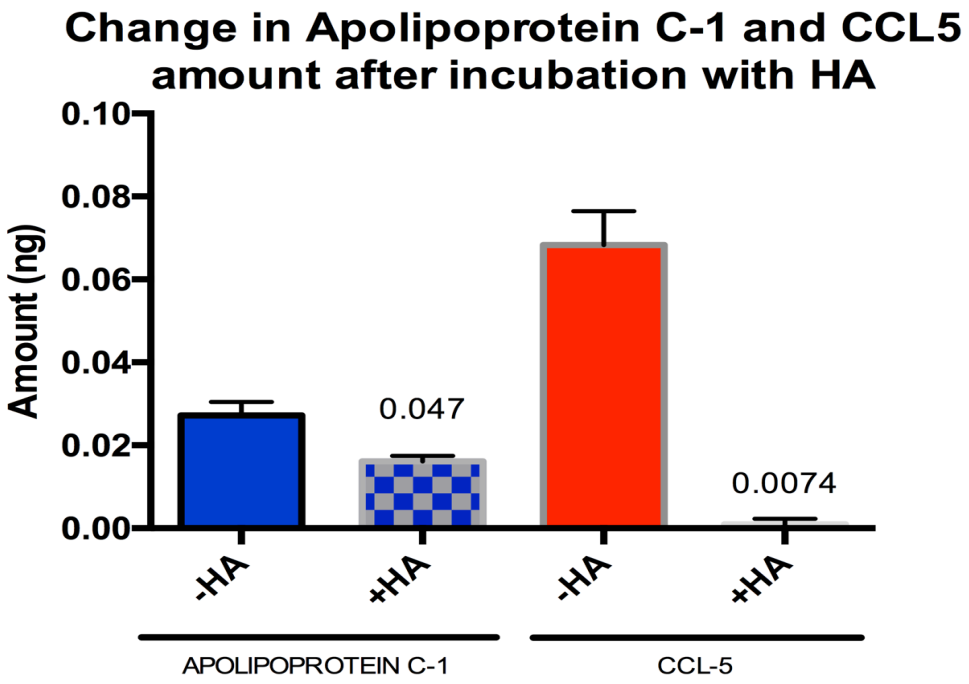

Figure 5.21: Amount of Apolipoprotein C-1 and CCL5 in control and samples incubated with HA-beads

Proteins were identified in HA-incubated and control platelet releasates by LS-MS/MS and quantified. Apolipoprotein C-1 and CCL5 were identified has being significantly reduced in treated samples. P-values calculated using standard paired t-test. Data show mean±SD; n=2.

As CCL5 was almost completely removed by HA-beads and apolipoprotein C-1 was only slightly reduced, combined with the fact that CCL5, is known to exert effects on monocytes, it is likely that this molecule is responsible for monocyte *procr* expression. However, due to time constraints no further work to confirm this could be carried out, although it is something that could be followed up in future studies.

5.4 Discussion

This chapter aimed to build on the results presented in chapter 3, further elucidating the mechanism(s) by which platelets regulate the expression of *tfpi* and *procr* in monocytes. To recap, monocyte *tfpi* expression was shown to be upregulated late in response to activation, not be dependent on monocyte platelet aggregate formation or MPs, induced by oxylipins released from platelets and reduced when either COX-1 or 12-LOX were inhibited. Monocyte *procr* expression was identical to that found for *tfpi* but its expression was induced by soluble proteins released from platelets. Using MS and RT-qPCR approaches, the main conclusions from this chapter are as follows:

I. GPVI-activated platelets release 10 oxylipins into the medium

II. Aspirin reduces release of 11- and 15-HETE, 9- and 13-HODE, TxB2 and PGD/E2
III. Esculetin and baicalein reduce the release of all measured metabolites with the exception of AA and possibly 9-HETE
IV. An additional 11 oxylipins were identified in plasma but these were unaffected by 12-LOX inhibitors suggesting extra-platelet sources
V. The effect of the COX-1 and 12-LOX inhibitors was not due to inhibition of platelet aggregation / signalling through GPIIbIIIa
VI. PPARγ agonists are able to upregulate *tfpi* and potentiate expression when co-incubated with CRP-XL, although inhibition was not seen with antagonists
VII. A number of proteins are released from CRP-XL-activated platelets that could regulate *procr* expression
VIII. The protein was thought to be ~10kDa and PF4 was identified as a likely candidate due to known effects in monocytes
IX. HA-beads were predicted to remove PF4 and a protein was removed between 10-25kDa but this was not PF4, and even though incubation with HA-beads did prevent *procr* expression, hPF4 could not rescue expression
X. LC-MS/MS measurement of releasates incubated with HA-beads identified CCL5 (RANTES) as a potential mediator of *procr* expression

The next few paragraphs will discuss the results beginning with the identification of oxylipins by MS. AA and LA can be metabolised by a number of enzymes belonging to COX, LOX and cytochrome pathways and currently a number of these have been identified as released from platelets, albeit using supra-physiological AA and LA concentrations (figure 5.22 green boxes). These results present the first evidence platelets are capable of metabolising endogenous AA and LA released upon activation to at least 7 other oxylipins in addition to TxA2 and 12-HETE. It is also the first to identify the contributions of COX-1 and 12-LOX to production of these and show it is not due to the inhibition of platelet aggregation / GPIIbIIIa signalling.

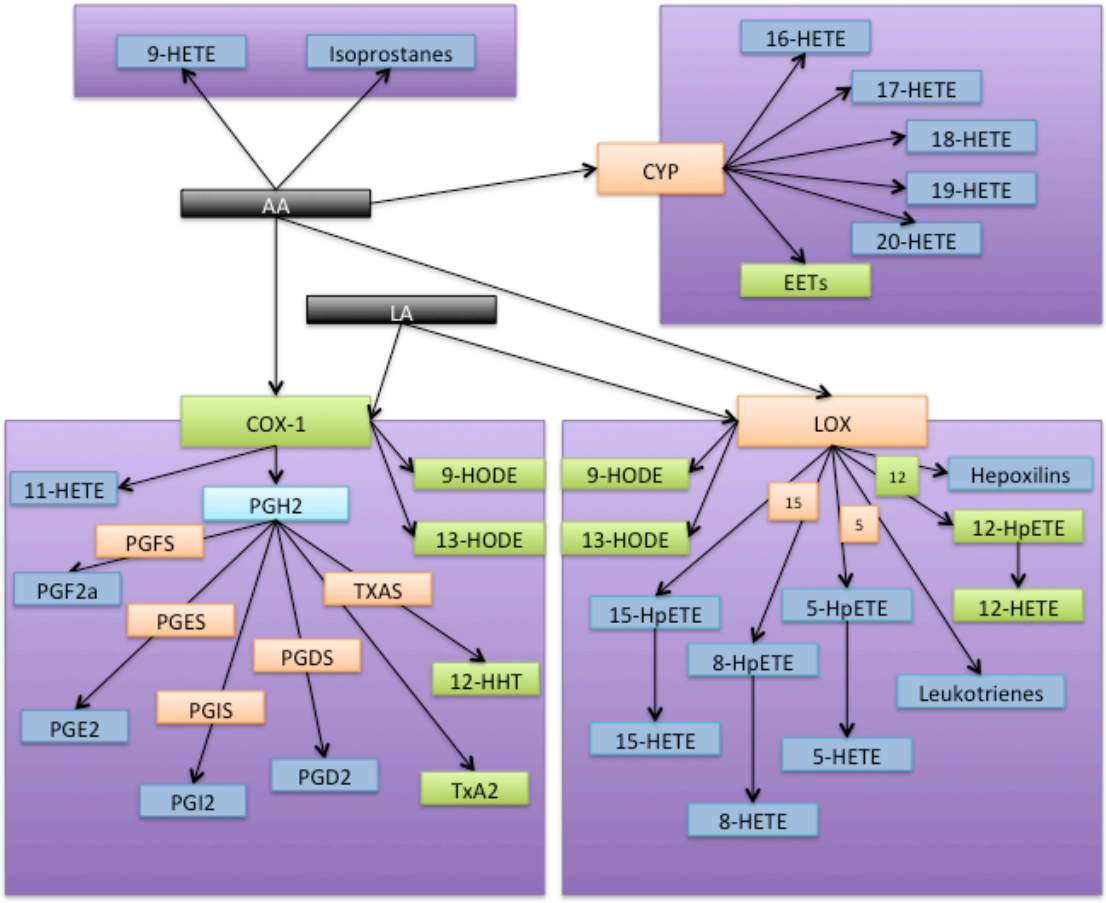

Figure 5.22: AA and LA metabolic pathways

Summary of metabolic pathway of AA and LA metabolism in man. Enzymes and products in green boxes are those currently identified in platelets.

Activating platelets through the GPVI collagen receptor has lead to observations that differ from a number of previously described results; the majority measuring oxylipins produced from exogenous oxylipin sources. For example, Daret et al added exogenous LA to washed platelets and observed its conversion to 9- and 13-HODE at the same rate as the production of 12-HETE and at the ratio of 1:5.66 (9- : 13-HODE) (Daret et al., 1989). Our results demonstrate that from endogenous sources of LA and AA, 9-HODE is 75 times and 13-HODE 114.5 times lower than 12-HETE and at a ratio of 1.5:1 (9-: 13-HODE). This study, however, was the first to identify the production of 9- and 13-HODE from both COX-1 and 12-LOX, which is supported by the findings here with the addition that 9-HODE is preferentially synthesised by COX-1 whereas 13-HODE is through 12-LOX.

Similarly, a recent paper from Jarrar et al reported the identification of 17 AA metabolites, a number of which are different from those identified here, including 5-, 8-, 9-, 11-, 12-, 15- and 20-HETE; 8,9-, 11,12- and 14,15-EET; 8,9-, 11,12- and

14,15-dihydroxyeicosatrienoic acid (DHET); leukotriene B4; 5,6-lipoxin A4; PGF2a; TxB_2 from addition of exogenous AA and nicotinamide adenine dinucleotide phosphate (NADPH) (Jarrar et al., 2013). Our study failed to identify any EET's or DHET's produced from endogenous AA and NADPH and may result from high concentrations of AA; since DHET's are formed through the hydrolysis of EET's by soluble epoxide hydrolase, which are at very low levels in platelets (Seidegård et al., 1984).

The identification of 12-HETE, TxB_2, AA and LA is not surprising and agrees with the large volume of research already carried out on platelet activation. The release of 11- and 15-HETE from human platelets, to our knowledge, has not been shown before, although production through COX-1 has been demonstrated in cultured rat aortic SMCs (BAILEY et al., 1983); an observation backed up by reduced formation of both 11- and 15-HETE with aspirin. Unfortunately, due to PGD_2 and PGE_2 being stereoisomers identification of each individual species was not achieved, however it is likely to be PGE_2 as only PGE synthase has been detected in platelet extracts by LC-MS/MS (Burkhart et al., 2012). 8-HETE has been shown to be produced by cytochrome P450 enzymes (CAPDEVILA et al., 1986), but as formation was inhibited with baicalein and esculetin but not aspirin it is likely 8-HETE is formed through 12-LOX activity in platelets. The 9-HETE product is formed through non-enzymatic conversion of AA (Guido et al., 1993) and formation is likely to be donor dependent and may account for the variability in detection seen here.

Inhibiting platelets with aspirin resulted in the significant decrease of several oxylipins that could play roles in a number of pathological processes. The most beneficial effect is seen with TxB_2 and the occurrence of secondary MI; providing a 25% reduction in all cause mortality (Antithrombotic Trialists' (ATT) Collaboration et al., 2009). Whilst this is desired it does not rule out the possibility that inhibiting platelets with aspirin is preventing other oxylipins having affects elsewhere. For example, 11-HETE has been shown to be chemotactic to neutrophils and eosinophil's and may play an important role in inflammation (Goetzl and Pickett, 1980). 15-HETE has been associated with a role in inhibiting 12-LOX and could act as an endogenous regulator of 12-HETE production (Fleteher-Cieutat et al., 1985). Preventing 15-HETE formation may therefore lead to increased 12-HETE, which has been associated with pro-thrombotic effects; although 15-HETE itself has been associated with unstable plaques, and inhibiting its production may result in a more stable plaque phenotype (Mallat et al., 1999). The decrease in 13-HODE could also be disadvantageous as it has been shown to sequester the

endothelial vitronectin receptor at the basolateral membrane, but upon damage it can dissociate and allow translocation of the receptor to the apical side where it binds vitronectin and promotes cell adhesion (Buchanan et al., 1998).

Although currently not thought to be clinically relevant, inhibition of 12-LOX with esculetin and baicalein gave interesting results. In these samples, Ca^{2+} was included as 12-LOX activity has been shown to be dependent on exogenous Ca^{2+} (Coffey et al., 2004b). As expected there was complete inhibition of 12-HETE. As mentioned earlier, the role of 12-HETE in platelet is conflicting and so further work is needed to elucidate its mode of action, if any. Interestingly, 12-HETE has recently been associated with cancer metastasis, cell adhesion and inflammation (Porro et al., 2014) and so may become a target for future therapies. Similarly is 8-HETE, which has been associated with a number of different cancers but without a clear role (Attar et al., 1985; Kim et al., 2005). Inhibition of 12-LOX significantly reduced the same oxylipins as aspirin and as such would have the same consequences. This could be due to off-target effects; baicalein has been shown to inhibit TxA2 synthase (Yeung et al., 2012) and esculetin NF-kB translocation (Hong et al., 2014) and HiF-prolyl isomerase (Yum et al., 2015). In future a more specific inhibitor should be used such as NCTT-956 (Luci et al., 2010).

To verify the effects seen with COX-1 and 12-LOX inhibition were not due to the inhibition of outside in signalling through GPIIbIIIa, which is needed for ADP induced TxA2 production (Jin et al., 2002), fibrinogen binding to GPIIbIIIa was prevented using the monoclonal antibody RFGP56. Our results indicated that inhibiting the aggregation of platelets in buffer or plasma had no effect on oxylipin production and did in fact have a tendency to increase the amount secreted. There were large decreases seen in the production of 9- and 13-oxoODE in plasma, which may suggest outside in signalling and/or aggregation is affecting for the oxidation of 9- and 13-HODE respectively.

The identification of these oxylipins and the effect of COX-1 and 12-LOX inhibitors related well to the initial hypothesis that PPARγ may regulate *tfpi* expression. A number of the identified oxylipins have been shown to activate PPARγ including 9- and 13-HODE (Itoh et al., 2008), 12-HETE and 15-HETE (Nagy et al., 1998). The differential effect of the COX-1 and 12-LOX inhibitors also correlates well with the RT-qPCR data and with current literature describing PPARγ as a general lipid sensor as opposed to having a specific ligand.

To determine whether PPARγ is able to regulate monocyte *tfpi* expression, whole blood was incubated with two agonists and antagonists of PPARγ in combination with CRP-XL. In the absence of platelet activation, 15d-PGJ2 increased monocyte *tfpi* expression to a similar level as CRP-XL alone, although rosiglitazone did not have the same effect. This is probably due to a dose effect rather than 15d-PGJ2 activating platelets as PPARγ agonists have been shown to attenuate platelet activation (Moraes et al., 2010). The antagonists showed no change in expression compared to the control. Both PPARγ agonists greatly potentiated monocyte *tfpi* expression when co-incubated with CRP-XL, which is probably a consequence of an increase in monocyte PPARγ induced by platelet activation. Antagonists of PPARγ failed to inhibit *tfpi* expression in monocytes induced by activated platelets. This may be due to concentration and timing as evidenced when antagonists were co-incubated with CRP-XL and 15d-PGJ2. Both antagonists failed to inhibit *tfpi* expression in these samples compared to controls. This could be a result of the short half life of GW9662 (~2.2h in cells) compared to rosiglitazone (~54h in cells) (X. Li et al., 2011). T007 has been shown to inhibit rosiglitazone mediated PPARγ activation but can be reversed by RXRα ligands (Lee et al., 2002), an avenue of regulation not explored here. Alternatively, PPARγ may be able to increase *tfpi* expression after it itself has been induced by activated platelets and the increase seen initially is PPARγ independent (figure 5.23).

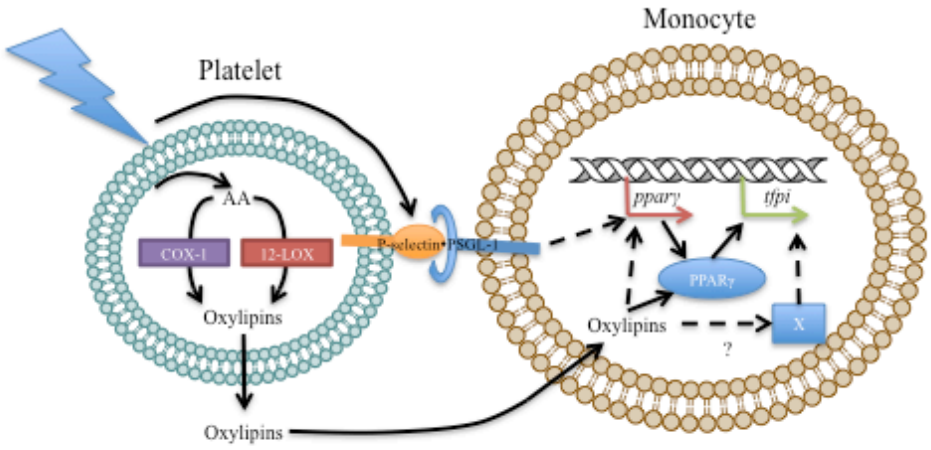

Figure 5.23: Potential mechanism of platelet-induced tfpi expression in monocytes

This could explain the difference between expression induced by rosiglitazone and 15d-PGJ2 without CRP-XL, as 15d-PGJ2 is known to affect other pathways independent of PPAR γ activation, such as the direct inhibition of NF-κB.

These results have not only provided novel findings on the oxylipins released from activated platelets and shown PPARγ agonists are able to increase *tfpi* expression in monocytes but also raised further questions regarding gene regulation. For example, why does 15d-PGJ2 increase *tfpi* expression but rosi does not in the absence of platelet activation? Is this due to PPARγ independent effects of 15d-PGJ2? This could be tested in one instance by inhibiting NF-kB in whole blood and measuring *tfpi* gene expression. Another question is whether the *tfpi* promoter contains PPARγ binding sites? Cloning the *tfpi* promoter upstream of the luciferase gene and carrying out transactivation assays with PPARγ would answer this.

As the results in chapter 3 had shown that soluble proteins released from platelets were important for the upregulation of monocyte *procr* expression, the first experiments used LC-MS/MS to identify the proteins present in the soluble material from GPVI-activated platelets. Over the last 9 years significant progress has been made in identifying the platelet proteome in terms of the whole proteome, secretome, sheddome and compartments. To 2012, there have been four studies specifically looking at the platelet secretome, three of these have used the PAR agonist thrombin or TRAP. The fourth study by Coppinger et al in 2007 used CRP-XL, TRAP and ADP with and without aspirin and identified 146 proteins. Interestingly, 2 of these proteins, PF4 and thrombospondin were found to be significantly reduced in the releasate from aspirin treated platelets (Coppinger et al., 2007; Zufferey et al., 2012). The results from this paper gave an indication of the molecules that could be responsible for *procr* expression, but with recent advances in MS, and the fact that other papers had reported over 300 proteins released from thrombin/TRAP stimulated platelets (Maynard et al., 2007; Piersma et al., 2009), it was decided to carry out our own MS analysis of CRP-XL stimulated proteins.

The releasate was run on 2 different machines and it was determined the Q-Exactive was superior to the Waters Synapt in terms of number of proteins detected. Next, a set of 4 donors platelet releasates were analysed for protein using the Q-Exactive MS. A core set of 386 proteins was identified as present in all 4 samples with a further 92 present in 3 of the 4 samples. Proteins detected in only 1 or 2 samples are likely to result from assignment of peptides to different protein isoforms. Unfortunately, comparison with the earlier landmark papers of Coppinger, Maynard and Piersma were not carried out due to the difficulty of converting the pre-2011 International protein identification (IPI) to the post-2011 Uniprot accession number. A comparison was made

to the recent Zufferey et al paper that identified 827 proteins (Zufferey et al., 2012). It was found only 70 of the proteins were common to both sets of data, however this is probably due to a large number of isoforms and specific protein chains that lead to alternative accession codes.

The large number of proteins identified would have made it impossible to narrow down potential regulators of *procr* expression. Fortunately, the observation that using different filters produced different *procr* expression profiles, with one showing expression with both less and more than 10kDa proteins and the other with just more than 10kDa, suggested the protein in question was likely to be ~10kDa. GO analysis of proteins between 10 and 15kDa based on biological process identified 8 groups, 3 of these, biological regulation, cellular process and response to stimulus were the most likely to contain a regulatory protein. Within all these groups appeared PF4, PF4v and PBP, which lead to selection of PF4, based on MW, abundance and known roles.

PF4 is a member of the chemokine family and can elicit a response by binding to the alternatively spliced form of CXCR3, CXCR3-B (Lasagni et al., 2003), however, monocytes do not express the CXCR3-B form on their surface (Pervushina et al., 2004). A well-known property of chemokines is their ability to bind to GAGs due to a cluster of positive amino acids at the c-terminal. PF4, however, has an additional cluster of basic residues that increase the affinity for GAGs 100-1000 fold (Witt and Lander, 1994). In addition to this PF4 is the only chemokine that has been shown to bind GAGs other than heparin and heparin sulphates in the form of chondroitin sulphates (Petersen et al., 1999). It is therefore possible that PF4 mediates its effects on monocytes by binding and eliciting signalling from GAGs. PF4 can induce monocyte survival, differentiation to macrophages (Scheuerer et al., 2000), production of reactive oxygen intermediates (Kasper et al., 2007), increases the release of TNFα and monocyte TF expression (Kasthuri et al., 2012) and activity in response to LPS (Engstad et al., 1995).

Unfortunately, as monocytes have no defined receptor for PF4 another approach was needed that would block the function of PF4. For this, HA beads were used as had been reported in the online patent to remove PF4 from platelet supernates. This is based on studies showing heparin is able to bind 2 molecules of PF4, and reflects its role in heparin induced thrombocytopenia (HIT) (Jordan et al., 1982), where auto-antibodies recognise the heparin-PF4 complex and mediate binding to the platelet FCyRIIa chain, promoting thrombosis (Kelton et al., 1994). Incubation of platelet releasates with HA-beads completely attenuated platelet-induced monocyte *procr* expression, however,

hPF4 was unable to rescue gene expression. This could have been for a number of reasons including i) some heparin is released from the beads and is able to bind the exogenously added PF4 (although heparin was not identified in the releasates by LC-MS/MS), ii) the hPF4 was past its expiry date, iii) the regulation was through another protein removed by the HA-beads or iv) the HA-beads were not removing PF4. The latter was the easiest to test by western blotting for PF4 and showed that the HA-beads removed only small amounts of PF4 from the platelet releasate. The Poncaeu reagent however, did show the reduction of a band between <25kDa. To identify whether the HA-beads removed any other proteins and to confirm limited removal of PF4, MS was carried out on platelet releasates incubated with and without HA-beads. This confirmed the reduction of a number of proteins. The complete reduction of CCL5/RANTES was considered the most likely in terms of *procr* regulation (figure 5.24).

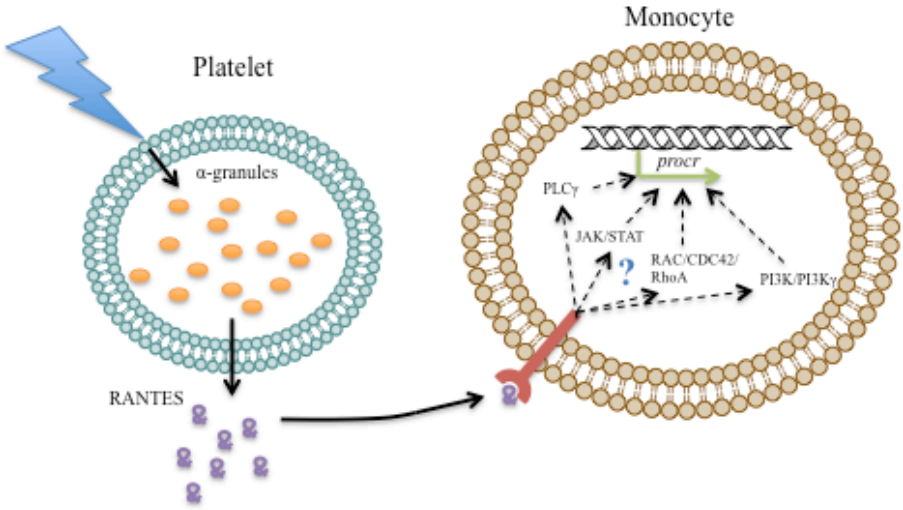

Figure 5.24: Potential mechanism of platelet-induced procr expression in monocytes

CCL5 was also present in the GO analysis of proteins 10-15kDa MW in the response to stimulus group refer to figure 5.13. CCL5 is a chemokine like PF4 but belonging to the C-C as opposed to C-X-C family. It is a 68 residue, 8kDa protein implicated in a number of biological roles (Appay and Rowland-Jones, 2001). CCL5 is derived mainly from T-lymphocytes and platelets and can bind to a number of receptors including CCR1, 3, 4 and 5, which are present on monocytes; although receptor levels may be dependent on the monocyte subset (C. Weber et al., 2000). In monocytes CCL5 is known to be chemotactic and promote arrest on endothelial cells. Studies have shown that CCL5 can be deposited on inflamed and damaged endothelium by platelets (Hundelshausen et al., 2001) and platelet-derived MPs (Schober et al., 2002) and act to

attract monocytes to these sites. Other roles of CCL5 in monocytes include release of granule enzymes and rapid and transient increase in calcium (Uguccioni et al., 1995). Some *in vitro* studies suggest high concentrations of CCL5, such as those found in thrombi and inflamed areas, may promote leukocyte activation, although whether this is relevant *in vivo* is unknown. Although the role of CCL5 in monocyte migration is well documented, its role in other monocyte functions is poorly researched. Whether or not platelet-derived CCL5 plays a role in monocyte anti-thrombotic gene expression remains to be seen.

Although these results have shown CCL5 and not PF4 is likely to be responsible for *procr* regulation in monocytes there are still a number of experiments required to confirm this. Firstly, although assumed, it has not been proven the effector molecule is protein in nature but could be confirmed by treating the protein releasate with proteinase K and incubating with autologous monocytes. If *procr* expression is attenuated then the molecule is protein. To complete this story, it is also necessary to confirm the molecule is CCL5, either by blocking the receptor using antagonists or by incubating whole blood and / or isolated monocytes with CCL5 and measuring *procr* expression.

In summary this chapter has identified novel oxylipins released from GPVI activated platelet and shown the effect of COX-1 inhibition on this release in washed platelets and 12-LOX inhibition in washed platelets and plasma. It has also shown that PPARγ agonists are able to potentiate the increase in *tfpi* expression observed with CRP-XL suggesting this as a regulatory pathway. Finally, this chapter has identified CCL5/RANTES as a likely candidate for regulating monocyte *procr* expression.

Chapter 6: Molecular and structural characterisation of 12- and 15-HETE as PPARγ agonists

6.1 Introduction

The previous three chapters focused on the regulation of anti-thrombotic genes in monocytes and the pathways involved in regulating transcription. From the previous chapter, PPARγ was identified as a transcription factor able to regulate monocyte *tfpi* gene transcription. This was evident from RT-qPCR data showing potentiation of platelet-induced monocyte *tfpi* expression by PPARγ agonists. In addition, LC-MS/MS analysis of platelet-derived oxylipins identified a number of potential PPARγ agonists released from activated platelets. A number of these, such as 9- and 13-HODE, have already been characterised as PPARγ agonists (Itoh et al., 2008). However, the 2 oxylipins of most interest, 12- and 15-HETE have only been partially characterised. Studies using 12-HETE have produced mixed reports, with some identifying it as a PPARγ agonist (Westergaard et al., 2003) and others showing no effect (Yu et al., 1995). While15-HETE has been shown to activate PPARγ (Nagy et al., 1998), neither of these molecules have been crystallised with PPARγ.

The aims of this chapter were to clarify whether 12- and 15-HETE increase PPARγ transcriptional activity and if they interact with PPARγ. This would be achieved using two approaches; a mammalian transactivation assay to assess the ability of 12/15-HETE to activate PPARγ, and to determine the crystal structures of PPARγ bound to 12/15-HETE.

6.2 Transactivation assays for PPARγ

6.2.1 Transactivation of PPARγ with known agonists

To determine the assay was working efficiently, the two known PPARγ agonist's, 15d-PGJ2 and rosiglitazone, were used to assess their ability to activate PPARγ. 15d-PGJ2 (0.05-1μM) produced a dose dependent increase in luciferase expression (figure 6.1a). Rosiglitazone (1-50μM) induced maximal luciferase expression at 1μM that decreased gradually with increasing concentration (figure 6.1b), unlikely to be due to the increasing DMSO concentration as this was only 0.2%. In both cases, the DMSO control was equal to the highest concentration in the experimental samples. These

results demonstrated the assay was working and able to measure PPARγ activation. 1μM 15d-PGJ2 was used as a positive control in all subsequent experiments.

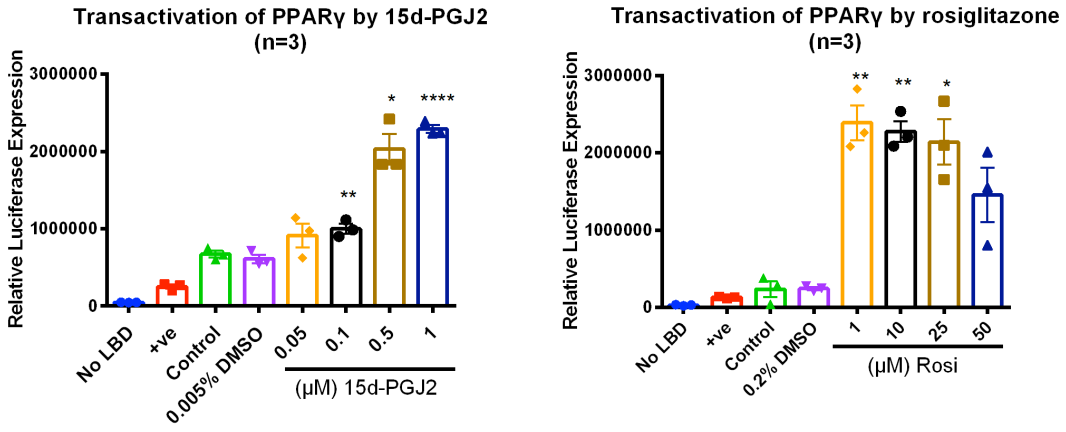

Figure 6.1: Activation of the PPARγ-LBD by 15d-PGJ2 and rosiglitazone

*293T cells were transfected with plasmids encoding β-galactosidase, TK-luciferase and the PPARγ-LBD/Gal4-DBD fusion protein before treatment for 24h with increasing concentrations of A) 15d-PGJ2 (0.05-1μM) and B) rosiglitazone (1-50μM). Statistical analysis was performed using a repeated measures ANOVA (*p<0.05, **p<0.01, ****p<0.0001). Data show mean±SEM; n=3.*

6.2.2 Transactivation of PPARγ with 12-HETE

293T cells were transfected with the β-gal, TK-Luc and PPARγ-LBD/Gal4-DBD plasmids and treated with 12-HETE (1-20μM) for 24h before cell lysis and measurement of β-gal and luciferase expression. The concentration of DMSO (2.2%) in the control was equal to the highest concentration of DMSO used for treatment with 12-HETE. This concentration had a marked effect on luciferase expression, probably due to cytotoxicity; therefore the decrease in luciferase activity seen with 12-HETE is most likely due to the toxic effects of the higher levels of DMSO (figure 6.2). For this reason, luciferase expression induced by 1 and 5μM 12-HETE was compared to the control without DMSO (control). There appeared to be a trend towards increae PPARγ activity with increasing 12-HETE concentration at 1 and 5μM although this did not reach significance. Due to the expense of 12-HETE, it was not practical to repeat the experiment with a normalised concentration of DMSO.

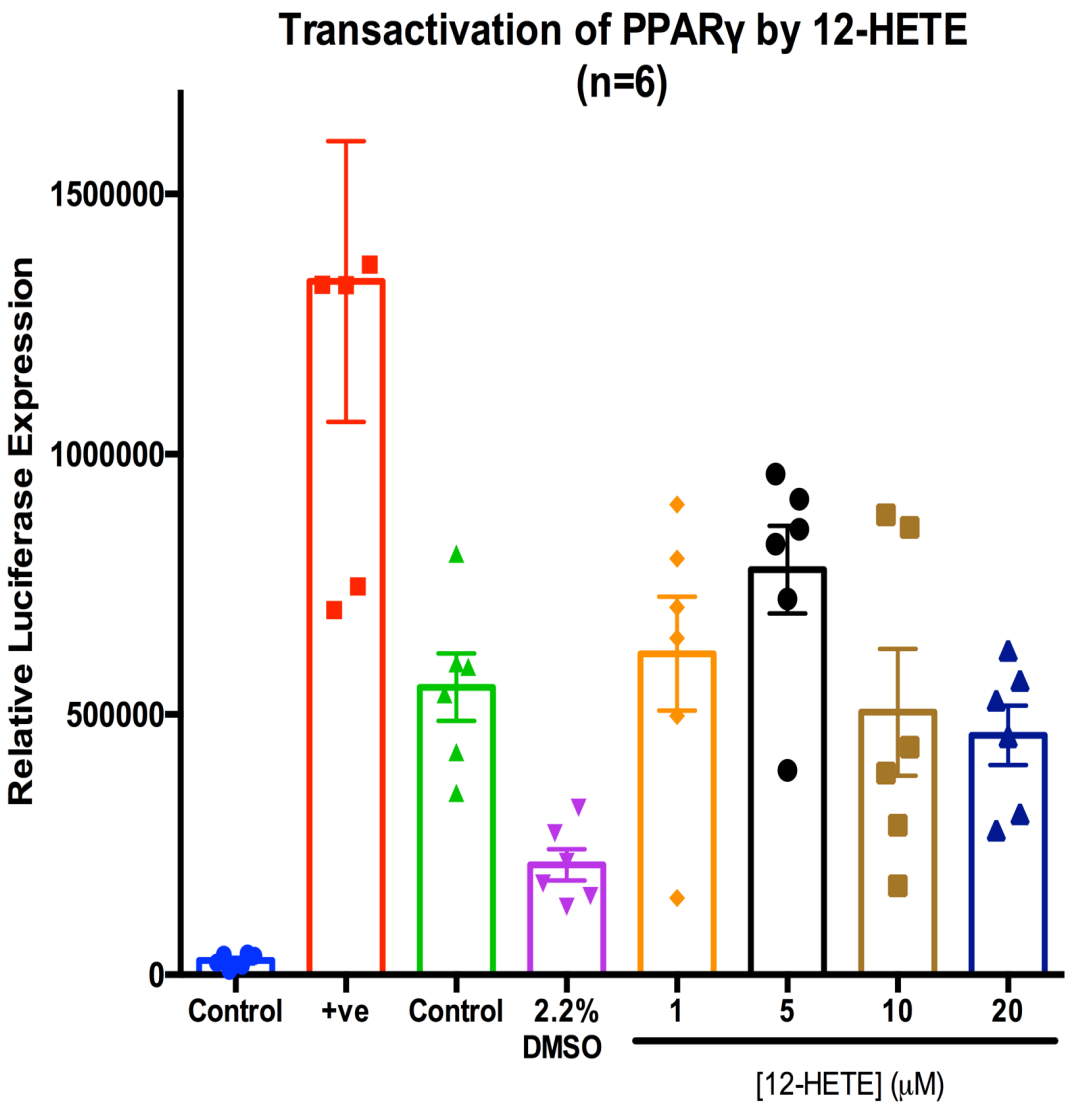

Figure 6.2: Activation of the PPARγ-LBD by 12-HETE

293T cells were transfected with plasmids encoding β-galactosidase, TK-luciferase and the PPARγ-LBD/Gal4-DBD fusion protein before treatment for 24h with increasing concentrations of 12-HETE (1-20μM). Statistical analysis was performed using a Friedman test . Data show mean±SEM; n=6.

6.2.3 Transactivation of PPARγ with 15-HETE

293T cells were transfected with the β-gal, TK-Luc and PPARγ-LBD/Gal4-DBD plasmids and incubated for 24h with 15-HETE (1-20μM) before cell lysis and measurement of β-gal and luciferase expression. For these experiments the 15-HETE was synthesised and kindly gifted by Toshimasa Itoh (University of Tokyo). Due to a high stock concentration of 15-HETE (100mM) in DMSO, dilutions were made using complete media and the concentration of DMSO (0.02%) was kept consistent in all

samples and did not affect luciferase expression when compared to untreated cells. 15-HETE produced a (almost) dose dependent increase in luciferase expression reaching a maximum at 20μM (figure 6.3). Concentrations of 1 and 5μM 15-HETE produced small increases in luciferase expression but were not significant. At 10μM, luciferase expression induced by 15-HETE was comparable to that induced by 15d-PGJ2 but was not significant and this increased further with 20μM (p=<0.01).

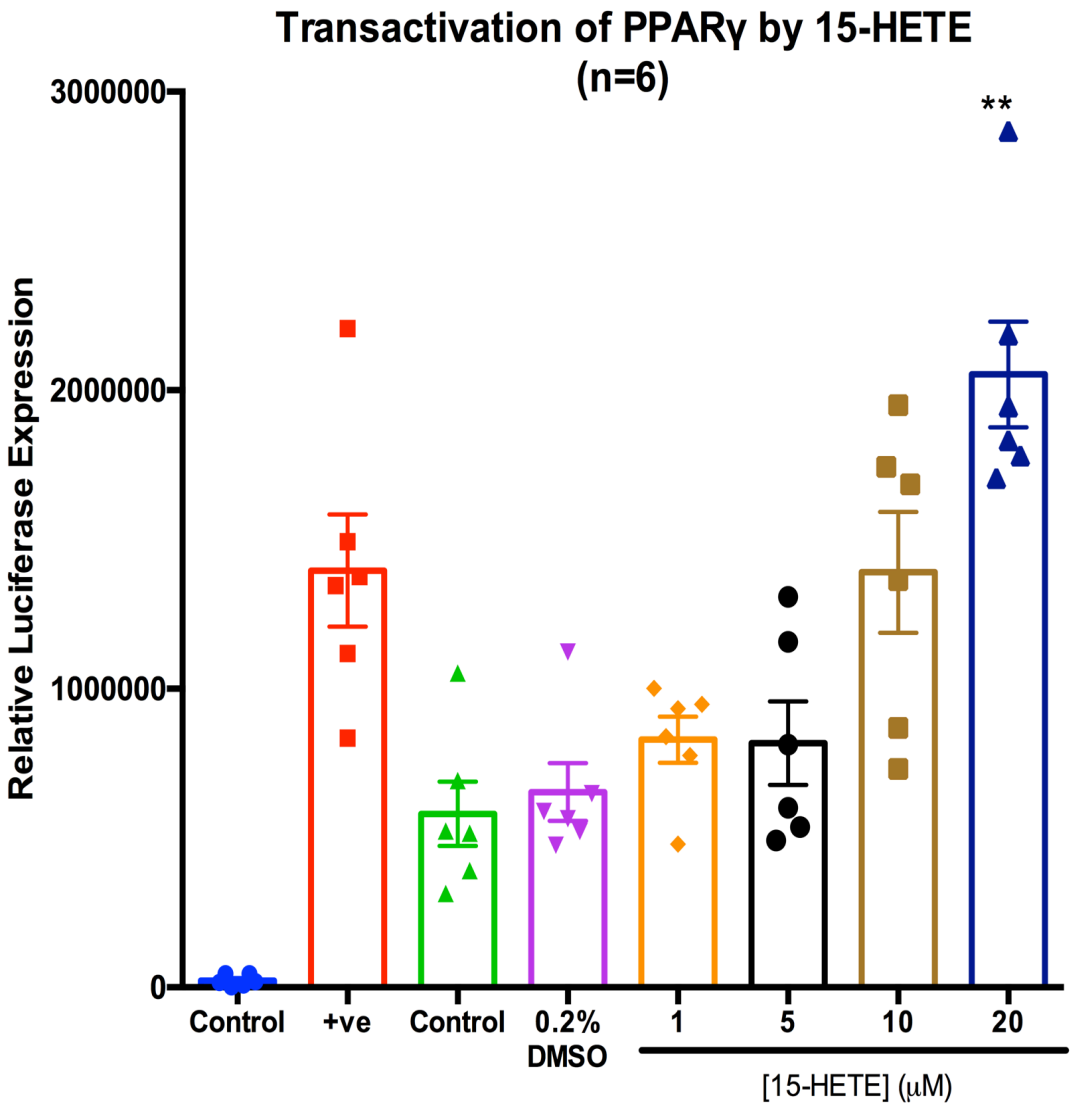

Figure 6.3: Activation of the PPARγ-LBD by 15-HETE

*293T cells were transfected with plasmids encoding β-galactosidase, TK-luciferase and the PPARγ-LBD/Gal4-DBD fusion protein before treatment for 24h with increasing concentrations of 15-HETE (1-20μM). Statistical analysis was performed using a Friedman test (**p<0.01). Data show mean±SEM; n=6.*

6.3 Structural characterisation of PPARγ

6.3.1 Purification of PPARγ-His6 construct

As described in section 2.14, purification of the His-tagged PPARγ-LBD proceeded through a number of steps (Itoh et al., 2008). Briefly, Rosetta *E.coli* were transformed with plasmid KA87 encoding the His-tagged PPARγ-LBD (residues 204-477), under control from the Lac operon, and kanamycin resistance. Protein expression was induced with IPTG for 16h at 20°C before cells were lysed and the crude protein extract isolated by ultra-centrifugation. The His-tagged protein was isolated from the crude extract by incubation with Ni-NTA agarose and, after washing, eluted with imidazole. The His-tag was subsequently cleaved overnight using TEV. The protein was further purified using a ResourceQ column followed by a Superdex S75 column. The PPARγ-LBD did not bind to the ResourceQ column, but other contaminants that did bind were removed (figure 6.4a). The Superdex S75 separates components of a mixture according to size and the PPARγ-LBD was eluted over several fractions, the fractions were run on a gel and the most concentrated combined to form the purified protein (figure 6.4b).

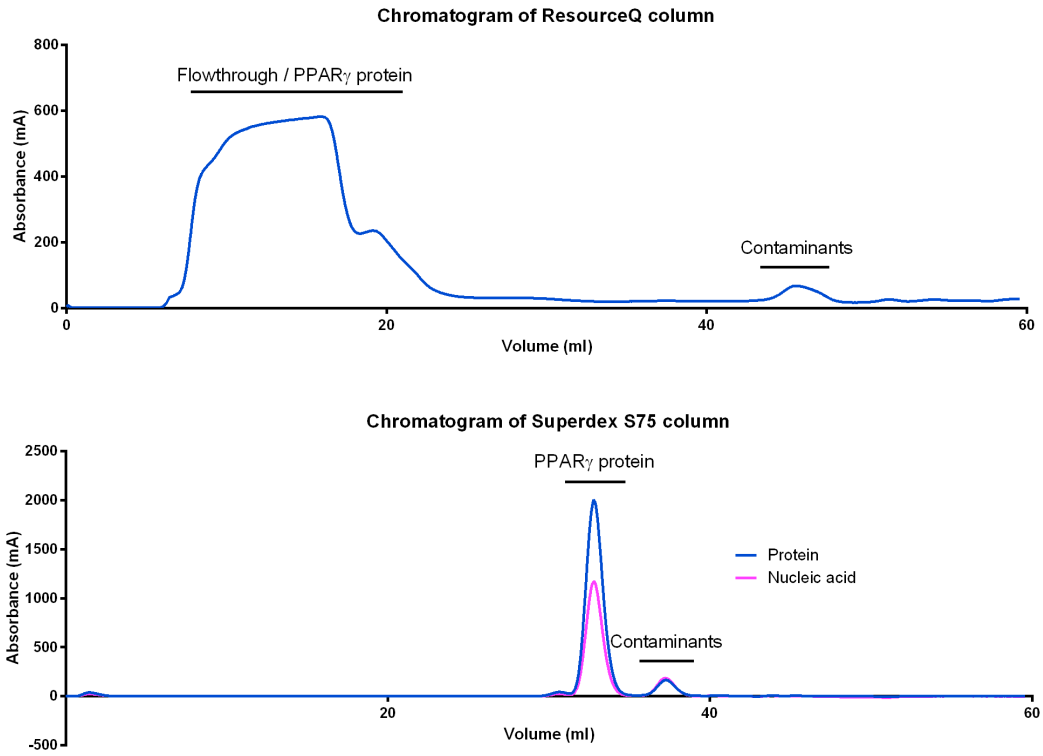

Figure 6.4: Chromatogram's of A280 from ResourceQ and Superdex S75 columns

After TEV cleavage and dialysis, protein samples were loaded onto the ResourceQ column and A280 measured (A). The protein was present in the flow through and was concentrated before loading onto the Superdex S75 column and fractionated (B).

At each stage of purification, a sample was retained for SDS-PAGE to determine protein purity (figure 6.5). From the gel, the eluted protein had a MW of ~35kDa that decreased to 31kDa after removal of the His-tag.

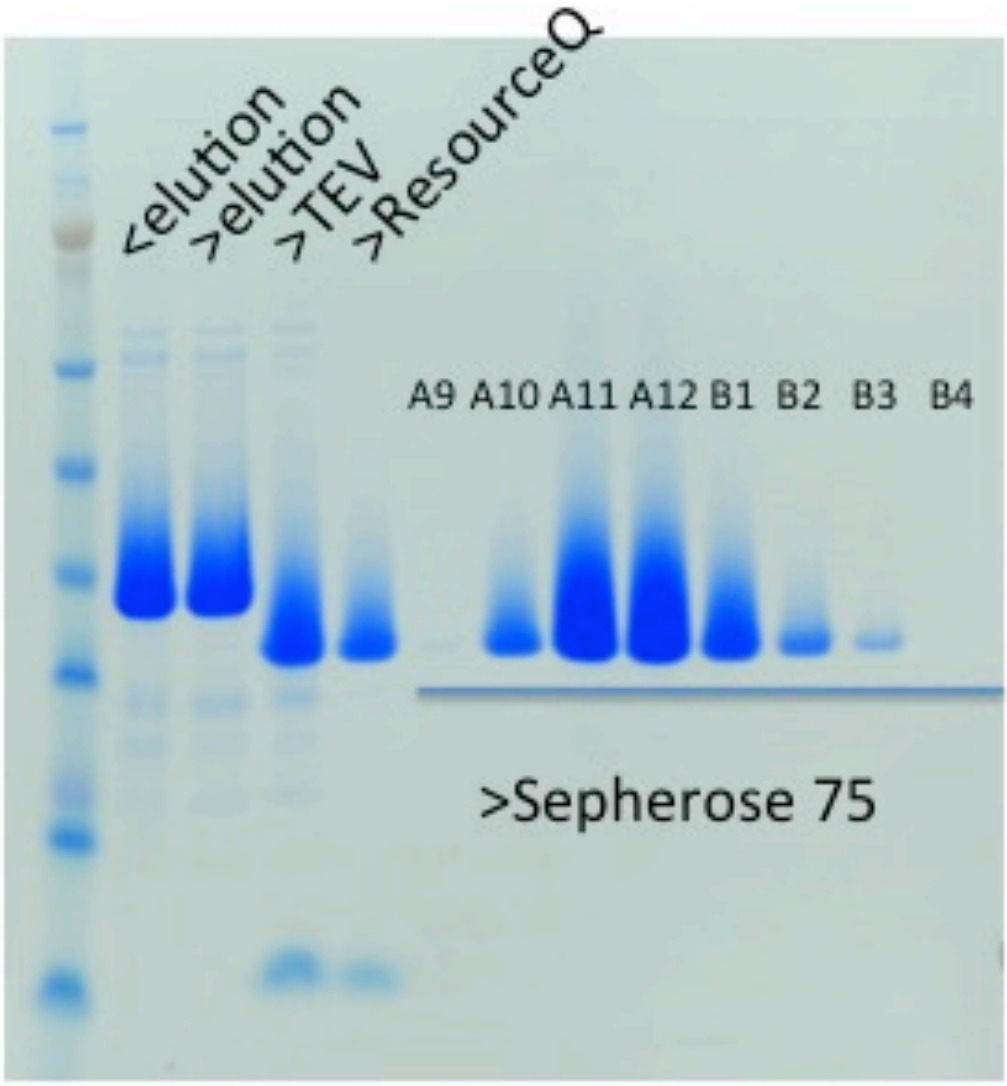

Figure 6.5: Protein gel showing purification of the PPARγ-LBD

After each stage of protein isolation and purification a sample was retained and ran on a gel. Lane 1: Pre Ni-NTA elution, 2: post Ni-NTA elution, 3: post TEV cleavage, 4: post ResourceQ purification, 5-10: Post Superdex S75 fractionation.

6.3.2 Preliminary studies

After the purification strategy had been established, preliminary crystallisation trials were performed to determine if i) DMSO effected crystallisation, as this was the solvent ligands were dissolved in, and ii) if crystals could be grown with 15d-PGJ2 and

rosiglitazone, as had been described previously. The molecular dimensions NR-LBD screen was used for all crystallisation experiments (appendix 1).

Without DMSO, the formation of crystals could be detected in 12 wells (table 6.1) and ranged from small and needle like to large and diamond shaped.

Table 6.1: Crystallisation conditions for apo PPARγ-LBD from the NR-LBD screen

Well	Salt	Buffer	pH	Precipitant
C2	None	0.1M Na HEPES	7.5	1.3M sodium citrate
C4	0.1M ammonium acetate	0.1M Tris	8.0	1.0M sodium citrate
C6	0.2M ammonium acetate	0.1M Na HEPES	7.5	1.2M sodium citrate
C7	0.4M sodium chloride	0.1M Na HEPES	7.5	1.3M sodium citrate
C10	0.1M ammonium acetate	0.1M Bis Tris	6.5	1.0M sodium citrate
D2	None	0.1M PIPES	7.0	1.5M sodium citrate
D6	0.4M sodium chloride	0.1M Bis Tris	6.5	1.0M sodium citrate
D7	0.1M ammonium acetate	0.1M Na HEPES	7.5	1.0M sodium citrate
G5	0.1M ammonium sulphate	0.1M Tris	8.0	1.1M sodium citrate
G10	0.5M ammonium sulphate	0.1M PIPES	7.0	0.9M sodium tartrate
H11	0.3M sodium chloride	0.1M Tris	8.0	1.7M ammonium sulphate
H12	0.2M sodium chloride	0.1M Tris	8.0	2.0M ammonium sulohate

With the addition of DMSO (0.1-1%), there was no observable effect on crystal formation in any of the wells, suggesting a final concentration of up to 1% DMSO can be used without hindering crystal formation. Figure 6.6 shows representative pictures of crystals from 3 wells formed with 0, 0.4 and 1% DMSO.

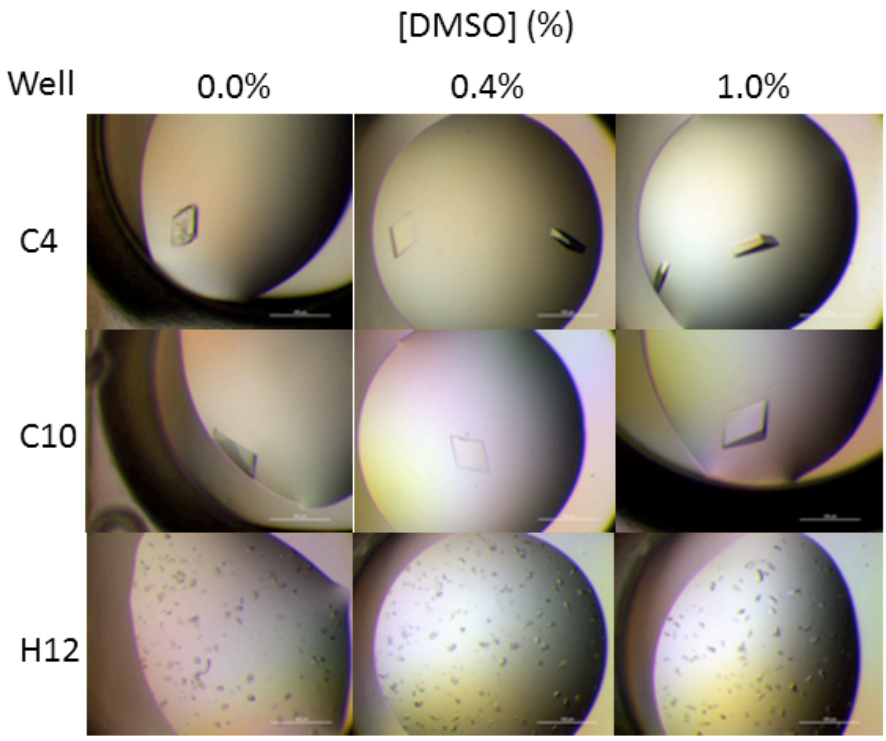

Figure 6.6: Formation of apo PPARγ-LBD crystals with increasing DMSO concentrations

The PPARγ-LBD protein was purified and incubated with increasing concentrations of DMSO (0.1-1%) before crystallisation plates set up using the NR-LBD. After 3 days the plates were inspected for crystal formation.

In order to determine if ligand binding to the PPARγ-LBD effected crystallisation, trials were set up with purified PPARγ-LBD with the PPARγ ligands 15d-PGJ2 (1mM) and rosiglitazone (1mM). After 3 days the plates were inspected and crystals were observed in the same wells as without ligand (not shown); suggesting incubation with ligand does not adversely effect crystallisation. For this reason initial crystallisation experiments used 15-HETE (1mM) with 8mg/ml PPARγ-LBD as had been done previously with other ligands (Itoh et al., 2008) however no crystals formed. It was hypothesised that it could be due to the excess of ligand. 15-HETE is a fatty acid eicosanoid and may bind to the surface of the PPARγ protein when added in high concentrations that could affect the crystal packing in solution and prevent ordered crystal formation.

In order to grow crystals with 15-HETE, purified PPARγ protein was concentrated to approximately 8.5mg/ml (250μM) and 13mg/ml (~400μM) and co-crystallised with increasing concentrations of 15-HETE, from a 0.5 : 1 to 4 : 1 ratio (15-HETE : PPARγ-LBD).

Crystals formed within 2 days in the majority of wells established previously. Interestingly, crystals were only observed in plates where the 15-HETE concentrations

were 0.5, 1 and 1.5 that of PPARγ. No crystals were observed at either protein concentration in any wells with the higher ligand concentration. Figure 6.7 shows representative examples from wells C10 and D7. On this basis, co-crystallisations using 12-HETE were set up using an approximate 1:1 ratio.

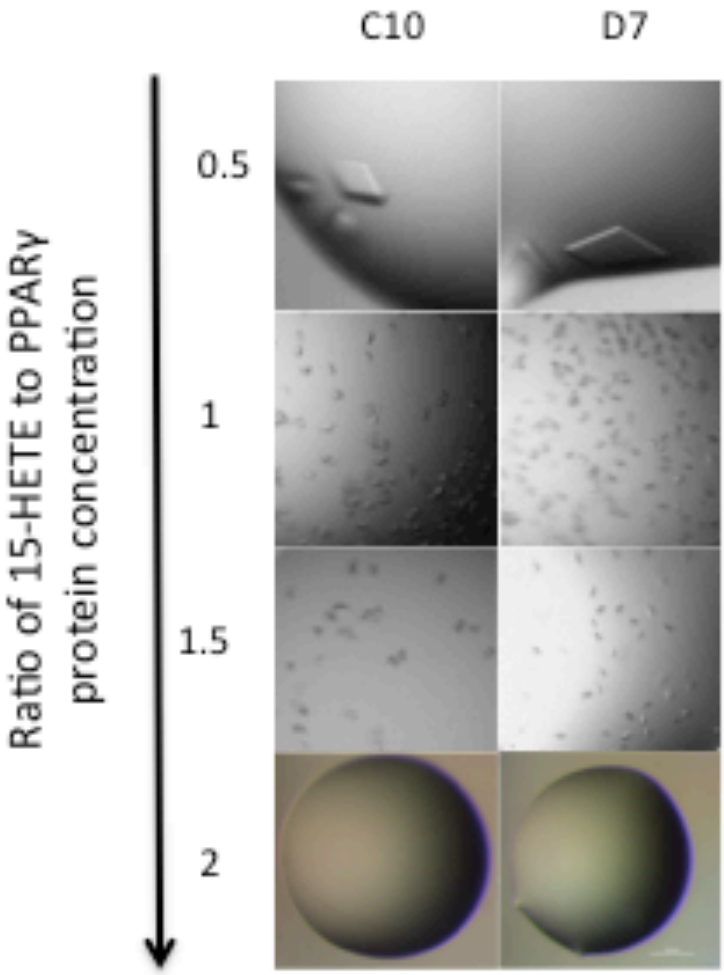

Figure 6.7: Effect of 15-HETE concentrations on crystal formation

Purified PPARγ protein was co-incubated with increasing molar ratios of the ligand 15-HETE before crystallisation trials were set up using the NR-LBD screen. Crystals formed after 3 days in wells similar to previous experiments up to a ratio of 1.5 : 1 (15-HETE : protein).

6.3.3 Crystallisation of the PPARγ-LBD with 12- and 15-HETE

6.3.3.1 Strategy for structure determination

Protein crystals were soaked in cryoprotectant (crystallisation condition with 20% glycerol), 'fished' into crystallisation loops and stored in liquid nitrogen. Initially, crystals were transported to the Diamond Light Source (Oxford) and X-rayed using beamline I24. Data were collected through 180° with diffraction recorded every 0.2°. Unfortunately, no ligand was detected in these crystals. Crystals collected at a later time

point, with 12- and 15-HETE, were X-rayed at the Swiss Light Source (SLS) (Villigen, Switzerland), using the micro-focus beam line. Data points were collected every 0.1° through 180° rotation and generated 1800 diffraction images. Images were processed using iMosflm and the CCP4 suite. Crystals used for data collection and example diffraction patterns are shown in figure 6.8.

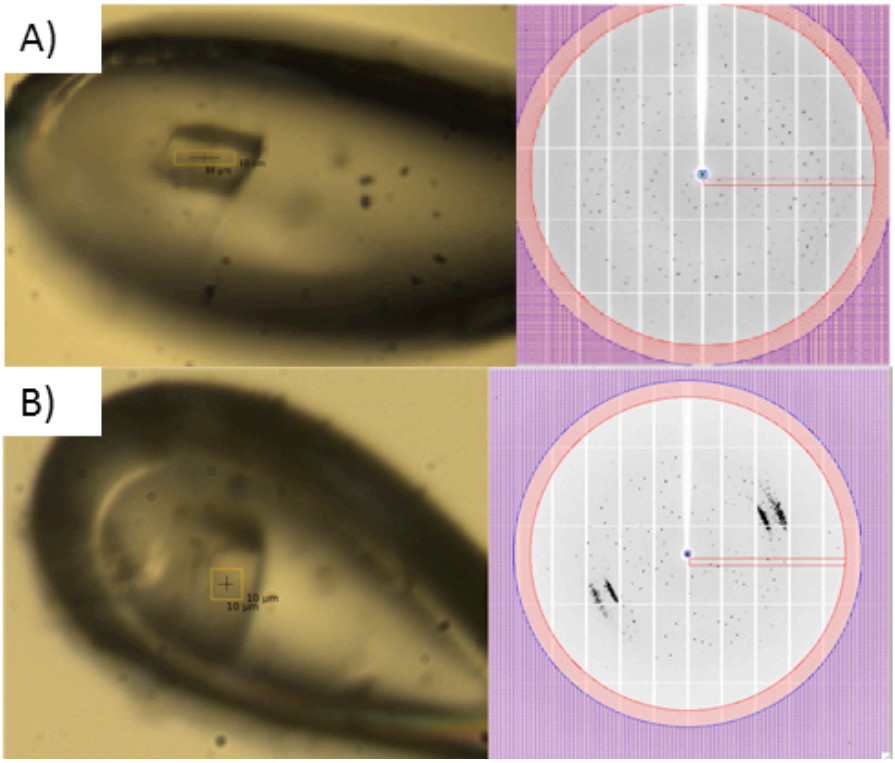

Figure 6.8: Crystals X-rayed using micro-focus beam and representative diffraction pattern
Crystals were soaked in cryoprotectant of the buffer in which they formed with added glycerol before being scooped and rapidly frozen in liquid nitrogen. At the light source crystals were positioned in the beam line and X-rayed, top: 12-HETE and bottom: 15-HETE. A representative diffraction pattern is shown for 12-HETE (top right) and 15-HETE (bottom right).

Using iMosflm, diffraction images 1 and 900, 90° apart, were auto-indexed, which, based on reflection intensities, predicted the space group C2 and initial unit cell dimensions, in agreement with previous crystal structures of PPARγ and integrated the data set (Leslie, 2006).

The resulting mtz file (map) was scaled using Aimless, a CCP4 program (Collaborative Computational Project, Number 4, 1994) that i) determined the Laue group (point group) based on the symmetry of the diffraction pattern, ii) scaled and merged identical reflections to obtain an average intensity and iii) converted intensities to amplitudes. A number of descriptive outputs are available that relate to the quality of the data with

three shown below (figure 6.9a-c). Firstly the output showed the observed intensities were untwined and did not result from 2 crystals that have similar symmetry but are in different orientations (figure 6.9a). The B-factor vs. image number (or time) is a measure of radiation damage and should be greater than -10 (figure 6.9b). Rmerge against image number shows if there are any poor datasets, the lower the Rmerge the better the data quality, usually below 0.6 is accepted (figure 6.9c).

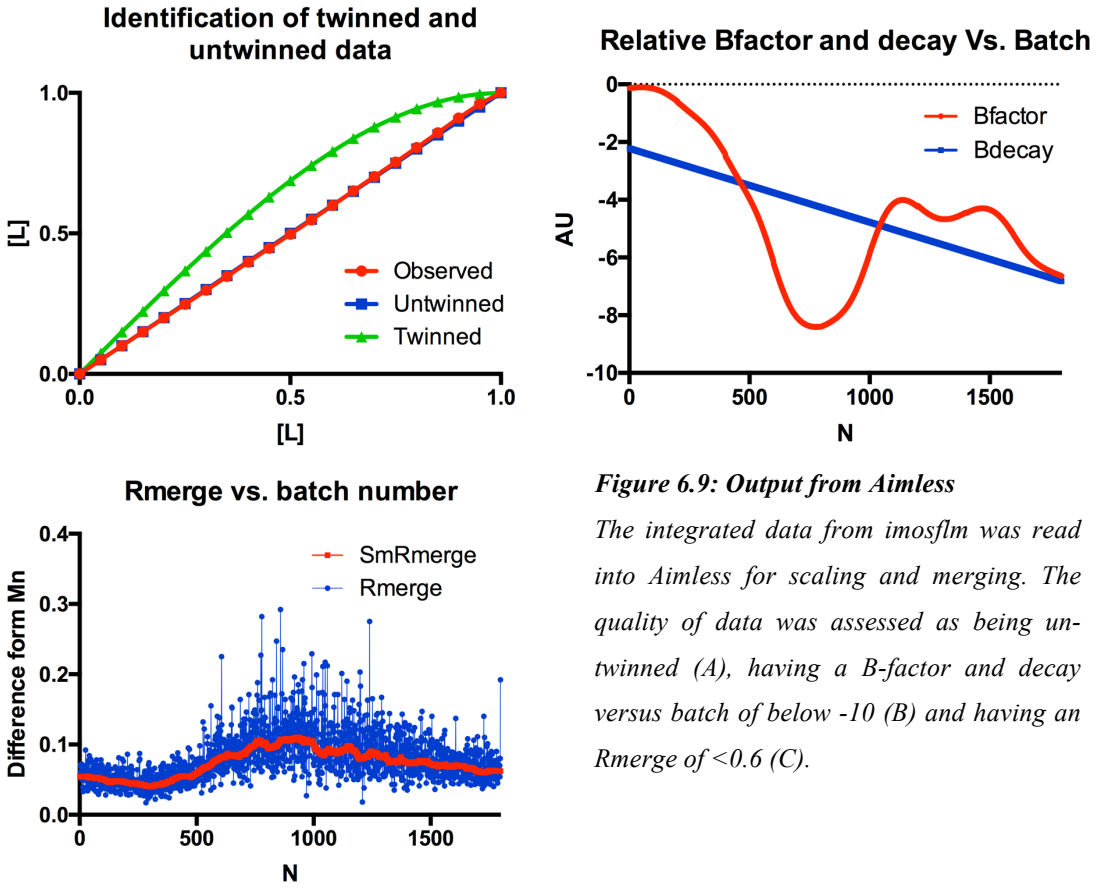

Figure 6.9: Output from Aimless

The integrated data from imosflm was read into Aimless for scaling and merging. The quality of data was assessed as being un-twinned (A), having a B-factor and decay versus batch of below -10 (B) and having an Rmerge of <0.6 (C).

The resulting file was used to determine a suitable resolution cut-off where *Rmerge* was ~0.5 and the signal to noise ratio (I/sd) >2. This information was used to re-run the data through the Aimless program. The new aimless map (mtz file) was used for all future tasks based on refining the electron density. The PPARγ structure was solved by molecular replacement using Phaser (Scapin, 2013) with the mtz file and the already solved 2VSR structure, with the ligand removed to avoid model bias. The structure was rebuilt using Coot (Emsley and Cowtan, 2004) and PDB-redo, an automated online program that carries out refinement (http://xtal.nki.nl/PDB_REDO/). The resulting structure and original mtz file from Aimless was used to calculate a Simulated Annealing Omit map using Phenix (Adams et al., 2010) to try to remove any model

bias. The resulting density maps from different crystals were compared and the map that looked most promising for density in the ligand-binding pocket used for further rebuilding (figure 6.10).

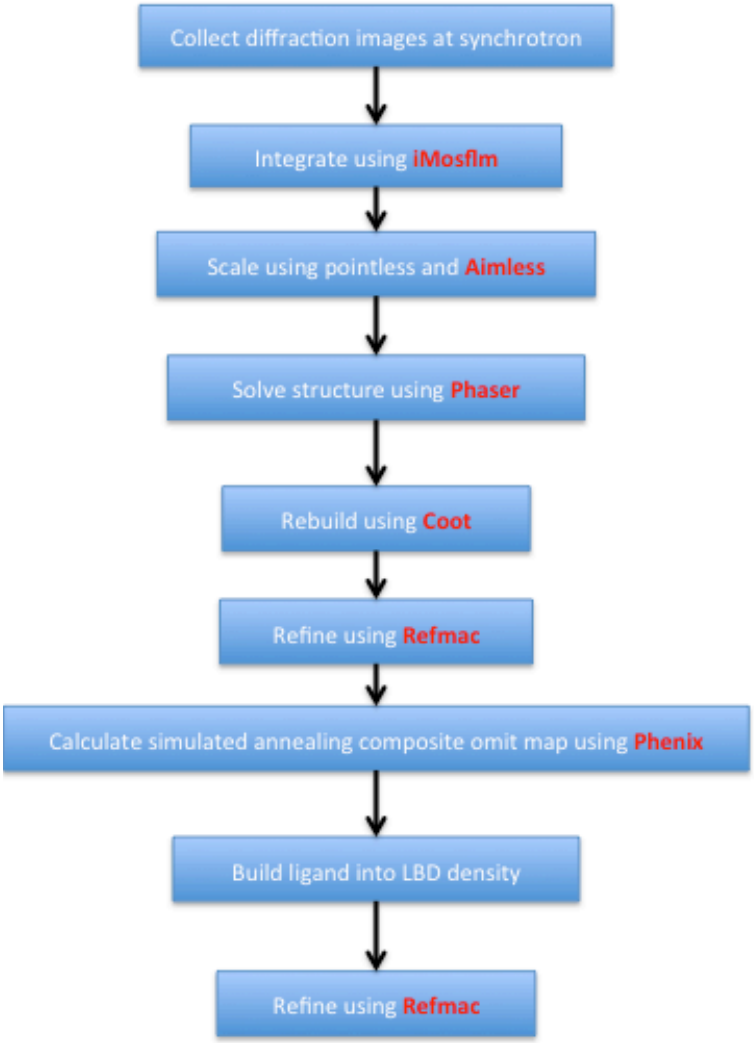

Figure 6.10: Flow chart for strategy of structure determination and optimisation

Process of solving, refining and building crystal structures. Text in red indicates software used for processing,

For model building the 12- and 15-HETE ligands were created using MarvinSketch, rendered in 3D and saved as a PDB file. This was merged with the protein model and orientated to best fit the density, before the complex was refined using Refmac5 (Murshudov et al., 1997). At the point of submission of this thesis, no further optimisation had been carried out on the structures due to time constraints. All figures were created using Pymol, with maps set to 1 σ. Data statistics for the 12- and 15-HETE structures are shown in table 6.2.

Table 6.2 Data statistics for 12- and 15-HETE structures

Data Collection	**12-HETE**	**15-HETE**
Space Group	C2	C2
Cell Dimensions		
a, b, c (Å)	92.5, 61.0, 118.2	92.7, 60.9, 118.6
α, β, γ (°)	90.0, 103.0, 90.0	90.0, 103.2, 90.0
Resolution (Å)	33.14-2.45 (2.55-2.45)	38,49-2.35 (2.43-2.35)
Rmerge	0.067 (0.400)	0.055 (0.491)
I/σI	41.7 (2.6)	9.4 (2.3)
Completeness (%)	97.7 (98.6)	97.2 (98.6)
Multiplicity	3.1 (3.1)	3.0 (3.1)

6.3.3.2 Structure comparison of the solved PPARγ-LBDs

Both the 12-HETE and 15-HETE crystals were solved by molecular replacement using 2VSR with the ligand removed. For both the 12-HETE and 15-HETE structures there are two molecules in the asymmetric unit as seen in other structures (figure 6.11a and b). As expected, molecule A from 12- and 15-HETE structures were identical when overlaid as were molecules B (figure 6.11c and d). For this reason any further comparisons used the 12-HETE structure only.

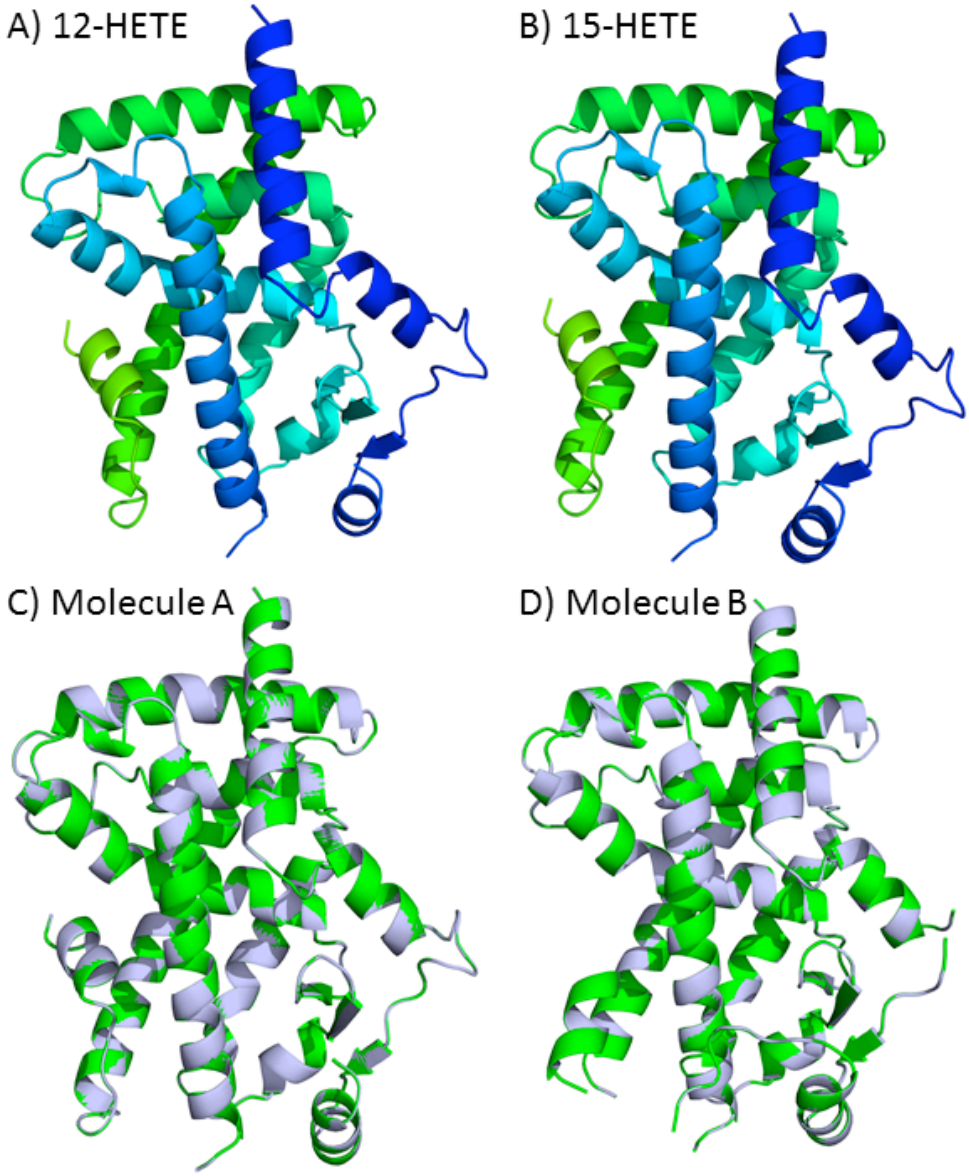

Figure 6.11: Overall structures of 12-HETE and 15-HETE PPARγ-LBDs

The structures of the PPARγ-LBDs were solved by molecular replacement. The structure of molecule A of 12-HETE A) and 15-HETE B) were similar to that of other structures and superimposed perfectly on each other C). The same was also true of molecule B D). 12-HETE: green, 15-HETE: grey.

To further evaluate our structure it was compared to the first crystal structure of apo PPARγ-LBD published by Nolte et al., (Nolte et al., 1998). Superimposing the two structures showed almost identical homology in the secondary structure regions for both molecule A and B (figure 6.12a and d) with a slight movement of a β-strand in the β-sheet between Hx5 and 6. The most noticeable differences were in the mobile loop regions of both subunits at the N-terminus and the C-terminus mobile loop and terminal helix. Molecule A showed differences in the loop between Hx2 and the β-strand and

between Hx2' and Hx3, which is absent in this structure (figure 6.12b arrows). The C-terminus shows similar homology in the loop but has a slightly different conformation in the terminal AmA (figure 6.12c arrow). These observations were similar in molecule B although the loop between Hx2' and Hx3 was more complete (figure 6.12E arrow) and conversely the loop between Hx11 and Hx12 was incomplete (figure 6.12F).

In vivo, PPARγ is found as a complex with RXR and DNA as the full-length protein, it was therefore relevant to compare the structure of the LBD model with that of the LBD from Chandra et al., who solved this structure (Chandra et al., 2008). When superimposed onto the LBD from the full length, DNA-bound structure the observations were similar as for the PPARγ-LBD homodimer described above. The majority of secondary structure elements superimposed (figure 6.13a) with the exception of the β-strand between Hx5 and Hx6 (figure 6.13b arrow 1) and Hx2' (arrow 2). There were also some differences in the mobile loop between Hx2 and the β-strand (arrow 3). Similar to this structure, there was no loop modelled between Hx2' and Hx3. There were also slight differences in the C-terminal mobile loop between Hx11 and Hx12 (figure 6.13c arrows).

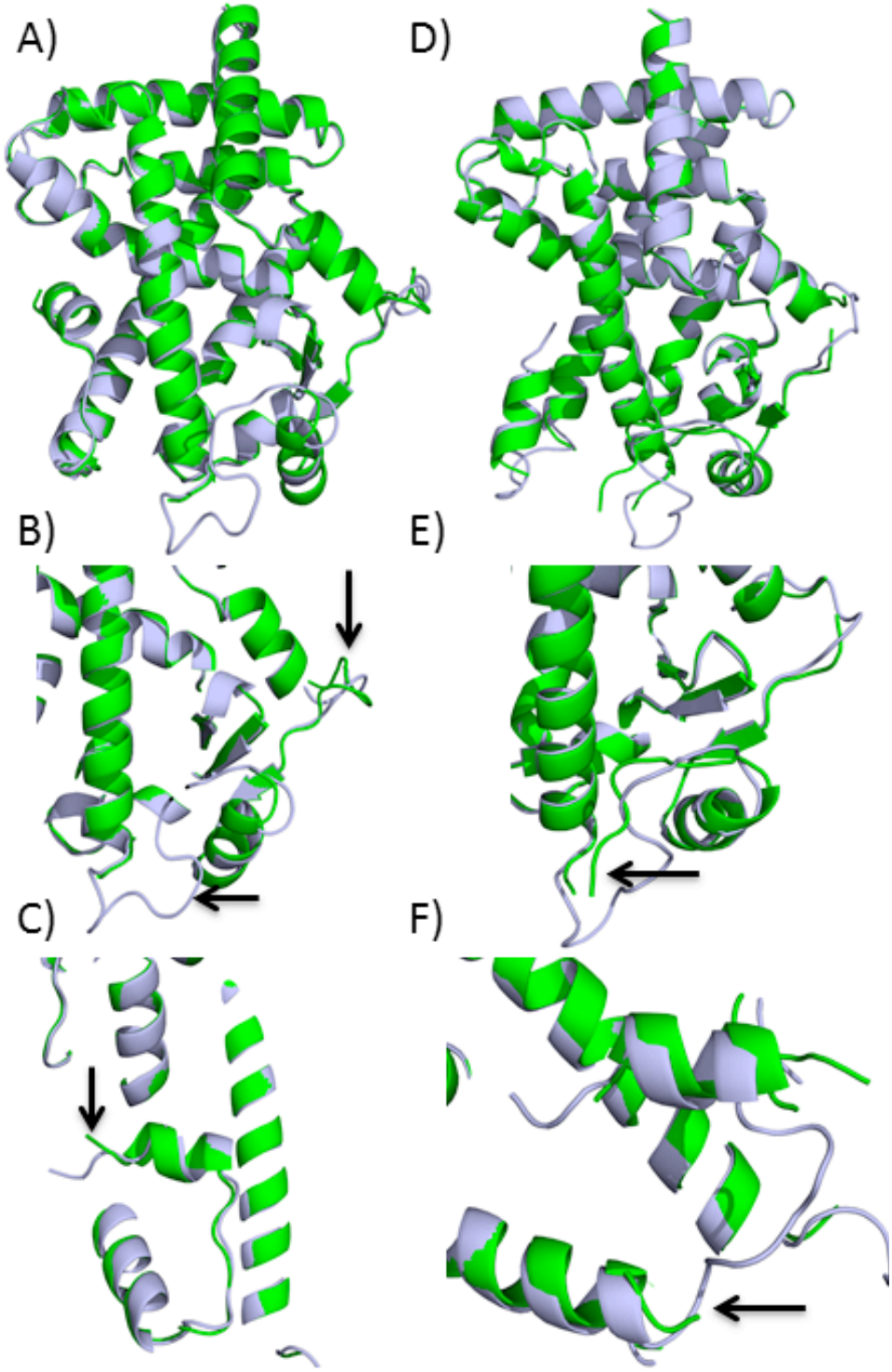

Figure 6.12: Comparison of PPARγ-LBD model with first published structure

Using Pymol, molecules A A) and B D) were superimposed onto molecules A and B of the first published PPARγ-LBD model by Nolte et al. The secondary structure conformations were similar between the structures with the main differences in the N-terminal mobile loops B) and the C-terminal Hx12 and loops C) for molecule A and the N-terminal loops E) and C-terminal loops F) for molecule B. Structure from this work is in green and that from the first model, 1PRG, is in grey.

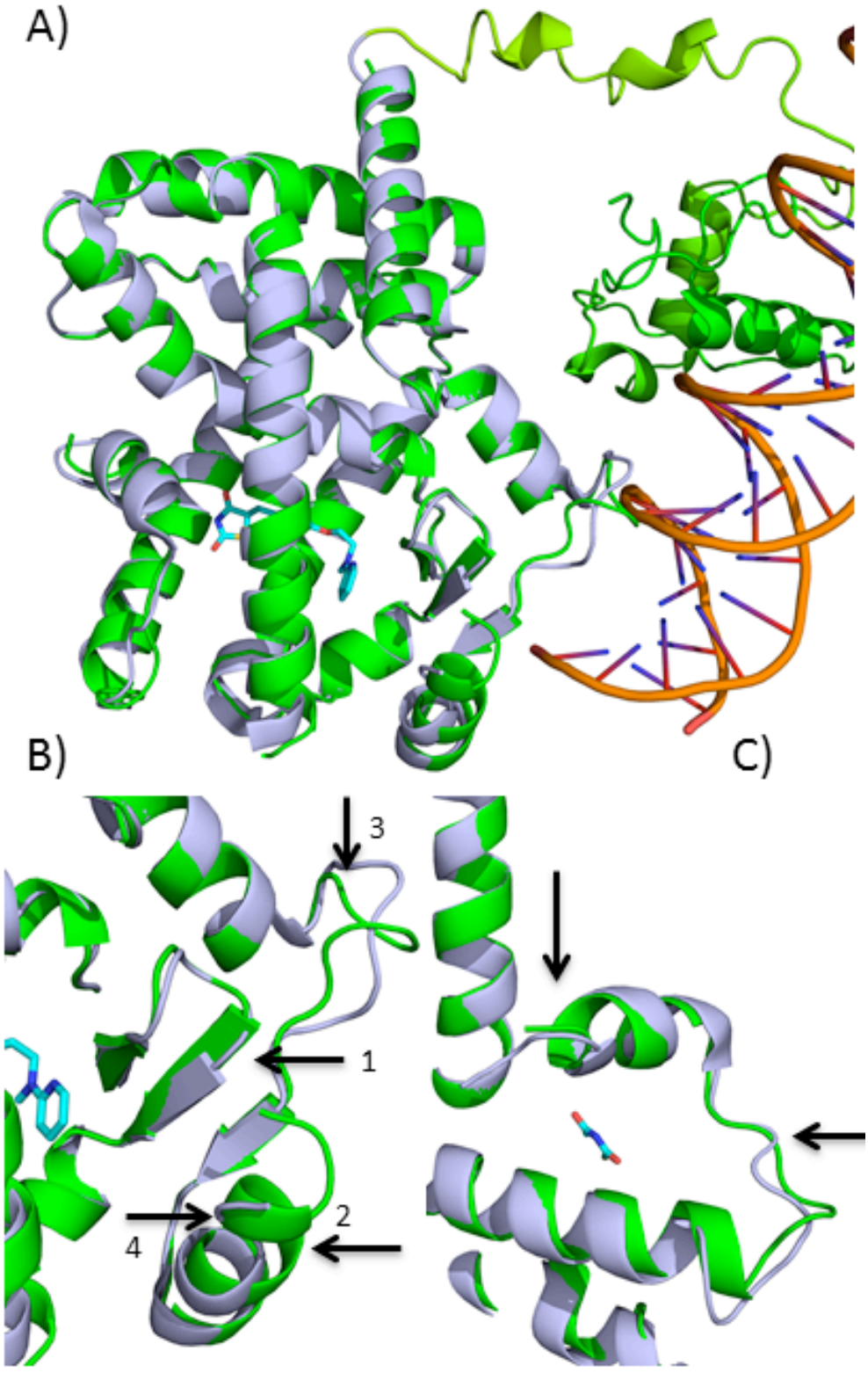

Figure 6.13: Comparison of PPARγ-LBD model with LBD from full-length PPARγ

The PPARγ-LBD from this work (green) was superimposed into the LBD (grey) from full length, DNA-bound and ligand bound PPARγ from Chandra et al A). The main differences can be seen in the N-terminal mobile loops with some difference in the conformation of the β-strand and Hx2' B). There are also some positional differences in the C-terminal Hx11 and Hx12 and the connecting loop C).

The observed differences described above between the structure solved in this thesis and the full-length, ligand bound heterodimer are not unusual. In fact, when 10 molecule A's with PPARγ ligands were superimposed, the largest differences in conformation were seen between Hx2' and Hx3, with many models having incomplete loops (figure 6.14). Less difference is seen in the mobile regions between Hx2 and the β-strand and Hx11 and Hx12 with some very minor differences in secondary structure positions.

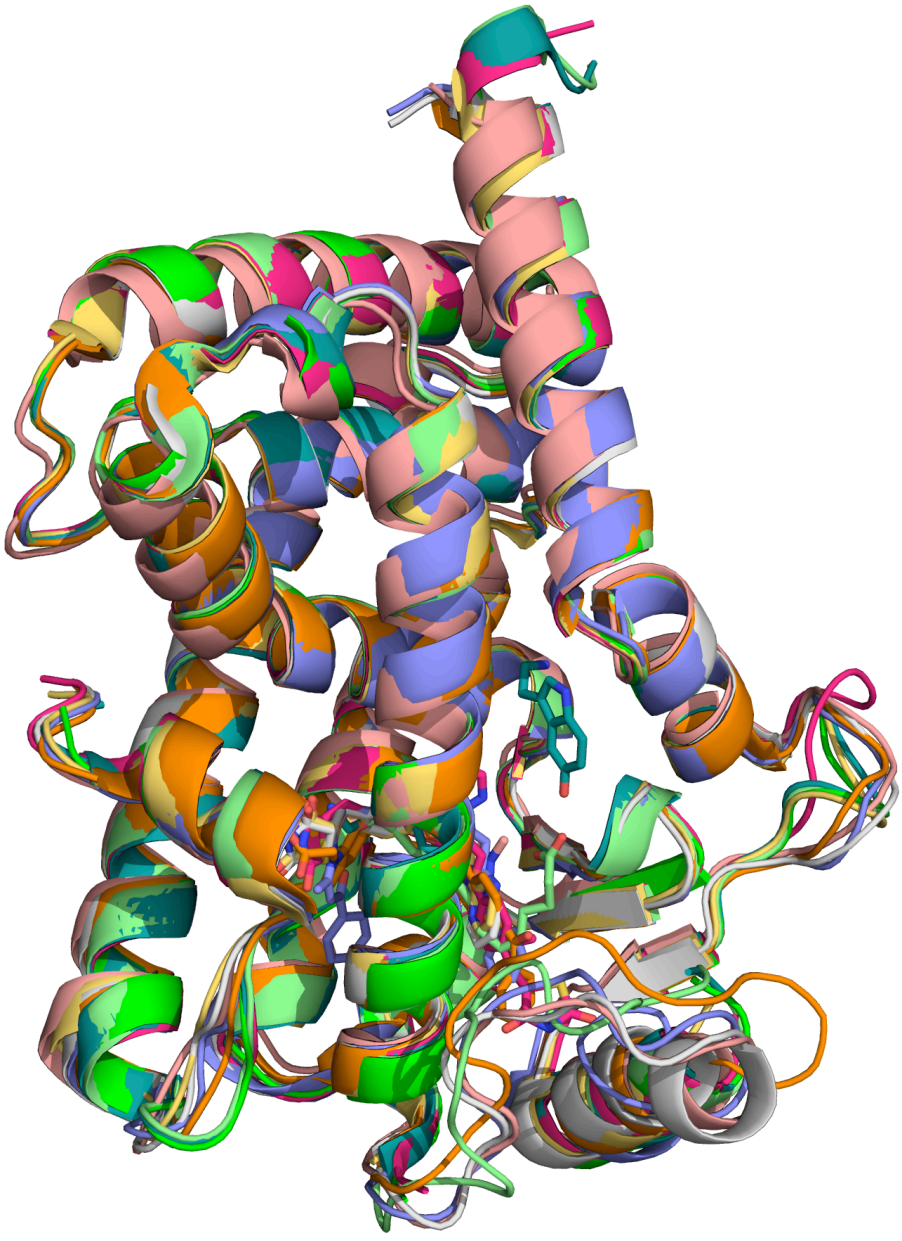

Figure 6.14: Comparison of the PPARγ-LBD from 10 different structures

The PPARγ-LBDs from molecule A of 10 different models were superimposed in Pymol. Whilst the major secondary structure elements are similar a large amount of variation is seen in the mobile loops connecting these elements together.

6.3.3.3 Modelling of 12- and 15-HETE ligands into the PPARγ-LBD

Density was observed in the LBD for both 12/15-HETE structures suggesting the presence of ligand. In order to build ligand into the density, 12/15-HETE were created in MarvinSketch, rendered in 3D and converted to a PDB file (figure 6.15a). The final positions at the point of submission of this thesis were different for both 12- and 15-HETE, which reflects the large capacity of the LBD to bind ligand and the difficulty in fitting ligands to the correct position (figure 6.15b).

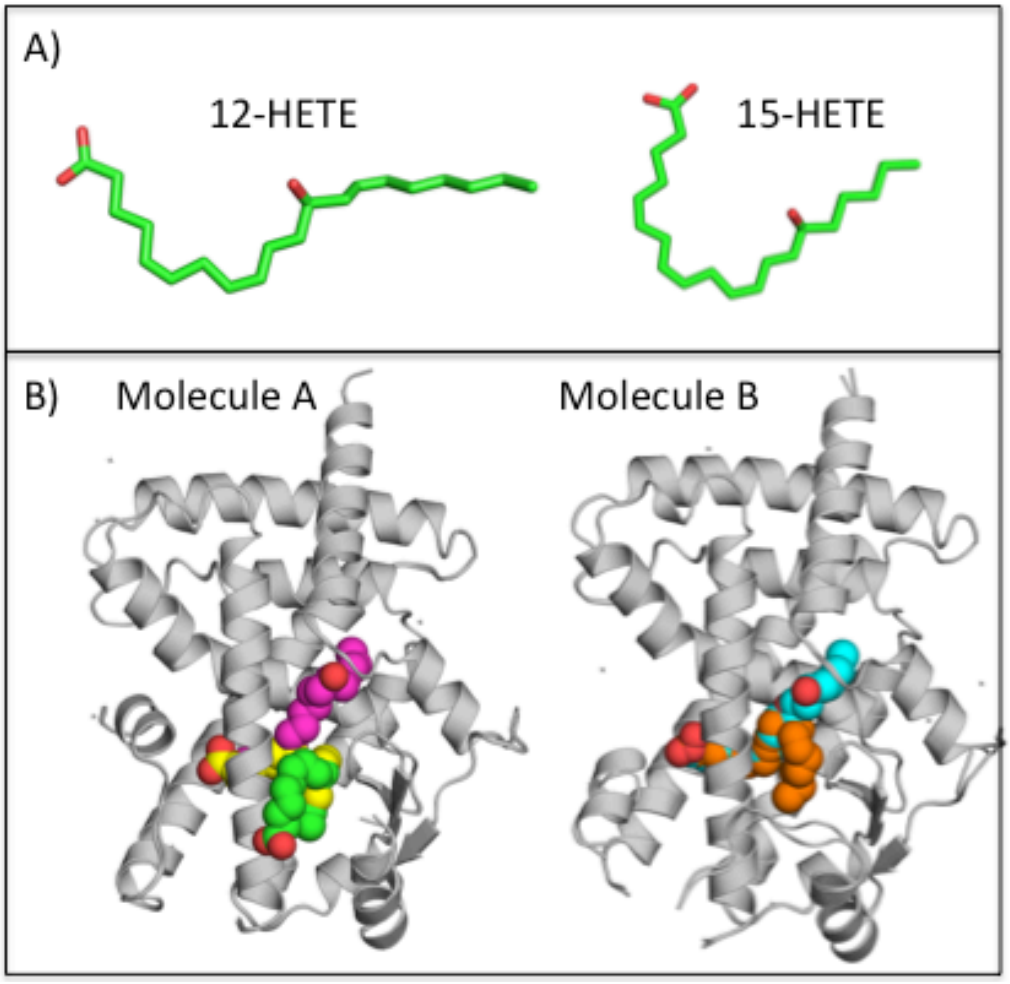

Figure 6.15: Structure of 12- and 15-HETE and position in PPARγ-LBD

A) 12- and 15-HETE were created using the program MarvinSketch, rendered in 3D and converted to a PDB file able to be merged with the 12- and 15-HETE PPARγ-LBD structures. B) Positions of 12- and 15-HETE within LBD. (12-HETE - Yellow and orange; 15-HETE - pink, green and blue).

The map from the 12-HETE rebuild showed promising electron density in the LBD, starting towards Hx12, where other ligands are known to make H-bonds to H323 and H449, and extending around Hx3, where a large loop of density could be seen (figure 6.16a). This was indicative of the presence of a ligand and was more compelling after

calculation of a simulated annealing composite omit map, which removed model bias and still showed density in the LBD (figure 6.16b). A masked map of unassigned density was used to fit the 12-HETE molecule in the LBD, which mapped into almost continuous density at 1 σ with a small gap between C5-7 (figure 6.16c). This conformation was favoured due the hydrogen bonds formed between the carboxyl group to H323 (Hx5), H449 (Hx11) and Y473 (Hx12), a common theme in ligand-coupled PPARγ structures. The double bond between C5 and C6 maps to density close to C285 (Hx3) that has been shown to mediate covalent attachment of ligands in other models. The hydrophobic terminus sits in a hydrophobic pocket in the LBD, formed by residues V339 and I341 (figure 6.16d). The final position of 12-HETE in molecule A is shown in figure 6.16e. After positioning the 12-HETE in the density, the structure was refined using refmac5 to improve the phases and the map and to avoid model bias. After refinement contiguous density could not be observed around the 12-HETE molecule (figure 6.16f).

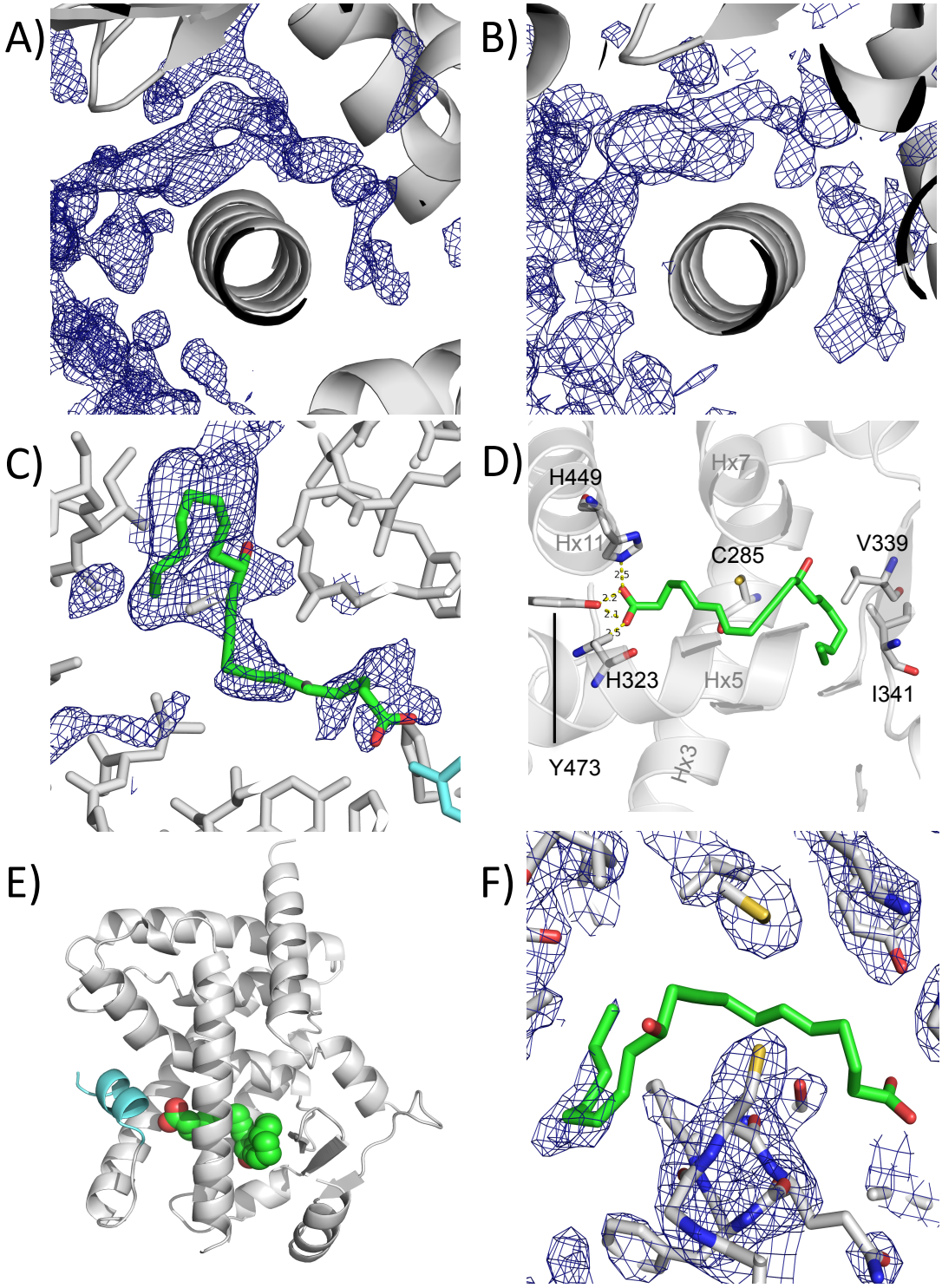

Figure 6.16: Identification and building of 12-HETE in the PPARγ-LBD molecule A

A) Density in the PPARγ-LBD after rebuilding and B) after calculation of simulated annealing composite omit map. C) Fitted 12-HETE molecule in density, D) specific contacts made between 12-HETE and the main chain, E) final position of 12-HETE in the PPARγ-LBD and F) density in the PPARγ-LBD after refinement.

The density observed in molecule B after the rebuild (figure 6.17a) and the simulated annealing composite omit map calculation (figure 6.17b) was similar to molecule A. Fitting of 12-HETE in the LBD positioned the carboxyl group in the canonical Hx12 position and the rest of the molecule followed continuous density around Hx3 to the β-sheet (figure 6.17c). The difference between molecule A and B is the position of the hydroxyl group, with it facing 'up' in B towards Hx5 and 'down' in A. Predicted contacts were similar to A at Hx12, although in this case the 12-HETE molecule was further away suggesting H-bonds may not form (figure 6.17d). This may be due to the structure of the PPARγ-LBD and may suggest rebuilding would be beneficial here. The hydrophobic region was positioned in a similar conformation to molecule A. The final position of 12-HETE in molecule B is shown in figure 6.17e. Similar to molecule A, after refinement the ligand density was removed indicating further building and refinement are required (figure 6.17f).

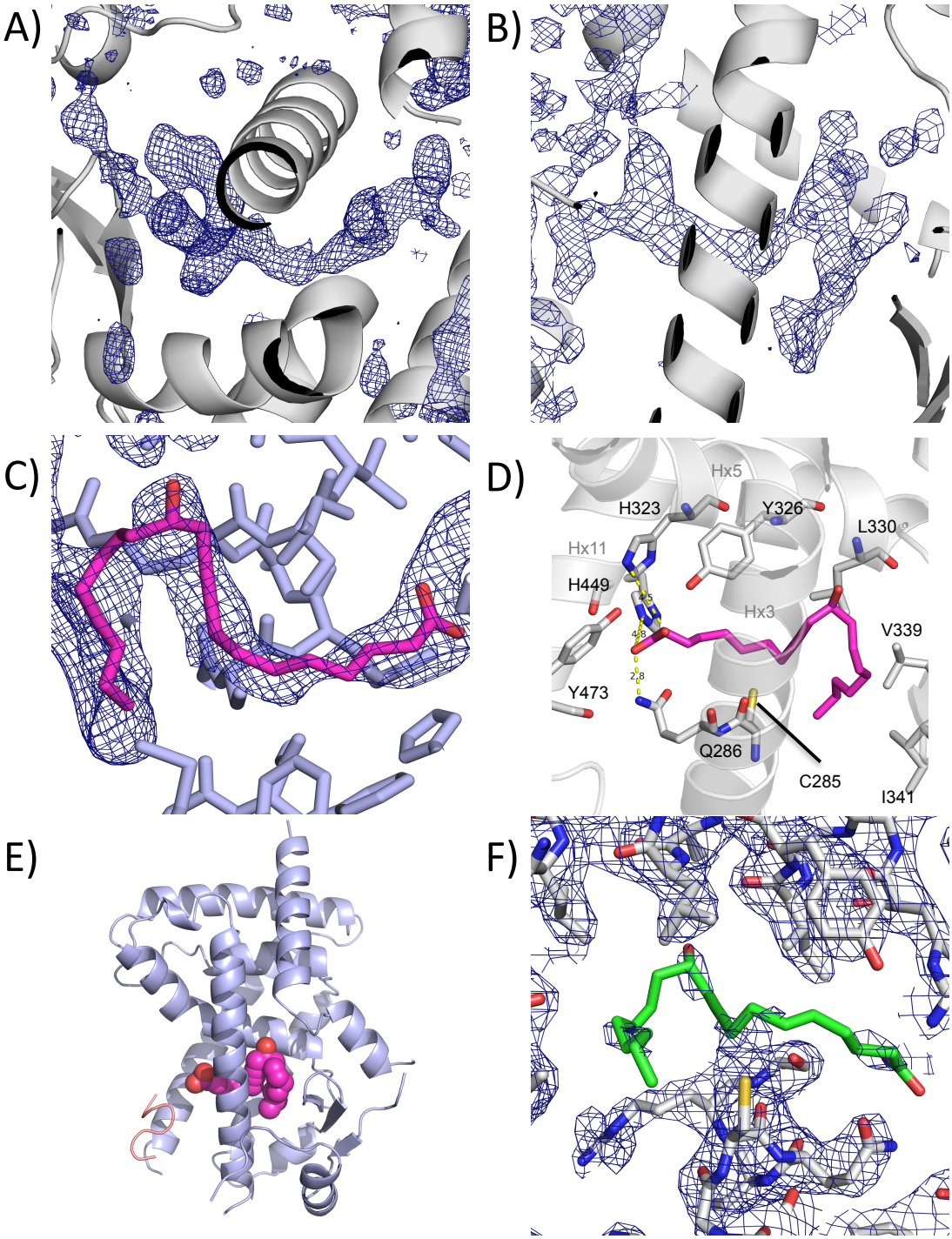

Figure 6.17: Identification and building of 12-HETE in the PPARγ-LBD molecule B

A) Density in the PPARγ-LBD after rebuilding and B) after calculation of simulated annealing composite omit map. C) Fitted 12-HETE molecule in density, D) specific contacts made between 12-HETE and the main chain, E) final position of 12-HETE in the PPARγ-LBD and F) density in PPARγ-LBD after refinement.

The 15-HETE structure showed a similar pattern of density in the LBD after rebuilding, with density beginning at Hx12 and extending around Hx3 where a large loop was also present as with the 12-HETE model (figure 6.18a). After calcualtion of a simulated annealing composite omit map, density was still observed in the LBD suggesting the 15-HETE ligand is present (figure 6.18b). In contrast to 12-HETE, two molecules of 15-HETE were fitted into the density in molecule A. The first started with the carboxyl group towards Hx12 but instead of extending around Hx3, extended towards Hx5 with the hydroxyl group at C_{15} pointing towards Hx2 (figure 6.18c, green molecule). This molecule mapped to almost continuous density with small gap between C12 and C14. Like with 12-HETE, this molecule was positioned to form H-bonds from the carboxyl group to H323, H449 and Y473. 15-HETE extended around Hx3 but instead of the hydrophobic terminus settling in the hydrophobic pocket, the hydroxyl group made contacts with R288 (Hx3) and the main chain O from L228 (loop connecting Hx1 and Hx2). This causes the end of the 15-HETE to point towards Hx5 in a hydrophobic region made of L333 (Hx5) and L384 (Hx8) (figure 6.18d). The second molecule of 15-HETE formed an upside down U-shape with the carboxyl group pointing towards the ligand entry site and extending parallel to Hx3, and eventually ends facing back towards Hx2', fitting to continuous density (figure 6.18e). This molecule appeared not to make any specific H-bonds, although it is possible some may form between E259 (Hx2') and R280 (Hx3) with the carboxyl group. The remainder of the molecule sits in the hydrophobic pocket made up of I281 (Hx3), V339 (Hx5), I341 (Hx5) and L353 (Hx6) (figure 6.18f). Although more convincing then the 12-HETE refinement, with more density surrounding the 15-HETE ligands, it is still not continuous suggesting further rebuilding and refining is necessary (figure 6.18g and h).

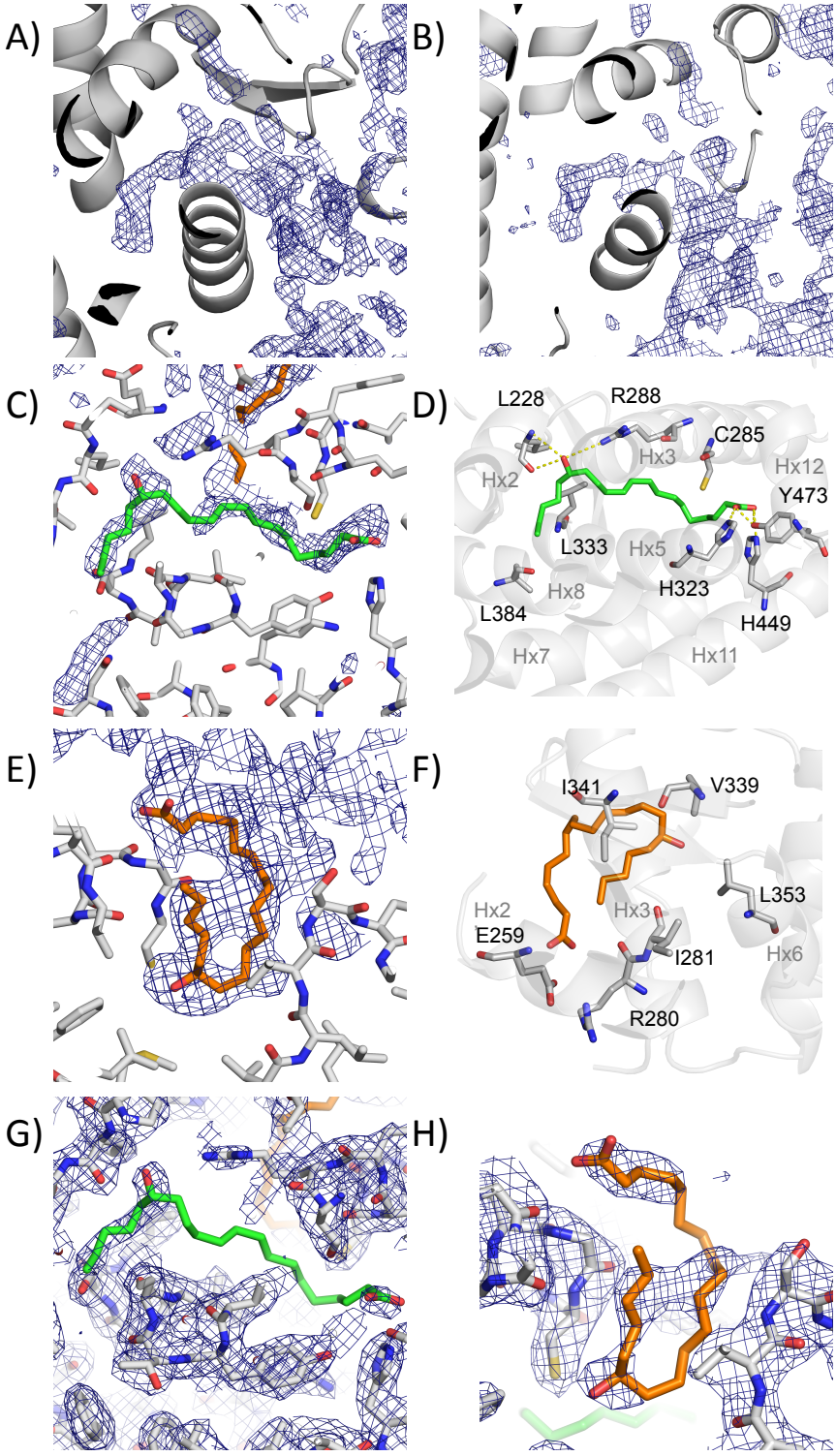

Figure 6.18: Identification and building of 15-HETE in the PPARγ-LBD molecule A

A) Density in the PPARγ-LBD after rebuilding and B) after calculation of simulated annealing composite omit map. C) Molecule 1 of 15-HETE fitted in density and D) specific contacts made between molecule 1 of the 15-HETE and the main chain. E) Molecule 2 of 15-HETE fitted in density and F) specific contacts made between molecule 2 of the 15-HETE and the main chain. Density in PPARγ-LBD after refinement for molecule 1 G) and molecule 2 H).

The density observed in the LBD in molecule B after rebuilding was similar to molecule A although not as pronounced (figure 6.19a) and this was also true for the simulated annealing composite omit map calculation (figure 6.19b). For this reason only one molecule of 15-HETE was positioned in molecule B in a similar conformation to molecule 1 of subunit A (figure 6.19c). The carboxyl group was positioned close to H323, H449 and Q286 although just out of H-bond distance. The hydroxyl group could make a H-bond to R288 and an additional H-bond to E295. The hydrophobic end was in a similar conformation to molecule A (figure 6.19d). The final position of the 15-HETE molecule in molecule B can be seen in figure 6.19e. As with the other molecules for both 12- and 15-HETE, after refinement the density was greatly reduced around the ligand (figure 6.19f).

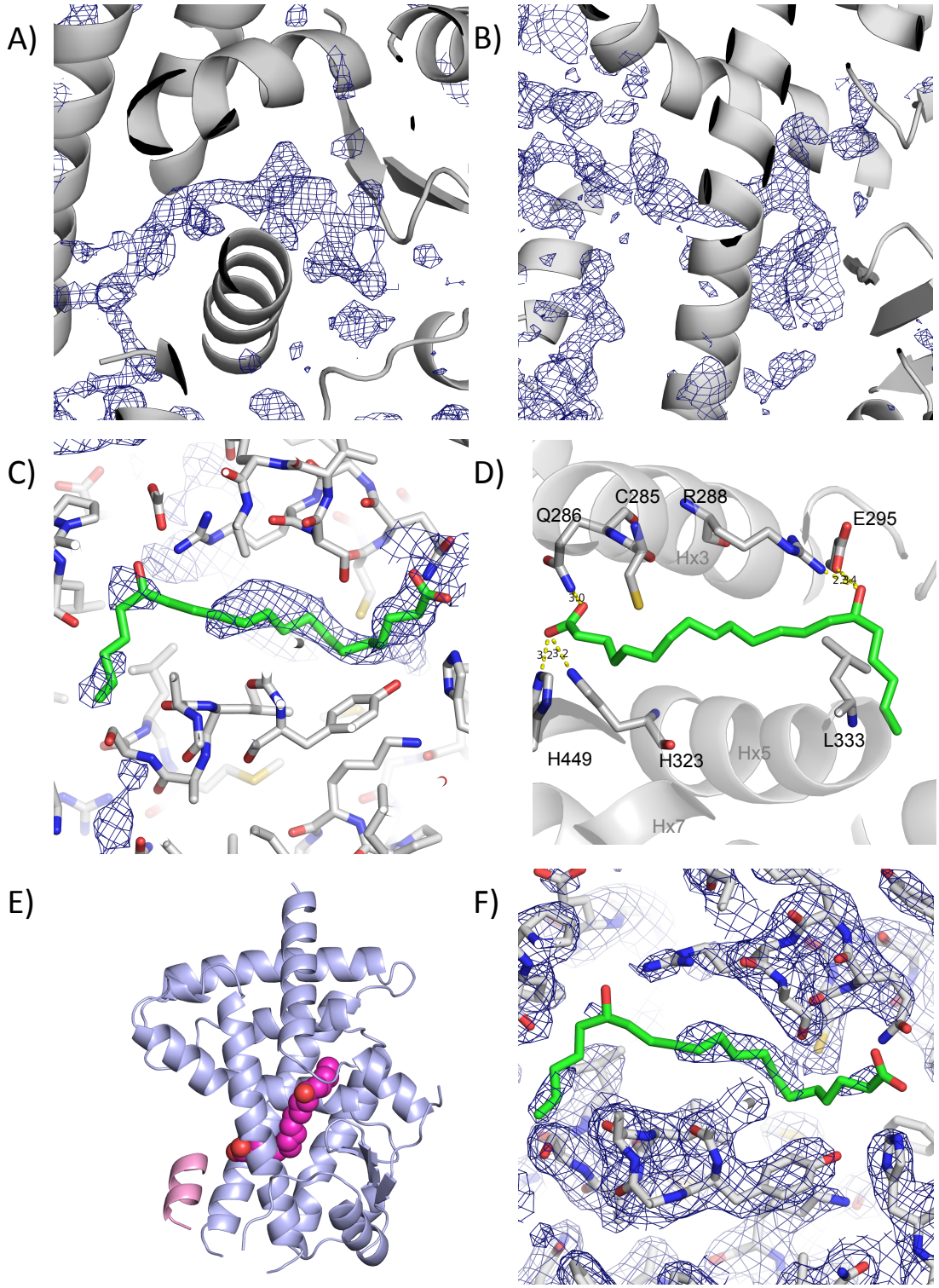

Figure 6.19: Identification and building of 15-HETE in the PPARγ-LBD molecule B

A) Density in the PPARγ-LBD after rebuilding and B) after calculation of simulated annealing composite omit map. C 15-HETE fitted in density and D) specific contacts made between 15-HETE and the main chain. E) Final position of 15-HETE in the PPARγ-LBD and F) density in PPARγ-LBD after refinement.

6.4 Discussion

The aim of this chapter was to extend the molecular findings of Chapter 5 that identified PPARγ as a regulator of monocyte *tfpi* expression and that activated platelets release potential PPARγ agonists. This would be achieved through biochemical and structural techniques aimed at identifying whether the most abundant 12-LOX metabolite 12-HETE could activate PPARγ as well its isomer 15-HETE, and if crystal structures could be solved of these 2 molecules in complex with the PPARγ-LBD. The main findings of this chapter are summarised below:

i. 12-HETE (5μM) caused a small but significant increase in PPARγ activity as measured by luciferase expression
ii. 15-HETE (10 and 20μM) caused large significant increase in PPARγ activity
iii. Crystal structures of the PPARγ-LBD were solved after co-crystallisation with both 12- and 15-HETE and were similar to those already published
iv. After re-building, potential density was observed in the ligand-binding site for the 12-HETE crystal and 1 molecule of 12-HETE was modelled into both molecules, however this was diminished after refinement
v. After rebuilding, potential density was observed in the ligand-binding site for the 15-HETE crystal and 2 molecules of 15-HETE were modelled into molecule A and 1 into molecule B. After refinement density was still present around some of the molecule but was not contiguous, possibly due to a not fully occupied pocket

The results from this chapter confirm that two oxylipins released from platelets are able to activate PPARγ and provides evidence of the structural characteristics of binding. As shown in chapter 5, 12-HETE was the most abundant oxylipin released by activated platelets and it was predicted that this may be relevant *in vivo*. The second oxylipin, 15-HETE, is i) structurally related to 12-HETE, ii) the major product produced by monocyte 15-LOX (Deleuran et al., 1995; KUHN et al., 1994; Nassar et al., 1994) and iii) has already been shown to activate PPARγ (Nagy et al., 1998). 15-HETE was chosen based on the RT-qPCR results from chapter 3 and MS experiments from chapter 5. Monocyte *tfpi* expression was reduced by a similar amount when either 12-LOX or COX-1 was inhibited (~45%) and although dual inhibition was additive, expression was only attenuated by a further ~20%. MS analysis revealed COX-1 inhibition abrogated TxA2 and PGD/E2 release and significantly reduced 11- and 15-HETE and 9- and

13-HODE suggesting one of these could mediate *tfpi* expression. 12-LOX inhibition also significantly reduced the same oxylipins (as well as all others bar AA and 9-HETE); with complete reduction in TxA2, PGD/E2, 11-HETE and 9- and 13-HODE. There was still a small amount of 15-HETE released. As 15-HETE was the only oxylipin not to be completely inhibited by either 12-LOX or COX-1 inhibition it is likely this is responsible for some monocyte *tfpi* induction.

Other oxylipins that could regulate PPARγ include TxA2, a carboxylic acid that is not dissimilar in structure to 15d-PGJ2, the most potent known natural ligand for PPARγ (figure 6.19a). However, due its short half life, predicted to be only ~30s (Hamberg and B, 1974), it would be impossible to use in experiments. The stable metabolite TxB2 is structurally similar to TxA2 (figure 6.19b) and has a much longer half-life, however evidence for a biological role for TxB2 is lacking with many reports associating increased levels with various pathological conditions (Dewitt et al., 1988; Lieb et al., 1983; Tada et al., 1981) but whose source is likely to be from platelet-derived TxA2. For these reasons, thromboxane's were not used in crystallography experiments.

PGD/E2, 9-HODE, 13-HODE and 11-HETE were not chosen for further work as we could not be sure which PG it was (D or E) and 9- and 13-HODE have already been shown to activate PPARγ and have been crystallised with PPARγ (Itoh et al., 2008). 11-HETE is related to 12-HETE but little is known regarding its production and function, with its most well documented role being in the neutrophil and eosinophil chemotactic response (Goetzl and Pickett, 1980; Goetzl et al., 1980). It would have been interesting to test the other oxylipins identified but for issues of time and cost the 12- and 15-HETE were the most appropriate.

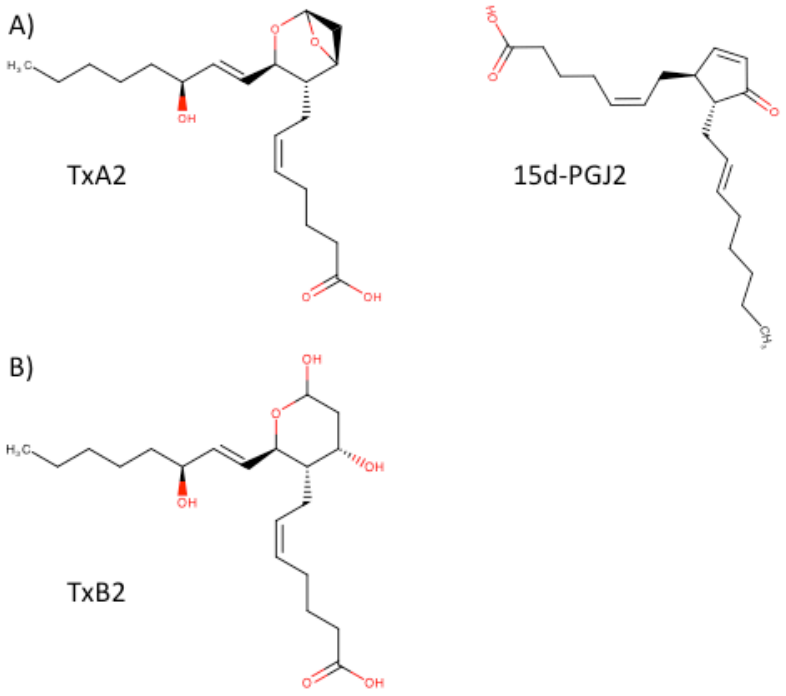

Figure 6.20: Structural comparison of 15d-PGJ2, TxA2 and TxB2

A) Comparison of 15d-PGJ2 with the second major platelet metabolite TxA2 and B) structure of the TxA2 stable metabolite TxB2. Figure made using Marvin Sketch.

The results from the transactivation assays confirmed reports from previous studies that 15d-PGJ2, rosiglitazone and 15-HETE can all activate PPARγ (Forman et al., 1995; Nagy et al., 1998; Thouennon et al., 2015). Interestingly, Nagy et al reported a 3-fold increase in PPARγ activity with 20µg/ml 15-HETE, equivalent to 62.5µM and here 15-HETE caused a 3.1-fold increase in activity with 20µM, which may reflect cell type used and construct. Results from the 12-HETE activation assays showed a 1.4-fold increase in PPARγ activity at 5µM. Higher concentrations of 12-HETE resulted in decreased activity, likely due to the concentration of DMSO, which was toxic to the cells. Due to the cost of 12-HETE and the relatively low stock concentration purchased the final concentration of DMSO in the experimental samples was high. If this were to be taken forward in the future, a collaboration with Toshimasa Itoh would be established who would synthesise 12-HETE in a powder form and allow higher stock concentrations to be made. Had the DMSO concentration been lower and uniform throughout the treatments, 12-HETE was likely to activate PPARγ to a similar if not higher degree as 15-HETE as at 5µM 12- and 15-HETE induced a 1.4 and 1.25-fold increase respectively. Previous reports in the literature have lead to confusion as to whether 12-HETE is able to activate PPARγ. The earliest paper by Yu et al showed no

activation of PPARγ with HETE's 8-15 (including 12-HETE) but this was probably due to using sub-micromolar concentrations (Yu et al., 1995). Then in 2003/4 Westergaard et al and Li et al showed 12-HETE, at 5μM, activated PPARγ (Q. Li et al., 2004; Westergaard et al., 2003). As with the results presented here, Li et al showed 12-HETE induced higher activity at 5μM than 15-HETE but this was reversed when PPARγ's partner RXR was co-expressed. Other papers have referenced work that does not show 12-HETE activation of PPARγ (Abdelrahman et al., 2005; Penumetcha and Santanam, 2012). These results are consistent with the 2003/4 papers and show that 12-HETE is able to activate PPARγ.

The crystallography results strongly indicated the presence of both 12- or 15-HETE in the PPARγ-LBD. Unfortunately, after refinement contiguous density around either ligand was not observed. Due to time constraints, further work on model building and refinement could not be carried out during the PhD, although there are a number of ways to continue building to improve the model and electron density maps. One such way is to merge the datasets from a number of crystals. As a crystal is rotated in the X-ray beam it begins to deteriorate through radiation damage, this leads to loss of resolution and data quality. By merging datasets from multiple crystals different regions will have deteriorated in different crystals, which may lead to a higher quality dataset (Foadi et al., 2013). Further work to improve the model and therefore the electron density may be achieved by adding residues into density. Missing residues are most likely to occur in mobile regions such as those found connecting secondary structure. Building in these residues may improve the overall density of the map as a small change in one part of the structure can have a large effect in another. Two such areas where this would be advantageous is the loop between Hx2' and Hx3 (figure 6.21a) in both subunits (12- and 15-HETE models) and C-terminus of subunit B in the 12-HETE model. Here the loop connecting Hx11 to Hx12 is truncated and Hx12 is not a well-defined helix (figure 6.21b).

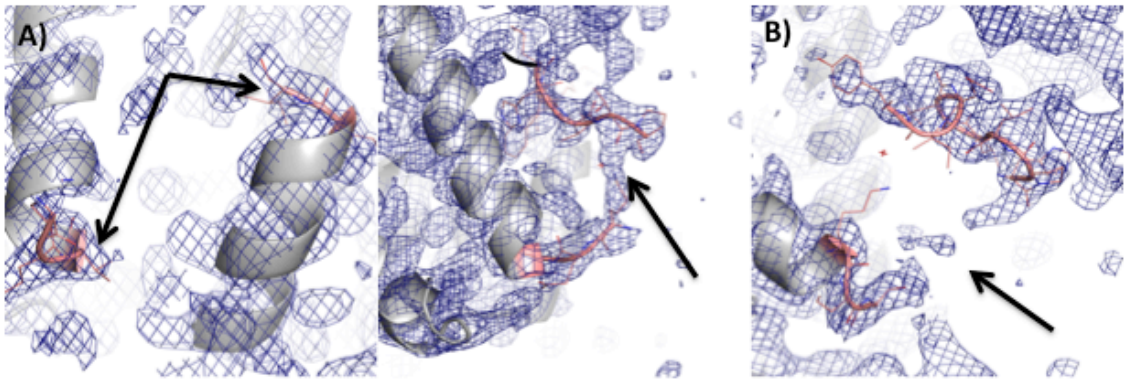

Figure 6.21: Missing regions in PPARγ-LBD models

A) Missing AA's in the loop region between Hx2' and Hx3 in both subunits A (left) and B (right). Representative figures using 12-HETE model but relevant for the 15-HETE model. B) Missing AA's between Hx11 and Hx12 and incomplete Hx12 in subunit B of 12-HETE model.

Finally, the position and number of ligands within the LBD can influence refinement and final electron density. Due to time constraints, the ligands where modelled based on where ligands are positioned in other deposited structures, with the carboxyl group within H-bond distance with H323, H449 and Y473 as both synthetic ligands (Furukawa et al., 2012; Ohashi et al., 2011) and potent natural ligands have been shown to bind close to the this cluster of AmA's, including 15d-PGJ2, 8-oxoETE (Waku et al., 2009), 9-HODE, 5-HEPA, 4-oxoDHA, 4-HDHA and 6-oxoOTE (Itoh et al., 2008). However, whilst the synthetic ligands usually adopt similar conformations around Hx3, natural ligands have been shown in multiple conformations (figure 6.22a). Some other natural ligands have been shown to adopt less conventional positions in the ligand binding domain such as 9-HODE, 13-HODE and 15-oxoETE (figure 6.22b) and 9-HODE has also been shown to have 2 molecules present in subunit A (figure 6.22c). As well as all the different conformations, due to the 1300Å^3 size of the LBD, some ligands have also been shown to bind covalently to C285 (figure 2.22d).

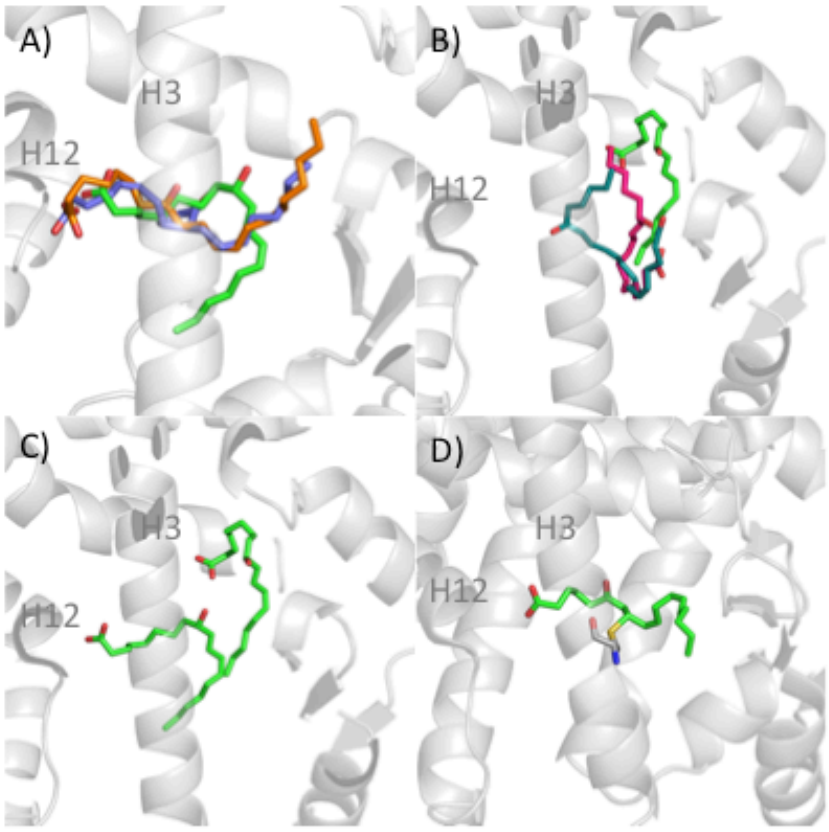

Figure 6.22: Alternative modes of ligand binding in the PPARγ-LBD

A) Alternative conformations of hydrophobic ligand tails when carboxyl group is positioned at Hx12. B) Alternative conformations of ligands when not in contact with Hx12. C) Multiple 9-HODE ligands occupying PPAR-LBD. D) 6-oxoOTE covalent bound to C285 in Hx3 (Itoh et al., 2008; Waku et al., 2009).

Additionally, if 12- and 15-HETE are weak agonists, they may adopt multiple conformations within the LBD. This would mean the crystal lattice would contain multiple PPARγ-LBD's in a uniform array but 12- or 15-HETE may adopt 1 of x number of conformations in a molecule. This would produce density in the LBD, but, as was shown here, would disappear when a single ligand was fit in one conformation. Fitting multiple ligands in different conformations and reducing the occupancy of each ligand by a certain factor can sidestep this problem. Taking all these factors together, there are a number of different approaches to improve and refine the model to show density around the ligand.

The implications of these results would suggest that the major oxylipin, 12-HETE is able to bind to and activate PPARγ. It also suggests 15-HETE is able to activate PPARγ and as it is only partially inhibited by 12-LOX and COX-1 inhibition, may be the major oxylipin regulating *tfpi* expression. Both these oxylipins appear to bind to PPARγ in a manner similar to ligands already described and this data adds to the growing list of

naturally occurring ligands for PPARγ. This also adds to the current premise that PPARγ has no single ligand and acts as a general oxylipin sensor (Bishop-Bailey and Wray, 2003). This is in contrast to the argument that the natural agonists are not present at high enough concentrations *in vivo* to activate PPARγ (Nosjean and Boutin, 2002). Having showed 12-HETE and 15-HETE activate PPARγ it is now possible to suggest that activated platelets are able to activate PPARγ. This is further augmented by the additional PPARγ ligands already identified as released from platelets such as 9- and 13-HODE as well as the distinct possibility 11-HETE and TxA/B2 may activate PPARγ. Using the data from chapter 5 showing 211.9ng/ml 12-HETE is released from 600 x 10^9 platelets.L^{-1}, which converts to 661nM. Whilst this is not enough to activate PPARγ *in vitro* the combined concentration of all oxylipins may be enough *in vivo*. In addition, the local effective concentration may be higher within a thrombus due to the tight packing of cells.

To conclude, this chapter has provided biochemical and structural evidence for the activation of PPARγ by 2 platelet-derived oxylipins, but the structures need more work to be interpreted fully.

Chapter 7: Perspectives

The current failure or lack off potent drugs to combat atherothrombosis raises the need for new targets to be identified. One such target is monocytes, whose importance in atherosclerosis is already well established but who are also becoming increasingly recognised as important contributors to both venous and arterial thrombosis. However, the current understanding of the role monocytes play within these processes is limited and more research is required if they are to be considered a viable target for treatment. Currently, most research surrounding monocytes has focused on their differentiation to macrophages in atherosclerosis and the induction of gene and protein expression in response to inflammatory stimuli or cytokines and chemokines. Much less research has looked at how activated platelets talk to monocytes; a process likely to be highly important due to the role platelets play in both atherosclerosis and thrombosis. The most well studied role of platelets is the induction of TF in monocytes by P-selectin (Celi et al., 1994), although there is some evidence for roles in the resolution of venous thrombosis through expression of tissue plasminogen activator and urokinase and in recanalization (Moldovan and Asahara, 2003; Soo et al., 1996).

The aim of this thesis therefore was to explore the mechanisms by which platelets, once activated through the primary signalling receptor GPVI, can 'talk' to monocytes, either through direct contact or secreted molecules and signal them to switch on the expression of a number of genes. This work was based on two previous studies, the first had investigated the effect of platelet activation on monocyte gene expression, a large number were found to be differentially expressed after incubation with activated platelets for 4h. Whilst all of the genes warrant further study to determine the role they may play in atherothrombosis, focus was drawn towards two genes in particular, *tfpi* and *procr,* which play important roles in regulation coagulation and their up-regulation is in contrast to the consensus that platelets induce a pro-thrombotic phenotype in monocytes by upregulating TF expression (Celi et al., 1994). Furthermore, these two genes were shown to be expressed at lower levels in STEMI patients. The second study measured platelet-induced monocyte gene expression after 2h and found the transcription factor PPARγ to be highly induced, a protein associated with negatively regulating atherosclerosis (Wang et al., 2011).

The results presented here can largely be divided into three sections; regulation of gene expression of monocyte *pparγ*, regulation of gene expression of monocyte *tfpi* and

regulation of gene expression of monocyte *procr*. The nuclear transcription factor Gene expression of *pparγ* was found to be induced in monocytes by activated platelets maximally at 2h, was largely through direct contact (P-selectin•PSGL-1 interaction) although there was some regulation through both released proteins (negative) and oxylipins (positive) and was increased in the presence of aspirin, probably as a consequence of increased MPA formation resulting from reduced platelet aggregation. Although further study would be required, this could be important in atherosclerosis and explain the origin of plaque macrophage PPARγ and, as will be discussed later, macrophage TFPI. Platelets are known to be important in the initiation of atherosclerosis, binding to monocytes and inducing the expression of adhesive proteins (Huo et al., 2003). In addition, this direct contact could induce the expression of PPARγ, which is present at low levels in circulating monocytes (Chinetti et al., 1998). The extravasation of monocytes through the endothelium and differentiation into macrophages could then result in the production of 15-HETE, one of the most abundant plaque oxylipins (T. C. Simon et al., 1989), and agonist for PPARγ. The activation of PPARγ by 15-HETE could drive expression of target genes such as TIMP's, LXR and TFPI as well negatively regulating inflammatory gene expression through modulation of NF-κB (figure 7.1). Interestingly, PPARγ has recently been shown to regulate macrophage expression of ADTRP (Chinetti-Gbaguidi et al., 2015), a protein associated with regulation and co-expression of TFPI (Lupu et al., 2011). Activation of PPARγ has already been proposed for the treatment of atherosclerosis, and *in vitro* and *in vivo* observations show PPARγ activation has many beneficial roles on processes related to atherosclerosis. For example, PPARγ activation has been shown to reduce inflammatory gene expression (C. Jiang et al., 1998) and increase cholesterol efflux (Chawla et al., 2001) in macrophages; inhibit the pro-inflammatory phenotype in endothelial cells (S. M. Jackson et al., 1999); and decrease SMC migration and proliferation (Heo et al., 2007).

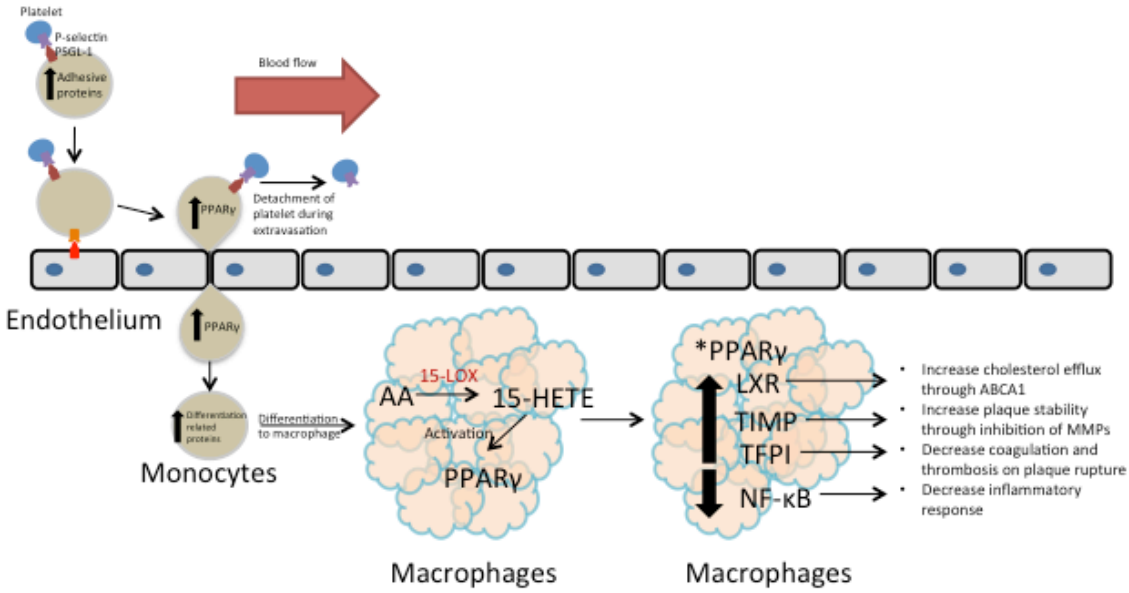

Figure 7. 1 Potential implications of platelet-induced monocyte pparγ in vivo

Increased monocyte expression of pparγ by activated platelets may lay the foundation for expression of PPARγ responsive genes in plaque macrophages in atherosclerosis.

Whilst the regulation of monocyte *pparγ* gene expression may be important in atherosclerosis, it may play an equally important role in thrombosis. PPARγ agonists have already been shown to increase the time to occlusive thrombi formation in an animal model (D. Li et al., 2005) and inhibit thrombus formation *in vitro* using human blood, with limited effects on thrombus stability (Moraes et al., 2010); although these effects have been attributed to activation of platelet, as opposed to monocyte, PPARγ. Concerns had been raised regarding an increased risk of heart failure and MI in diabetes patients taking rosiglitazone or pioglitazone (Nissen and Wolski, 2007) but this has since been revised on reanalysis of the data (Stone et al., 2015). PPARγ agonists have not been associated with decreased events in diabetes patients, although this is likely to be confounded by other pathologies commonly associated with diabetes such as obesity and metabolic syndrome. Whilst it is unlikely PPARγ regulates *tfpi* expression under normal conditions, after a thrombotic event such as an acute MI when patients are at increased risk of another infarction, and activated platelets have induced PPARγ protein expression, treatment with PPARγ agonists may prove beneficial in upregulating *tfpi* expression. Currently, results from clinical trials in man have been conflicting with both beneficial and deleterious effects such as those associated with rosiglitazone, highlighting that the regulation and role of PPARγ in CVD needs to be explored further (Wang et al., 2011).

Gene expression of monocyte *tfpi* and *procr* followed a similar pattern to begin with; both induced by activated platelets from 4h onwards, with no change when MPA formation was inhibited (suggesting a released molecule) and no difference in expression between platelet releasate and MP-free soluble mediators. Both were also similarly affected by inhibitors of COX-1 and 12-LOX. At this point it was found that proteins, most likely ~10kDa, were responsible for inducing monocyte *procr* expression and further experimental evidence pointed towards RANTES as a possible mediator, although this needs to be confirmed (figure 7.2). Expression of *tfpi*, in contrast, was found to be largely oxylipin mediated. Further experiments showed induction of *tfpi* expression on co-incubation with CRP-XL and PPARγ agonists although a similar indication was not seen in the absence of platelet-activation suggesting an initial PPARγ independent pathway (figure 7.2). Identified oxylipins released from platelets included a number of known and potential PPARγ agonists and two of the most interesting of these, 12- and 15-HETE were confirmed to both activate PPARγ and co-crystallise with the LBD.

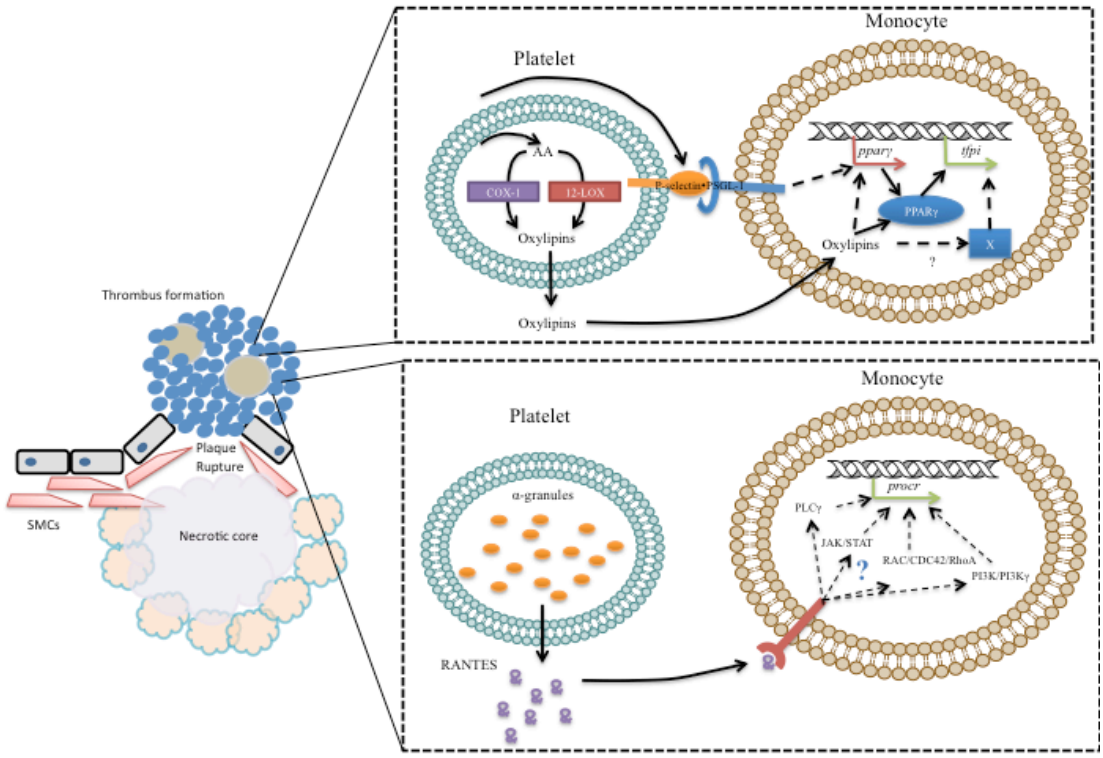

Figure 7. 2 Potential signalling pathway from platelets to monocytes for tfpi and procr in vivo

Potential signalling pathways that may regulate monocyte tfpi and procr expression by activated platelets within thrombus formation.

Whilst both *tfpi* and *procr* were found to be regulated by soluble mediators released from platelets, it is likely the regulation *in vivo* requires the formation of MPA's to allow the controlled transfer of these metabolites. MPA formation is dependent on platelet activation and are not normally present in significant numbers in the circulation of healthy individuals but have been shown to be increased in situations where platelets become activated in vivo; for example in acute MI (Furman et al., 2001), unstable angina (Zeng et al., 2014) and in response to inflammatory stimuli (Passacquale et al., 2011). In the circulation, formation of MPAs allows signalling through direct contact and for the transfer of soluble mediators to monocytes, which would otherwise be diluted in the blood stream.

It is well understood that soluble mediators derived from platelets can influence monocytes. To date, most evidence comes from the study of changes leading to the recruitment of monocytes to damaged endothelium during atherogenesis (Baltus et al., 2005). The majority of these studies have focused on the monocyte response to individual, known, platelet-derived molecules such as PF4, which has been shown to cause monocytes to differentiate into antigen presenting cells (Fricke et al., 2004). .Whilst these experiments have tried to single out specific molecules regulating expression of the genes being studied, the situation *in vivo* is likely to be complex; supported by the findings here that inhibiting COX-1 and 12-LOX gave only partial (~50%) inhibition of *tfpi* and *procr* expression (discussed in more detail below), suggesting there is likely to be redundancy in the factors involved in regulation of these genes.

Inhibition of both COX-1 and 12-LOX resulted in reduced expression of monocyte antithrombotic genes and whilst 12-LOX is yet to become a viable therapeutic target, COX-1 is inhibited in 100% of MI patients. As such these results may raise some questions regarding the clinical use of aspirin. Aspirin is effective for the immediate treatment of thrombosis. However if it also can simultaneously reduce the expression of key antithrombotic genes this might adversely affect thrombus stability. While the levels of *tfpi* and *procr* expression is probably not relevant in acute arterial thrombi, which are usually short-lived, this may be relevant in treatment of secondary MI and in venous thrombosis (e.g. DVT) where clots can persist for long periods of time. Increased levels of both TFPI (Dahm et al., 2003) and EPCR (Gandrille, 2008) are already associated with venous thrombosis. Being able to increase *tfpi* or *procr* expression over a few hours is probably a way of regulating clot growth and stability

In terms of acute thrombosis, the reduction in *tfpi* and *procr* by aspirin, mirrored by results from STEMI patients may explain the limitation of aspirin preventing secondary MI, which is effective in only 25% of patients (Antithrombotic Trialists' (ATT) Collaboration et al., 2009). An association between aspirin and plasma TFPI levels has been reported by Cheng et al., who observed decreased levels in stable STEMI patients (<3 months after an event) who were aspirin sensitive compared to those who were aspirin resistant (Cheng et al., 2007). Conversely, Bratseth et al., reported increased plasma levels in CAD patients (of which 44% had had a previous MI) who had taken aspirin for 12 months (Bratseth et al., 2012). This could suggest a mechanism whereby normal TFPI levels are predominantly endothelial cell-derived and aspirin independent, but after a thrombotic event or during CAD, the balance is tipped towards other sources such as monocytes that are dependent on oxylipin metabolites for *tfpi* transcription. Following resolution of thrombosis and inflammation (>3 months after the event), endothelial cells once again become the main contributor. It would be interesting to look at the effect of length of aspirin treatment on TFPI levels in plasma in STEMI patients over 12 months compared to healthy controls.

Aspirin has not been associated with EPCR levels but other oral anti-coagulants have been shown to lead to decreased levels of soluble EPCR compared to controls (Stearns-Kurosawa et al., 2002). However, whilst soluble EPCR can be measured in the plasma, it is derived from the cleavage of membrane bound EPCR and may not reflect gene regulation, but relate to the rate of cleavage and/or expression of the ADAM17 protease. To determine if aspirin does affect levels of membrane-bound EPCR an *in vivo* animal model could be used and EPCR levels measured histologically by analysis of the endothelium or alternatively, membrane-bound EPCR could be measured on peripheral blood monocytes and compared between people taking aspirin and controls.

Additionally, the role of RANTES warrants further study. Firstly it needs to be confirmed whether this chemokine can regulate *procr* expression. Further work identifying the signalling pathway may open new avenues to increase the level of EPCR, which could provide a route to reduce the thrombotic response, leading to improved outcomes.

Although inhibition of 12-LOX is not yet practised clinically, research suggests it could be an effective target in the future. Inhibition of 12-LOX has been shown to inhibit almost all platelet responses in response to agonists (Yeung et al., 2014; 2013). Research into the role of 12-LOX in platelets is limited and contradictory. The clearest

understanding of its role comes from a series of recent papers from Michael Holinstat's group in the US, who were also the first to suggest 12-LOX as a therapeutic target (Yeung and Holinstat, 2011). 12-LOX is unlikely to be involved in the initial formation of a platelet plug, as its activity is dependent in AA release and initial Ca^{2+} increase and so, like COX-1 and P2Y12 inhibitors, would act to inhibit the secondary phase of platelet activation making it an attractive therapeutic target. However, much more work is needed *ex vivo* using human platelets and *in vivo* animal studies to dissect out the exact mechanism of 12-LOX activity.

In addition to the potential regulatory pathways outlined above, this research was also the first, to our knowledge, to profile oxylipins formed from endogenous platelets AA and LA after activation through GPVI. These oxylipins are not only involved in activation of PPARγ but are, in their own right, signalling molecules that can elicit responses in a number of cell types. From this study, 15-HETE was identified as an important signalling molecule likely to be involved in *tfpi* regulation. The effect of 15-HETE on monocyte gene expression is unknown and it would be interesting to measure the global effect of this oxylipin via a genome-wide study. This would also be true for the other molecules where limited biological roles have been studied such as 11-HETE.

On a more global scale, GWE profiling of resting and 2h platelet-activated monocytes incubated with PPARγ agonists would identify the regulatory network in monocytes and could add weight to the idea of targeting PPARγ for the treatment of atherosclerosis and thrombosis. It would also be interesting to determine gene expression changes in monocytes in response to PF4 and RANTES. These experiments would show whether these elicit a response in monocytes characteristic of an anti-thrombotic phenotype rather than be specific for only *tfpi* and/or *procr*. Similarly longer-term culture of these monocytes to understand their pattern of differentiation would help clarify the likely consequences of the effects of platelets on monocytes.

Finally, these results could contribute to the management of bleeding disorders such as haemophilia's. A number of papers have recently demonstrated that blocking TFPI improves clotting time (Gorczyca et al., 2012) and thrombin generation in blood from haemophilia patients, mitigates bleeding in mice with haemophilia (Maroney et al., 2012), and shortens the bleeding time of haemophilia rabbits *in vivo* (Erhardtsen et al., 1995). Results from a recent phase I clinical trial using an anti-TFPI antibody showed increased clotting with minimal side effects (Chowdary et al., 2015). If TFPI levels

could be reduced through inhibition of PPARγ or oxylipin production via 12-LOX or COX-1, this may offer additional protection to patients with haemophilia. It would be interesting to note in diabetes patients with haemophilia whether aspirin reduces clotting time or, if they are on PPARγ agonists, increases bleeding time.

In summary, the work presented in this thesis makes an important contribution to the current understanding of cross-talk between platelets and monocytes. For the first time, monocyte *tfpi* and *procr* expression have been shown to be regulated by molecules released from activated platelets, which led to the identification of a novel oxylipin profile released from platelets activated through the GPVI receptor. It has also shown that *tfpi* expression can be increased in platelet-activated monocytes through activation of PPARγ and that 15-HETE is a potentially important signalling molecule released from platelets. This work opens up a number of exciting prospects relating to the regulation of monocyte gene expression by platelets for future consideration and may explain some clinical observations in the literature leading to better management of atherothrombotic disease.

Appendix

Appendix 1: NR-LBD screen from molecular dimensions

Well	Salt	Buffer	pH	Precipitant
A1	None	0.1 M Na HEPES	7.5	10 % w/v PEG 8K
A2	0.9 M sodium chloride	0.1 M Tris	8	6 % w/v PEG 8K
A3	0.5 M sodium chloride	0.1 M Bis Tris	6.5	19 % w/v PEG 4K
A4	0.2 M ammonium acetate	0.1 M Tris	8	13 % w/v PEG 6K
A5	None	0.1 M Tris	8	9% w/v PEG 8K
A6	0.2 M sodium chloride	0.1 M Na HEPES	7.5	24 % w/v PEG 4K
A7	None	0.1 M Na HEPES	7.5	12 % w/v PEG 8K
A8	None	0.1 M Na HEPES	7.5	18 % w/v PEG 6K
A9	None	0.1 M PIPES	7	7 % w/v PEG 8K
A10	0.1 M ammonium acetate	0.1 M Na HEPES	7.5	18 % w/v PEG 4K
A11	0.1 M ammonium acetate	0.1 M Na HEPES	7.5	8 % w/v PEG 4K
A12	0.3 M sodium chloride	0.1 M Bis Tris	6.5	27 % w/v PEG 4K
B1	0.3 M sodium chloride	0.1 M Bis Tris	6.5	16 % w/v PEG 4K
B2	None	0.1 M PIPES	7	23 % w/v PEG 4K
B3	1.2 M ammonium acetate	0.1 M Tris	8.5	14 % w/v PEG 4K
B4	0.4 M sodium chloride	0.1 M Tris	8	19 % w/v PEG 4K
B5	0.6 M sodium chloride	0.1 M PIPES	7	7 % w/v PEG 4K
B6	None	0.1 M Tris	8	15 % w/v PEG 6K
B7	None	0.1 M Tris	8	8 % w/v PEG 8K
B8	None	0.1 M PIPES	7	22 % w/v PEG 4K
B9	0.2 M sodium chloride	0.1 M Tris	8.5	10 % w/v PEG 8K
B10	0.5 M sodium chloride	0.1 M PIPES	7	14 % w/v PEG 6K
B11	0.4 M sodium chloride	0.1 M PIPES	7	20 % w/v PEG 4K
B12	None	0.1 M PIPES	7	17 % w/v PEG 4K
C1	None	0.1 M PIPES	7	1.0 M sodium acetate
C2	None	0.1 M Na HEPES	7.5	1.3 M sodium citrate
C3	0.2 M ammonium acetate	0.1 M Tris	8.5	3.0 M sodium formate
C4	0.1 M ammonium acetate	0.1 M Tris	8	1.0 M sodium citrate
C5	0.1 M ammonium acetate	0.1 M Na HEPES	7.5	1.6 M sodium acetate
C6	0.2 M ammonium acetate	0.1 M Na HEPES	7.5	1.2 M sodium citrate
C7	0.4 M sodium chloride	0.1 M Na HEPES	7.5	1.3 M sodium citrate
C8	None	0.1 M Na HEPES	7.5	1.6 M sodium acetate
C9	0.5 M sodium chloride	0.1 M Tris	8	0.9 M sodium acetate
C10	0.1 M ammonium acetate	0.1 M Bis Tris	6.5	1.0 M sodium citrate
C11	0.3 M sodium chloride	0.1 M Na HEPES	7.5	1.5 M sodium acetate
C12	0.3 M sodium chloride	0.1 M PIPES	7	2.6 M sodium formate
D1	None	0.1 M Bis Tris	6.5	1.4 M sodium acetate
D2	None	0.1 M PIPES	7	1.5 M sodium citrate
D3	0.8 M sodium chloride	0.1 M PIPES	7	1.2 M sodium citrate
D4	0.1 M ammonium acetate	0.1 M PIPES	7	2.5 M sodium formate

D5	0.1 M sodium chloride	0.1 M Bis Tris	6.5	2.0 M sodium formate
D6	0.4 M sodium chloride	0.1 M Bis Tris	6.5	1.0 M sodium citrate
D7	0.1 M ammonium acetate	0.1 M Na HEPES	7.5	1.0 M sodium citrate
D8	None	0.1 M Tris	8.5	1.3 M sodium acetate
D9	None	0.1 M Na HEPES	7.5	0.8 M sodium acetate
D10	None	0.1 M Tris	8	3.5 M sodium formate
D11	0.2 M ammonium acetate	0.1 M PIPES	7	2.7 M sodium formate
D12	0.5 M sodium chloride	0.1 M Na HEPES	7.5	2.2 M sodium formate
E1	0.1 M ammonium acetate	0.1M PIPES	7	21 % v/v PEG 400
E2	0.3 M sodium chloride	0.1M Na HEPES	7.5	25 % v/v PEG 400
E3	0.2 M ammonium sulfate	0.1M Bis Tris	6.5	28 % v/v PEG 400
E4	0.2 M magnesium chloride	0.1M Tris	8	20 % w/v PEG 2K MME
E5	0.1 M sodium chloride	0.1M PIPES	7	22 % w/v PEG 2K MME
E6	0.2 M sodium chloride	0.1M Bis Tris	6.5	19 % w/v PEG 2K MME
E7	None	0.1M Na HEPES	7.5	22 % w/v PEG 2K MME
E8	0.3 M ammonium sulfate	0.1M PIPES	7	11 % w/v PEG 4K
E9	0.5 M ammonium sulfate	0.1M PIPES	7	12 % w/v PEG 4K
E10	0.4 M sodium thiocyanate	0.1M Tris	8.5	13 % w/v PEG 4K
E11	0.2 M magnesium chloride	0.1M Na HEPES	7.5	15 % w/v PEG 4K
E12	0.2 M magnesium chloride	0.1M PIPES	7	22 % w/v PEG 4K
F1	0.2 M sodium thiocyanate	0.1M Bis Tris	6.5	23 % w/v PEG 4K
F2	Non e	0.1M Na HEPES	7.5	22 % w/v PEG 5K MME
F3	0.3 M ammonium sulfate	0.1M Tris	8.5	25 % w/v PEG 5K MME
F4	0.2 M ammonium acetate	0.1M PIPES	7	26 % w/v PEG 5K MME
F5	0.2 M magnesium chloride	0.1M Tris	8.5	7 % w/v PEG 6K
F6	0.2 M ammonium sulfate	0.1M Na HEPES	7.5	11 % w/v PEG 6K
F7	0.4 M sodium thiocyanate	0.1M Bis Tris	6.5	17 % w/v PEG 6K
F8	0.2 M sodium thiocyanate	0.1M Bis Tris	6.5	10 % w/v PEG 8K
F9	0.2 M magnesium chloride	0.1M PIPES	7	12 % w/v PEG 8K
F10	0.2 M ammonium sulfate	0.1M Bis Tris	6.5	14 % w/v PEG 8K
F11	0.1 M sodium thiocyanate	0.1M PIPES	7	15 % w/v PEG 8K
F12	0.1 M magnesium chloride	0.1M Na HEPES	7.5	18 % w/v PEG 8K
G1	0.1 M sodium thiocyanate	0.1M Tris	8.5	9 % w/v PEG 10K
G2	0.1 M ammonium sulfate	0.1M Na HEPES	7.5	12 % w/v PEG 10K
G3	0.2 M ammonium acetate	0.1M PIPES	7	16 % w/v PEG 10K
G4	0.2 M sodium thiocyanate	0.1M Tris	8.5	1.0 M sodium acetate
G5	0.1 M ammonium sulfate	0.1M Tris	8	1.1 M sodium citrate
G6	0.2 M magnesium chloride	0.1M Na HEPES	7.5	2.7 M sodium formate
G7	0.3 M ammonium acetate	0.1M Na HEPES	7.5	0.8 M sodium tartrate
G8	0.2 M sodium chloride	0.1M Bis Tris	6.5	0.8 M sodium tartrate
G9	0.1 M sodium thiocyanate	0.1M Tris	8	0.9 M sodium tartrate
G10	0.5 M ammonium sulfate	0.1M PIPES	7	0.9 M sodium tartrate
G11	0.2 M ammonium sulfate	0.1M Tris	8	1.1 M sodium tartrate
G12	0.1 M magnesium chloride	0.1M Na HEPES	7.5	1.1 M sodium tartrate
H1	0.2 M sodium thiocyanate	0.1M Bis Tris	6.5	0.7 M lithium sulfate

H2	0.1 M ammonium acetate	0.1M Na HEPES	7.5	0.8 M lithium sulfate
H3	0.2 M sodium chloride	0.1M Tris	8.5	1.0 M lithium sulfate
H4	0.1 M magnesium chloride	0.1M Na HEPES	7.5	1.1 M lithium sulfate
H5	Non e	0.1M Na HEPES	7.5	1.3 M lithium sulfate
H6	Non e	0.1M Bis Tris	6.5	1.4 M lithium sulfate
H7	0.2 M sodium chloride	0.1M PIPES	7	1.3 M ammonium sulfate
H8	0.2 M ammonium acetate	0.1M Na HEPES	7.5	1.4 M ammonium sulfate
H9	0.1 M magnesium chloride	0.1M Tris	8.5	1.5 M ammonium sulfate
H10	0.2 M sodium thiocyanate	0.1M PIPES	7	1.6 M ammonium sulfate
H11	0.3 M sodium chloride	0.1M Tris	8	1.7 M ammonium sulfate
H12	0.2 M sodium chloride	0.1M Tris	8	2.0 M ammonium sulfate

References

Abdelrahman, M., Sivarajah, A., Thiemermann, C., 2005. Beneficial effects of PPAR-{gamma} ligands in ischemia-reperfusion injury, inflammation and shock. Cardiovasc Res 65, 772–781. doi:10.1016/j.cardiores.2004.12.008

Adams, P.D., Afonine, P.V., Bunkóczi, G., Chen, V.B., Davis, I.W., Echols, N., Headd, J.J., Hung, L.W., Kapral, G.J., Grosse-Kunstleve, R.W., McCoy, A.J., Moriarty, N.W., Oeffner, R., Read, R.J., Richardson, D.C., Richardson, J.S., Terwilliger, T.C., Zwart, P.H., 2010. PHENIX: a comprehensive Python-based system for macromolecular structure solution. Acta Crystallogr Sect D Biol Crystallogr 66, 213–221.

Adler, D.H., Cogan, J.D., Phillips, J.A., Schnetz-Boutaud, N., Milne, G.L., Iverson, T., Stein, J.A., Brenner, D.A., Morrow, J.D., Boutaud, O., Oates, J.A., 2008. Inherited human cPLA2α deficiency is associated with impaired eicosanoid biosynthesis, small intestinal ulceration, and platelet dysfunction. J Clin Invest 118, 2121–2131. doi:10.1172/JCI30473

Ahamed, J., Belting, M., Ruf, W., 2005. Regulation of tissue factor-induced signaling by endogenous and recombinant tissue factor pathway inhibitor 1. Blood 105, 2384–2391. doi:10.1182/blood-2004-09-3422

Ahmad, F., Boulaftali, Y., Greene, T.K., Ouellette, T.D., Poncz, M., Feske, S., Bergmeier, W., 2011. Relative contributions of stromal interaction molecule 1 and CalDAG-GEFI to calcium-dependent platelet activation and thrombosis. J. Thromb. Haemost. 9, 2077–2086. doi:10.1111/j.1538-7836.2011.04474.x

Aleem, A.M., Jankun, J., Dignam, J.D., Walther, M., Kuehn, H., Svergun, D.I., Skrzypczak-Jankun, E., 2008. Human platelet 12-lipoxygenase, new findings about its activity, membrane binding and low-resolution structure. Journal of Molecular Biology 376, 193–209. doi:10.1016/j.jmb.2007.11.086

Andreou, A., Feussner, I., 2009. Lipoxygenases - Structure and reaction mechanism. Phytochemistry 70, 1504–1510. doi:10.1016/j.phytochem.2009.05.008

Antithrombotic Trialists' (ATT) Collaboration, Baigent, C., Blackwell, L., Collins, R., Emberson, J., Godwin, J., Peto, R., Buring, J., Hennekens, C., Kearney, P., Meade, T., Patrono, C., Roncaglioni, M.C., Zanchetti, A., 2009. Aspirin in the primary and secondary prevention of vascular disease: collaborative meta-analysis of individual participant data from randomised trials. Lancet 373, 1849–1860. doi:10.1016/S0140-6736(09)60503-1

Appay, V., Rowland-Jones, S.L., 2001. RANTES: a versatile and controversial chemokine. Trends Immunol. 22, 83–87.

Aprile, M., Ambrosio, M.R., D'Esposito, V., Beguinot, F., Formisano, P., Costa, V., Ciccodicola, A., 2014. PPARG in Human Adipogenesis: Differential Contribution of Canonical Transcripts and Dominant Negative Isoforms. PPAR Research 2014, 537865–11. doi:10.1155/2014/537865

Attar, El, T., Lin, H.S., Vanderhoek, J.Y., 1985. Biosynthesis of prostaglandins and hydroxy fatty acids in primary squamous carcinomas of head and neck in humans. Cancer letters. doi:10.1016/0304-3835(85)90182-X

Baba, A., Sakuma, S., Okamoto, H., Inoue, T., Iwata, H., 1989. Calcium induces membrane translocation of 12-lipoxygenase in rat platelets. J. Biol. Chem. 264, 15790–15795.

Bailey, J.M., Bryant, R.W., Whiting, J., Salata, K., 1983. Characterization of 11-Hete

and 15-Hete, Together with Prostacyclin, as Major Products of the Cyclooxygenase Pathway in Cultured Rat Aorta Smooth-Muscle Cells. J. Lipid Res. 24, 1419–1428.
Bajaj, M.S., Ghosh, M., Bajaj, S.P., 2007. Fibronectin-adherent monocytes express tissue factor and tissue factor pathway inhibitor whereas endotoxin-stimulated monocytes primarily express tissue factor: physiologic and pathologic implications. Journal of Thrombosis and Haemostasis 5, 1493–1499. doi:10.1111/j.1538-7836.2007.02604.x
Baltus, T., Hundelshausen, von, P., Mause, S.F., Buhre, W., Rossaint, R., Weber, C., 2005. Differential and additive effects of platelet-derived chemokines on monocyte arrest on inflamed endothelium under flow conditions. J Leukoc Biol 78, 435–441. doi:10.1189/jlb.0305141
Barclay, J.W., Craig, T.J., Fisher, R.J., Ciufo, L.F., Evans, G.J.O., Morgan, A., Burgoyne, R.D., 2003. Phosphorylation of Munc18 by protein kinase C regulates the kinetics of exocytosis. J. Biol. Chem. 278, 10538–10545. doi:10.1074/jbc.M211114200
Barstad, R.M., Hamers, M., Kierulf, P., Westvik, AB, Sakariassen, K.S., 1995. Procoagulant Human Monocytes Mediate Tissue Factor Factor Viia-Dependent Platelet-Thrombus Formation When Exposed to Flowing Nonanticoagulated Human Blood. Arterioscler. Thromb. Vasc. Biol. 15, 11–16.
Basavaraj, M.G., Gruber, F.X., Sovershaev, M., Appelbom, H.I., Østerud, B., Petersen, L.C., Hansen, J.-B., 2010. The role of TFPI in regulation of TF-induced thrombogenicity on the surface of human monocytes. Thromb. Res. 126, 418–425. doi:10.1016/j.thromres.2010.07.014
Belaaouaj, A.A., Li, A., Wun, T.C., Welgus, H.G., Shapiro, S.D., 2000. Matrix metalloproteinases cleave tissue factor pathway inhibitor. Effects on coagulation. J. Biol. Chem. 275, 27123–27128. doi:10.1074/jbc.M004218200
Benjamin A Garcia, David M Smalley, HyungJun Cho, Jeffrey Shabanowitz, Klaus Ley, A., Donald F Hunt, 2005. The Platelet Microparticle Proteome. J. Proteome Res. 4, 1516–1521. doi:10.1021/pr0500760
Bentfeld-Barker, M.E., Bainton, D.F., 1982. Identification of primary lysosomes in human megakaryocytes and platelets. Blood 59, 472–481.
Berger, J., Bailey, P., Biswas, C., Cullinan, C.A., Doebber, T.W., Hayes, N.S., Saperstein, R., Smith, R.G., Leibowitz, M.D., 1996. Thiazolidinediones produce a conformational change in peroxisomal proliferator-activated receptor-gamma: binding and activation correlate with antidiabetic actions in db/db mice. Endocrinology 137, 4189–4195. doi:10.1210/endo.137.10.8828476
Berger, J., Moller, D.E., 2002. The mechanisms of action of PPARs. Annu. Rev. Med. 53, 409–435. doi:10.1146/annurev.med.53.082901.104018
Berger, J.S., Roncaglioni, M.C., Avanzini, F., Pangrazzi, I., Tognoni, G., Brown, D.L., 2006. Aspirin for the Primary Prevention of Cardiovascular Events in Women and Men: A Sex-Specific Meta-analysis of Randomized Controlled Trials. JAMA 295, 306–313. doi:10.1001/jama.295.3.306
Bergmeier, W., Piffath, C.L., Goerge, T., Cifuni, S.M., Ruggeri, Z.M., Ware, J., Wagner, D.D., 2006. The role of platelet adhesion receptor GPIbalpha far exceeds that of its main ligand, von Willebrand factor, in arterial thrombosis. PNAS 103, 16900–16905. doi:10.1073/pnas.0608207103
Berliner, J.A., Navab, M., Fogelman, A.M., Frank, J.S., Demer, L.L., Edwards, P.A., Watson, A.D., Lusis, A.J., 1995. Atherosclerosis - Basic Mechanisms - Oxidation, Inflammation, and Genetics. Circulation 91, 2488–2496.
Berridge, M.J., Bootman, M.D., Roderick, H.L., 2003. Calcium signalling: dynamics,

homeostasis and remodelling. Nat. Rev. Mol. Cell Biol. 4, 517–529. doi:10.1038/nrm1155

Bishop-Bailey, D., Wray, J., 2003. Peroxisome proliferator-activated receptors: a critical review on endogenous pathways for ligand generation. Prostaglandins Other Lipid Mediat. 71, 1–22.

Blair, P., Flaumenhaft, R., 2009. Platelet α-granules: Basic biology and clinical correlates. Blood Reviews 23, 177–189. doi:10.1016/j.blre.2009.04.001

Blajchman, M.A., 1994. An overview of the mechanism of action of antithrombin and its inherited deficiency states. Blood Coagulation & Fibrinolysis 5 Suppl 1, S5–11–discussion S59–64.

Bouhlel, M.A., Derudas, B., Rigamonti, E., Dièvart, R., Brozek, J., Haulon, S., Zawadzki, C., Jude, B., Torpier, G., Marx, N., Staels, B., Chinetti-Gbaguidi, G., 2007. PPARgamma activation primes human monocytes into alternative M2 macrophages with anti-inflammatory properties. Cell Metab. 6, 137–143. doi:10.1016/j.cmet.2007.06.010

Boyle, J.J., Weissberg, P.L., Bennett, M.R., 2003. Tumor necrosis factor-alpha promotes macrophage-induced vascular smooth muscle cell apoptosis by direct and autocrine mechanisms. Arterioscler. Thromb. Vasc. Biol. 23, 1553–1558. doi:10.1161/01.ATV.0000086961.44581.B7

Bratseth, V., Pettersen, A.A., Opstad, T.B., Arnesen, H., Seljeflot, I., 2012. Markers of hypercoagulability in CAD patients. Effects of single aspirin and clopidogrel treatment. Thromb J 10, 12. doi:10.1186/1477-9560-10-12

Braunersreuther, V., Steffens, S., Arnaud, C., Pelli, G., Burger, F., Proudfoot, A., Mach, F., 2008. A novel RANTES antagonist prevents progression of established atherosclerotic lesions in mice. Arterioscler. Thromb. Vasc. Biol. 28, 1090–1096. doi:10.1161/ATVBAHA.108.165423

Braunersreuther, V., Zernecke, A., Arnaud, C., Liehn, E.A., Steffens, S., Shagdarsuren, E., Bidzhekov, K., Burger, F., Pelli, G., Luckow, B., Mach, F., Weber, C., 2007. Ccr5 but not Ccr1 deficiency reduces development of diet-induced atherosclerosis in mice. Arterioscler. Thromb. Vasc. Biol. 27, 373–379. doi:10.1161/01.ATV.0000253886.44609.ae

Brown, M.S., Ho, Y.K., Goldstein, J.L., 1980. The cholesteryl ester cycle in macrophage foam cells. Continual hydrolysis and re-esterification of cytoplasmic cholesteryl esters. J. Biol. Chem. 255, 9344–9352.

Broze, G.J., 1995. Tissue factor pathway inhibitor and the current concept of blood coagulation. Blood Coagulation & Fibrinolysis 6 Suppl 1, S7–13.

Broze, G.J., 1992. The role of tissue factor pathway inhibitor in a revised coagulation cascade. Semin. Hematol. 29, 159–169.

Buchanan, M.R., Horsewood, P., Brister, S.J., 1998. Regulation of endothelial cell and platelet receptor-ligand binding by the 12- and 15-lipoxygenase monohydroxides, 12-, 15-HETE and 13-HODE. Prostaglandins Leukot. Essent. Fatty Acids 58, 339–346. doi:10.1016/S0952-3278(98)90069-2

Burkhart, J.M., Vaudel, M., Gambaryan, S., Radau, S., Walter, U., Martens, L., Geiger, J., Sickmann, A., Zahedi, R.P., 2012. The first comprehensive and quantitative analysis of human platelet protein composition allows the comparative analysis of structural and functional pathways. Blood 120, e73–82. doi:10.1182/blood-2012-04-416594

Capdevila, J., Yadagiri, P., Manna, S., Falck, J.R., 1986. Absolute configuration of the hydroxyeicosatetraenoic acids (HETEs) formed during catalytic oxygenation of arachidonic acid by microsomal cytochrome P-450. Biochemical and Biophysical

Research Communications 141, 1007–1011.
Caplice, N.M., Mueske, C.S., Kleppe, L.S., Peterson, T.E., Broze, G.J., Simari, R.D., 1998. Expression of tissue factor pathway inhibitor in vascular smooth muscle cells and its regulation by growth factors. Circ. Res. 83, 1264–1270.
Catella-Lawson, F., Reilly, M.P., Kapoor, S.C., Cucchiara, A.J., DeMarco, S., Tournier, B., Vyas, S.N., FitzGerald, G.A., 2001. Cyclooxygenase inhibitors and the antiplatelet effects of aspirin. N. Engl. J. Med. 345, 1809–1817. doi:10.1056/NEJMoa003199
Celi, A., Pellegrini, G., Lorenzet, R., Deblasi, A., Ready, N., Furie, B.C., Furie, B., 1994. P-Selectin Induces the Expression of Tissue Factor on Monocytes. PNAS 91, 8767–8771.
Chandra, V., Huang, P., Hamuro, Y., Raghuram, S., Wang, Y., Burris, T.P., Rastinejad, F., 2008. Structure of the intact PPAR-gamma-RXR- nuclear receptor complex on DNA. Nature 456, 350–356. doi:10.1038/nature07413
Chawla, A., Boisvert, W.A., Lee, C.-H., Laffitte, B.A., Barak, Y., Joseph, S.B., Liao, D., Nagy, L., Edwards, P.A., Curtiss, L.K., Evans, R.M., Tontonoz, P., 2001. A PPARγ-LXR-ABCA1 Pathway in Macrophages Is Involved in Cholesterol Efflux and Atherogenesis. Mol. Cell 7, 161–171. doi:10.1016/S1097-2765(01)00164-2
Chen, L., Chen, Y., Zhang, S., Ye, L., Cui, J., Sun, Q., Li, K., Wu, H., Liu, L., 2015. MiR-540 as a Novel Adipogenic Inhibitor Impairs Adipogenesis Via Suppression of PPARγ. J. Cell. Biochem. n/a–n/a. doi:10.1002/jcb.25050
Chen, V.M., Hogg, P.J., 2013. Encryption and decryption of tissue factor. J. Thromb. Haemost. 11 Suppl 1, 277–284. doi:10.1111/jth.12228
Cheng, G., Shan, J., Xu, G., Liu, P., Zhou, Y., Zhu, Y., Lu, X., 2007. Relationship between endothelial dysfunction, oxidant stress and aspirin resistance in patients with stable coronary heart disease. J Clin Pharm Ther 32, 287–292. doi:10.1111/j.1365-2710.2007.00823.x
Chinetti, G., Griglio, S., Antonucci, M., Torra, I.P., Delerive, P., Majd, Z., Fruchart, J.-C., Chapman, J., Najib, J., Staels, B., 1998. Activation of Proliferator-activated Receptors α and γ Induces Apoptosis of Human Monocyte-derived Macrophages. J. Biol. Chem. 273, 25573–25580. doi:10.1074/jbc.273.40.25573
Chinetti-Gbaguidi, G., Copin, C., Derudas, B., Vanhoutte, J., Zawadzki, C., Jude, B., Haulon, S., Pattou, F., Marx, N., Staels, B., 2015. The coronary artery disease-associated gene C6ORF105 is expressed in human macrophages under the transcriptional control of PPARγ. FEBS Lett. doi:10.1016/j.febslet.2015.01.002
Cho, H.-Y., Gladwell, W., Wang, X., Chorley, B., Be, D., Reddy, S.P., Kleeberger, S.R., 2010. Nrf2-regulated PPAR gamma Expression Is Critical to Protection against Acute Lung Injury in Mice. American Journal of Respiratory and Critical Care Medicine 182, 170–182. doi:10.1164/rccm.200907-1047OC
Chowdary, P., Lethagen, S., Friedrich, U., Brand, B., Hay, C., Abdul Karim, F., Klamroth, R., Knoebl, P., Laffan, M., Mahlangu, J., Miesbach, W., Dalsgaard Nielsen, J., Martín-Salces, M., Angchaisuksiri, P., 2015. Safety and pharmacokinetics of anti-TFPI antibody (concizumab) in healthy volunteers and patients with hemophilia: a randomized first human dose trial. J. Thromb. Haemost. 13, 743–754. doi:10.1111/jth.12864
Christersson, C., Johnell, M., Siegbahn, A., 2008. Tissue factor and IL8 production by P-selectin-dependent platelet-monocyte aggregates in whole blood involves phosphorylation of Lyn and is inhibited by IL10. J. Thromb. Haemost. 6, 986–994. doi:10.1111/j.1538-7836.2008.02956.x
Chung, S.H., Polgar, J., Reed, G.L., 2000. Protein kinase C phosphorylation of syntaxin

4 in thrombin-activated human platelets. J. Biol. Chem. 275, 25286–25291. doi:10.1074/jbc.M004204200

Cifuni, S.M., Wagner, D.D., Bergmeier, W., 2008. CalDAG-GEFI and protein kinase C represent alternative pathways leading to activation of integrin alphaIIbbeta3 in platelets. Blood 112, 1696–1703. doi:10.1182/blood-2008-02-139733

Clemetson, K.J., 2012. Platelets and Primary Haemostasis. Thromb. Res. 129, 220–224. doi:10.1016/j.thromres.2011.11.036

Coffey, M.J., Coles, B., Locke, M., Bermúdez-Fajardo, A., Williams, P.C., Jarvis, G.E., O'Donnell, V.B., 2004a. Interactions of 12-lipoxygenase with phospholipase A2 isoforms following platelet activation through the glycoprotein VI collagen receptor. FEBS Lett. 576, 165–168. doi:10.1016/j.febslet.2004.09.007

Coffey, M.J., Jarvis, G.E., Gibbins, J.M., Coles, B., Barrett, N.E., Wylie, O.R.E., O'Donnell, V.B., 2004b. Platelet 12-lipoxygenase activation via glycoprotein VI: involvement of multiple signaling pathways in agonist control of H(P)ETE synthesis. Circ. Res. 94, 1598–1605. doi:10.1161/01.RES.0000132281.78948.65

Collaborative Computational Project, Number 4, 1994. The CCP4 suite: programs for protein crystallography. Acta Crystallogr Sect D Biol Crystallogr 50, 760–763. doi:10.1107/S0907444994003112

Collaborative overview of randomised trials of antiplatelet therapy Prevention of death, myocardial infarction, and stroke by prolonged antiplatelet therapy in various categories of patients, 1994. Collaborative overview of randomised trials of antiplatelet therapy Prevention of death, myocardial infarction, and stroke by prolonged antiplatelet therapy in various categories of patients. Br Med J (Clin Res Ed) 308, 81–106. doi:10.1136/bmj.308.6921.81

Combadiere, C., Potteaux, S., Rodero, M., Simon, T., Pezard, A., Esposito, B., Merval, R., Proudfoot, A., Tedgui, A., Mallat, Z., 2008. Combined inhibition of CCL2, CX3CR1, and CCR5 abrogates Ly6C(hi) and Ly6C(lo) monocytosis and almost abolishes atherosclerosis in hypercholesterolemic mice. Circulation 117, 1649–1657. doi:10.1161/Circulationaha.107.745091

Coppinger, J.A., Cagney, G., Toomey, S., Kislinger, T., Belton, O., McRedmond, J.P., Cahill, D.J., Emili, A., Fitzgerald, D.J., Maguire, P.B., 2004. Characterization of the proteins released from activated platelets leads to localization of novel platelet proteins in human atherosclerotic lesions. Blood 103, 2096–2104. doi:10.1182/blood-2003-08-2804

Coppinger, J.A., O'Connor, R., Wynne, K., Flanagan, M., Sullivan, M., Maguire, P.B., Fitzgerald, D.J., Cagney, G., 2007. Moderation of the platelet releasate response by aspirin. Blood 109, 4786–4792. doi:10.1182/blood-2006-07-038539

Corte, Della, A., Maugeri, N., Pampuch, A., Cerletti, C., de Gaetano, G., Rotilio, D., 2008. Application of 2-dimensional difference gel electrophoresis (2D-DIGE) to the study of thrombin-activated human platelet secretome. Platelets 19, 43–50. doi:10.1080/09537100701609035

Cosemans, J.M.E.M., Angelillo-Scherrer, A., Mattheij, N.J.A., Heemskerk, J.W.M., 2013. The effects of arterial flow on platelet activation, thrombus growth, and stabilization. Cardiovasc Res 99, 342–352. doi:10.1093/cvr/cvt110

Cunningham, A.C., Hasty, K.A., Enghild, J.J., Mast, A.E., 2002. Structural and functional characterization of tissue factor pathway inhibitor following degradation by matrix metalloproteinase-8. Biochem. J. 367, 451–458. doi:10.1042/BJ20020696

Dahm, A., van Hylckama Vlieg, A., Bendz, B., Rosendaal, F., Bertina, R.M., Sandset, P.M., 2003. Low levels of tissue factor pathway inhibitor (TFPI) increase the risk of venous thrombosis. Blood 101, 4387–4392. doi:10.1182/blood-2002-10-3188

Daret, D., Blin, P., Larrue, J., 1989. Synthesis of hydroxy fatty acids from linoleic acid by human blood platelets. Prostaglandins 38, 203–214.

Davies, M.J., 1996. Stability and instability: two faces of coronary atherosclerosis. The Paul Dudley White Lecture 1995. Circulation.

Deleuran, B., Iversen, L., Deleuran, M., Yssel, H., Kragballe, K., Stengaard-Pedersen, K., Thestrup-Pedersen, K., 1995. Interleukin 13 suppresses cytokine production and stimulates the production of 15-HETE in PBMC. Cytokine 7, 319–324. doi:10.1006/cyto.1995.0040

Denis, M.M., Tolley, N.D., Bunting, M., Schwertz, H., Jiang, H., Lindemann, S., Yost, C.C., Rubner, F.J., Albertine, K.H., Swoboda, K.J., Fratto, C.M., Tolley, E., Kraiss, L.W., McIntyre, T.M., Zimmerman, G.A., Weyrich, A.S., 2005. Escaping the nuclear confines: signal-dependent pre-mRNA splicing in anucleate platelets. Cell 122, 379–391. doi:10.1016/j.cell.2005.06.015

Dennis, E.A., Deems, R.A., Harkewicz, R., Quehenberger, O., Brown, H.A., Milne, S.B., Myers, D.S., Glass, C.K., Hardiman, G., Reichart, D., Merrill, A.H., Sullards, M.C., Wang, E., Murphy, R.C., Raetz, C.R.H., Garrett, T.A., Guan, Z., Ryan, A.C., Russell, D.W., McDonald, J.G., Thompson, B.M., Shaw, W.A., Sud, M., Zhao, Y., Gupta, S., Maurya, M.R., Fahy, E., Subramaniam, S., 2010. A mouse macrophage lipidome. J. Biol. Chem. 285, 39976–39985. doi:10.1074/jbc.M110.182915

DeWitt, D.L., el-Harith, E.A., Kraemer, S.A., Andrews, M.J., Yao, E.F., Armstrong, R.L., Smith, W.L., 1990. The aspirin and heme-binding sites of ovine and murine prostaglandin endoperoxide synthases. J. Biol. Chem. 265, 5192–5198.

Dewitt, D.S., Kong, D.L., Lyeth, B.G., Jenkins, L.W., Hayes, R.L., Wooten, E.D., Prough, D.S., 1988. Experimental traumatic brain injury elevates brain prostaglandin E2 and thromboxane B2 levels in rats. J. Neurotrauma 5, 303–313.

Dixon, R.A., Diehl, R.E., Opas, E., Rands, E., Vickers, P.J., Evans, J.F., Gillard, J.W., Miller, D.K., 1990. Requirement of a 5-lipoxygenase-activating protein for leukotriene synthesis. Nature 343, 282–284. doi:10.1038/343282a0

Díaz-González, F., Sánchez-Madrid, F., 2015. NSAIDs: learning new tricks from old drugs. European Journal of Immunology 45, 679–686. doi:10.1002/eji.201445222

Dole, V.S., Bergmeier, W., Patten, I.S., Hirahashi, J., Mayadas, T.N., Wagner, D.D., 2007. PSGL-I regulates platelet P-selectin-mediated endothelial activation and shedding of P-selectin from activated platelets. Thromb. Haemost. 98, 806–812. doi:10.1160/TH07-03-0207

Domon, B., Aebersold, R., 2006. Mass spectrometry and protein analysis. Science 312, 212–217. doi:10.1126/science.1124619

Dopheide, S.M., Maxwell, M.J., Jackson, S.P., 2002. Shear-dependent tether formation during platelet translocation on von Willebrand factor. Blood 99, 159–167.

Drake, T.A., Morrissey, J.H., Edgington, T.S., 1989. Selective cellular expression of tissue factor in human tissues. Implications for disorders of hemostasis and thrombosis. Am. J. Pathol. 134, 1087–1097.

Dweep, H., Gretz, N., 2015. miRWalk2.0: a comprehensive atlas of microRNA-target interactions. Nat. Methods 12, 697–697. doi:10.1038/nmeth.3485

Eidelman, R.S., Hebert, P.R., Weisman, S.M., Hennekens, C.H., 2003. An Update on Aspirin in the Primary Prevention of Cardiovascular Disease. Arch Intern Med 163, 2006–2010. doi:10.1001/archinte.163.17.2006

Ellery, P.E.R., Maroney, S.A., Martinez, N.D., Wickens, M.P., Mast, A.E., 2014. Translation of human tissue factor pathway inhibitor-β mRNA is controlled by alternative splicing within the 5' untranslated region. Arterioscler. Thromb. Vasc. Biol. 34, 187–195. doi:10.1161/ATVBAHA.113.302660

Emsley, P., Cowtan, K., 2004. Coot: model-building tools for molecular graphics. Acta Crystallogr Sect D Biol Crystallogr 60, 2126–2132. doi:10.1107/S0907444904019158

Engstad, C.S., Lia, K., Rekdal, O., Olsen, J.O., Osterud, B., 1995. A novel biological effect of platelet factor 4 (PF4): enhancement of LPS-induced tissue factor activity in monocytes. J Leukoc Biol 58, 575–581.

Erhardtsen, E., Ezban, M., Madsen, M.T., Diness, V., Glazer, S., Hedner, U., Nordfang, O., 1995. Blocking of tissue factor pathway inhibitor (TFPl) shortens the bleeding time in rabbits with antibody induced haemophilia A. Blood Coagulation & Fibrinolysis 6, 388.

Evangelista, V., Manarini, S., Rotondo, S., Martelli, N., Polischuk, R., McGregor, J.L., de Gaetano, G., Cerletti, C., 1996. Platelet/polymorphonuclear leukocyte interaction in dynamic conditions: evidence of adhesion cascade and cross talk between P-selectin and the beta 2 integrin CD11b/CD18. Blood 88, 4183–4194.

Evans, R.M., 2013. Journal of Molecular Endocrinology 25th anniversary special issue. J. Mol. Endocrinol. 51, E1–E3. doi:10.1530/JME-13-0257

Ezumi, Y., Shindoh, K., Tsuji, M., Takayama, H., 1998. Physical and functional association of the Src family kinases Fyn and Lyn with the collagen receptor glycoprotein VI-Fc receptor gamma chain complex on human platelets. J Exp Med 188, 267–276.

Ezzelarab, M.B., Liu, Y.W., Lin, C.C., Long, C., 2014. Role of P-selectin and P-selectin glycoprotein ligand-1 interaction in the induction of tissue factor expression on human platelets after incubation with porcine aortic endothelial cells. Xenotransplantation 21, 16-24.. doi:10.1111/xen.12068

Fager, A.M., Hoffman, M., 2014. Endothelial Protein C Receptor Is Expressed on Procoagulant Platelets and Contributes to Factor VIIa Binding and Activity. Blood 124, 4224–4224.

Fajas, L., Auboeuf, D., Raspé, E., Schoonjans, K., Lefebvre, A.M., Saladin, R., Najib, J., Laville, M., Fruchart, J.C., Deeb, S., Vidal-Puig, A., Flier, J., Briggs, M.R., Staels, B., Vidal, H., Auwerx, J., 1997. The organization, promoter analysis, and expression of the human PPARgamma gene. J. Biol. Chem. 272, 18779–18789.

Fajas, L., Fruchart, J.-C., Auwerx, J., 1998. PPARγ3 mRNA: a distinct PPARγ mRNA subtype transcribed from an independent promoter. FEBS Lett. 438, 55–60. doi:10.1016/S0014-5793(98)01273-3

Fajas, L., Schoonjans, K., Gelman, L., Kim, J.B., Najib, J., Martin, G., Fruchart, J.C., Briggs, M., Spiegelman, B.M., Auwerx, J., 1999. Regulation of peroxisome proliferator-activated receptor gamma expression by adipocyte differentiation and determination factor 1/sterol regulatory element binding protein 1: implications for adipocyte differentiation and metabolism. Mol. Cell. Biol. 19, 5495–5503.

Fenn, J.B., Mann, M., Meng, C.K., Wong, S.F., Whitehouse, C.M., 1989. Electrospray ionization for mass spectrometry of large biomolecules. Science 246, 64–71.

Feske, S., Gwack, Y., Prakriya, M., Srikanth, S., Puppel, S.-H., Tanasa, B., Hogan, P.G., Lewis, R.S., Daly, M., Rao, A., 2006. A mutation in Orai1 causes immune deficiency by abrogating CRAC channel function. Nature 441, 179–185. doi:10.1038/nature04702

FitzGerald, G.A., 1991. Mechanisms of platelet activation: thromboxane A2 as an amplifying signal for other agonists. Am. J. Cardiol. 68, 11B–15B.

Fleteher-Cieutat, M., Vanderhoek, J.Y., Bryant, R.W., 1985. Aspirin enhances the sensitivity of human platelet 12-lipoxygenase to inhibition by 15-HETE, an endogenous regulator. Prostaglandins 18, 255–259. doi:10.1016/0262-

1746(85)90025-3
Floyd, C.N., Ferro, A., 2014. Mechanisms of aspirin resistance. Pharmacol. Ther. 141, 69–78. doi:10.1016/j.pharmthera.2013.08.005
Floyd, Z.E., Stephens, J.M., 2002. Interferon-{gamma}-mediated Activation and Ubiquitin-Proteasome-dependent Degradation of PPAR{gamma} in Adipocytes. J. Biol. Chem. 277, 4062–4068. doi:10.1074/jbc.M108473200
Foadi, J., Aller, P., Alguel, Y., Cameron, A., Axford, D., Owen, R.L., Armour, W., Waterman, D.G., Iwata, S., Evans, G., 2013. Clustering procedures for the optimal selection of data sets from multiple crystals in macromolecular crystallography. Acta Crystallogr Sect D Biol Crystallogr 69, 1617–1632. doi:10.1107/S0907444913012274
Fong, K.P., Barry, C., Tran, A.N., Traxler, E.A., Wannemacher, K.M., Tang, H.-Y., Speicher, K.D., Blair, I.A., Speicher, D.W., Grosser, T., Brass, L.F., 2011. Deciphering the human platelet sheddome. Blood 117, 15–26. doi:10.1182/blood-2010-05-283838
Forman, B.M., Tontonoz, P., Chen, J., Brun, R.P., Spiegelman, B.M., Evans, R.M., 1995. 15-Deoxy-Δ12,14-Prostaglandin J2 is a ligand for the adipocyte determination factor PPARγ. Cell 83, 803–812. doi:10.1016/0092-8674(95)90193-0
Fricke, I., Mitchell, D., Petersen, F., Bohle, A., Bulfone-Paus, S., Brandau, S., 2004. Platelet factor 4 in conjunction with IL-4 directs differentiation of human monocytes into specialized antigen-presenting cells. FASEB J 18, 1588–. doi:10.1096/fj.03-1435fje
Fukudome, K., Esmon, C.T., 1994. Identification, cloning, and regulation of a novel endothelial cell protein C/activated protein C receptor. J. Biol. Chem. 269, 26486–26491.
Funk, C.D., Funk, L.B., Kennedy, M.E., Pong, A.S., FitzGerald, G.A., 1991. Human platelet/erythroleukemia cell prostaglandin G/H synthase: cDNA cloning, expression, and gene chromosomal assignment. FASEB J 5, 2304–2312.
Furie, B., Furie, B.C., 1996. P-Selectin Induction of Tissue Factor Biosynthesis and Expression. Pathophysiol Haemos Thromb 26, 60–65. doi:10.1159/10.1159/000217242
Furman, M.I., Barnard, M.R., Krueger, L.A., Fox, M.L., Shilale, E.A., Lessard, D.M., Marchese, P., Frelinger, A.L., Goldberg, R.J., Michelson, A.D., 2001. Circulating monocyte-platelet aggregates are an early marker of acute myocardial infarction. J Am Coll Cardiol 38, 1002–1006. doi:10.1016/S0735-1097(01)01485-1
Furukawa, A., Arita, T., Fukuzaki, T., Mori, M., Honda, T., Satoh, S., Matsui, Y., Wakabayashi, K., Hayashi, S., Nakamura, K., Araki, K., Kuroha, M., Tanaka, J., Wakimoto, S., Suzuki, O., Ohsumi, J., 2012. Synthesis and biological evaluation of novel (-)-Cercosporamide derivatives as potent selective PPARγ modulators. Eur J Med Chem 54, 522–533. doi:10.1016/j.ejmech.2012.05.040
Gailani, D., Bane, C.E., Gruber, A., 2015. Factor XI and Contact Activation as Targets for Antithrombotic Therapy. J. Thromb. Haemost. n/a–n/a. doi:10.1111/jth.13005
Galis, Z.S., Sukhova, G.K., Lark, M.W., Libby, P., 1994. Increased Expression of Matrix Metalloproteinases and Matrix-Degrading Activity in Vulnerable Regions of Human Atherosclerotic Plaques. J Clin Invest 94, 2493–2503. doi:10.1172/JCI117619
Galligan, L., Livingstone, W., Volkov, Y., Hokamp, K., Murphy, C., Lawler, M., Fukudome, K., Smith, O., 2001. Characterization of protein C receptor expression in monocytes. British Journal of Haematology 115, 408–414. doi:10.1046/j.1365-2141.2001.03187.x

Gampe, R.T., Montana, V.G., Lambert, M.H., Miller, A.B., Bledsoe, R.K., Milburn, M.V., Kliewer, S.A., Willson, T.M., Xu, H.E., 2000. Asymmetry in the PPARgamma/RXRalpha crystal structure reveals the molecular basis of heterodimerization among nuclear receptors. Mol. Cell 5, 545–555.

Gandrille, S., 2008. Endothelial cell protein C receptor and the risk of venous thrombosis. Haematologica 93, 812–816. doi:10.3324/haematol.13243

Garavito, R.M., Malkowski, M.G., DeWitt, D.L., 2002. The structures of prostaglandin endoperoxide H synthases-1 and -2. Prostaglandins Other Lipid Mediat. 68-69, 129–152.

Gawaz, M.P., Loftus, J.C., Bajt, M.L., Frojmovic, M.M., Plow, E.F., Ginsberg, M.H., 1991. Ligand bridging mediates integrin alpha IIb beta 3 (platelet GPIIB-IIIA) dependent homotypic and heterotypic cell-cell interactions. Journal of Clinical Investigation 88, 1128–1134. doi:10.1172/JCI115412

Gebuhrer, V., Murphy, J.F., Bordet, J.C., Reck, M.P., McGregor, J.L., 1995. Oxidized Low-Density-Lipoprotein Induces the Expression of P-Selectin (Gmp140/Padgem/Cd62) on Human Endothelial-Cells. Biochem. J. 306, 293–298.

Gerrard, J.M., White, J.G., Rao, G.H., Townsend, D., 1976. Localization of platelet prostaglandin production in the platelet dense tubular system. Am. J. Pathol. 83, 283–298.

Ghosh, S., Pendurthi, U.R., Steinoe, A., Esmon, C.T., Rao, L.V.M., 2007. Endothelial cell protein C receptor acts as a cellular receptor for factor VIIa on endothelium. J. Biol. Chem. 282, 11849–11857. doi:10.1074/jbc.M609283200

Gibbins, J., Asselin, J., Farndale, R., Barnes, M., Law, C.L., Watson, S.P., 1996. Tyrosine phosphorylation of the Fc receptor gamma-chain in collagen-stimulated platelets. J. Biol. Chem. 271, 18095–18099.

Gibbins, J.M., Okuma, M., Farndale, R., Barnes, M., Watson, S.P., 1997. Glycoprotein VI is the collagen receptor in platelets which underlies tyrosine phosphorylation of the Fc receptor γ-chain. FEBS Lett. 413, 255–259. doi:10.1016/S0014-5793(97)00926-5

Gilio, K., van Kruchten, R., Braun, A., Berna-Erro, A., Feijge, M.A.H., Stegner, D., van der Meijden, P.E.J., Kuijpers, M.J.E., Varga-Szabo, D., Heemskerk, J.W.M., Nieswandt, B., 2010. Roles of platelet STIM1 and Orai1 in glycoprotein VI- and thrombin-dependent procoagulant activity and thrombus formation. J. Biol. Chem. 285, 23629–23638. doi:10.1074/jbc.M110.108696

Gillmor, S.A., Villaseñor, A., Fletterick, R., Sigal, E., Browner, M.F., 1997. The structure of mammalian 15-lipoxygenase reveals similarity to the lipases and the determinants of substrate specificity. Nat. Struct. Biol. 4, 1003–1009. doi:10.1038/nsb1297-1003

Girard, T.J., Eddy, R., Wesselschmidt, R.L., Macphail, L.A., Likert, K.M., Byers, M.G., Shows, T.B., Broze, G.J., 1991. Structure of the Human Lipoprotein-Associated Coagulation Inhibitor Gene - Intro Exon Gene Organization and Localization of the Gene to Chromosome-2. J. Biol. Chem. 266, 5036–5041.

Glagov, S., Zarins, C., Giddens, D.P., Ku, D.N., 1988. Hemodynamics and Atherosclerosis - Insights and Perspectives Gained From Studies of Human Arteries. Arch. Pathol. Lab. Med. 112, 1018–1031.

Glass, C.K., Rosenfeld, M.G., 2000. The coregulator exchange in transcriptional functions of nuclear receptors. Genes Dev. 14, 121–141.

Gleissner, C.A., Shaked, I., Little, K.M., Ley, K., 2010. CXC chemokine ligand 4 induces a unique transcriptome in monocyte-derived macrophages. J Immunol 184, 4810–4818. doi:10.4049/jimmunol.0901368

Goetzl, E.J., Pickett, W.C., 1980. The human PMN leukocyte chemotactic activity of complex hydroxy-eicosatetraenoic acids (HETEs). J Immunol 125, 1789–1791.
Goetzl, E.J., Weller, P.F., Sun, F.F., 1980. The regulation of human eosinophil function by endogenous mono-hydroxy-eicosatetraenoic acids (HETEs). J Immunol 124, 926–933.
Goldstein, J.L., Brown, M.S., 1985. Familial hypercholesterolemia: a genetic receptor disease. Hosp. Pract. (Off. Ed.) 20, 35–41– 45–6.
Goldstein, J.L., Kita, T., Brown, M.S., 1983. Defective lipoprotein receptors and atherosclerosis. Lessons from an animal counterpart of familial hypercholesterolemia. N. Engl. J. Med. 309, 288–296. doi:10.1056/NEJM198308043090507
Gomez, K., McVey, J.H., 2006. Tissue factor initiated blood coagulation. Front Biosci.
Goodman, C.A., Pierre, P., Hornberger, T.A., 2012. Imaging of protein synthesis with puromycin. PNAS 109, 989–E989. doi:10.1073/pnas.1202000109
Gorczyca, M.E., Nair, S.C., Jilma, B., Priya, S., Male, C., Reitter, S., Knoebl, P., Gilbert, J.C., Schaub, R.G., Dockal, M., McGinness, K.E., Pabinger, I., Srivastava, A., 2012. Inhibition of tissue factor pathway inhibitor by the aptamer BAX499 improves clotting of hemophilic blood and plasma. J. Thromb. Haemost. 10, 1581–1590. doi:10.1111/j.1538-7836.2012.04790.x
Gordon, S., Taylor, P.R., 2005. Monocyte and macrophage heterogeneity. Nat. Rev. Immunol. 5, 953–964. doi:10.1038/nri1733
Gough, P.J., Gomez, I.G., Wille, P.T., Raines, E.W., 2006. Macrophage expression of active MMP-9 induces acute plaque disruption in apoE-deficient mice. J Clin Invest 116, 59–69. doi:10.1172/JCI25074
Grage-Griebenow, E., Zawatzky, R., Kahlert, H., Brade, L., Flad, H., Ernst, M., 2001. Identification of a novel dendritic cell-like subset of CD64(+) / CD16(+) blood monocytes. European Journal of Immunology 31, 48–56. doi:10.1002/1521-4141(200101)31
Green, S., Chambon, P., 1987. Oestradiol induction of a glucocorticoid-responsive gene by a chimaeric receptor. Nature 325, 75–78. doi:10.1038/325075a0
Griffin, J.H., Fernandez, J.A., Gale, A.J., 2007. Activated protein C. Journal of Thrombosis and Haemostasis 5 (Suppl. 1), 73-80
Guido, D.M., McKenna, R., Mathews, W.R., 1993. Quantitation of hydroperoxy-eicosatetraenoic acids and hydroxy-eicosatetraenoic acids as indicators of lipid peroxidation using gas chromatography-mass spectrometry. Anal. Biochem. 209, 123–129. doi:10.1006/abio.1993.1091
Hackeng, T.M., Seré, K.M., Tans, G., Rosing, J., 2006. Protein S stimulates inhibition of the tissue factor pathway by tissue factor pathway inhibitor. PNAS 103, 3106–3111. doi:10.1073/pnas.0504240103
Hamberg, M., B, S., 1974. Prostaglandin Endoperoxides - Novel Transformations of Arachidonic-Acid in Human Platelets. PNAS 71, 3400–3404. doi:10.1073/pnas.71.9.3400
Hamik, A., Setiadi, H., Bu, G., McEver, R.P., 1999. Down-regulation of monocyte tissue factor mediated by tissue factor pathway inhibitor and the low density lipoprotein receptor-related protein. Journal of Biological … 274, 4962–4969. doi:10.1074/jbc.274.8.4962
Hansson, G.K., 2005. Inflammation, Atherosclerosis, and Coronary Artery Disease. N. Engl. J. Med. 352, 1685–1695. doi:10.1056/NEJMra043430
Harker, L.A., 1977. The kinetics of platelet production and destruction in man. Clin Haematol 6, 671–693.

Harper, M.T., Poole, A.W., 2010. Diverse functions of protein kinase C isoforms in platelet activation and thrombus formation. Journal of Thrombosis and Haemostasis 8, 454–462. doi:10.1111/j.1538-7836.2009.03722.x

Havugimana, P.C., Hart, G.T., Nepusz, T., Yang, H., Turinsky, A.L., Li, Z., Wang, P.I., Boutz, D.R., Fong, V., Phanse, S., Babu, M., Craig, S.A., Hu, P., Wan, C., Vlasblom, J., Dar, V.-U.-N., Bezginov, A., Clark, G.W., Wu, G.C., Wodak, S.J., Tillier, E.R.M., Paccanaro, A., Marcotte, E.M., Emili, A., 2012. A census of human soluble protein complexes. Cell 150, 1068–1081. doi:10.1016/j.cell.2012.08.011

Heery, D.M., Kalkhoven, E., Hoare, S., Parker, M.G., 1997. A signature motif in transcriptional co-activators mediates binding to nuclear receptors. Nature 387, 733–736. doi:10.1038/42750

Heijnen, H.F.G., Schiel, A.E., Fijnheer, R., Geuze, H.J., Sixma, J.J., 1999. Activated Platelets Release Two Types of Membrane Vesicles: Microvesicles by Surface Shedding and Exosomes Derived From Exocytosis of Multivesicular Bodies and α-Granules. Blood 94, 3791–3799. doi:10.1007/BF00228075

Heinlein, C.A., Chang, C., 2013. Androgen Receptor in Prostate Cancer. Endocrine Reviews 25, 276–308. doi:10.1210/er.2002-0032

Henderson, W.R., Rashed, M., Yong, E.C., Fritsche, T.R., Chiang, G.K., 1992. Toxoplasma-Gondii Stimulates the Release of 13-Hydroxyoctadecadienoic and 9-Hydroxyoctadecadienoic Acids by Human Platelets. Biochemistry 31, 5356–5362.

Hennekens, C.H., Buring, J.E., Sandercock, P., Collins, R., Peto, R., 1989. Aspirin and other antiplatelet agents in the secondary and primary prevention of cardiovascular disease. Circulation 80, 749–756. doi:10.1161/01.CIR.80.4.749

Heo, K.-S., Kim, D.-U., Ryoo, S., Nam, M., Baek, S.T., Kim, L., Park, S.-K., Myung, C.-S., Hoe, K.-L., 2007. PPARgamma activation abolishes LDL-induced proliferation of human aortic smooth muscle cells via SOD-mediated down-regulation of superoxide. Biochemical and Biophysical Research Communications 359, 1017–1023. doi:10.1016/j.bbrc.2007.06.006

Holinstat, M., Boutaud, O., Apopa, P.L., Vesci, J., Bala, M., Oates, J.A., Hamm, H.E., 2011. Protease-activated receptor signaling in platelets activates cytosolic phospholipase A2α differently for cyclooxygenase-1 and 12-lipoxygenase catalysis. Arterioscler. Thromb. Vasc. Biol. 31, 435–442. doi:10.1161/ATVBAHA.110.219527

Hong, S.H., Jeong, H.-K., Han, M.H., Park, C., Choi, Y.H., 2014. Esculetin suppresses lipopolysaccharide-induced inflammatory mediators and cytokines by inhibiting nuclear factor-κB translocation in RAW 264.7 macrophages. Mol Med Rep 10, 3241–3246. doi:10.3892/mmr.2014.2613

Honn, K.V., Tang, D.G., Gao, X., Butovich, I.A., Bin Liu, Timár, J., Hagmann, W., 1994. 12-Lipoxygenases and 12(S)-HETE: role in cancer metastasis. Cancer Metast Rev 13, 365–396. doi:10.1007/BF00666105

Howard, G., Wagenknecht, L.E., Burke, G.L., Diez-Roux, A., Evans, G.W., McGovern, P., Nieto, F.J., Tell, G.S., 1998. Cigarette smoking and progression of atherosclerosis: The Atherosclerosis Risk in Communities (ARIC) Study. JAMA 279, 119–124.

Hristov, M., Weber, C., 2011. Differential role of monocyte subsets in atherosclerosis. Thromb. Haemost. 106, 757–762. doi:10.1160/TH11-07-0500

Hu, Q., Noll, R.J., Li, H., Makarov, A., Hardman, M., Graham Cooks, R., 2005. The Orbitrap: a new mass spectrometer. J Mass Spectrom 40, 430–443. doi:10.1002/jms.856

Hu, X., Lazar, M.A., 1999. The CoRNR motif controls the recruitment of corepressors

by nuclear hormone receptors. Nature 402, 93–96. doi:10.1038/47069
Hua, Y., Xue, J., Sun, F., Zhu, L., Xie, M., 2009. Aspirin inhibits MMP-2 and MMP-9 expressions and activities through upregulation of PPARalpha/gamma and TIMP gene expressions in ox-LDL-stimulated macrophages derived from human monocytes. Pharmacology 83, 18–25. doi:10.1159/000166183
Huang, Y., Tsang, S.-Y., Yao, X., Chen, Z.-Y., 2005. Biological Properties of Baicalein in Cardiovascular System. CDTCHD 5, 177–184. doi:10.2174/1568006043586206
Huang, Z.F., Higuchi, D., Lasky, N., Broze, G.J., 1997. Tissue factor pathway inhibitor gene disruption produces intrauterine lethality in mice. Blood 90, 944–951.
Hundelshausen, von, P., Weber, K.S., Huo, Y., Proudfoot, A.E., Nelson, P.J., Ley, K., Weber, C., 2001. RANTES deposition by platelets triggers monocyte arrest on inflamed and atherosclerotic endothelium. Circulation 103, 1772–1777. doi:10.1161/01.CIR.103.13.1772
Hunter, M.P., Ismail, N., Zhang, X., Aguda, B.D., Lee, E.J., Yu, L., Xiao, T., Schafer, J., Lee, M.-L.T., Schmittgen, T.D., Nana-Sinkam, S.P., Jarjoura, D., Marsh, C.B., 2008. Detection of microRNA expression in human peripheral blood microvesicles. PLoS ONE 3, e3694. doi:10.1371/journal.pone.0003694
Huo, Y., Ley, K., 2001. Adhesion molecules and atherogenesis. Acta Physiologica Scandinavica 173, 35–43. doi:10.1046/j.1365-201X.2001.00882.x
Huo, Y.Q., Schober, A., Forlow, S.B., Smith, D.F., Hyman, M.C., Jung, S., Littman, D.R., Weber, C., Ley, K., 2003. Circulating activated platelets exacerbate atherosclerosis in mice deficient in apolipoprotein E. Nat. Med. 9, 61–67. doi:10.1038/nm810
Italiano, J.E., Lecine, P., Shivdasani, R.A., Hartwig, J.H., 1999. Blood platelets are assembled principally at the ends of proplatelet processes produced by differentiated megakaryocytes. J Cell Biol 147, 1299–1312.
Italiano, J.E., Richardson, J.L., Patel-Hett, S., Battinelli, E., Zaslavsky, A., Short, S., Ryeom, S., Folkman, J., Klement, G.L., 2008. Angiogenesis is regulated by a novel mechanism: pro- and antiangiogenic proteins are organized into separate platelet alpha granules and differentially released. Blood 111, 1227–1233. doi:10.1182/blood-2007-09-113837
Itoh, T., Fairall, L., Amin, K., Inaba, Y., Szanto, A., Balint, B.L., Nagy, L., Yamamoto, K., Schwabe, J.W.R., 2008. Structural basis for the activation of PPAR|[gamma]| by oxidized fatty acids. Nature Structural & Molecular Biology 15, 924–931. doi:10.1038/nsmb.1474
Ivanov, I., Heydeck, D., Hofheinz, K., Roffeis, J., O'Donnell, V.B., Kühn, H., Walther, M., 2010. Molecular enzymology of lipoxygenases. Arch. Biochem. Biophys. 503, 161–174. doi:10.1016/j.abb.2010.08.016
Jackson, S.M., Parhami, F., Xi, X.P., Berliner, J.A., Hsueh, W.A., Law, R.E., Demer, L.L., 1999. Peroxisome proliferator-activated receptor activators target human endothelial cells to inhibit leukocyte-endothelial cell interaction. Arterioscler. Thromb. Vasc. Biol. 19, 2094–2104. doi:10.1161/01.ATV.19.9.2094
Jackson, S.P., Schoenwaelder, S.M., 2003. Antiplatelet therapy: in search of the “magic bullet.” Nature Reviews Drug Discovery 2, 775–789. doi:10.1038/nrd1198
Jakubowski, J.A., Riesmeyer, J.S., Close, S.L., Leishman, A.G., Erlinge, D., 2012. TRITON and beyond: new insights into the profile of prasugrel. Cardiovasc Ther 30, e174–82. doi:10.1111/j.1755-5922.2011.00263.x
Jarrar, Y.B., Cho, S.-A., Oh, K.-S., Kim, D.-H., Shin, J.-G., Lee, S.-J., 2013. Identification of cytochrome P450s involved in the metabolism of arachidonic acid in human platelets. Prostaglandins Leukot. Essent. Fatty Acids 89, 227–234.

doi:10.1016/j.plefa.2013.06.008
Jiang, C., Ting, A.T., Seed, B., 1998. PPAR-gamma agonists inhibit production of monocyte inflammatory cytokines. Nature 391, 82–86. doi:10.1038/34184
Jiang, X., Ye, X., Guo, W., Lu, H., Gao, Z., 2014. Inhibition of HDAC3 promotes ligand-independent PPAR gamma activation by protein acetylation. J. Mol. Endocrinol. 53, 191–200. doi:10.1530/JME-14-0066
Jin, J., Quinton, T.M., Zhang, J., Rittenhouse, S.E., Kunapuli, S.P., 2002. Adenosine diphosphate (ADP)-induced thromboxane A(2) generation in human platelets requires coordinated signaling through integrin alpha(IIb)beta(3) and ADP receptors. Blood 99, 193–198.
Jonnalagadda, D., Izu, L.T., Whiteheart, S.W., 2012. Platelet secretion is kinetically heterogeneous in an agonist-responsive manner. Blood 120, 5209–5216. doi:10.1182/blood-2012-07-445080
Jordan, R.E., Favreau, L.V., Braswell, E.H., Rosenberg, R.D., 1982. Heparin with two binding sites for antithrombin or platelet factor 4. J. Biol. Chem. 257, 400–406.
Kadoglou, N.P.E., Iliadis, F., Liapis, C.D., 2008. Exercise and Carotid Atherosclerosis. European Journal of Vascular and Endovascular Surgery 35, 264–272. doi:10.1016/j.ejvs.2007.08.022
Kaplan, G., Gaudernack, G., 1982. In vitro differentiation of human monocytes. Differences in monocyte phenotypes induced by cultivation on glass or on collagen. J Exp Med 156, 1101–1114. doi:10.1084/jem.156.4.1101
Kappelmayer, J., Kunapuli, S.P., Wyshock, E.G., Colman, R.W., 1993. Characterization of monocyte-associated factor V. Thromb. Haemost. 70, 273–280.
Karas, M., Hillenkamp, F., 1988. Laser desorption ionization of proteins with molecular masses exceeding 10,000 daltons. Anal. Chem. 60, 2299–2301.
Kasirer-Friede, A., Ware, J., Leng, L., Marchese, P., Ruggeri, Z.M., Shattil, S.J., 2002. Lateral clustering of platelet GP Ib-IX complexes leads to up-regulation of the adhesive function of integrin alpha IIbbeta 3. J. Biol. Chem. 277, 11949–11956. doi:10.1074/jbc.M108727200
Kasper, B., Brandt, E., Brandau, S., Petersen, F., 2007. Platelet factor 4 (CXC chemokine ligand 4) differentially regulates respiratory burst, survival, and cytokine expression of human monocytes by using distinct signaling pathways. J Immunol 179, 2584–2591.
Kasthuri, R.S., Glover, S.L., Jonas, W., McEachron, T., Pawlinski, R., Arepally, G.M., Key, N.S., Mackman, N., 2012. PF4/heparin-antibody complex induces monocyte tissue factor expression and release of tissue factor positive microparticles by activation of FcγRI. Blood 119, 5285–5293. doi:10.1182/blood-2011-06-359430
Keizo, S., Hiromichi, O., 1982. Selective inhibition of platelet lipoxygenase by baicalein. Biochemical and biophysical research …. doi:10.1016/0006-291X(82)91081-6
Keizo, S., Hiromichi, O., Shigeru, A., 1982. Selective inhibition of platelet lipoxygenase by esculetin. … et Biophysica Acta (BBA)-Lipids and …. doi:10.1016/0005-2760(82)90167-9
Kelton, J.G., Smith, J.W., Warkentin, T.E., Hayward, C.P., Denomme, G.A., Horsewood, P., 1994. Immunoglobulin G from patients with heparin-induced thrombocytopenia binds to a complex of heparin and platelet factor 4. Blood 83, 3232–3239.
Kenyon, V., Rai, G., Jadhav, A., Schultz, L., Armstrong, M., Jameson, J.B., Perry, S., Joshi, N., Bougie, J.M., Leister, W., Taylor-Fishwick, D.A., Nadler, J.L., Holinstat, M., Simeonov, A., Maloney, D.J., Holman, T.R., 2011. Discovery of potent and

selective inhibitors of human platelet-type 12- lipoxygenase. J. Med. Chem. 54, 5485–5497. doi:10.1021/jm2005089

Kiechl, S., Willeit, J., Rungger, G., Egger, G., Oberhollenzer, F., Bonora, E., 1998. Alcohol consumption and atherosclerosis: what is the relation? Prospective results from the Bruneck Study. Stroke 29, 900–907.

Kim, E., Rundhaug, J.E., Benavides, F., Yang, P., Newman, R.A., Fischer, S.M., 2005. An antitumorigenic role for murine 8S-lipoxygenase in skin carcinogenesis. Oncogene 24, 1174–1187. doi:10.1038/sj.onc.1208269

Kliewer, S.A., Lenhard, J.M., Willson, T.M., Patel, I., Morris, D.C., Lehmann, J.M., 1995. A prostaglandin J2 metabolite binds peroxisome proliferator-activated receptor gamma and promotes adipocyte differentiation. Cell 83, 813–819.

Klinkhardt, U., Bauersachs, R., Adams, J., Graff, J., Lindhoff-Last, E., Harder, S., 2003. Clopidogrel but not aspirin reduces P-selectin expression and formation of platelet-leukocyte aggregates in patients with atherosclerotic vascular disease. Clin. Pharmacol. Ther. 73, 232–241. doi:10.1067/mcp.2003.13

Knight, C.G., Morton, L.F., Onley, D.J., Peachey, A.R., Ichinohe, T., Okuma, M., Farndale, R.W., Barnes, M.J., 1999. Collagen–platelet interaction: Gly-Pro-Hyp is uniquely specific for platelet Gp VI and mediates platelet activation by collagen. Cardiovasc Res 41, 450–457. doi:10.1016/S0008-6363(98)00306-X

Kopp, E., Ghosh, S., 1994. Inhibition of NF-kappa B by sodium salicylate and aspirin. Science 265, 956–959. doi:10.1126/science.8052854

Kuhn, H., Belkner, J., Suzuki, H., Yamamoto, S., 1994. Oxidative modification of human lipoproteins by lipoxygenases of different positional specificities. J. Lipid Res. 35, 1749–1759.

Kunjathoor, V.V., Febbraio, M., Podrez, E.A., Moore, K.J., Andersson, L., Koehn, S., Rhee, J.S., Silverstein, R., Hoff, H.F., Freeman, M.W., 2002. Scavenger receptors class A-I/II and CD36 are the principal receptors responsible for the uptake of modified low density lipoprotein leading to lipid loading in macrophages. J. Biol. Chem. 277, 49982–49988. doi:10.1074/jbc.M209649200

Kurosawa, S., Stearns-Kurosawa, D.J., Hidari, N., Esmon, C.T., 1997. Identification of functional endothelial protein C receptor in human plasma. J Clin Invest 100, 411–418. doi:10.1172/JCI119548

Kühn, H., Banthiya, S., van Leyen, K., 2014. Mammalian lipoxygenases and their biological relevance. doi:10.1016/j.bbalip.2014.10.002

Landry, P., Plante, I., Ouellet, D.L., Perron, M.P., Rousseau, G., Provost, P., 2009. Existence of a microRNA pathway in anucleate platelets. Nature Structural & Molecular Biology 16, 961–966. doi:10.1038/nsmb.1651

Lannan, K.L., Sahler, J., Kim, N., Spinelli, S.L., Maggirwar, S.B., Garraud, O., Cognasse, F., Blumberg, N., Phipps, R.P., 2015. Breaking the mold: transcription factors in the anucleate platelet and platelet-derived microparticles. Front Immunol 6, 48. doi:10.3389/fimmu.2015.00048

Lasagni, L., Francalanci, M., Annunziato, F., Lazzeri, E., Giannini, S., Cosmi, L., Sagrinati, C., Mazzinghi, B., Orlando, C., Maggi, E., Marra, F., Romagnani, S., Serio, M., Romagnani, P., 2003. An alternatively spliced variant of CXCR3 mediates the inhibition of endothelial cell growth induced by IP-10, Mig, and I-TAC, and acts as functional receptor for platelet factor 4. J Exp Med 197, 1537–1549. doi:10.1084/jem.20021897

Le Guyader, A., Davis-Gorman, G., Copeland, J.G., McDonagh, P.F., 2004. A flow cytometric method for determining the binding of coagulation factor X to monocytes in whole human blood. Journal of Immunological Methods 292, 207–

215. doi:10.1016/j.jim.2004.03.016
Lee, G., Elwood, F., McNally, J., Weiszmann, J., Lindstrom, M., Amaral, K., Nakamura, M., Miao, S., Cao, P., Learned, R.M., Chen, J.-L., Li, Y., 2002. T0070907, a selective ligand for peroxisome proliferator-activated receptor gamma, functions as an antagonist of biochemical and cellular activities. J. Biol. Chem. 277, 19649–19657. doi:10.1074/jbc.M200743200
Lefkovits, J., Plow, E.F., Topol, E.J., 1995. Mechanisms of Disease - Platelet Glycoprotein Iib/Iiia Receptors in Cardiovascular Medicine. N. Engl. J. Med. 332, 1553–1559. doi:10.1056/NEJM199506083322306
Leslie, A.G.W., 2006. The integration of macromolecular diffraction data. Acta Crystallogr Sect D Biol Crystallogr 62, 48–57. doi:10.1107/S0907444905039107
Lesnik, P., Vonica, A., Guérin, M., Moreau, M., Chapman, M.J., 1993. Anticoagulant activity of tissue factor pathway inhibitor in human plasma is preferentially associated with dense subspecies of LDL and HDL and with Lp(a). Arterioscler. Thromb. 13, 1066–1075.
Lhermusier, T., Chap, H., Payrastre, B., 2011. Platelet membrane phospholipid asymmetry: from the characterization of a scramblase activity to the identification of an essential protein mutated in Scott syndrome. J. Thromb. Haemost. 9, 1883–1891. doi:10.1111/j.1538-7836.2011.04478.x
Li, D., Chen, K., Sinha, N., Zhang, X., Wang, Y., Sinha, A.K., Romeo, F., Mehta, J.L., 2005. The effects of PPAR-gamma ligand pioglitazone on platelet aggregation and arterial thrombus formation. Cardiovasc Res 65, 907–912. doi:10.1016/j.cardiores.2004.11.027
Li, Q., Cheon, Y.-P., Kannan, A., Shanker, S., Bagchi, I.C., Bagchi, M.K., 2004. A novel pathway involving progesterone receptor, 12/15-lipoxygenase-derived eicosanoids, and peroxisome proliferator-activated receptor gamma regulates implantation in mice. J. Biol. Chem. 279, 11570–11581. doi:10.1074/jbc.M311773200
Li, W., Zheng, X., Gu, J.-M., Ferrell, G.L., Brady, M., Esmon, N.L., Esmon, C.T., 2005. Extraembryonic expression of EPCR is essential for embryonic viability. Blood 106, 2716–2722. doi:10.1182/blood-2005-01-0406
Li, X., Ycaza, J., Blumberg, B., 2011. The environmental obesogen tributyltin chloride acts via peroxisome proliferator activated receptor gamma to induce adipogenesis in murine 3T3-L1 preadipocytes. J. Steroid Biochem. Mol. Biol. 127, 9–15. doi:10.1016/j.jsbmb.2011.03.012
Li, Y., Lambert, M.H., Xu, H.E., 2003. Activation of Nuclear Receptors. Structure 11, 741–746. doi:10.1016/S0969-2126(03)00133-3
Lieb, J., Karmali, R., Horrobin, D., 1983. Elevated levels of prostaglandin E2 and thromboxane B2 in depression. Prostaglandins, Leukotrienes and Medicine 10, 361–367.
Lindmark, E., Tenno, T., Siegbahn, A., 2000. Role of platelet P-selectin and CD40 ligand in the induction of monocytic tissue factor expression. Arterioscler. Thromb. Vasc. Biol. 20, 2322–2328.
Lisman, T., 2009. Factor XI Binding to Platelets Glycoprotein Ib alpha Has an Accomplice. Arterioscler. Thromb. Vasc. Biol. 29, 1409–1410. doi:10.1161/ATVBAHA.109.195412
Liu, F., Morris, S., Epps, J., Carroll, R., 2002. Demonstration of an activation regulated NF-kappaB/I-kappaBalpha complex in human platelets. Thromb. Res. 106, 199–203.
López, J.A., Andrews, R.K., Afshar-Kharghan, V., Berndt, M.C., 1998. Bernard-Soulier

Syndrome. Blood 91, 4397–4418.
López, J.A., del Conde, I., Shrimpton, C.N., 2005. Receptors, rafts, and microvesicles in thrombosis and inflammation. Journal of Thrombosis and Haemostasis 3, 1737–1744. doi:10.1111/j.1538-7836.2005.01463.x
Luci, D., Jameson, J.B., Yasgar, A., Diaz, G., Joshi, N., Kantz, A., Markham, K., Perry, S., Kuhn, N., Yeung, J., Schultz, L., Holinstat, M., Nadler, J., Taylor-Fishwick, D.A., Jadhav, A., Simeonov, A., Holman, T.R., Maloney, D.J., 2010. Discovery of ML355, a Potent and Selective Inhibitor of Human 12-Lipoxygenase. National Center for Biotechnology Information (US), Bethesda (MD).
Luo, B.-H., Carman, C.V., Springer, T.A., 2007. Structural basis of integrin regulation and signaling. Annu. Rev. Immunol. 25, 619–647. doi:10.1146/annurev.immunol.25.022106.141618
Luo, S.-Z., Mo, X., Afshar-Kharghan, V., Srinivasan, S., López, J.A., Li, R., 2007. Glycoprotein Ibα forms disulfide bonds with 2 glycoprotein Ibβ subunits in the resting platelet. Blood 109, 603–609. doi:10.1182/blood-2006-05-024091
Lupu, C., Goodwin, C.A., Westmuckett, A.D., Emeis, J.J., Scully, M.F., Kakkar, V.V., Lupu, F., 1997. Tissue factor pathway inhibitor in endothelial cells colocalizes with glycolipid microdomains/caveolae. Regulatory mechanism(s) of the anticoagulant properties of the endothelium. Arterioscler. Thromb. Vasc. Biol. 17, 2964–2974.
Lupu, C., Zhu, H., Popescu, N.I., Wren, J.D., Lupu, F., 2011. Novel protein ADTRP regulates TFPI expression and function in human endothelial cells in normal conditions and in response to androgen. Blood 118, 4463–4471. doi:10.1182/blood-2011-05-355370
Malaver, E., Romaniuk, M.A., D'atri, L.P., Pozner, R.G., Negrotto, S., Benzadón, R., Schattner, M., 2009. NF-kappaB inhibitors impair platelet activation responses. J. Thromb. Haemost. 7, 1333–1343. doi:10.1111/j.1538-7836.2009.03492.x
Mallat, Z., Nakamura, T., Ohan, J., Lesèche, G., Tedgui, A., Maclouf, J., Murphy, R.C., 1999. The relationship of hydroxyeicosatetraenoic acids and F2-isoprostanes to plaque instability in human carotid atherosclerosis. J Clin Invest 103, 421–427. doi:10.1172/JCI3985
Mancini, J.A., Abramovitz, M., Cox, M.E., Wong, E., Charleson, S., Perrier, H., Wang, Z., Prasit, P., Vickers, P.J., 1993. 5-lipoxygenase-activating protein is an arachidonate binding protein. FEBS Lett. 318, 277–281.
Mangelsdorf, D.J., Thummel, C., Beato, M., Herrlich, P., Schütz, G., Umesono, K., Blumberg, B., Kastner, P., Mark, M., Chambon, P., Evans, R.M., 1995. The nuclear receptor superfamily: The second decade. Cell 83, 835–839. doi:10.1016/0092-8674(95)90199-X
Manning-Tobin, J.J., Moore, K.J., Seimon, T.A., Bell, S.A., Sharuk, M., Alvarez-Leite, J.I., de Winther, M.P.J., Tabas, I., Freeman, M.W., 2009. Loss of SR-A and CD36 activity reduces atherosclerotic lesion complexity without abrogating foam cell formation in hyperlipidemic mice. Arterioscler. Thromb. Vasc. Biol. 29, 19–26. doi:10.1161/ATVBAHA.108.176644
Mantovani, A., Sica, A., Sozzani, S., Allavena, P., Vecchi, A., Locati, M., 2004. The chemokine system in diverse forms of macrophage activation and polarization. Trends Immunol. 25, 677–686. doi:10.1016/j.it.2004.09.015
Maroney, S.A., Cooley, B.C., Ferrel, J.P., Bonesho, C.E., Nielsen, L.V., Johansen, P.B., Hermit, M.B., Petersen, L.C., Mast, A.E., 2012. Absence of hematopoietic tissue factor pathway inhibitor mitigates bleeding in mice with hemophilia. Proc. Natl. Acad. Sci. U.S.A. 109, 3927–3931. doi:10.1073/pnas.1119858109
Maroney, S.A., Haberichter, S.L., Friese, P., Collins, M.L., Ferrel, J.P., Dale, G.L.,

Mast, A.E., 2007. Active tissue factor pathway inhibitor is expressed on the surface of coated platelets. Blood 109, 1931–1937. doi:10.1182/blood-2006-07-037283
Maroney, S.A., Mast, A.E., 2008. Expression of tissue factor pathway inhibitor by endothelial cells and platelets. Transfus. Apher. Sci. 38, 9–14. doi:10.1016/j.transci.2007.12.001
Martinez, F.O., 2009. The transcriptome of human monocyte subsets begins to emerge. J. Biol. 8, 99. doi:10.1186/jbiol206
Maxfield, F.R., Tabas, I., 2005. Role of cholesterol and lipid organization in disease. Nature 438, 612–621. doi:10.1038/nature04399
Maynard, D.M., Heijnen, H.F.G., Horne, M.K., White, J.G., Gahl, W.A., 2007. Proteomic analysis of platelet α-granules using mass spectrometry. Journal of Thrombosis and Haemostasis 5, 1945–1955. doi:10.1111/j.1538-7836.2007.02690.x
McGee, M.P., Foster, S., Wang, X., 1994. Simultaneous expression of tissue factor and tissue factor pathway inhibitor by human monocytes. A potential mechanism for localized control of blood coagulation. J Exp Med 179, 1847–1854. doi:10.1084/jem.179.6.1847
McNicol, A., Israels, S.J., 1999. Platelet dense granules: structure, function and implications for haemostasis. Thrombosis research.
McPherson, R., Pertsemlidis, A., Kavaslar, N., Stewart, A., Roberts, R., Cox, D.R., Hinds, D.A., Pennacchio, L.A., Tybjaerg-Hansen, A., Folsom, A.R., Boerwinkle, E., Hobbs, H.H., Cohen, J.C., 2007. A common allele on chromosome 9 associated with coronary heart disease. Science 316, 1488–1491. doi:10.1126/science.1142447
Miltenyi, S., Müller, W., Weichel, W., Radbruch, A., 1990. High gradient magnetic cell separation with MACS. Cytometry 11, 231–238. doi:10.1002/cyto.990110203
Moldovan, N.I., Asahara, T., 2003. Role of Blood Mononuclear Cells in Recanalization and Vascularization of ThrombiPast, Present, and Future. Trends Cardiovasc. Med. 13, 265–269. doi:10.1016/S1050-1738(03)00108-7
Moller, D.E., Greene, D.A., 2001. Peroxisome proliferator-activated receptor (PPAR) gamma agonists for diabetes. Adv. Protein Chem. 56, 181–212.
Moore, K.J., Tabas, I., 2011. Macrophages in the Pathogenesis of Atherosclerosis. Cell 145, 341–355. doi:10.1016/j.cell.2011.04.005
Moraes, L.A., Spyridon, M., Kaiser, W.J., Jones, C.I., Sage, T., Atherton, R.E.L., Gibbins, J.M., 2010. Non-genomic effects of PPARγ ligands: inhibition of GPVI-stimulated platelet activation. J. Thromb. Haemost. 8, 577–587. doi:10.1111/j.1538-7836.2009.03732.x
Murphy, R.C., Gaskell, S.J., 2011. New applications of mass spectrometry in lipid analysis. J. Biol. Chem. 286, 25427–25433. doi:10.1074/jbc.R111.233478
Murshudov, G.N., Vagin, A.A., Dodson, E.J., 1997. Refinement of Macromolecular Structures by the Maximum-Likelihood Method. Acta Crystallogr Sect D Biol Crystallogr 53, 240–255. doi:10.1107/S0907444996012255
Nagalla, S., Shaw, C., Kong, X., Kondkar, A.A., Edelstein, L.C., Ma, L., Chen, J., McKnight, G.S., López, J.A., Yang, L., Jin, Y., Bray, M.S., Leal, S.M., Dong, J.-F., Bray, P.F., 2011. Platelet microRNA-mRNA coexpression profiles correlate with platelet reactivity. Blood 117, 5189–5197. doi:10.1182/blood-2010-09-299719
Nagy, L., Schwabe, J.W.R., 2004. Mechanism of the nuclear receptor molecular switch. Trends Biochem. Sci. 29, 317–324. doi:10.1016/j.tibs.2004.04.006
Nagy, L., Tontonoz, P., Alvarez, J.G.A., Chen, H., Evans, R.M., 1998. Oxidized LDL Regulates Macrophage Gene Expression through Ligand Activation of PPARγ. Cell 93, 229–240. doi:10.1016/S0092-8674(00)81574-3
Nan, B., Lin, P., Lumsden, A.B., Yao, Q., Chen, C., 2005. Effects of TNF-alpha and

curcumin on the expression of thrombomodulin and endothelial protein C receptor in human endothelial cells. Thromb. Res. 115, 417–426. doi:10.1016/j.thromres.2004.10.010

Narahara, N., Enden, T., Wiiger, M., Prydz, H., 1994. Polar expression of tissue factor in human umbilical vein endothelial cells. Arterioscler. Thromb. 14, 1815–1820.

Nassar, G.M., Morrow, J.D., Roberts, L.J., Lakkis, F.G., Badr, K.F., 1994. Induction of 15-lipoxygenase by interleukin-13 in human blood monocytes. J. Biol. Chem. 269, 27631–27634.

Nieswandt, B., Watson, S.P., 2003. Platelet-collagen interaction: is GPVI the central receptor? Blood 102, 449–461. doi:10.1182/blood-2002-12-3882

Nissen, S.E., Wolski, K., 2007. Effect of rosiglitazone on the risk of myocardial infarction and death from cardiovascular causes. N. Engl. J. Med. 356, 2457–2471. doi:10.1056/NEJMoa072761

Nolte, R.T., Wisely, G.B., Westin, S., Cobb, J.E., Lambert, M.H., Kurokawa, R., Rosenfeld, M.G., Willson, T.M., Glass, C.K., Milburn, M.V., 1998. Ligand binding and co-activator assembly of the peroxisome proliferator-activated receptor-gamma. Nature 395, 137–143. doi:10.1038/25931

Nosjean, O., Boutin, J.A., 2002. Natural ligands of PPAR gamma: Are prostaglandin J(2) derivatives really playing the part? Cellular signalling 14, 573–583. doi:10.1016/S0898-6568(01)00281-9

Novotny, W.F., Girard, T.J., Miletich, J.P., Broze, G.J., 1988. Platelets secrete a coagulation inhibitor functionally and antigenically similar to the lipoprotein associated coagulation inhibitor. Blood 72, 2020–2025.

Nyby, M.D., Sasaki, M., Ideguchi, Y., Wynne, H.E., Hori, M.T., Berger, M.E., Golub, M.S., Brickman, A.S., Tuck, M.L., 1996. Platelet lipoxygenase inhibitors attenuate thrombin- and thromboxane mimetic-induced intracellular calcium mobilization and platelet aggregation. J Pharmacol Exp Ther 278, 503–509.

Oeth, P.A., Parry, G.C., Kunsch, C., Nantermet, P., Rosen, C.A., Mackman, N., 1994. Lipopolysaccharide induction of tissue factor gene expression in monocytic cells is mediated by binding of c-Rel/p65 heterodimers to a kappa B-like site. Mol. Cell. Biol. 14, 3772–3781. doi:10.1128/MCB.14.6.3772

Offermans, S., n.d. Activation of Platelet Function Through G Protein-Coupled Receptors. Circ. Res.

Oganesyan, V., Oganesyan, N., Terzyan, S., Qu, D., Dauter, Z., Esmon, N.L., Esmon, C.T., 2002. The crystal structure of the endothelial protein C receptor and a bound phospholipid. J. Biol. Chem. 277, 24851–24854. doi:10.1074/jbc.C200163200

Ohashi, M., Oyama, T., Nakagome, I., Satoh, M., Nishio, Y., Nobusada, H., Hirono, S., Morikawa, K., Hashimoto, Y., Miyachi, H., 2011. Design, synthesis, and structural analysis of phenylpropanoic acid-type PPARγ-selective agonists: discovery of reversed stereochemistry-activity relationship. J. Med. Chem. 54, 331–341. doi:10.1021/jm101233f

Osterud, B., 1998. Tissue factor expression by monocytes: regulation and pathophysiological roles. Blood Coagulation & Fibrinolysis 9 Suppl 1, S9–14.

Osterud, B., Bajaj, M.S., Bajaj, S.P., 1995. Sites of tissue factor pathway inhibitor (TFPI) and tissue factor expression under physiologic and pathologic conditions. On behalf of the Subcommittee on Tissue factor Pathway Inhibitor (TFPI) of the Scientific and Standardization Committee of the ISTH. Thromb. Haemost. 73, 873–875.

Ott, I., Andrassy, M., Zieglgänsberger, D., Geith, S., Schömig, A., Neumann, F.-J., 2001. Regulation of monocyte procoagulant activity in acute myocardial infarction:

role of tissue factor and tissue factor pathway inhibitor-1. Blood 97, 3721–3726. doi:10.1182/blood.V97.12.3721

Ottow, E., Weinmann, H., 2008. Nuclear receptors as drug targets. Wiley-VCH.

Pasmant, E., Laurendeau, I., Héron, D., Vidaud, M., Vidaud, D., Bièche, I., 2007. Characterization of a germ-line deletion, including the entire INK4/ARF locus, in a melanoma-neural system tumor family: identification of ANRIL, an antisense noncoding RNA whose expression coclusters with ARF. Cancer Res 67, 3963–3969. doi:10.1158/0008-5472.CAN-06-2004

Pasquet, J.M., Gross, B., Quek, L., Asazuma, N., Zhang, W., Sommers, C.L., Schweighoffer, E., Tybulewicz, V., Judd, B., Lee, J.R., Koretzky, G., Love, P.E., Samelson, L.E., Watson, S.P., 1999. LAT is required for tyrosine phosphorylation of phospholipase cgamma2 and platelet activation by the collagen receptor GPVI. Mol. Cell. Biol. 19, 8326–8334.

Passacquale, G., Vamadevan, P., Pereira, L., Hamid, C., Corrigall, V., Ferro, A., 2011. Monocyte-platelet interaction induces a pro-inflammatory phenotype in circulating monocytes. PLoS ONE 6, e25595. doi:10.1371/journal.pone.0025595

Passlick, B., Flieger, D., Ziegler-Heitbrock, H.W., 1989. Identification and characterization of a novel monocyte subpopulation in human peripheral blood. Blood 74, 2527–2534.

Paysant, J., Soria, C., Cornillet Lefèbvre, P., Nguyen, P., Lenormand, B., Mishal, Z., Vannier, J.P., Vasse, M., 2005. Long-term incubation with IL-4 and IL-10 oppositely modifies procoagulant activity of monocytes and modulates the surface expression of tissue factor and tissue factor pathway inhibitor. British Journal of Haematology 131, 356–365. doi:10.1111/j.1365-2141.2005.05783.x

Pellegrini, G., Malandra, R., Celi, A., Furie, B.C., Furie, B., 1998. 12-Hydroxyeicosatetraenoic acid upregulates P-selectin-induced tissue factor activity on monocytes. FEBS Lett. 441, 463–466. doi:10.1016/S0014-5793(98)01610-X

Penumetcha, M., Santanam, N., 2012. Nutraceuticals as Ligands of PPARγ. PPAR Research 2012, 858352–7. doi:10.1155/2012/858352

Pervushina, O., Scheuerer, B., Reiling, N., Behnke, L., Schröder, J.M., Kasper, B., Brandt, E., Bulfone-Paus, S., Petersen, F., 2004. Platelet factor 4/CXCL4 induces phagocytosis and the generation of reactive oxygen metabolites in mononuclear phagocytes independently of Gi protein activation or intracellular calcium transients. J Immunol 173, 2060–2067. doi:10.4049/jimmunol.173.3.2060

Petersen, F., Brandt, E., Lindahl, U., Spillmann, D., 1999. Characterization of a neutrophil cell surface glycosaminoglycan that mediates binding of platelet factor 4. J. Biol. Chem. 274, 12376–12382.

Petit, L., Lesnik, P., Dachet, C., Moreau, M., Chapman, M.J., 1999. Tissue factor pathway inhibitor is expressed by human monocyte-derived macrophages - Relationship to tissue factor induction by cholesterol and oxidized LDL. Arterioscler. Thromb. Vasc. Biol. 19, 309–315.

Picot, D., Loll, P.J., Garavito, R.M., 1994. The X-ray crystal structure of the membrane protein prostaglandin H2 synthase-1. Nature 367, 243–249. doi:10.1038/367243a0

Piersma, S.R., Broxterman, H.J., Kapci, M., de Haas, R.R., Hoekman, K., Verheul, H.M.W., Jimenez, C.R., 2009. Proteomics of the TRAP-induced platelet releasate. Journal of Proteomics 72, 91–109. doi:10.1016/j.jprot.2008.10.009

Pignone, M., Alberts, M.J., Colwell, J.A., Cushman, M., Inzucchi, S.E., Mukherjee, D., Rosenson, R.S., Williams, C.D., Wilson, P.W., Kirkman, M.S., 2010. Aspirin for Primary Prevention of Cardiovascular Events in People With Diabetes. J Am Coll Cardiol 55, 2878–2886. doi:10.1016/j.jacc.2010.04.003

Piro, O., Broze, G.J., 2005. Comparison of cell-surface TFPIalpha and beta. Journal of Thrombosis and Haemostasis 3, 2677–2683. doi:10.1111/j.1538-7836.2005.01636.x

Piro, O., Broze, G.J., 2004. Role for the Kunitz-3 domain of tissue factor pathway inhibitor-alpha in cell surface binding. Circulation 110, 3567–3572. doi:10.1161/01.CIR.0000148778.76917.89

Polgar, J., Lane, W.S., Chung, S.-H., Houng, A.K., Reed, G.L., 2003. Phosphorylation of SNAP-23 in activated human platelets. J. Biol. Chem. 278, 44369–44376. doi:10.1074/jbc.M307864200

Porro, B., Songia, P., Squellerio, I., Tremoli, E., Cavalca, V., 2014. Analysis, physiological and clinical significance of 12-HETE: A neglected platelet-derived 12-lipoxygenase product. J. Chromatogr. B Analyt. Technol. Biomed. Life Sci. 964, 26–40. doi:10.1016/j.jchromb.2014.03.015

Preston, R.J.S., Ajzner, E., Razzari, C., Karageorgi, S., Dua, S., Dahlbäck, B., Lane, D.A., 2006. Multifunctional specificity of the protein C/activated protein C Gla domain. J. Biol. Chem. 281, 28850–28857. doi:10.1074/jbc.M604966200

Qu, D., Wang, Y., Esmon, N.L., Esmon, C.T., 2007. Regulated endothelial protein C receptor shedding is mediated by tumor necrosis factor-alpha converting enzyme/ADAM17. Journal of Thrombosis and Haemostasis 5, 395–402. doi:10.1111/j.1538-7836.2007.02347.x

Ramos, C.L., Huo, Y.Q., Jung, U.S., Ghosh, S., Manka, D.R., Sarembock, I.J., Ley, K., 1999. Direct demonstration of P-selectin- and VCAM-1-dependent mononuclear cell rolling in early atherosclerotic lesions of apolipoprotein E-deficient mice. Circ. Res. 84, 1237–1244. doi:10.1161/01.RES.84.11.1237

Rastinejad, F., Huang, P., Chandra, V., Khorasanizadeh, S., 2013. Understanding nuclear receptor form and function using structural biology. J. Mol. Endocrinol. 51, T1–T21. doi:10.1530/JME-13-0173

Ray, D.M., Spinelli, S.L., Pollock, S.J., Murant, T.I., O'Brien, J.J., Blumberg, N., Francis, C.W., Taubman, M.B., Phipps, R.P., 2008. Peroxisome Proliferator-Activated Receptor γ and Retinoid X Receptor transcription factors are released from activated human platelets and shed in microparticles. Thromb. Haemost. 99, 86–95. doi:10.1160/TH07-05-0328

Regan, L.M., Stearns-Kurosawa, D.J., Kurosawa, S., Mollica, J., Fukudome, K., Esmon, C.T., 1996. The endothelial cell protein C receptor. Inhibition of activated protein C anticoagulant function without modulation of reaction with proteinase inhibitors. J. Biol. Chem. 271, 17499–17503.

Rendu, F., Brohard-Bohn, B., 2001. The platelet release reaction: granules' constituents, secretion and functions. Platelets 12, 261–273. doi:10.1080/09537100120068170

Ricote, M., Huang, J., Fajas, L., Li, A., Welch, J., Najib, J., Witztum, J.L., Auwerx, J., Palinski, W., Glass, C.K., 1998. Expression of the peroxisome proliferator-activated receptor {gamma} (PPAR{gamma}) in human atherosclerosis and regulation in macrophages by colony stimulating factors and oxidized low density lipoprotein. PNAS 95, 7614–7619. doi:10.1073/pnas.95.13.7614

Risitano, A., Beaulieu, L.M., Vitseva, O., Freedman, J.E., 2012. Platelets and platelet-like particles mediate intercellular RNA transfer. Blood 119, 6288–6295. doi:10.1182/blood-2011-12-396440

Roos, J., DiGregorio, P.J., Yeromin, A.V., Ohlsen, K., Lioudyno, M., Zhang, S., Safrina, O., Kozak, J.A., Wagner, S.L., Cahalan, M.D., Veliçelebi, G., Stauderman, K.A., 2005. STIM1, an essential and conserved component of store-operated Ca2+ channel function. J Cell Biol 169, 435–445. doi:10.1083/jcb.200502019

Ross, R., 1993. The Pathogenesis of Atherosclerosis - a Perspective for the 1990s.

Nature 362, 801–809. doi:10.1038/362801a0
Rossmann, M.G., 1990. The molecular replacement method. Acta Crystallogr Sect A Found Crystallogr 46 (Pt 2), 73–82.
Rossmann, M.G., Blow, D.M., 1962. The detection of sub-units within the crystallographic asymmetric unit. Acta Crystallogr 15, 24–31. doi:10.1107/S0365110X62000067
Roth, G.J., Majerus, P.W., 1975. The mechanism of the effect of aspirin on human platelets. I. Acetylation of a particulate fraction protein. Journal of Clinical Investigation 56, 624–632. doi:10.1172/JCI108132
Ruggeri, Z.M., 2002. Platelets in atherothrombosis. Nat. Med. 8, 1227–1234. doi:10.1038/nm1102-1227
Sabatino, L., Casamassimi, A., Peluso, G., Barone, M.V., Capaccio, D., Migliore, C., Bonelli, P., Pedicini, A., Febbraro, A., Ciccodicola, A., Colantuoni, V., 2005. A novel peroxisome proliferator-activated receptor gamma isoform with dominant negative activity generated by alternative splicing. J. Biol. Chem. 280, 26517–26525. doi:10.1074/jbc.M502716200
Samani, N.J., Erdmann, J., Hall, A.S., Hengstenberg, C., Mangino, M., Mayer, B., Dixon, R.J., Meitinger, T., Braund, P., Wichmann, H.-E., Barrett, J.H., König, I.R., Stevens, S.E., Szymczak, S., Tregouet, D.-A., Iles, M.M., Pahlke, F., Pollard, H., Lieb, W., Cambien, F., Fischer, M., Ouwehand, W., Blankenberg, S., Balmforth, A.J., Baessler, A., Ball, S.G., Strom, T.M., Braenne, I., Gieger, C., Deloukas, P., Tobin, M.D., Ziegler, A., Thompson, J.R., Schunkert, H., WTCCC and the Cardiogenics Consortium, 2007. Genomewide association analysis of coronary artery disease. N. Engl. J. Med. 357, 443–453. doi:10.1056/NEJMoa072366
Santoso, S., Sachs, U.J.H., Kroll, H., Linder, M., Ruf, A., Preissner, K.T., Chavakis, T., 2002. The junctional adhesion molecule 3 (JAM-3) on human platelets is a counterreceptor for the leukocyte integrin Mac-1. J Exp Med 196, 679–691. doi:10.1084/jem.20020267
Satta, N., Freyssinet, J.M., Toti, F., 1997. The significance of human monocyte thrombomodulin during membrane vesiculation and after stimulation by lipopolysaccharide. British Journal of Haematology 96, 534–542.
Savage, B., Saldívar, E., Ruggeri, Z.M., 1996. Initiation of platelet adhesion by arrest onto fibrinogen or translocation on von Willebrand factor. Cell 84, 289–297.
Scapin, G., 2013. Molecular replacement then and now. Acta Crystallogr Sect D Biol Crystallogr 69, 2266–2275.
Schall, T.J., Bacon, K., Toy, K.J., Goeddel, D.V., 1990. Selective attraction of monocytes and T lymphocytes of the memory phenotype by cytokine RANTES. , Published online: 18 October 1990; | doi:10.1038/347669a0 347, 669–671. doi:10.1038/347669a0
Scheuerer, B., Ernst, M., Dürrbaum-Landmann, I., Fleischer, J., Grage-Griebenow, E., Brandt, E., Flad, H.-D., Petersen, F., 2000. The CXC-chemokine platelet factor 4 promotes monocyte survival and induces monocyte differentiation into macrophages. Blood 95, 1158–1166. doi:10.1146/annurev.iy.09.040191.003153
Schewe, T., Halangk, W., Hiebsch, C., Rapoport, S.M., 1975. A lipoxygenase in rabbit reticulocytes which attacks phospholipids and intact mitochondria. FEBS Lett. 60, 149–152.
Schmitz, B., Radbruch, A., Kümmel, T., Wickenhauser, C., Korb, H., Hansmann, M.L., Thiele, J., Fischer, R., 1994. Magnetic activated cell sorting (MACS) — a new immunomagnetic method for megakaryocytic cell isolation: Comparison of different separation techniques. Scandinavian Journal of Haematology 52, 267–275.

doi:10.1111/j.1600-0609.1994.tb00095.x
Schneider, S.W., Nuschele, S., Wixforth, A., Gorzelanny, C., Alexander-Katz, A., Netz, R.R., Schneider, M.F., 2007. Shear-induced unfolding triggers adhesion of von Willebrand factor fibers. PNAS 104, 7899–7903. doi:10.1073/pnas.0608422104
Schober, A., Manka, D., Hundelshausen, von, P., Huo, Y., Hanrath, P., Sarembock, I.J., Ley, K., Weber, C., 2002. Deposition of platelet RANTES triggering monocyte recruitment requires P-selectin and is involved in neointima formation after arterial injury. Circulation 106, 1523–1529. doi:10.1161/01.CIR.0000028590.02477.6F
Schubert, S., Weyrich, A.S., Rowley, J.W., 2014. A tour through the transcriptional landscape of platelets. Blood 123, E37–E45. doi:10.1182/blood-2013-12-544692
Scigelova, M., Hornshaw, M., Giannakopulos, A., Makarov, A., 2011. Fourier Transform Mass Spectrometry. Mol Cell Proteomics 10, 111009431–M111.009431. doi:10.1074/mcp.M111.009431
Sehgal, S., Storrie, B., 2007. Evidence that differential packaging of the major platelet granule proteins von Willebrand factor and fibrinogen can support their differential release. Journal of Thrombosis and Haemostasis 5, 2009–2016. doi:10.1111/j.1538-7836.2007.02698.x
Seidegård, J., DePierre, J.W., Pero, R.W., 1984. Measurement and characterization of membrane-bound and soluble epoxide hydrolase activities in resting mononuclear leukocytes from human blood. Cancer Res 44, 3654–3660.
Sevinsky, J.R., Rao, L.V., Ruf, W., 1996. Ligand-induced protease receptor translocation into caveolae: a mechanism for regulating cell surface proteolysis of the tissue factor-dependent coagulation pathway. J Cell Biol 133, 293–304. doi:10.1097/MOH.0b013e3283634412
Shackelford, R.E., Alford, P.B., Xue, Y., Thai, S.F., Adams, D.O., Pizzo, S., 1997. Aspirin inhibits tumor necrosis factoralpha gene expression in murine tissue macrophages. Mol Pharmacol 52, 421–429.
Shantsila, E., Lip, G.Y.H., 2009. The role of monocytes in thrombotic disorders. Insights from tissue factor, monocyte-platelet aggregates and novel mechanisms. Thromb. Haemost. 102, 916–924. doi:10.1160/TH09-01-0023
Shiau, A.K., Barstad, D., Loria, P.M., Cheng, L., Kushner, P.J., Agard, D.A., Greene, G.L., 1998. The structural basis of estrogen receptor/coactivator recognition and the antagonism of this interaction by tamoxifen. Cell 95, 927–937.
Si-Tahar, M., Renesto, P., Falet, H., Rendu, F., Chignard, M., 1996. The phospholipase C/protein kinase C pathway is involved in cathepsin G-induced human platelet activation: comparison with thrombin. Biochem. J. 313 (Pt 2), 401–408.
Simmonds, R.E., Lane, D.A., 1999. Structural and functional implications of the intron/exon organization of the human endothelial cell protein C/activated protein C receptor (EPCR) gene: comparison with the structure of CD1/major histocompatibility complex alpha1 and alpha2 domains. Blood 94, 632–641.
Simon, D.I., Chen, Z., Xu, H., Li, C.Q., Dong, J.F., McIntire, L.V., Ballantyne, C.M., Zhang, L., Furman, M.I., Berndt, M.C., López, J.A., 2000. Platelet glycoprotein ibalpha is a counterreceptor for the leukocyte integrin Mac-1 (CD11b/CD18). J Exp Med 192, 193–204.
Simon, D.I., Ezratty, A.M., Francis, S.A., Rennke, H., Loscalzo, J., 1993. Fibrin(ogen) is internalized and degraded by activated human monocytoid cells via Mac-1 (CD11b/CD18): a nonplasmin fibrinolytic pathway. Blood 82, 2414–2422.
Simon, L.M., Edelstein, L.C., Nagalla, S., Woodley, A.B., Chen, E.S., Kong, X., Ma, L., Fortina, P., Kunapuli, S., Holinstat, M., McKenzie, S.E., Dong, J., Shaw, C.A., Bray, P.F., 2014. Human platelet microRNA-mRNA networks associated with age

and gender revealed by integrated plateletomics. Blood.
Simon, T.C., Makheja, A.N., Martyn Bailey, J., 1989. Formation of 15-hydroxyeicosatetraenoic acid (15-HETE) as the predominant eicosanoid in aortas from Watanabe Heritable Hyperlipidemic and cholesterol-fed rabbits. Atherosclerosis 75, 31–38. doi:10.1016/0021-9150(89)90204-9
Smith, W.L., Song, I., 2002. The enzymology of prostaglandin endoperoxide H synthases-1 and -2. Prostaglandins Other Lipid Mediat. 68-69, 115–128.
Soboloff, J., Spassova, M.A., Tang, X.D., Hewavitharana, T., Xu, W., Gill, D.L., 2006. Orai1 and STIM reconstitute store-operated calcium channel function. J. Biol. Chem. 281, 20661–20665. doi:10.1074/jbc.C600126200
Soo, K.S., Northeast, A., Happerfield, L.C., Burnand, K.G., Bobrow, L.G., 1996. Tissue plasminogen activator production by monocytes in venous thrombolysis. J. Pathol. 178, 190–194. doi:10.1002/(SICI)1096-9896(199602)178:2<190::AID-PATH454>3.0.CO;2-3
Southern, E.M., 1975. Detection of specific sequences among DNA fragments separated by gel electrophoresis. Journal of Molecular Biology 98, 503–517. doi:10.1016/S0022-2836(75)80083-0
Spinelli, S.L., Casey, A.E., Pollock, S.J., Gertz, J.M., McMillan, D.H., Narasipura, S.D., Mody, N.A., King, M.R., Maggirwar, S.B., Francis, C.W., Taubman, M.B., Blumberg, N., Phipps, R.P., 2010. Platelets and Megakaryocytes Contain Functional Nuclear Factor-{kappa}B. Arterioscler. Thromb. Vasc. Biol. 30, 591–598. doi:10.1161/ATVBAHA.109.197343
Stavik, B., Tinholt, M., Sletten, M., Skretting, G., Sandset, P.M., Iversen, N., 2013. TFPIα and TFPIβ are expressed at the surface of breast cancer cells and inhibit TF-FVIIa activity. J Hematol Oncol 6, 5. doi:10.1186/1756-8722-6-5
Stearns-Kurosawa, D.J., Kurosawa, S., Mollica, J.S., Ferrell, G.L., Esmon, C.T., 1996. The endothelial cell protein C receptor augments protein C activation by the thrombin-thrombomodulin complex. PNAS 93, 10212–10216.
Stearns-Kurosawa, D.J., Swindle, K., D'Angelo, A., Valle, Della, P., Fattorini, A., Caron, N., Grimaux, M., Woodhams, B., Kurosawa, S., 2002. Plasma levels of endothelial protein C receptor respond to anticoagulant treatment. Blood 99, 526–530.
Steering Committee of the Physicians' Health Study Research Group*, 1989. Final report on the aspirin component of the ongoing Physicians“ Health Study. Steering Committee of the Physicians” Health Study Research Group. N. Engl. J. Med. 321, 129–135. doi:10.1056/NEJM198907203210301
Steger, D.J., Grant, G.R., Schupp, M., Tomaru, T., Lefterova, M.I., Schug, J., Manduchi, E., Stoeckert, C.J., Lazar, M.A., 2010. Propagation of adipogenic signals through an epigenomic transition state. Genes Dev. 24, 1035–1044. doi:10.1101/gad.1907110
Stegner, D., Nieswandt, B., 2011. Platelet receptor signaling in thrombus formation. J. Mol. Med. 89, 109–121. doi:10.1007/s00109-010-0691-5
Stenberg, P.E., McEver, R.P., Shuman, M.A., Jacques, Y.V., BAINTON, D.F., 1985. A platelet alpha-granule membrane protein (GMP-140) is expressed on the plasma membrane after activation. J Cell Biol 101, 880–886. doi:10.1083/jcb.101.3.880
Stone, J.C., Furuya-Kanamori, L., Barendregt, J.J., Doi, S.A.R., 2015. Was there really any evidence that rosiglitazone increased the risk of myocardial infarction or death from cardiovascular causes? Pharmacoepidemiol Drug Saf 24, 223–227. doi:10.1002/pds.3736
Storey, R.F., Judge, H.M., Wilcox, R.G., Heptinstall, S., 2002. Inhibition of ADP-

induced P-selectin expression and platelet-leukocyte conjugate formation by clopidogrel and the P2Y12 receptor antagonist AR-C69931MX but not …. Thromb Haemost.

Strong, J.P., Malcom, G.T., McMahan, C.A., Tracy, R.E., Newman, W.P., Herderick, E.E., Cornhill, J.F., 1999. Prevalence and extent of atherosclerosis in adolescents and young adults - Implications for prevention from the pathobiological determinants of atherosclerosis in youth study. JAMA 281, 727–735. doi:10.1001/jama.281.8.727

Tabas, I., 2010a. Macrophage death and defective inflammation resolution in atherosclerosis. Nat. Rev. Immunol. 10, 36–46. doi:10.1038/nri2675

Tabas, I., 2010b. The Role of Endoplasmic Reticulum Stress in the Progression of Atherosclerosis. Circ. Res. 107, 839–850. doi:10.1161/CIRCRESAHA.110.224766

Tada, M., Kuzuya, T., Inoue, M., Kodama, K., Mishima, M., Yamada, M., Inui, M., Abe, H., 1981. Elevation of thromboxane B2 levels in patients with classic and variant angina Pectoris. Circulation 64, 1107–1115.

Takagi, J., Petre, B.M., Walz, T., Springer, T.A., 2002. Global conformational rearrangements in integrin extracellular domains in outside-in and inside-out signaling. Cell 110, 599–511.

Taylor, F.B., Peer, G.T., Lockhart, M.S., Ferrell, G., Esmon, C.T., 2001a. Endothelial cell protein C receptor plays an important role in protein C activation in vivo. Blood 97, 1685–1688. doi:10.1182/blood.V97.6.1685

Taylor, F.B., Peer, G.T., Lockhart, M.S., Ferrell, G., Esmon, C.T., 2001b. Endothelial cell protein C receptor plays an important role in protein C activation in vivo. Blood 97, 1685–1688.

Temple, K.A., Cohen, R.N., Wondisford, S.R., Yu, C., Deplewski, D., Wondisford, F.E., 2005. An Intact DNA-binding Domain Is Not Required for Peroxisome Proliferator-activated Receptor {gamma} (PPAR{gamma}) Binding and Activation on Some PPAR Response Elements. J. Biol. Chem. 280, 3529–3540. doi:10.1074/jbc.M411422200

Thomas, C.P., Morgan, L.T., Maskrey, B.H., Murphy, R.C., Kühn, H., Hazen, S.L., Goodall, A.H., Hamali, H.A., Collins, P.W., O'Donnell, V.B., 2010. Phospholipid-esterified eicosanoids are generated in agonist-activated human platelets and enhance tissue factor-dependent thrombin generation. J. Biol. Chem. 285, 6891–6903. doi:10.1074/jbc.M109.078428

Thomas, P.D., Kejariwal, A., Guo, N., Mi, H., Campbell, M.J., Muruganujan, A., Lazareva-Ulitsky, B., 2006. Applications for protein sequence-function evolution data: mRNA/protein expression analysis and coding SNP scoring tools. Nucleic Acids Res. 34, W645–50. doi:10.1093/nar/gkl229

Thouennon, E., Cheng, Y., Falahatian, V., Cawley, N.X., Loh, Y.P., 2015. Rosiglitazone-activated PPARγ induces neurotrophic factor-α1 transcription contributing to neuroprotection. J. Neurochem. 134, 463–470. doi:10.1111/jnc.13152

Tonin, A., Aylward, P., Colquhoun, D., Glasziou, P., 1998. Prevention of cardiovascular events and death with pravastatin in patients with coronary heart disease and a broad range of initial cholesterol levels. The Long-Term Intervention with Pravastatin in Ischaemic Disease (LIPID) Study Group. N. Engl. J. Med. 339, 1349–1357. doi:10.1056/NEJM199811053391902

Tontonoz, P., Hu, E., Spiegelman, B.M., 1994. Stimulation of adipogenesis in fibroblasts by PPAR gamma 2, a lipid-activated transcription factor. Cell 79, 1147–1156.

Tontonoz, P., Nagy, L., Alvarez, J.G.A., Thomazy, V.A., Evans, R.M., 1998. PPARγ Promotes Monocyte/Macrophage Differentiation and Uptake of Oxidized LDL. Cell 93, 241–252. doi:10.1016/S0092-8674(00)81575-5

Towbin, H., Staehelin, T., Gordon, J., 1979. Electrophoretic transfer of proteins from polyacrylamide gels to nitrocellulose sheets: procedure and some applications. PNAS 76, 4350–4354.

Tran, H., Mehta, S.R., Eikelboom, J.W., 2006. Clinical update on the therapeutic use of clopidogrel: treatment of acute ST-segment elevation myocardial infarction (STEMI). Vasc Health Risk Manag 2, 379–387.

Traut, R.R., Monro, R.E., 1964. The puromycin reaction and its relation to protein synthesis. Journal of Molecular Biology 10, 63–72. doi:10.1016/S0022-2836(64)80028-0

Tremoli, E., Camera, M., Toschi, V., Colli, S., 1999. Tissue factor in atherosclerosis. Atherosclerosis 144, 273–283.

Trowbridge, E., Martin, J., Slater, D., Kishk, Y., Warren, C., Harley, P., Woodcock, B., 1984. The origin of platelet count and volume. Clin Phys Physiol Meas 5, 145–170. doi:10.1088/0143-0815/5/3/007

Tucker, M.E., 2013. FDA panel advises easing restrictions on rosiglitazone. BMJ 346, f3769–f3769. doi:10.1136/bmj.f3769

Uguccioni, M., D'Apuzzo, M., Loetscher, M., Dewald, B., Baggiolini, M., 1995. Actions of the chemotactic cytokines MCP-1, MCP-2, MCP-3, RANTES, MIP-1α and MIP-1β on human monocytes. European Journal of Immunology 25, 64–68. doi:10.1002/eji.1830250113

van der Logt, C.P.E., Dirven, R.J., Reitsma, P.H., Bertina, R.M., 1994. Expression of tissue factor and tissue factor pathway inhibitor in monocytes in response to bacterial lipopolysaccharide and phorbolester. Blood Coagulation & Fibrinolysis 5, 211.

van Gils, J.M., Zwaginga, J.J., Hordijk, P.L., 2009a. Molecular and functional interactions among monocytes, platelets, and endothelial cells and their relevance for cardiovascular diseases. J Leukoc Biol 85, 195–204. doi:10.1189/jlb.0708400

van Gils, J.M., Zwaginga, J.J., Hordijk, P.L., 2009b. Molecular and functional interactions among monocytes, platelets, and endothelial cells and their relevance for cardiovascular diseases. J Leukoc Biol 85, 195–204. doi:10.1189/jlb.0708400

van Leyen, K., Duvoisin, R.M., Engelhardt, H., Wiedmann, M., 1998. A function for lipoxygenase in programmed organelle degradation. Nature 395, 392–395. doi:10.1038/26500

Vane, J.R., DSc, FRS, Botting, R.M., PhD, 1998. Mechanism of Action of Nonsteroidal Anti-inflammatory Drugs. The American Journal of Medicine 104, 2S–8S. doi:10.1016/S0002-9343(97)00203-9

Wagner, M., Zollner, G., Trauner, M., 2011. Nuclear receptors in liver disease. Hepatology 53, 1023–1034. doi:10.1002/hep.24148

Waku, T., Shiraki, T., Oyama, T., Fujimoto, Y., Maebara, K., Kamiya, N., Jingami, H., Morikawa, K., 2009. Structural insight into PPARgamma activation through covalent modification with endogenous fatty acids. Journal of Molecular Biology 385, 188–199. doi:10.1016/j.jmb.2008.10.039

Wang, N., Yin, R., Liu, Y., Mao, G., Xi, F., 2011. Role of Peroxisome Proliferator-Activated Receptor-γ in Atherosclerosis. Circulation Journal 75, 528–535. doi:10.1253/circj.CJ-11-0060

Watson, P.J., Fairall, L., Schwabe, J.W.R., 2012. Nuclear hormone receptor co-repressors: structure and function. Mol. Cell. Endocrinol. 348, 440–449.

doi:10.1016/j.mce.2011.08.033
Watson, S.P., Auger, J.M., McCarty, O.J.T., Pearce, A.C., 2005. GPVI and integrin αIIbβ3 signaling in platelets. J. Thromb. Haemost. 3, 1752–1762. doi:10.1111/j.1538-7836.2005.01429.x
Weber, C., Belge, K.U., Hundelshausen, von, P., Draude, G., Steppich, B., Mack, M., Frankenberger, M., Weber, K.S., Ziegler-Heitbrock, H.W., 2000. Differential chemokine receptor expression and function in human monocyte subpopulations. J Leukoc Biol 67, 699–704.
Weber, E., 1988. Randomised trial of prophylactic daily aspirin in British male doctors. Br Med J (Clin Res Ed) 296, 1193–316.
Werling, R.W., Zacharski, L.R., Kisiel, W., Bajaj, S.P., Memoli, V.A., Rousseau, S.M., 1993. Distribution of Tissue Factor Pathway Inhibitor in Normal and Malignant Human Tissues. Thromb. Haemost. 69, 366–369.
Westergaard, M., Henningsen, J., Johansen, C., 2003. Expression and localization of peroxisome proliferator-activated receptors and nuclear factor κB in normal and lesional psoriatic skin. Journal of investigative … 121, 1104–1117. doi:10.1046/j.1523-1747.2003.12536.x
Westmuckett, A.D., Lupu, C., Roquefeuil, S., Krausz, T., Kakkar, V.V., Lupu, F., 2000. Fluid flow induces upregulation of synthesis and release of tissue factor pathway inhibitor in vitro. Arterioscler. Thromb. Vasc. Biol. 20, 2474–2482.
Weyrich, A.S., McIntyre, T.M., McEver, R.P., Prescott, S.M., Zimmerman, G.A., 1995. Monocyte Tethering by P-Selectin Regulates Monocyte Chemotactic Protein-1 and Tumor-Necrosis-Factor-Alpha Secretion - Signal Integration and Nf-Kappa-B Translocation. J Clin Invest 95, 2297–2303. doi:10.1172/JCI117921
Whitelaw, D.M., 1966. The intravascular lifespan of monocytes. Blood 28, 455–464.
Williamson, D., Pikovski, I., Cranmer, S.L., Mangin, P., Mistry, N., Domagala, T., Chehab, S., Lanza, F., Salem, H.H., Jackson, S.P., 2002. Interaction between platelet glycoprotein Ibalpha and filamin-1 is essential for glycoprotein Ib/IX receptor anchorage at high shear. J. Biol. Chem. 277, 2151–2159. doi:10.1074/jbc.M109384200
Witt, D.P., Lander, A.D., 1994. Differential binding of chemokines to glycosaminoglycan subpopulations. Curr. Biol. 4, 394–400.
Wood, J.P., Ellery, P.E.R., Maroney, S.A., Mast, A.E., 2014. Biology of tissue factor pathway inhibitor. Blood 123, 2934–2943. doi:10.1182/blood-2013-11-512764
Woollard, K.J., Geissmann, F., 2010. Monocytes in atherosclerosis: subsets and functions. Nat Rev Cardiol 7, 77–86. doi:10.1038/nrcardio.2009.228
Wu, Z., Rosen, E.D., Brun, R., Hauser, S., Adelmant, G., Troy, A.E., McKeon, C., Darlington, G.J., Spiegelman, B.M., 1999. Cross-regulation of C/EBP alpha and PPAR gamma controls the transcriptional pathway of adipogenesis and insulin sensitivity. Mol. Cell 3, 151–158.
Wu, Z., Xie, Y., Bucher, N.L., Farmer, S.R., 1995. Conditional ectopic expression of C/EBP beta in NIH-3T3 cells induces PPAR gamma and stimulates adipogenesis. Genes Dev. 9, 2350–2363. doi:10.1101/gad.9.19.2350
Wun, T.C., Kretzmer, K.K., Girard, T.J., Miletich, J.P., Broze, G.J., 1988. Cloning and characterization of a cDNA coding for the lipoprotein-associated coagulation inhibitor shows that it consists of three tandem Kunitz-type inhibitory domains. J. Biol. Chem. 263, 6001–6004.
Wurtz, J.-M., Bourguet, W., Renaud, J.-P., Vivat, V., Chambon, P., Moras, D., Gronemeyer, H., 1996. A canonical structure for the ligand-binding domain of nuclear receptors. Nature Structural & Molecular Biology 3, 87–94.

doi:10.1038/nsb0196-87
Xue, J., Hua, Y.N., Xie, M.L., Gu, Z.L., 2010. Aspirin inhibits MMP-9 mRNA expression and release via the PPARalpha/gamma and COX-2/mPGES-1-mediated pathways in macrophages derived from THP-1 cells. Biomed. Pharmacother. 64, 118–123. doi:10.1016/j.biopha.2009.04.033
Yang, H., Kim, A., David, T., Palmer, D., Jin, T., Tien, J., Huang, F., Cheng, T., Coughlin, S.R., Jan, Y.N., Jan, L.Y., 2012. TMEM16F Forms a Ca2+-Activated Cation Channel Required for Lipid Scrambling in Platelets during Blood Coagulation. Cell 151, 111–122. doi:10.1016/j.cell.2012.07.036
Yap, C.L., Hughan, S.C., Cranmer, S.L., Nesbitt, W.S., Rooney, M.M., Giuliano, S., Kulkarni, S., Dopheide, S.M., Yuan, Y., Salem, H.H., Jackson, S.P., 2000. Synergistic adhesive interactions and signaling mechanisms operating between platelet glycoprotein Ib/IX and integrin alpha IIbbeta 3. Studies in human platelets ans transfected Chinese hamster ovary cells. J. Biol. Chem. 275, 41377–41388. doi:10.1074/jbc.M005590200
Yarmolinsky, M.B., Haba, G.L., 1959. Inhibition by puromycin of amino acid incorporation into protein. PNAS 45, 1721–1729.
Yáñez-Mó, M., Siljander, P.R.-M., Andreu, Z., Zavec, A.B., Borràs, F.E., Buzas, E.I., Buzas, K., Casal, E., Cappello, F., Carvalho, J., Colás, E., Cordeiro-da Silva, A., Fais, S., Falcon-Perez, J.M., Ghobrial, I.M., Giebel, B., Gimona, M., Graner, M., Gursel, I., Gursel, M., Heegaard, N.H.H., Hendrix, A., Kierulf, P., Kokubun, K., Kosanovic, M., Kralj-Iglic, V., Krämer-Albers, E.-M., Laitinen, S., Lässer, C., Lener, T., Ligeti, E., Linē, A., Lipps, G., Llorente, A., Lötvall, J., Manček-Keber, M., Marcilla, A., Mittelbrunn, M., Nazarenko, I., Nolte-'t Hoen, E.N.M., Nyman, T.A., O'Driscoll, L., Olivan, M., Oliveira, C., Pállinger, É., Del Portillo, H.A., Reventós, J., Rigau, M., Rohde, E., Sammar, M., Sánchez-Madrid, F., Santarém, N., Schallmoser, K., Ostenfeld, M.S., Stoorvogel, W., Stukelj, R., Van der Grein, S.G., Vasconcelos, M.H., Wauben, M.H.M., De Wever, O., 2015a. Biological properties of extracellular vesicles and their physiological functions. J Extracell Vesicles 4, 27066. doi:10.3402/jev.v4.27066
Yáñez-Mó, M., Siljander, P.R.-M., Andreu, Z., Zavec, A.B., Borràs, F.E., Buzas, E.I., Buzas, K., Casal, E., Cappello, F., Carvalho, J., Colás, E., Silva, A.C.-D., Fais, S., Falcon-Perez, J.M., Ghobrial, I.M., Giebel, B., Gimona, M., Graner, M., Gursel, I., Gursel, M., Heegaard, N.H.H., Hendrix, A., Kierulf, P., Kokubun, K., Kosanovic, M., Kralj-Iglic, V., Krämer-Albers, E.-M., Laitinen, S., Lässer, C., Lener, T., Ligeti, E., Linē, A., Lipps, G., Llorente, A., Lötvall, J., Manček-Keber, M., Marcilla, A., Mittelbrunn, M., Nazarenko, I., Hoen, E.N.M.N., Nyman, T.A., O'Driscoll, L., Olivan, M., Oliveira, C., Pállinger, É., Del Portillo, H.A., Reventós, J., Rigau, M., Rohde, E., Sammar, M., Sánchez-Madrid, F., Santarém, N., Schallmoser, K., Ostenfeld, M.S., Stoorvogel, W., Stukelj, R., Van der Grein, S.G., Vasconcelos, M.H., Wauben, M.H.M., De Wever, O., 2015b. Biological properties of extracellular vesicles and their physiological functions. J Extracell Vesicles 4, 319. doi:10.3402/jev.v4.27066
Yeung, J., Apopa, P.L., Vesci, J., Kenyon, V., Rai, G., Jadhav, A., Simeonov, A., Holman, T.R., Maloney, D.J., Boutaud, O., Holinstat, M., 2012. Protein kinase C regulation of 12-lipoxygenase-mediated human platelet activation. Mol Pharmacol 81, 420–430. doi:10.1124/mol.111.075630
Yeung, J., Apopa, P.L., Vesci, J., Stolla, M., Rai, G., Simeonov, A., Jadhav, A., Fernandez-Perez, P., Maloney, D.J., Boutaud, O., Holman, T.R., Holinstat, M., 2013. 12-lipoxygenase activity plays an important role in PAR4 and GPVI-

mediated platelet reactivity. Thromb. Haemost. 110, 569–581. doi:10.1160/TH13-01-0014

Yeung, J., Holinstat, M., 2011. 12-lipoxygenase: a potential target for novel anti-platelet therapeutics. Cardiovasc Hematol Agents Med Chem 9, 154–164.

Yeung, J., Tourdot, B.E., Fernandez-Perez, P., Vesci, J., Ren, J., Smyrniotis, C.J., Luci, D.K., Jadhav, A., Simeonov, A., Maloney, D.J., Holman, T.R., McKenzie, S.E., Holinstat, M., 2014. Platelet 12-LOX is essential for FcγRIIa-mediated platelet activation. Blood 124, 2271–2279. doi:10.1182/blood-2014-05-575878

Yiqin, Y., Meilin, X., Jie, X., Keping, Z., 2009. Aspirin inhibits MMP-2 and MMP-9 expression and activity through PPARalpha/gamma and TIMP-1-mediated mechanisms in cultured mouse celiac macrophages. Inflammation 32, 233–241. doi:10.1007/s10753-009-9125-3

Yu, K., Bayona, W., Kallen, C.B., Harding, H.P., Ravera, C.P., McMahon, G., Brown, M., Lazar, M.A., 1995. Differential activation of peroxisome proliferator-activated receptors by eicosanoids. J. Biol. Chem. 270, 23975–23983.

Yum, S., Jeong, S., Lee, S., Kim, W., Nam, J., Jung, Y., 2015. HIF-prolyl hydroxylase is a potential molecular target for esculetin-mediated anti-colitic effects. Fitoterapia 103, 55–62. doi:10.1016/j.fitote.2015.03.013

Zand, T., Hoffman, A.H., Savilonis, B.J., Underwood, J.M., Nunnari, J.J., Majno, G., Joris, I., 1999. Lipid Deposition in Rat Aortas with Intraluminal Hemispherical Plug Stenosis. Am. J. Pathol. 155, 85–92. doi:10.1016/S0002-9440(10)65103-6

Zeng, S., Zhou, X., Ge, L., Ji, W.-J., Shi, R., Lu, R.-Y., Sun, H.-Y., Guo, Z.-Z., Zhao, J.-H., Jiang, T.-M., Li, Y.-M., 2014. Monocyte subsets and monocyte-platelet aggregates in patients with unstable angina. J. Thromb. Thrombolysis 38, 439–446. doi:10.1007/s11239-014-1083-4

Zhang, J.-H., Pearson, T., Matharoo-Ball, B., Ortori, C.A., Warren, A.Y., Khan, R., Barrett, D.A., 2007. Quantitative profiling of epoxyeicosatrienoic, hydroxyeicosatetraenoic, and dihydroxyeicosatetraenoic acids in human intrauterine tissues using liquid chromatography/electrospray ionization tandem mass spectrometry. Anal. Biochem. 365, 40–51. doi:10.1016/j.ab.2007.03.001

Zhao, C., Zhang, H., Wong, W.-C., Sem, X., Han, H., Ong, S.-M., Tan, Y.-C., Yeap, W.-H., Gan, C.-S., Ng, K.-Q., Koh, M.B.-C., Kourilsky, P., Sze, S.-K., Wong, S.-C., 2009. Identification of novel functional differences in monocyte subsets using proteomic and transcriptomic methods. J. Proteome Res. 8, 4028–4038. doi:10.1021/pr900364p

Zhou, J., Tang, P.C.Y., Qin, L., Gayed, P.M., Li, W., Skokos, E.A., Kyriakides, T.R., Pober, J.S., Tellides, G., 2010. CXCR3-dependent accumulation and activation of perivascular macrophages is necessary for homeostatic arterial remodeling to hemodynamic stresses. J Exp Med 207, 1951–1966. doi:10.1084/jem.20100098

Zufferey, A., Fontana, P., Reny, J.L., Nolli, S., Sanchez, J.C., 2012. Platelet proteomics. Mass Spectrometry Reviews 31, 331–351. doi:10.1002/mas.20345

Zufferey, A., Schvartz, D., Nolli, S., Reny, J.L., Sanchez, J.C., Fontana, P., 2014. Characterization of the platelet granule proteome: evidence of the presence of MHC1 in alpha-granules. Journal of Proteomics 101, 130–140. doi:10.1016/j.jprot.2014.02.008

Zwaal, R., Comfurius, P., Bevers, E.M., 2004. Scott syndrome, a bleeding disorder caused by defective scrambling of membrane phospholipids. Biochim. Biophys. Acta 1636, 119–128. doi:10.1016/j.bbalip.2003.07.003

Zwaal, R., Comfurius, P., Bevers, E.M., 1998. Lipid-protein interactions in blood coagulation. Biochim. Biophys. Acta 1376, 433–453.